

New Analytical Approach Based on Thin Film and Nanomaterials

Sirilak Sattayasamitsathit

**A Thesis Submitted in Fulfillment of the Requirements
for the Degree of Doctor of Philosophy in Chemistry
Prince of Songkla University**

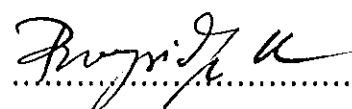
2008

Copyright of Prince of Songkla University

Library	QD115. S54 2008 C. 2
Bib Key	302967
	26 Nov. 2552

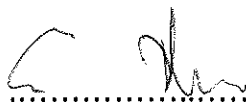
Thesis Title New Analytical Approach Based on Thin Film and
Nanomaterials
Author Miss Sirilak Sattayasamitsathit
Major Program Chemistry

Major Advisor



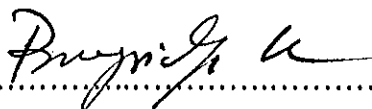
(Assoc. Prof. Dr. Proespichaya Kanatharana)

Examining Committee :



.....Chairperson

(Prof. Dr. Eric Bakker)

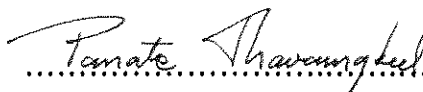


(Assoc. Prof. Dr. Proespichaya Kanatharana)

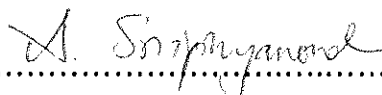
Co-advisor



(Assoc. Prof. Dr. Panote Thavarungkul)

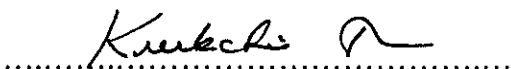


(Assoc. Prof. Dr. Panote Thavarungkul)



(Asst. Prof. Dr. Atitaya Siripinyanond)

The Graduate School, Prince of Songkla University, has approved this thesis as fulfillment of the requirements for the Doctor of Philosophy Degree in Chemistry



(Assoc. Prof. Dr. Kerkchai Thongnoo)

Dean of Graduate School

ชื่อวิทยานิพนธ์	เทคนิควิเคราะห์แบบใหม่โดยใช้ฟิล์มบางและวัสดุนาโน
ผู้เขียน	นางสาวศิริลักษณ์ สัตยสมิทธิศิต
สาขาวิชา	เคมี
ปีการศึกษา	2551

บทคัดย่อ

วิทยานิพนธ์นี้แบ่งงานวิจัยออกเป็นสองส่วน ส่วนแรกศึกษาการพัฒนาเทคนิคการเตรียมตัวอย่างและการวิเคราะห์สารทางไฟฟ้าเคมีโดยใช้ฟิล์มบางและวัสดุนาโน ในส่วนที่สองศึกษาการเตรียมเส้นลวดนาโนโดยใช้เทคนิคการเกาะติดทางไฟฟ้า

เทคนิคแรกที่พัฒนา คือ การวิเคราะห์สารอินทรีย์ระเหยง่ายแบบออนไลน์ โดยอาศัยเทคนิคการซึมผ่านและการระเหยเป็นไอ (pervaporation) สำหรับวิเคราะห์เมทานอล เอทานอล โพรพานอล เมทิลไอโซบิวทิลคีโตน (MIBK) และ เมทิลเทอร์เทียรีบิวทิล อีเธอร์ (MTBE) ศึกษาอัตราการแพร่และประสิทธิภาพของระบบ ผลการทดลองพบว่าอัตราการแพร่ของเมทิลเทอร์เทียรีบิวทิล อีเธอร์ เร็วที่สุด ส่วนอัตราการแพร่ที่ช้าที่สุด คือ เมทานอลและเอทานอล นอกจากนี้ได้นำระบบที่พัฒนาไปใช้กับตัวอย่างจริง คือ ตัวอย่างน้ำเสียและไบโอโพลีเมอร์ ศึกษาผลของตัวรบกวนและเปอร์เซ็นต์การได้กลับคืน จากการวิเคราะห์ตัวอย่างจริงไม่พบสารที่วิเคราะห์ทั้งทั้งในตัวอย่างน้ำเสียและไบโอโพลีเมอร์

ต่อมาเพื่อเป็นการแก้ปัญหาจากตัวดูดซับทางการค้า จึงได้พัฒนาท่อสำหรับดูดซับสารอินทรีย์ระเหยง่าย ได้แก่ ไคลโอโรมีเทน (DCM) ไคลโอโรอีเทน (DCE) ไตรคลโอโรมีเทน (TCM) ไตรคลโอโรอีเทน (TCE) เบนซีน (Benzene) โทลูอิน (Toluene) ไซลีน (Xylene) ในตัวอย่างอากาศภายในอาคาร โดยท่อที่พัฒนาสำหรับดูดซับสารอินทรีย์ระเหยง่ายจะเคลือบด้วยโซล-เจลของโพลีเอทิลีนไกลคอลและโซล-เจลของโพลีเอทิลีนไกลคอลร่วมกับท่อนาโนคาร์บอน (multiwall carbon nanotubes) เพื่อให้ได้ประสิทธิภาพการดูดซับและคายการดูดซับสูงที่สุดจึงศึกษาปัจจัยต่างๆ ที่ส่งผลต่อสัญญาณการวิเคราะห์ ศึกษาความสามารถในการทำซ้ำได้ ความเสถียร และประสิทธิภาพของระบบ โดยเปรียบเทียบกับคาร์โบแนค บี พบว่าท่อสำหรับดูดซับสารอินทรีย์ระเหยง่ายที่พัฒนาขึ้นให้ค่าความไววิเคราะห์สูงกว่าและขีดจำกัดการตรวจวัดที่ต่ำกว่าคาร์โบแนค บี จากนั้นจึงนำท่อที่พัฒนาไปดูดซับสารอินทรีย์ระเหยง่ายในตัวอย่างอากาศภายในอาคารพบโทลูอินและไซลีนในช่วงที่ไม่สามารถตรวจวัดได้จนถึง 3.3 ส่วนในพันล้านส่วนโดยปริมาตร และช่วงที่ไม่สามารถตรวจวัดได้จนถึง 1.1 ส่วน ในพันล้านส่วนโดยปริมาตร ตามลำดับ

ลำดับต่อมาได้ศึกษาการตรวจวัดยาปฏิชีวนะ คือ เตตราไซคลิน โดยใช้ขั้วไฟฟ้าฟิล์มบางบิสมีส โดยการเตรียมฟิล์มบางบิสมีสบนขั้วกลาสซี คาร์บอนโดยอาศัยการเกาะติดทางไฟฟ้าเคมี นำขั้วไฟฟ้าที่พัฒนาขึ้นไปติดตั้งในระบบไหลผ่านเพื่อใช้ตรวจวัดเตตราไซคลินที่ศักย์ไฟฟ้ารีดักชัน -1.3 โวลต์ โดยขั้วไฟฟ้าฟิล์มบางบิสมีสให้ความไววิเคราะห์สูงกว่าขั้วกลาสซี คาร์บอนถึง 4.6 เท่า ในช่วงความเป็นเส้นตรง 1.0 ถึง 6.0 มิลลิโมลาร์ และขีดจำกัดการตรวจวัด 1.2 ไมโครโมลาร์ บิสมีสฟิล์มสามารถเตรียมซ้ำได้ดีโดยให้ค่าการเบี่ยงเบนมาตรฐานสัมพัทธ์ 4.7% และสามารถใช้ได้ถึง 40 ครั้ง จากนั้นจึงศึกษาตัวอย่างจริง คือ ยาแคปซูลเตตราไซคลิน 250 มิลลิกรัม ผลการวิเคราะห์โดยใช้ขั้วไฟฟ้าฟิล์มบางบิสมีสในระบบไหลผ่านให้ผลอยู่ในช่วง 240 - 260 มิลลิกรัม ซึ่งสอดคล้องกับฉลากยา นอกจากนี้ยังให้เปอร์เซ็นต์การได้กลับคืน 86 - 106%

ในการพัฒนาเทคนิคการเตรียมเส้นลวดนาโนอัลลอยด์ ได้อาศัยเทคนิคการเกาะติดทางไฟฟ้าและใช้เมมเบรนเป็นแม่แบบ โดยใช้สารละลายผสมของโลหะโคบอลต์ นิกเกิล และคอปเปอร์ เกาะติดทางไฟฟ้าที่ศักย์ไฟฟ้า -1.4 โวลต์ เพื่อให้ได้เส้นลวดนาโนอัลลอยด์แบบซิงเกิลเชกเมนต์ และสารละลายผสมของเงินและทอง เกาะติดทางไฟฟ้าที่ศักย์ไฟฟ้า -0.5 ถึง -1.2 โวลต์ ในการเตรียมเส้นลวดนาโนอัลลอยด์แบบมัลติเชกเมนต์ นอกจากนี้เส้นลวดนาโนของทองที่มีรูพรุนแบบลำดับชั้นสามารถเตรียมได้จากสารละลายผสมของเงินและทอง เกาะติดทางไฟฟ้าที่ศักย์ไฟฟ้า -0.9 ถึง -1.1 โวลต์ ตามด้วยการกัดองค์ประกอบเงิน จากนั้นจึงละลายแม่แบบเพื่อให้ได้เส้นลวดนาโน ใช้เทคนิคเอกซเรย์ฟลูออเรสเซนส์ในการตรวจวัดองค์ประกอบโลหะในเส้นลวดนาโนอัลลอยด์แบบซิงเกิลเชกเมนต์ และการสะท้อนกลับของแสงในการตรวจวัดเส้นลวดนาโนอัลลอยด์แบบมัลติเชกเมนต์ จากสัญญาณการตรวจวัดสามารถแปลผลได้เป็นรูปแบบโค้ด เอกซเรย์ฟลูออเรสเซนซ์สเปกโตรเมตรีแบบกระจายพลังงาน (EDX) ใช้ในการศึกษาปริมาณเงินและทองที่ศักย์ไฟฟ้าต่าง ๆ สำหรับเส้นลวดนาโนอัลลอยด์แบบมัลติเชกเมนต์และเส้นลวดนาโนของทองที่มีรูพรุนแบบลำดับชั้น ใช้กล้องจุลทรรศน์อิเล็กตรอนแบบส่องกราดในการศึกษาการกระจายตัวของรูพรุน ขนาดของรูพรุนที่องค์ประกอบของเงินกับทองต่าง ๆ กัน และลักษณะของเส้นลวดนาโน เทคนิคเอกซเรย์ฟลูออเรสเซนส์และการสะท้อนกลับของแสงเป็นเทคนิคที่มีประสิทธิภาพในการในการอ่านสัญญาณของเส้นลวดนาโนอัลลอยด์ กล้องจุลทรรศน์อิเล็กตรอนแบบส่องกราดแสดงลักษณะของเส้นลวดนาโนของทองที่มีรูพรุนแบบลำดับชั้นและวัสดุคอมโพสิต จากหลักการปรับองค์ประกอบและรูปร่างของเส้นลวดนาโนนำไปสู่การสังเคราะห์เส้นลวดนาโนที่มีคุณสมบัติหลากหลายขึ้นอยู่กับองค์ประกอบโลหะและวัสดุคอมโพสิต วัสดุนาโนสามารถนำไปใช้ได้อย่างกว้างขวาง เช่น การตรวจสอบสินค้าและอุปกรณ์นาโน

Thesis Title	New Analytical Approach Based on Thin Film and Nanomaterials
Author	Miss Sirilak Sattayasamitsathit
Major Program	Chemistry
Academic Year	2008

Abstract

This thesis consists of two parts. For the first part sample preparation and electrochemical detection techniques were developed using thin film layer and nanomaterials. The second part focused on the preparation of nanowires via electrodeposition technique.

The first developed technique was on on-line system for volatile organic compounds (VOCs) based on pervaporation technique for methanol, ethanol, 1-propanol, methyl-isobutyl ketone (MIBK) and tert-butyl methyl ether (MTBE) analysis. The diffusion rate and system performance of each compound was studied. The results show that diffusion rate of MTBE was the highest and the lowest was methanol and ethanol. In addition, this technique was applied for the analysis of environmental sample, *i.e.*, wastewater and biosolids. Matrix effect and the percentage of relative recovery were also investigated. From real sample analysis, none of the studied compounds were detected in the wastewater and biosolids in this area.

The second development aimed to overcome the drawback from commercial adsorbent. Trapping tubes for volatile organic compounds (VOCs), dichloromethane (DCM), 1, 2-dichloroethane (DCE), trichloromethane (TCM), trichloroethene (TCE), benzene (B), toluene (T) and xylene (X) in indoor air were developed using silico-steel tube (1.02 mm I.D. and 1.59 mm O.D.) coated with sol-gel polyethylene glycol (PEG), sol-gel polyethylene glycol mixed with multi-walled carbon nanotubes (PEG/MWCNTs). To achieve the highest adsorption and desorption efficiencies, parameters affecting the response of the system were optimized. The reproducibility, stability and system performance of developed trapping tube were

investigated and compared to Carbopack B. The trapping tubes provided higher sensitivity and lower detection limit than Carbopack B. The developed trapping tubes were applied for the monitoring of VOCs in indoor air and only toluene and xylene were found in the range of N.D.-3.3 ppmv and N.D.-1.1 ppmv, respectively.

For the third project, electrochemical detection of tetracycline was investigated using bismuth thin film electrode (BiFE). A bismuth film was prepared on glassy carbon electrode (GCE) via electrodeposition technique. This modified electrode was set in a flow injection amperometric system for analysis of tetracycline at -1.3 V. It provided higher sensitivity, 4.6 times, than bare GCE. Linear dynamic range was between 1.0 and 6.0 mM with a low detection limit of 1.2 μ M. Good reproducibility of bismuth film preparation was obtained with relative standard deviation 4.7% where one preparation could be used to analyze tetracycline up to 40 times. The BiFE was validated with three different lots of real sample, 250 mg tetracycline capsules, the results showed good agreement *i.e.*, between 240 and 260 mg per capsule. Good relative recoveries were also obtained in the range of 86-106%.

For the development of alloy nanowires preparation, electrodeposition technique with template-assisted was carried out whereas the mixture of metal plating solution was used for single segment alloy nanowires (Co, Ni and Cu mixture, deposition potential -1.4 V) and multi segment alloy nanowires (Ag and Au, alternative deposition potential between -0.5 to -1.2 V) including step-like porous gold nanowires (Ag and Au, changing deposition potential between -0.9 to -1.1 V following etching silver component). Finally, the template was dissolved to obtain free standing nanowires. Composition profile of single-segment alloy nanowire, qualitatively and quantitatively, was detected by X-ray fluorescence (XRF) whereas optical reflectivity was used to qualify the multi-segment alloy nanowires. These can be interpreted for coding pattern. Energy dispersive X-ray fluorescence (EDX) was used to study the amount (% atom) of gold and silver at different deposition potential for multi-segment and porous gold nanowires. Scanning electron microscope (SEM) was used to study the pore distribution, the diameter of porous gold at different composition of gold/silver and the characteristic of all nanowires. XRF and optical reflectance are effective readout techniques of alloy nanowires. SEM illustrated the

step-like porous gold and also the composite materials. These versatile composition- and shape- tailored concept can be extended to nanowires which have diverse properties based on different metals and also composite material. These production can be used for a wide range of application *i.e.*, product tagging and nano-devices.

Acknowledgements

The completion of this thesis would be impossible without the help of many people, whom I would like to thank.

I am very grateful to my advisors Associate Professor Dr. Proespichaya Kanatharana and Associate Professor Dr. Panote Thavarungkul for their support, valuable opportunities and for all the excellent teaching, guidance and supervision.

I would like to thank my beloved mom, sister, grandfather and grandmother for their support.

I would like to thank Professor Dr. Joseph Wang for giving me a chance to learn and conduct an exciting research at the Department of Chemical Engineering, Biodesign institute, Arizona state University, Arizona, USA. I would especially like to thank, Dr. Rawiwan Laocharoensuk, Jared Burdick, Ralph Bash, Andrea Bulbarello, and Agustin G. Crevillen for their friendship and support.

I would like to thank examination committee members of this thesis for their valuable time. All the help in some technical aspects rendered by staffs of the Department of Chemistry, Faculty of Science, Prince of Songkla University

I am deeply indebted to the Royal Golden Jubilee Ph.D. Program (RGJ) of the Thailand Research Fund (TRF) for scholarship; the Center of Excellence for Innovation in Chemistry (PERCH-CIC), Commission on Higher Education, Ministry of Education is gratefully acknowledged.

And lastly, I would like to thank the member of Trace Analysis and Biosensor Research Center for their support and friendship forever.

Sirilak Sattayasamitsathit

The Relevant of the Research Work to Thailand

The purpose of this Doctor of Philosophy thesis in chemistry (analytical chemistry) is to develop and evaluate the sample preparation techniques for the analysis of organic compounds. These developed methods are simple, cost effective and easy to operate. The first technique is membrane extraction of organic compounds in aqueous sample followed with preconcentration using μ -trap. This technique is suitable for on-line analysis of volatile organic compounds (VOCs) in aqueous sample. The second method is the development of trapping tube by coating the silico-steel tube with polymer film (polyethylene glycol, PEG) and PEG incorporated with multiwall carbon nanotubes to be applied to monitor volatile organic compounds in indoor air. This will be useful for the evaluation of indoor air quality in work place. The third method is the electrode modification using bismuth thin film for tetracycline detection in flow injection system. This electrode can be used replacing mercury film electrode and useful for other organic compounds detection. The last developed method is the preparation technique of single- and multi- segment nanowires including porous gold nanowires via electrochemical deposition with template-assisted. Using the mixture of plating solution then all nanowires can be synthesized. These nanowires will be useful for the security system, nano-sensor and nano-hardware.

Government and private organizations in Thailand which are the Ministry of Public Health, the Ministry of Industry, the Ministry of Environment and the Ministry of Education can use these sample preparation techniques and electrode modification for quantitative analysis of trace amount of organic compounds. For nanowires synthesis, they can be used to improve the security system and nano-sensor device.

Contents

	Page
List of Tables	xxi
List of Figures	xxiv
List of Abbreviation	xli
CHAPTER 1: Introduction	1
1.1 Background and Rationale	1
1.2 Objective of the research	3
1.2.1 Gas injection membrane extraction for trace organic compounds	3
1.2.2 High efficiency coating film for VOCs preconcentration device	4
1.2.3 Bismuth film electrode for analysis of tetracycline in flow injection system	4
1.2.4 Alloy nanowires	4
1.2.5 Shape-tailored porous gold nanowires	5
1.3 Benefit	5
CHAPTER 2: Sample preparation	6
2.1 Introduction	6
2.2 Sample preparation methods for VOC analysis in liquid sample	6
2.2.1 Direct aqueous injection	6
2.2.2 Liquid liquid extraction	7
2.2.3 Enrichment using immersed immobilized sorbents	11
2.2.3.1 Solid phase extraction	11
2.2.3.2 Solid phase microextraction	12
2.2.3.3 Stir bar sorptive extraction	13
2.2.3.4 Solid phase dynamic extraction	14

Contents (continued)

	Page
2.2.4 Membrane extraction	15
2.2.4.1 Supported liquid membrane	16
2.2.4.2 Microporous membrane liquid-liquid extraction	17
2.2.4.3 Polymeric membrane extraction	18
2.2.4.4 Membrane extraction with sorbent interfaces	19
2.2.4.5 Enrichment in membrane extraction	23
2.2.5 Headspace techniques	24
2.2.5.1 Static headspace techniques	24
2.2.5.2 Dynamic headspace techniques	25
2.3 Sample preparation methods for VOC analysis in air	26
2.3.1 Enrichment using immobilized sorbents	26
2.3.1.1 Adsorbent on solid sorbent	26
2.3.1.2 Thermal desorption and type of adsorbent	29
2.3.2 Membrane extraction	31
2.4 Conclusions	33
CHAPTER 3: Electrochemical analysis of organic compounds	35
3.1 Introduction	35
3.2 Electrochemical detection technique	35
3.2.1 Voltammetry	35
3.2.2 Amperometry	37
3.3 Electrode material	39
3.3.1 Mercury electrode	39
3.3.2 Solid electrode	40
3.3.3 Chemically modified electrode	40
3.4 Other electrodes	47

Contents (continued)

	Page
3.4.1 Microelectrodes	47
3.4.2 Screen print electrode	49
3.5 Flow injection system with electrochemical detection	50
3.6 Conclusion	53
CHAPTER 4: Nanowires	54
4.1 Introduction	54
4.2 Nanowires fabrication and characterization	55
4.2.1 The top down technique	55
4.2.2 The bottom up technique	57
4.2.2.1 Soft template	57
4.2.2.2 Hard template	58
4.2.2.2.1 Track etched membranes	58
4.2.2.2.2 Porous alumina membrane	60
4.3 Electrochemical deposition	63
4.3.1 Metals and alloy	65
4.3.2 Metal oxide nanowires	68
4.3.3 Semiconductor	68
4.3.4 Conductive polymers	69
4.3.5 Composite nanowires	70
4.4 Characterizations of nanowires	72
4.4.1 Optical microscope	72
4.4.2 Electron microscopes	72
4.4.2.1 Scanning electron microscope	73
4.4.2.2 Transmission electron microscope	73
4.4.3 Atomic force microscope	74

Contents (continued)

	Page
4.4.4 X-ray fluorescence	75
4.5 Applications	75
4.5.1 Nanowires for bioapplications	75
4.5.2 Nanowires for non-bioapplication	78
4.5.2.1 Security system	78
4.5.2.2 Chemical sensor	80
4.6 Conclusions	82
CHAPTER 5: Gas injection membrane extraction for trace organic compounds	84
5.1 Introduction	84
5.2 Experimental	85
5.2.1 Chemical and reagent	85
5.2.2 Instrumentation	85
5.2.3 Extractor module	87
5.2.4 Preconcentrator	88
5.2.5 Sample mixture	88
5.2.6 System performance	89
5.2.7 Real sample analysis	90
5.2.7.1 Wastewater sample	90
5.2.7.2 Biosolids sample	90
5.2.7.3 Ground water sample	91
5.3 Results and Discussion	91
5.3.1 Optimum conditions of gas chromatograph	91
5.3.2 Pervaporation	92

Contents (continued)

	Page
5.3.3 Membrane temperature	93
5.3.4 Extraction time	94
5.3.5 Preconcentrator	95
5.3.6 Injector	97
5.3.7 Sample mixture	100
5.3.8 Linearity and limit of detection	101
5.3.9 Stability	102
5.3.10 Real sample analysis	103
5.3.10.1 Wastewater	103
5.3.10.2 Bisolids sample	104
5.3.10.3 Ground water sample	105
5.4 Conclusions	106
CHAPTER 6: High efficiency coating film for VOCs preconcentration device	108
6.1 Introduction	108
6.2 Experimental	110
6.2.1 Materials	110
6.2.2 Instrumentation	110
6.2.3 Standard gas vapor generator	112
6.2.4 Trapping tube preparation	113
6.2.5 Analytical procedure	115
6.2.6 System performance	115
6.2.7 Real sample analysis	116
6.3 Results and Discussion	116
6.3.1 Gas chromatograph optimum conditions	116
6.3.2 Standard gas vapor generator validation	117

Contents (continued)

	Page
6.3.2.1 Calculation of diffusion rate and concentration	117
6.3.2.2 Stability	118
6.3.2.3 Effect of diffusion tube position	119
6.3.3 Optimization of desorption conditions	120
6.3.4 Validation of trapping tube	125
6.3.4.1 Reproducibility	125
6.3.4.2 Stability	126
6.3.5 Performance of trapping tubes	126
6.3.6 Measurements of VOCs in indoor air	129
6.4 Conclusions	131
CHAPTER 7: Bismuth Film Electrode for Tetracycline Analysis in Flow Injection System	133
7.1 Introduction	133
7.2 Experimental	135
7.2.1 Chemical and reagents	135
7.2.2 Preparation of BiFE	135
7.2.3 Flow injection system for tetracycline	136
7.2.4 System performances	137
7.3 Results and discussion	138
7.3.1 Reduction and oxidation of Bi(III) onto GCE	138
7.3.2 Optimization of BiFE preparation	139
7.3.3 Working potential of BiFE	141
7.3.4 Reduction potential of tetracycline	142
7.3.5 Optimization of flow injection system	143
7.3.5.1 Detection potential	143
7.3.5.2 Carrier flow rate	144

Contents (continued)

	Page
7.3.5.3 Sample volume	145
7.3.5.4 Supporting solution concentration	146
7.3.5.5 Concentration and pH of borate buffer	146
7.3.6 System performance	149
7.3.7 Stability of bismuth film	151
7.3.8 Reproducibility of bismuth preparation	152
7.3.9 Real sample analysis	153
7.4 Conclusions	154
 CHAPTER 8: Alloy Nanowires Barcodes	 156
8.1 Introduction	156
8.2 Experimental	157
8.2.1 Apparatus	157
8.2.2 Materials	158
8.2.3 Preparation of multi-segmented (stripe) alloy nanowires barcodes	159
8.2.4 Optical barcode images processing of multi-segment alloy nanowires	161
8.2.5 Preparation of single-segment alloy nanowires	162
8.2.6 Analytical procedure of single-segment alloy nanowires	164
8.3 Results and discussion	164
8.3.1 Multi-segment alloy nanowires	164
8.3.1.1 Multi-segment alloy nanowires synthesis	164
8.3.1.2 Alloy composition	165
8.3.1.3 Bar coding signature generation	166
8.3.2 Characteristic of single-segment alloy nanowires	169

Contents (continued)

	Page
8.3.2.1 Scanning electron micrographs of alloy nanowires	169
8.3.2.2 Non-destructive readout	170
8.3.2.3 Two and three dimension responses	171
8.3.2.4 Generation of barcode signature	173
8.3.2.5 Single-segment alloy nanowires validations	176
8.3.2.5.1 Reproducibility	176
8.3.2.5.2 Uniformity	176
8.3.2.5.3 Kevex and hand-held XRF readout	178
8.3.2.5.4 Limit of detection	180
8.3.2.5.5 Tracking applications	183
8.4 Conclusions	186
CHAPTER 9: Shape-tailored porous gold nanowires	187
9.1 Introduction	187
9.2 Experimental	188
9.2.1 Chemical and reagents	188
9.2.2 Apparatus	188
9.2.3 Preparation of nanowires	189
9.2.3.1 Porous gold nanowires	189
9.2.3.2 Composite porous gold/polymer nanowires	190
9.3 Results and discussion	192
9.3.1 Porous gold nanowires	192
9.3.1.1 Porous gold nanowires synthesis	192
9.3.1.2 Diameter characterization	193
9.3.1.3 Shape-tailored porous gold nanowires	195
9.3.2 Metal/Polymer composite material	197
9.4 Conclusions	198

Contents (continued)

	Page
CHAPTER 10: Conclusions	200
References	205
Appendices	246
Appendix A	247
Appendix B	252
Appendix C	258
Appendix D	265
Vitae	270

List of Tables

Table	Page
2.1 Summarization of membrane extraction techniques	22
5.1 Optimum conditions of the gas chromatograph; 5 mL of standard solution mixture was used, <i>i.e.</i> , 1 mg L ⁻¹ MTBE, 500 mg L ⁻¹ methanol, 500 mg L ⁻¹ ethanol, 500 mg L ⁻¹ 1-propanol and 20 mg L ⁻¹ MIBK.	92
5.2 Optimum conditions of the preconcentrator and injector system	99
5.3 Linear dynamic range and limit of detection of GIME system	102
5.4 A: The percentages of relative recoveries of spike sample from Songklanakarin Hospital wastewater pond.	104
B: The percentages of relative recoveries of spike sample from garage wastewater.	104
5.5 The percentages of relative recoveries of spike biosolids sample.	105
5.6 The percentages of relative recoveries of spike ground water sample.	106
6.1 Optimum gas chromatographic conditions for DCM, DCE, TCM, TCE and BTX	117
6.2 Effective values used for diffusion rate calculation (equation 6.6) <i>X</i> is the diffusion coefficient obtained from the experiments, ρ is the density of analyte and <i>A</i> is the cross sectional area of the diffusion tube	118
6.3 Performances of sol-gel polyethylene glycol (sol-gel PEG) and sol-gel polyethylene glycol/multiwall carbon nanotubes (sol-gel PEG/MWCNTs) trapping tubes compare to Carbopack B for determination of selected VOCs in indoor air	128
6.4 Concentration of toluene detected in indoor air from 5 replications using 3 types of trapping tube	130

List of Tables (Continued)

Table	Page
6.5 Concentration of xylene detected in indoor air from 5 replications using 3 types of trapping tube	130
6.6 Two-way ANOVA of toluene	131
6.7 Two-way ANOVA of xylene	131
7.1 The optimum conditions for GCE and BiFE in flow injection system 3	148
7.2 Statistical values for the comparison between the slopes of the regression line from three different BiFE using two-way ANOVA by R software.	153
7.3 % relative recovery of spiked samples	154
8.1 Percentage of atomic silver at difference deposition potential using 85/15 of Au/Ag	165
8.2 Reproducibility of 6 sections from one membrane template	176
8.3 Normalized peak intensity of Co, Ni and Cu showing peak ratios of the fluorescence signature.	177
8.4 The intensity of background noise measurement from 20 blanks	182
9.1 The percentage of reduction of normalization diameter at different deposition potential	194
10.1 Comparison of the analytical features of 4 different sample preparation for VOCs determination	201
10.2 Comparison of the analytical features of 4 different adsorption tubes for VOCs determination	202
10.3 Comparison of the analytical features of 4 different methods for tetracycline analysis	203

List of Figures

Figure	Page
2.1 Schematic representation of (A) Headspace-single drop microextraction (HS-SDME) (B) Liquid phase microextraction (LPME) by immersion of organic solvent into a sample solution	8
2.2 Schematic representation of the SDME procedure	9
2.3 Liquid phase microextraction (LPME) using a hollow fibre (HF) Membrane	10
2.4 Dispersive liquid-liquid microextraction (DLLME)	11
2.5 Mode of SPME operation (A) Direct extraction by immersion SPME into sample (B) Headspace-Solid phase microextraction (HS-SPME) (C) Membrane-protected SPME for direct extraction	12
2.6 Experimental set-up of sequential SBSE	14
2.7 Schematic diagram of solid phase dynamic extraction	15
2.8 Membrane extraction construction (A) Membrane unit with 1 ml channel volume (B) Membrane unit with 10 μ l channel volume (C) Hollow fiber membrane unit	16
2.9 Schematic diagram illustrate extraction technique using supported liquid membrane (SLM)	17
2.10 Schematic diagram illustrate extraction technique using Microporous membrane liquid-liquid extraction (MMLLE)	18
2.11 Membrane pervaporation process	19
2.12 Membrane extraction with sorbent interfaces (MESI) where the sample flows inside the hollow fiber membrane	20
2.13 Membrane extraction with sorbent interfaces (MESI) where the sample flow inside the hollow fiber membrane	21
2.14 Purge and trap system	25
2.15 Chromatographic techniques used for the determination of the specific breakthrough/retention volume (A) Frontal technique	28

List of Figures (Continued)

Figure	Page
(B) Elution technique	
2.16 Relationship of breakthrough to sample loss in a typical two-section sample tube sampling an atmosphere of constant sorbate concentration, showing the difference between 5% breakthrough volume and 5% sample loss to the back-up section. Actual shape of the curves will vary with sorbent, sorbate, concentration, temperature and the presence of other sorbates	29
2.17 Schematic diagram of membrane inlet mass spectrometry (MIMS) (A) the extracted analyte from hollow fiber membrane module directly flow MS and (B) the extracted analyte from hollow fiber membrane module flow through the cryotrap to preconcentrate before carrying to MS	32
2.18 Schematic diagram of membrane extraction with a sorbent interface (MESI), flat membrane was used in this work	33
3.1 Cyclic voltammograms for quantitative analysis, (A) CoPC/CPE (solid line) and the CPE (broken line) of 1.0 mmol L^{-1} solutions of ephedrine in 0.10 mol L^{-1} NaOH. Scan rate: 100 mV s^{-1} (B) Square wave voltammograms for 4 ppm TNT analyte only, 4 ppm DNT analyte only, and for a 4 ppm DNT+ 4 ppm TNT mixture I: The working electrode was bare gold, II: The working electrode was gold modified with an MCP monolayer reversible redox couple peak process	37
3.3 Modification of CNTs via covalent bonding (A) The redox reaction for 9, 10-anthraquinone covalently attached to MWCNTs (B) The proposed reduction mechanism for nitrobenzene covalently attached to MWCNTs	42

List of Figures (Continued)

Figure	Page
3.4 SEM images of composite CNTs modified electrode (A) Ppy-MWCNTs (B) Pt-Pb/MWCNT	43
3.5 SEM image of nanowires modified electrodes (A) Gold nanoparticles (B) Pd nanowire arrays (PdNWAs)	45
3.6 Repetitive cyclic voltammograms of 2.0×10^{-2} M DBA in 0.1 M NaCl solution. Initial potential: -1.5 V; terminal potential: +2.5 V; scan rate: 100 mV s^{-1}	46
3.7 Polypyrrole film deposited onto microporous polycarbonate membranes to form conducting polymer organic electrode	47
3.8 (A) Capillary electrophoresis chip for carbon fiber microelectrode assembly. B. Layout of the chip (B) Scheme of the working area of the device	49
3.9 Screen printed electrode (SPE) (A) SPE coated with nafion layer for cholinesterase biosensor design (B) SEM image of multiwall carbon nanotubes (CNTs) modified screen-printed (SP) electrochemical sensors (C) SEM of polyaniline polymer nanoparticle films modified on screen printed electrode	50
3.10 The comparison between the amperometric responses to hydrazine injections using (A) Rhodium- modified carbon fiber microelectrodes (Rh) (B) Rhodium-modified glassy carbon electrode in flow injection system	52
4.1 Schematic diagram of photolithography, (A) Photosensitive material was exposed to the radiation resulting changing its property (B) Positive material was used as template for nanowires synthesis	51
4.2 Schematic illustrate of micelle soft template used for nanowires synthesis (a) spherical micelles for spherical	58

List of Figures (Continued)

Figure	Page
particles (b) cylindrical micelle for rod-shape nanowires	
4.3 Track-etch process for nanoporous membranes	59
A) heavy-charged particle pass through substrate	
B) Cylindrical pore in a mica C) Top view of nanomembrane	
4.4 Electron micrograph of polycarbonate template membrane	60
with 1 μm diameter pores	
4.5 Electron micrograph of alumina membrane with 200 nm	61
diameter pore	
4.6 Schematic diagram of a porous anodic alumina film on	62
aluminum, showing honeycomb pores structure in cross-section.	
4.7 Schematic diagram showing a reduction (a) and oxidation	64
(b) process of a species A in solution. MO: molecular orbital.	
4.8 Experimental set up of (A) the template-based assist	65
electrodeposition technique (B) Current-time for the	
electrodeposition of Ni nanowires into a polycarbonate	
membrane with 60 nm diameter pores at -1.0 V	
4.9 Images of metal nanowires using electrodeposition technique	67
(A) TEM image of Bi nanowire (B) SEM image of free	
standing Pd nanowires (C) SEM image of porous gold nanowires	
(D) TEM image of Fe/Au nanowires (E) TEM image of the Fe-Pd	
alloy nanowires (F) SEM image of Ni-Fe-Co alloy nanowires	
4.10 SEM image of (A) SnO_2 nanowires (B) Ag_2Se nanowire arrays	69
4.11 SEM image of conducting polymer nanowires prepared by	70
electrochemical technique: (A) Polypyrrole (B) Polyaniline and	
polypyrrole (C) Poly(methyl pyrrole) nanowires	
4.12 SEM image of composite nanowires (A) Polyaniline deposited	71
inside alumina membrane and work as a second-order template,	
inset show Bi_2Te_3 nanowires surrounded by polyaniline	

List of Figures (Continued)

Figure	Page
(B) Polypyrrole/porous gold nanowires	
(C) Nickel/3,4-ethylene-dioxythiophene nanowires.	
4.13 Schematic diagram of atomic force microscope (AFM)	74
4.14 Barcode nanowires for bioanalysis (A) reflectivity can be used to identify and quantify particles (B) Reflectivity and fluorescence intensity is performed for each particle	76
4.15 Schematic diagram illustrated the encoding process of strip nanowires for biological detection. A) Analogy between a conventional barcode and a metallic stripe encoded nanowire. B) Schematic of the sandwich immunoassay performed on a nanowire. C) Reflectance and fluorescence readout of the nanowires	78
4.16 Optical images of different strip pattern nanowires prepared from sequential electrodeposition of gold and silver	79
4.17 Alloy nanowires barcodes prepared from chemically electrodeposition following with SWV measurement. SEM image shows alloy nanowires prepared	80
4.18 Au-nanoparticle/polypyrrole composite nanowires modified glassy carbon electrode for hydrazine and hydroxylamine detection	81
4.19 (A) Electrochemical test set up (B) Cross-sectional schematic of the test cell, with nanowires aligned on the platinum (C) Micro-fluidic platform in silicon with electrodes/gold nanowires and SU-8 chamber. (D) Platinum "assembly" lines for nanowire alignment. (E) Hard-baked SU-8 micro-fluidic chamber	82
5.1 Schematic diagram of the gas injection membrane extraction	86

List of Figures (Continued)

Figure	Page
(GIME) system for trace organic compounds analysis	
5.2 Pervaporation process through the hollow fiber membrane	87
5.3 Effect of membrane temperature to the response of the analytes	94
5.4 Effect of extraction time to the response of the analytes; 0.8 mL min ⁻¹ sample flow rate and 2 mL min ⁻¹ of stripping gas	95
5.5 Effect of desorption voltage to the response of the analytes; 0.8 mL min ⁻¹ sample flow rate and 2 mL min ⁻¹ of stripping gas	96
5.6 Effect of desorption time to the response of the analytes; 0.8 mL min ⁻¹ sample flow rate and 2 mL min ⁻¹ of stripping gas	97
5.7 Effect of loading time to the response of the analytes; 0.8 mL min ⁻¹ sample flow rate and 2 mL min ⁻¹ of stripping gas	98
5.8 Effect of injection time to the response of the analytes; 0.8 mL min ⁻¹ sample flow rate and 2 mL min ⁻¹ of stripping gas	99
5.9 Chromatograms of an on-line system at the optimum conditions for trace organic compounds analysis. A 5-mL of 1 mg L ⁻¹ MTBE, 20 mg L ⁻¹ MIBK, 500 mg L ⁻¹ methanol, ethanol and 1-propanol were used.	100
5.10 Effect of 1 mg L ⁻¹ MTBE and 20 mg L ⁻¹ MIBK to the response of (A) 100- 700 mg L ⁻¹ Ethanol (B) 500-800 mg L ⁻¹ Methanol	101
5.11 Stability of the extraction and preconcentration systems	103
6.1 Schematic diagram showing (A) the loading position of the 10-port valve where the analytes generated by a standard gas generator were flowed and adsorbed inside the trapping tube held in the 10-port valve and (B) the injection position where the analytes were thermally desorbed and injected into a gas chromatograph. Adsorption and desorption time was controlled by a custom-built	111

List of Figures (Continued)

Figure	Page
heating box and timer	
6.2 Coating of sol-gel PEG inside silico-steel tube using N ₂ gas to purge the sol solution through the silico-steel tube	114
6.3 Stability of standard gases vapor from 35 injections	119
6.4 Responses obtained from changing the position of standard solutions in the diffusion tube. Position 1 is DCM, DCE, TCM, TCE and BTX, the reverse of the position 1 is XTB, TCE, TCM, DCE and DCM. The percentage differences of the response between position 1 and the reverse of position 1 were shown above the columns	120
6.5 Delayed time of injection valve between switching and before analytes were thermally desorbed	121
6.6 Effect of injection time to the response of analyte	122
6.7 Effect of heating voltage to the response of analyte using (A) sol-gel PEG (B) Sol-gel PEG/MWCNTs (C) Carbopack B	123
6.8 Effect of heating time to the response of analyte using (A) sol-gel PEG (B) Sol-gel PEG/MWCNTs (C) Carbopack B	124
6.9 Chromatogram obtained from MWCNTs/PEG trapping tube injection where 1: TCE ($t_R = 3.4$ min), 2: DCM ($t_R = 3.9$ min), 3: Benzene ($t_R = 4.2$ min), 4: TCM ($t_R = 5.2$ min), 5: Toluene ($t_R = 5.7$ min), 6: DCE ($t_R = 6.0$ min) and 7: Xylene ($t_R = 7.3$ min).	125
6.10 Linear dynamic range and sensitivity of (A) DCM (B) DCE (C) TCM (D) TCE (E) Benzene (F) Toluene (G) Xylene	127
7.1 Schematic diagram of the flow injection system for tetracycline detection	137
7.2 Cyclic voltammogram of 1.5 mM Bi(III) on GCE using 1.0 M, pH 4.5 sodium acetate as a running buffer, scan rate 0.1 V s ⁻¹	138

List of Figures (Continued)

Figure	Page
7.3 The relationship between anodic stripping peak current of Bi(III) and concentration of Bi(III). 0.1 M, pH 4.5 sodium acetate buffer was used for deposition and stripping bismuth film	139
7.4 Effect of deposition potential of 1.5 mM Bi(III) onto GCE. 0.1 M, pH 4.5 sodium acetate buffer was used for deposition and stripping bismuth film	140
7.5 Effect of deposition time of 1.5 mM Bi(III) onto GCE. 0.1 M, pH 4.5 sodium acetate buffer was used for deposition and stripping bismuth film	141
7.6 Cyclic voltammograms of blank (25.0 mM borate buffer pH 8.7) and 1.0 mM of tetracycline in 25.0 mM borate buffer pH 8.7 containing 0.1 M KCl on GCE and BiFE at a scan rate of 50 mV s ⁻¹	143
7.7 Effect of detection potential on the response of 1.0 mM tetracycline using (A) BiFE and (B) GCE. System contains 25.0 mM borate buffer solution, 200 µL of sample volume	144
7.8 Effect of carrier solution flow rate on the response to 200 µL of 1.0 mM tetracycline in 25.0 mM borate buffer, detection potential -1.3 V	145
7.9 Effect of sample volume on the response of 1.0 mM tetracycline in 25.0 mM borate buffer, detection potential -1.3 V	146
7.10 Effect of buffer concentration on the response to 200 µL of 1.0 mM tetracycline in flow injection system; borate buffer solution, 0.2 mL min ⁻¹ flow rate and -1.3 V detection potential	147
7.11 Effect of pH of buffer on the response to 200 µL of 1.0 mM tetracycline in flow injection system; 25.0 mM borate buffer solution, 0.2 mL min ⁻¹ flow rate and -1.3 V detection potential	148

List of Figures (Continued)

Figure	Page
7.12 The current responses of tetracycline obtained from GCE and BiFE at 1.0, 2.0, 3.0, 4.0 mM tetracycline at different concentration; 25.0 mM borate buffer pH 8.70 containing 0.1 M KCl, applied potential -1.3 V	149
7.13 Current responses of GCE and BiFE to tetracycline at different concentration in the flow injection system with 25.0 mM borate buffer pH 8.70 containing 0.1 M KCl	150
7.14 Stability of the BiFE by injecting 2.0 mM of tetracycline for 50 times at the optimum conditions of flow injection system	151
7.15 The reproducibility of the responses from analysis of 1.0, 4.0 and 6.0 mM tetracycline using three new film modified electrodes	153
8.1 Alumina membrane template (A) show a pore structure of the membrane (B) Gold was sputtered on the branch side of the membrane (C) Membrane was placed at the bottom of the plating cell	159
8.2 Preparation of ternary alloy nanowires using alumina membrane as a porous template which have pore size 200 nm (A) Deposited gold into the branch (B) Deposited gold/silver at -1.20 V (C) Deposited gold/silver at -0.50 V (D) Deposited gold/silver at -0.85 V (E) Membrane was polished to remove sputtered metal and branch side of the template and (F) Dissolve membrane template to release alloy nanowires from template	161
8.3 Preparation of ternary alloy nanowires using alumina membrane as a porous template (A) Deposited silver into the branch at -0.9 V for 2.0 C (B) Deposited gold at -0.9 V for 1.0 C (C) Alloy nanowires was deposited at -1.4 V for 15.0 C and (D) Membrane was polished to remove sputtered metal and branch side of the template	163

List of Figures (Continued)

Figure	Page
8.4 (A) The relationship between normalized reflectance intensity and deposition potential (B) A reflectance microscopy image of a multi-segment nanowire containing three alloy compositions (deposited over the -0.50 to -1.20 V range) and pure gold and silver segments (at the ends, deposited at -0.90 V)	166
8.5 Reflectance images (top) and intensity lines (bottom) for different multisegment alloy nanowire barcodes prepared from an 85/15 (v/v) Au/Ag plating solution. The sequences of the deposition potentials for each nanowire image are (from left to right) (A) -1.20, -0.50, -1.20, -0.85, -0.50 and -1.20 V (B) -0.50, -1.20, -0.85, -0.50, -1.20, and -0.5 V (C) -0.50, -1.20, -0.85, -0.50, -0.85, -1.20 and -0.50 V	167
8.6 (A) SEM and (B) optical reflectance images of multi-segment alloy nanobarcode clearly show different color of each segment when changing plating potential. In optical microscopy technique, the most reflective is at -0.5 V (bright) and the least less reflective is -1.2 V (dark) while -0.85 V provides intermediate color	168
8.7 Scanning electron micrographs of alloy nanowires deposited at -1.4 V for 15.0 C. (A) Alloy nanowires embedded in alumina membrane template and (B) after dissolve membrane template	169
8.8 XRF spectrum of alloy nanowires showing peak energies of K_{α} and K_{β} photons of Co, Ni and Cu (A) Co/Ni/Cu at the concentration of 30/50/5 mg L ⁻¹ (B) Co/Ni/Cu at the concentration of 30/50/10 mg L ⁻¹	171
8.9 Comparison of X-ray fluorescence readout of alloy nanowires obtained before (A) and after (B) dissolving the membrane template. The nanowires were prepared by electrodeposition at -1.4 V for a	172

List of Figures (Continued)

Figure	Page
<p>total charge of 15.0 C. The nanowires were prepared using plating solutions with different Co, Ni and Cu concentrations (in g L⁻¹): (a) 30Co/40Ni/10Cu (b) 30Co/60Ni/10Cu (c) 30Co/ 90Ni/10Cu (d) 30Co/120Ni/10Cu</p>	
8.10 X-ray fluorescence of single-segment alloy nanowires prepared by changing concentration of one metals (Co (A), Ni (B) and Cu (C)) while keeping the level of others constant. (A) Changing the Co concentration (a-d: 10, 20, 30, 40 g L ⁻¹) with Ni and Cu at 50 and 10 g L ⁻¹ , respectively. (B) Changing the Ni concentration (a-d: 40, 60, 90, 120 g L ⁻¹) with Co and Cu at 30 and 10 g L ⁻¹ . (C) Changing the Cu concentration (a-d: 5, 10, 15 and 20 g L ⁻¹) with Co and Ni at 30 and 50 g L ⁻¹ . All alloy nanowires were electrodeposited at a potential of -1.4 V using a total charge of 15.0 C.	174
8.11 Relationship between concentration and normalized intensity. (A) Changing Co concentration (10, 20, 30, 40 g L ⁻¹) with Ni and Cu at 50 and 10 g L ⁻¹ , respectively. (B) Changing Ni concentration (40, 60, 90, 120 g L ⁻¹) with Co and Cu at 30 and 10 g L ⁻¹ . (C) Changing Cu concentration (5, 10, 15 and 20 g L ⁻¹) with Co and Ni at 30 and 50 g L ⁻¹ . All alloy nanowires were electrodeposited at a potential of -1.4 V using a total charge of 15.0 C	175
8.12 XRF readout of Co-Ni-Cu alloy nanowires of different lengths, prepared by increasing deposition charges (total charge) from 2.0 to 15.0 C (A) Linear relationship of deposition charge and peak intensity: (B) XRF signal obtained from various deposition charge 2.0 C (a), 5.0 C (b), 10.0 C (c), and 15.0 C (d) and a plating solution containing 5.0 g L ⁻¹ of the corresponding metal salts	178
8.13 Non-destructive XRF readout of barcoded alloy nanowires. Barcoded	179

List of Figures (Continued)

Figure	Page
nanowires (shown in the SEM photomicrograph of inset a) are embedded in packaging materials of a commercial product and detected with a hand-held XRF analyzer (b). The resulting XRF signature (c) is used for the product identification	
8.14 Comparison of the nanowire XRF readout obtained with a handheld XRF (Niton) unit (A) and a laboratory-based (Kevex XRF) instrument (B). Alloy nanowires (in membrane) prepared using plating solutions with the following Co/Ni/Cu concentration ratios: (a) 30/45/10, (b) 30/50/10, (c) 30/65/10	180
8.15 Calibration curve of single-segment alloy nanowires dried on the paper with different amount of nanowires	181
8.16 XRF signatures of alloy nanowires incorporated within inks or plastics. (A) Nanowire XRF signatures recorded with the nanowires (i) embedded in the membrane template or (ii) dispersed within an ink dispensed on a white printing paper. The nanowires were prepared using a plating solution containing 30-, 50-, 10- g L ⁻¹ of the Co, Ni and Cu salts. (B) Nanowire XRF signatures for (i) nanowires embedded in the membrane template or (ii) nanowires embedded between fused plastic (COC) sheets. The nanowires were prepared using a plating solution containing 30-, 90-, 10- g L ⁻¹ of the Co, Ni and Cu salts	184
8.17 Detection of increasing amounts of multi-metal nanowires that are imbedded between COC plastic sheets. The above was performed with 30-90-10 (g L ⁻¹) multi-metal nanowires using the Kevex XRF. (A) XRF signature at various amount of nanowires (a) Blank Plastic (b) 0.5 mg (c) 1.5 mg (d) 3.0 mg of multi-metal nanowires (B) linear relationship of amount of nanowires embedded in COC plastic sheet	185

List of Figures (Continued)

Figure		Page
	and counts	
9.1	Scheme illustrating the template-assisted electrochemical preparation of the porous gold nanowires: (a) Sputtering gold on alumina membrane; (b) copper deposition for a total charge of 10 C; (c) Au deposition (d) 9/1 (e) 8.5/21.5 (f) 8/2 (g) 7.5/2.5, all deposition steps were performed using a deposition potential of -0.9 V (vs. Ag/AgCl) for a charge of 0.2 C each; (h) dealloy the silver component using a 35% HNO ₃ solution; (i) removal of the sputtered gold layer (j) removal of copper layer using 0.1 M CuCl ₂ with 20% HCl; (k) dissolution of the membrane template	190
9.2	Scheme illustrating the electrochemical preparation of the composite porous gold/polymer nanowires: (a) Sputtering gold on alumina membrane; (b) copper deposition for a total charge of 10 C; (c) Au deposition for a total charge of 1 C (d) 1.0 mL of silver plating solution was added into gold plating solution (e) 0.5 mL of silver plating solution was added into plating solution (f) 0.5 mL of silver plating solution was added into plating solution (g) dealloy the silver component using a 35% HNO ₃ solution; (h) PPy was electropolymerized for 0.5 C (i) removal of the sputtered gold layer and removal of copper layer using 0.1 M CuCl ₂ with 20% HCl; (j) dissolution of the membrane template	192
9.3	Diameter characterization (A) Normalized diameters of asymmetric porous gold nanowires at various plating composition (Au/Ag) and deposition potentials of (a) -1.1 V; (b) -1.0 V, and (c) -0.9 V using plating solution ratios 10/0, 9/1, 8/2, 7/3 and 6/4 at each deposition potential. (B) SEM image of a porous step-cone created by changing the potential from -1.1 to -0.9 V while keeping the alloy plating	194

List of Figures (Continued)

Figure		Page
	solution ratio constant at 7/3 (Au/Ag)	
9.4	SEM and TEM images of multisegment asymmetric porous gold nanowires prepared at a deposition potential -0.9 V and using plating solutions of different gold/silver composition ratios. SEM (A) and TEM (B) images of the porous step-cone nanostructure prepared by plating sequentially alloy segments from plating solutions with gold/silver ratios of 10/0, 9/1, 8.5/1.5/, 8/2, 7.5/2.5 and 7/3. (C) SEM (C) and TEM (D) images of porous nano-barbell nanostructures prepared using plating solutions with gold/silver composition ratios 9/1 and 7/3	196
9.5	SEM and TEM image of asymmetric porous gold/PPy composite (step cone shape) by changing the ratio of the plating solution (Au/Ag ratios of 8.8/12, 8.2/1.8 and 7.8/2.2) while keeping the deposition potential constant at -0.9 V (A) SEM image of porous step cone/PPy composite (B) TEM image of porous step cone/PPy composite and (C) SEM image of nano porous gold/PPy composite wire grown with varying cross-section emulating "barcode" type wire. The five segments after the solid gold are plated from 7/3 Au/Ag alloy plating solution with the following recipe: -1.1 V for 0.3 C, -0.8 V for 0.2 C, -1.1 V for 0.15 C, -0.8 V for 0.15 C, and -1.1 V for 0.2 C all potentials are in reference to Ag/AgCl reference	198

CHAPTER 1

Introduction

1.1 Background and rationale

Sample preparation is an important procedure in analytical techniques. In most cases contaminated compounds are at very low concentration with complicated matrices, making direct analysis by analytical devices not possible. Therefore, cleaning and preconcentrating processes are also necessary (Dettmer and Engewald, 2002). Trends in sample preparation are aiming toward miniaturization, fast detection, green chemistry and on-line analysis system. These lead many researchers to try to develop preconcentration devices which can reduce the sample size, use minimal organic solvent and can directly connect to analysis tools.

Many sample preparation methods such as solid phase extraction (SPE) (Bruzzoniti *et al.*, 2006), solid phase microextraction (SPME) (Bruzzoniti *et al.*, 2006), liquid-phase microextraction (LPME) (Zou *et al.*, 2008) and membrane extraction (ME) (Bishop and Mitra, 2004; Esrafil *et al.*, 2007) can achieve some goals such as being small and use small amounts of organic solvent, however, they still suffer from long extraction times, are off-line systems and require organic solvents. In a move toward green analytical techniques, sample preparation by headspace technique was developed (Knivinen and Johnsson, 1999). This technique can reduce or eliminate the use of organic solvent. However, sometimes its sensitivity is not sufficient for analytical purposes. Techniques that were brought in to help improve sensitivity include single drop microextraction-headspace (SDME-HS) (Gupta *et al.*, 2007) and solid phase microextraction-headspace (SPME-HS) (Knupp *et al.*, 2005). However, they are off-line systems, time-consuming, laborious and still require organic solvent.

To overcome these problems, a number of on-line analysis systems were investigated. For liquid samples one such example is the use of membrane extraction technique (Guo and Mitra, 1998). In this system no organic solvent is

required but it is still time consuming due to the cleaning step of the membrane. For gas samples, adsorption of VOCs on solid adsorbent is a widely used technique and this led to the development of continuous analysis of VOCs in air using “sorbent trapping” (Harper, 2000) and later the development of “microtrap” for methane adsorption in high purity gas (Thammakhet *et al.*, 2005). Since one adsorbent can not trap all volatile organic compounds, in other studies multi-bed adsorbent was introduced. For example, the mixture of Tenax TA and Carbopack B have been used to trap VOCs from C5-C12 (Kuntasal *et al.*, 2005). However, porous polymer adsorbents are still limited by their instability at high temperature and only a few adsorbent can be applied for multi-bed adsorption tubes.

In view of these we are interested in the development of a simple, cost effective and environmental-friendly sample preparation technique using polymers coated on porous membranes coupled with adsorbent tube to extract and preconcentrate organic compounds in liquid samples. In addition, to overcome the limitation of commercial adsorbents, we investigate the preparation of a preconcentration tube by coating it with thin film of polymer incorporated with nanomaterials and used it to preconcentrate organic compounds in gas samples.

Besides chromatography, an alternative technique to detect organic compounds is electrochemical detection. In general, electrochemical techniques can provide fast detection, be cost effective, highly specific (Deo and Wang, 2004) and easily developed into an on-line analysis system (Luque *et al.*, 2007). Electrochemical detection techniques such as amperometry, potentiometry (Chen and Hibbert, 1997), and voltammetry (Vaze and Srivastava, 2007) can be applied with modified electrodes using biological material (Limbut *et al.*, 2006; Park *et al.*, 2006), conducting polymer (Kozlowski and Frackowiak, 2005), carbon nanotubes (Musameh *et al.*, 2005; Wang *et al.*, 2007) and nanoparticles (Jia *et al.*, 2007; Valentini *et al.*, 2007). However, the number of steps required for electrode preparation, electrode stability and analytical conditions are the main limitations of these techniques. In this work we investigated a simple modification of the electrode for electrochemical detection of organic compounds using electrodeposition technique of metal thin film onto the bare electrode.

Another interesting and relatively new research field which can be applied to analytical techniques are nanomaterials such as nanoparticles, nanorods and nanowires. Among these, nanowires based on electrochemical deposition technique have attracted some attention (Nicewarner-Peña *et al.*, 2001; Saedi and Ghorbani, 2005) since they can be used to provide simpler analytical technique. For examples, multisegment of gold and silver nanowires were used for multiplexed bioanalysis (Keating and Natan, 2003), biological barcodes (Walton *et al.*, 2002) and product tracking (Walton *et al.*, 2002; Wang *et al.*, 2003). However, the preparation technique are generally based on sequential deposition of each metal to obtain different segment of metal making it quite complicated and time consuming (Nicewarner-Peña *et al.*, 2001; Saedi and Ghorbani, 2005; Keating and Natan, 2003; Walton *et al.*, 2002; Walton *et al.*, 2002 and Wang *et al.*, 2003). In this study, a simple technique for nanowires preparation and their application will be investigated.

1.2 Objectives

The aim of this study is to investigate some new analytical approaches based on thin film and nanomaterials. This involves on one hand the use of thin film and nanomaterials concepts in sample preparation techniques and electrochemical detection of organic compounds using electrode coated thin films. On the other hand, preparation technique for nanowires is developed to obtain a simple route for versatile nanowires synthesis. To achieve these objectives five research projects were carried out as follows.

1.2.1 Gas injection membrane extraction for trace organic compounds

In this research, hollow fiber membrane coupled to a microtrap was used as an extraction and preconcentration device for on-line analysis of VOCs from water samples. The aim of this study is to use polymer thin film coated on porous membranes to extract the analyte from liquid sample based on pervaporation of analytes vapor. Analytes in carrier gas were then preconcentrated with multi-bed adsorbent, thermally desorped and injected into a gas chromatograph. This system

does not require any organic solvent and there is no complicated sample preparation step. This can prevent the loss of analyte, reducing analysis time and is an environmentally friendly technique.

1.2.2 High efficiency coating film for VOCs preconcentration device

The purpose of this study is to develop a preconcentration device with high thermal stability that can adsorb a wide range of VOCs. In this project, a VOC preconcentration device was developed by coating polymer thin film and polymer coupled with multiwall carbon nanotubes inside silico-steel tubes followed by thermal desorption. The device could be used for on-line analysis of VOCs contaminant in air samples.

1.2.3 Bismuth film electrode for analysis of tetracycline in flow injection system

For this part, a chemically modified electrode based on electrochemical deposition of bismuth thin film onto glassy carbon electrode was investigated. The aim is to use bismuth film modified electrode instead of the highly toxic mercury film. This electrode was applied in a flow injection system for fast and sensitive detection of an antibiotic compound.

1.2.4 Alloy nanowires

In this study, electrochemical synthesis of alloy nanowires using template-assisted electrodeposition technique was proposed. To obtain alloy nanowires, a mixture of metal plating solution was used. Two types of alloy nanowires were synthesized which are Co/Ni/Cu and Ag/Au alloy nanowires and applied as a barcode systems using X-ray fluorescence (XRF) and reflectance as detection principles. It is expected that fast and reliable response could be accomplished.

1.2.5 Shape-tailored porous gold nanowires

A new route for porous gold nanowires preparation was studied via Au/Ag alloy nanowires and chemical etching of electro-active component (Ag) to obtain the porous structure of gold. Due to different composition of gold and silver the diameter of porous gold, different shape of porous gold nanowires could be synthesized. This facilitates an easy, fast and controllable size and shape of nanowires which could be applied to various devices such as nano-hardware, chemical and biological sensors.

1.3 Benefits

Expectations are that the new sample preparation and electrochemical detection approaches involving thin film layer and nanomaterials could become alternative techniques for on-line analysis of organic compounds since they are simple, cost effective and environmental friendly. And as for nanomaterials, it is our hope that the new, simple and fast technique to synthesize versatile nanowires could be obtained.

CHAPTER 2

Sample Preparation Techniques for Volatile Organic Compounds

2.1 Introduction

Volatile organic compounds (VOCs) are organic compounds with a vapor pressure greater than 13.3 Pa at 25 °C and a vapor pressure of at least 10 Pa at 20 °C (Michulec *et al.*, 2005). Environmental and human health problems arise from the volatile organic compounds (VOCs) are on the increase every year (US EPA, 1994; Zogorski, 2006), hence bring up the awareness of VOCs impacts. Generally, VOCs contaminated are at very low concentration *i.e.*, pg L⁻¹ to µg L⁻¹ (Michulec *et al.*, 2005), making it very difficult to directly monitor or detect contaminated VOCs particularly in environmental matrices. Hence appropriate sampling is necessary to separate the target analyte from the matrices. To meet the sensitivity of the analytical instrument, preconcentration techniques are also required. Several conventional and novel techniques have been used to separate and enhance the response of the instrument for VOCs determination. Some of the commonly used techniques for VOCs analysis in liquid and air sample are summarized in this chapter.

2.2 Sample preparation methods for VOCs analysis in liquid sample

The techniques applied for liquid sample is limited due to low concentrations of VOCs and complicated matrix. Therefore, high preconcentration factors are required in the sample preparation technique. In this section, the classical and new sample preparation approaches for liquid sample are reviewed.

2.2.1 Direct aqueous injection (DAI)

Direct injection of an aqueous sample into a chromatographic column can eliminate sample pre-treatment and preconcentration, minimizing losses of

volatile analytes and sample contamination from sample preparation step. However, the main disadvantages are interferences from sample matrices to the obtained responses. In most cases, the stationary phases are non-polar and not compatible with water. For example, direct injection of 2 μL real water sample to gas chromatographic system for volatile organohalogen compounds was reported by Kot-wasik and co-workers (Kot-Wasik *et al.*, 2004) providing a limit of detection between 1 and 50 ng L^{-1} . In another report, Polkowska and co worker (Polkowska, 2004) injected 2-5 μL DAI of volatile organohalogen compounds (cold on column injector) using gas chromatograph coupled with electron capture detector a limit of detection was 50 ng L^{-1} . However, this technique is not suitable for complicated samples.

2.2.2 Liquid-liquid extraction (LLE)

Liquid-liquid extraction (LLE), known as solvent extraction and partitioning, is the separation technique based on different solutes being soluble to two liquids phases which is immiscible. Generally, one phase is hydrophilic (water) and the other is a hydrophobic (organic solvent). However, conventional LLE required a large volume of organic solvent that can cause environmental and human health problems and this has lead to the development of liquid phase microextraction (LPME) or single drop microextraction (SDME) which can reduce the usage of organic solvent from mL to μL and miniaturize the system (Farahani *et al.*, 2008; Hyötyläinen and Riekkola, 2008).

In SDME a microdrop of solvent is hanged from the tip of a microsyringe and then is either exposed to the headspace of the sample called headspace-single drop microextraction (HS-SDME) (Figure 2.1A) (Yamini *et al.*, 2004) or immersed in a sample solution in which it is immiscible (Figure 2.1B) (Farahani *et al.*, 2008). The latter SDME is a simple mode of LPME where analytes are extracted from a stirred aqueous sample into a drop of organic solvent (ca. 1–3 μL) at the tip of a microsyringe. Once the extraction is completed, the solvent drop is retracted into the microsyringe and injected to the chromatographic system for analysis (Figure 2.2) (Farahani *et al.*, 2008). Advantages of this SDME technique are

that a wide range of solvents can be used to extract a wide range of analytes, low solvent consumption and cost and elimination of memory effect. However, its limitation is the drop instability causing the loss of organic drop from the needle tip of the syringe during the extraction and is not suitable for the extraction of highly volatile analytes.

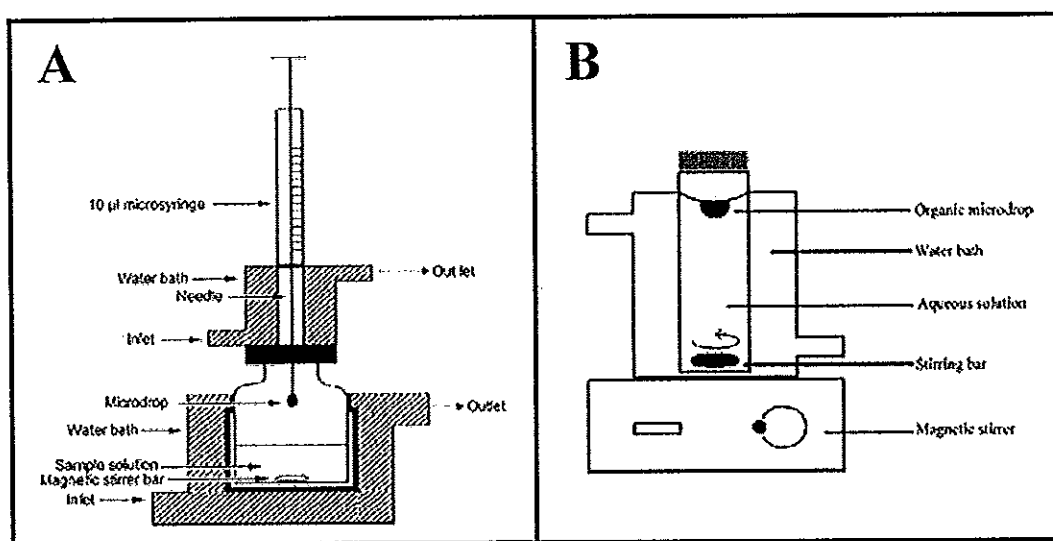


Fig. 2.1 Schematic representation of (A) Headspace-single drop microextraction (HS-SDME) (Yamini *et al.*, 2004) (B) Liquid phase microextraction (LPME) by immersion of organic solvent into a sample solution (Farahani *et al.*, 2008).

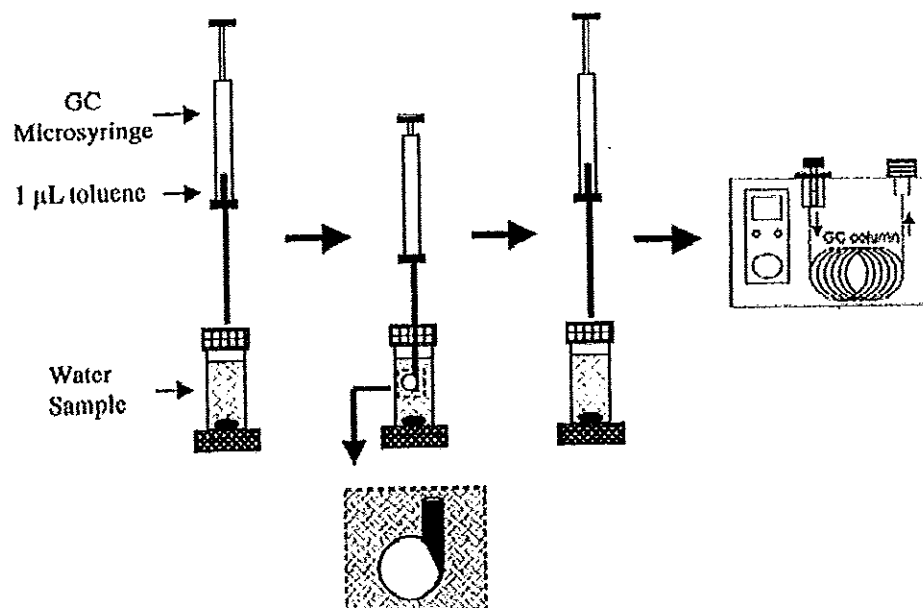


Fig. 2.2 Schematic representation of the SDME procedure (Farahani *et al.*, 2008).

From the limitation of drop stability, LPME using a porous hollow fiber (HF) membrane was developed (Figure 2.3). In this technique, organic solvent is impregnated in the pores and filled the inside of HF membrane therefore the loss of organic solvent can be eliminated and sample matrix is also reduced. After extraction, organic solvent was drawn into the syringe and injected to the analytical system (Pavón *et al.*, 2008).

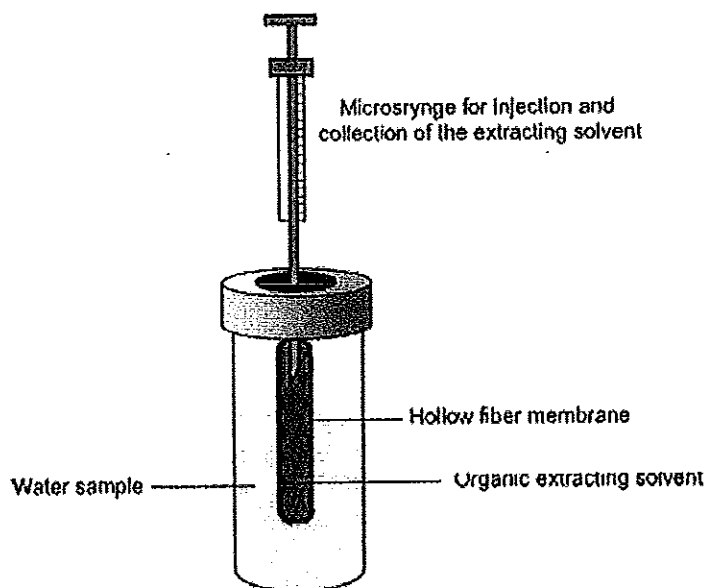


Fig. 2.3 Liquid phase microextraction (LPME) using a hollow fiber (HF) membrane (Pavón *et al.*, 2008).

In addition, a new solvent microextraction technique called dispersive liquid–liquid microextraction (DLLME) has also been developed (Figure 2.4) (Pavón *et al.*, 2008). In this method, an organic solvent, usually hydrophobic, is dispersed into water sample by agitation for a period of time. The analyte is allowed to transfer from water to the organic solvent, following centrifugation to separate between water and organic phase. Organic phase is further injected into analytical system. The advantages of DLLME are the extraction time and efficiency since the small drop of organic solvent is used which much improves the contact surface area with water sample. Therefore, less extraction time and high extraction efficiency than conventional LLE could be accomplished.

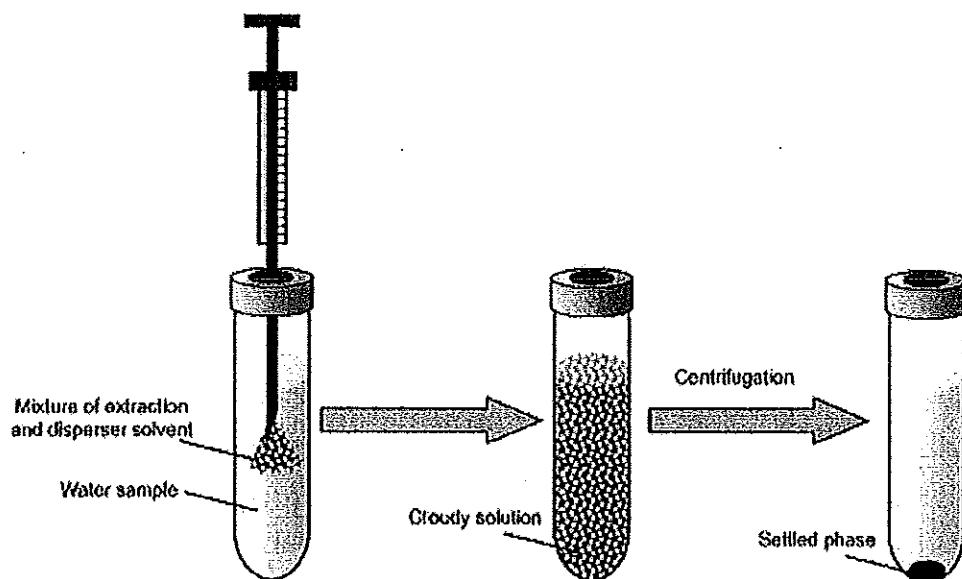


Fig 2.4 Dispersive liquid-liquid microextraction (DLLME) (Pavón *et al.*, 2008).

2.2.3 Enrichment using immersed immobilized sorbents

2.2.3.1 Solid phase extraction (SPE)

Solid phase extraction (SPE) is the liquid-solid separation and was made commercially available by Water Co., in 1978 (Meloan, 1999). SPE has several benefits over conventional LLE, *i.e.*, it is faster and requires less organic solvent for trace organic compounds analysis. SPE is widely use for semi-volatile organic compounds analysis (Santos and Galceran, 2002) but there were only a few reports of SPE applications for VOC preconcentration due of the risk of losing the compounds because of their volatility. For example, SPE with Carbograph 1 packed tube called "Trap" was used to adsorb benzene, toluene, xylene, ethylbenzne and styrene (Mangani *et al.*, 1998). However, in this technique a large sample volume was required making the transportation and storage steps very critical.

2.2.3.2 Solid phase microextraction (SPME)

Solid phase microextraction (SPME) is based on sorptive extraction, *i.e.* the analytes are extracted from either a headspace or from a liquid sample into a polymeric coating material. It is a fast, universal, sensitive, solventless and economical method of sample preparation for analysis by gas chromatography (GC). It has important advantages over conventional extraction techniques *i.e.*, solvent-free, fast, portable and easy to use. For example, ametryn, parathion, prometryn, simetryn and terbutyn was selected for direct adsorption from aqueous samples using a 100 μm poly(dimethylsiloxane) fiber (Eisert and Pawliszyn, 1997). The effectiveness of analyte preconcentration by SPME depends on many parameters such as fiber type, mode of extraction (Figure 2.5), sample volume (stationary phase), temperature and extraction time and salting-out among others (Meloan, 1999; Mitra, 2003). However, fibers are fragile and easily broken. Carry-over of the fiber may also be a problem and it is difficult to eliminate even at high desorption temperature.

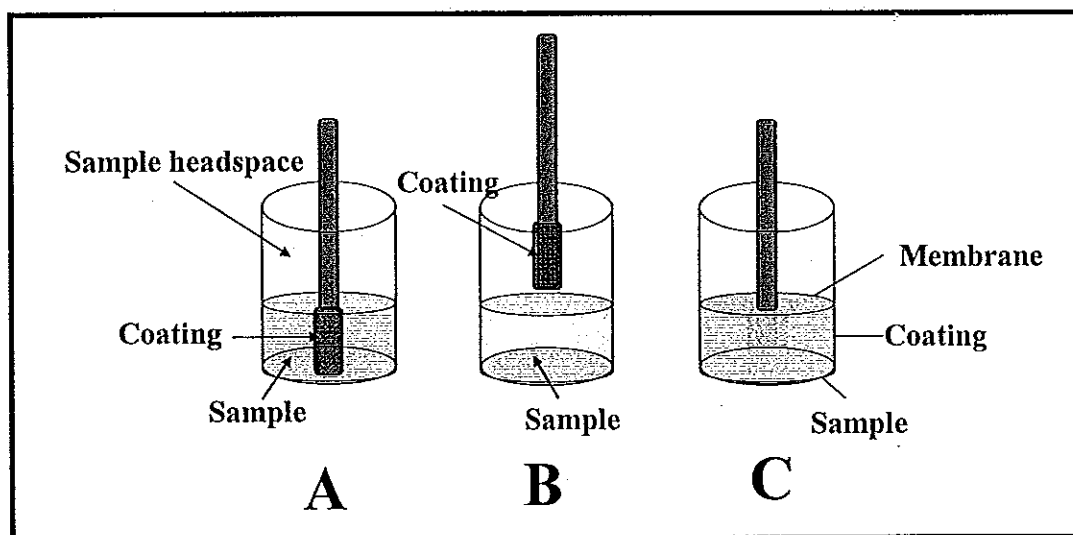


Fig. 2.5 Mode of SPME operation (A) Direct extraction by immersion SPME into sample (B) Headspace-Solid phase microextraction (HS-SPME) (C) Membrane-protected SPME for direct extraction (Mitra, 2003).

2.2.3.3 Stir bar sorptive extraction (SBSE)

Stir bar sorptive extraction (SBSE) was introduced in 1999 to be used as a solventless (environmental friendly) sample preparation technique. SBSE can be used simultaneously for the extraction and enrichment of organic compounds from aqueous matrices. SBSE is based on sorptive extraction where the solutes are extracted from the matrix (liquid or gaseous) into a polymer coating (non-miscible liquid phase) on a magnetic stirring rod. In contrast to the use of adsorbents, analytes interact with active sites on a surface, then migrate into the sorbent phase. Consequently, the total amount of extraction phase of SBSE technique is very important in sorptive extraction technique (David and Sandra, 2007).

Recently, a novel extraction procedure based on stir bar sorptive extraction (SBSE) was developed for sequential extraction as shown in Figure 2.6 (Ochiai *et al.*, 2008). SBSE was performed on a 5-mL sample, first without modifier using one stir bar, then using the same sample after addition of 30% NaCl using a second stir bar to extract the target analyte. The first extraction is mainly targeting solutes with high K_{ow} , the second extraction with modified sample solution (containing 30% NaCl) is targeting solutes with low and medium K_{ow} . Therefore, a wide range of compounds was extracted in this novel idea.

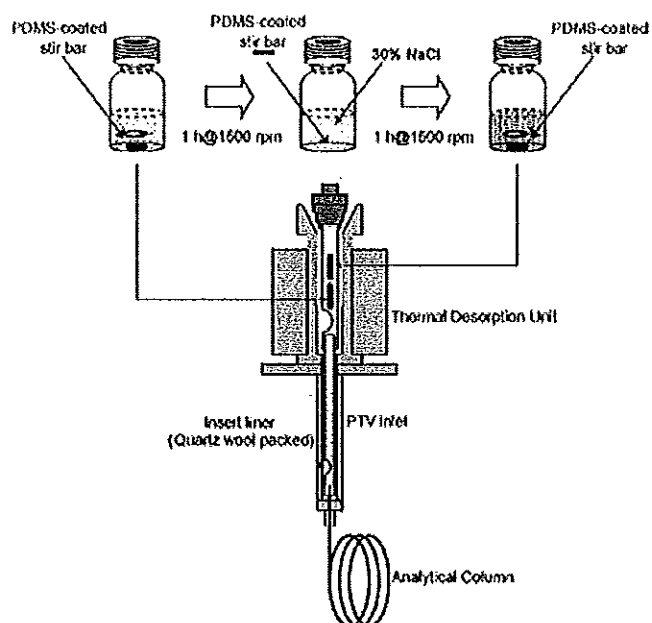


Fig. 2.6 Experimental set-up of sequential SBSE (Ochiai *et al.*, 2008).

2.2.3.4 Solid phase dynamic extraction (SPDE)

Solid phase dynamic extraction (SPDE) a newly released technology developed by CHROMTECH GmbH of Idstein, Germany, is a micro extraction method (Sofia GmbH, 2007). SPDE is based on the usage of injection needle which is coated with a polymeric material inside (Figure 2.7) in contrast to SPME where a coating film is outside the needle. Liquid sample is repeatedly drawn through the needle and pushed out again, with the organic analytes preconcentrated in the polymer film. The needle is transferred to the injection port whereby analyte is thermally desorbed (Sofia GmbH, 2007).

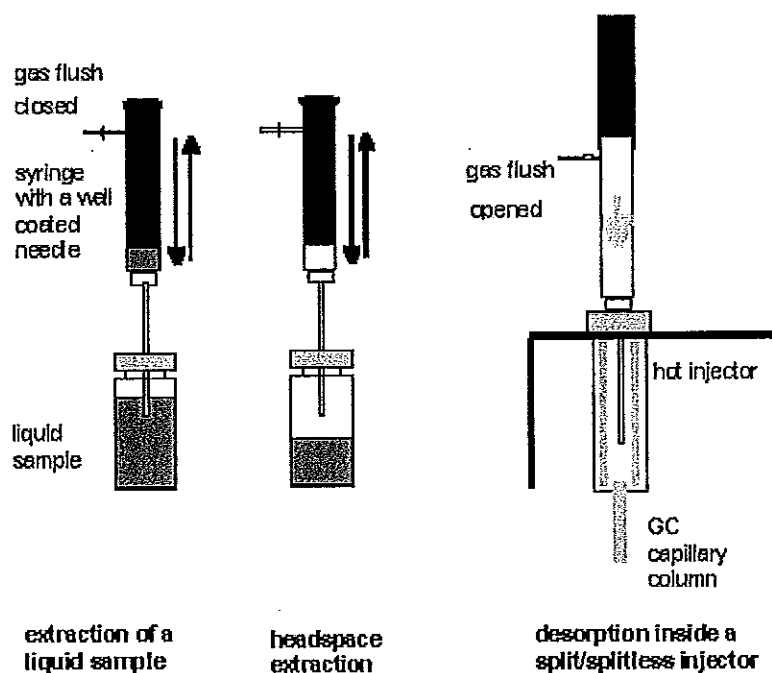


Fig. 2.7 Schematic diagram of solid phase dynamic extraction (Sofia GmbH, 2007)

2.2.4 Membrane extraction

Membrane extraction is a method which offers a high degree of selectivity and enrichment power and uses small amounts of organic solvents. It also provides convenient possibilities for direct and automated connecting with chromatography systems and other analytical instruments (Jönsson and Mathiasson, 2003). The application of membrane extraction as a sample preparation method was introduced by G. Audunsson (Audunsson, 1986). Several membrane extraction techniques were further developed. In this section we focus on the principles and application of non-porous membrane extraction techniques for sample preparation

Typically, membrane uses in extraction technique can be either flat or hollow fiber membrane. Therefore, the membrane holder must be properly constructed to obtain the highest extraction efficiency. Generally, the holder is constructed from two blocks of inert material, the membrane is placed between the two blocks and clamped together where a flow-through channel is formed on each side of the membrane (Figure 2.8) (Jönsson and Mathiasson, 2000).

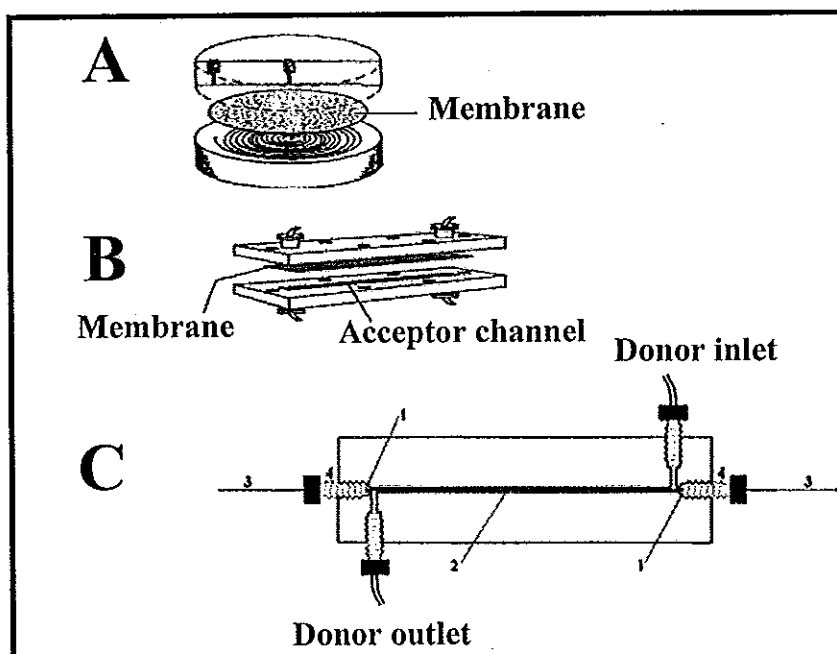


Fig. 2.8 Membrane extraction construction (A) Membrane unit with 1 ml channel volume (B) Membrane unit with 10 μl channel volume (C) Hollow fiber membrane unit (Jönsson and Mathiasson, 2000)

2.2.4.1 Supported liquid membrane (SLM) extraction

Membrane extraction or liquid-liquid membrane extraction is a widely used technique (Liu and Shi). In this technique, a microporous membrane is used to hold organic solvent and separate between sample phase (donor) and acceptor phase (strip). There are three and two phase systems. The three-phase system namely “supported liquid membrane” is aqueous-organic-aqueous where the organic phase is held between the two aqueous phases by a porous hydrophobic supporting membrane with capillary forces. Widely used solvents are long-chain hydrocarbons like n-undecane or kerosene and more polar compounds like dihexyl ether, dioctyl phosphate and others. Analytes are extracted through an organic phase. Figure 2.9 shows the principle of SLM extraction for a basic compound (B), the pH of the sample is adjusted to a value that is high enough for analyte (B) to be uncharged and therefore they can be extracted into the organic membrane phase. The acceptor

channel on the other side of the membrane is filled with acidic buffer. After the analyte diffuses through the membrane, it immediately becomes protonated (B^+) at the membrane–acceptor interface and, therefore, prevented from re-entering the membrane. After the extraction the acceptor phase is transferred to an analytical instrument, either manually or on-line by a flow system.

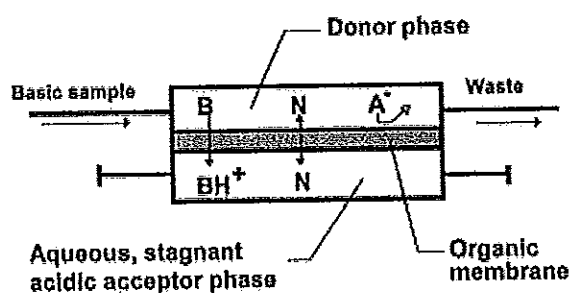


Fig. 2.9 Schematic diagram illustrated extraction technique using supported liquid membrane (SLM) (Jönsson and Mathiasson, 2000).

2.2.4.2 Microporous membrane liquid–liquid extraction (MMLLE)

In a two-phase system, one phase is aqueous and the other is organic. A microporous hydrophobic membrane separates the two phases, the pores of the membrane is filled with organic phase to provide a direct contact through a liquid–liquid interface (Figure 2.10). These systems were called “microporous membrane liquid–liquid extraction” (Jönsson and Mathiasson, 2003). MMLLE is more suitable for highly hydrophobic compounds than SLM since they can not be back extracted into a sample (aqueous) phase as in the SLM technique (Zorita *et al.*, 2007).

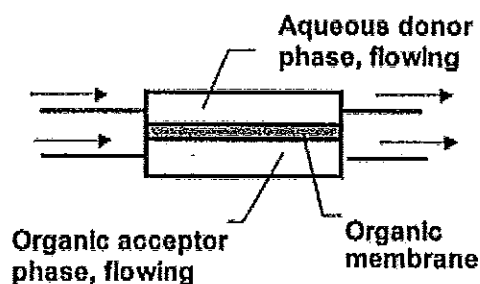


Fig. 2.10 Schematic diagram illustrated extraction technique using Microporous membrane liquid-liquid extraction (MMLLE) (Jönsson and Mathiasson, 2000).

2.2.4.3 Polymeric membrane extraction (PME)

Another type of membrane is the polymeric membrane. In this mode, a polymeric membrane is used to separate sample phase and organic phase. The commonly used membrane material is silicon material. There are possibilities for either aqueous-polymer-aqueous or aqueous-polymer-organic extraction (two-phase and three phase system). In the aqueous-polymer-organic system, organic solvent penetrates through the polymer causing membrane swelling and work similar to MMLLE (Jönsson and Mathiasson, 2000).

Generally, there are three steps in the extraction process, the analyte is first transferred from the bulk sample to the surface of a semipermeable membrane, then diffuses across the membrane and evaporate from the other side (Figure 2.11) (Creaser *et al.*, 1998).

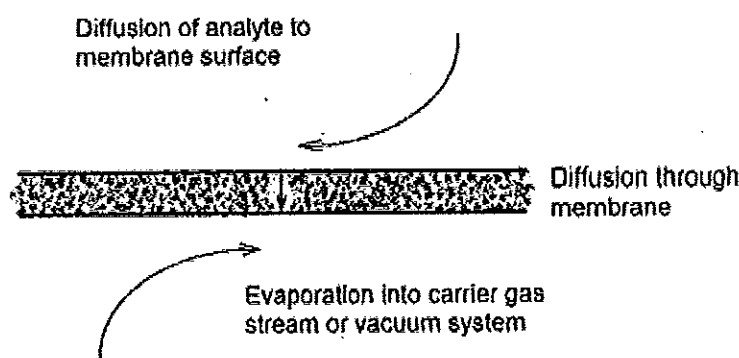


Fig. 2.11 Membrane pervaporation process (Creaser *et al.*, 1998).

Diffusion coefficients (K) of the analyte through the silicone membrane (polymer) can be calculated using Hildebrand solubility parameters as a given in equation 2.1 (Li *et al.*, 2004);

$$\ln K = \frac{\nu_i}{RT} \left((\delta_i - \delta_w)^2 - (\delta_i - \delta_m)^2 \right) - \frac{\nu_i}{\nu_w} \quad (2.1)$$

Where δ_i , δ_m , δ_w are the solubility parameters of organic compound, membrane and water respectively while ν_i and ν_w are the molar volume of organic compound and water (Li *et al.*, 2004).

2.2.4.4 Membrane extraction with sorbent interfaces (MESI)

The last type of membrane extraction that will be described is membrane extraction with sorbent interfaces (MESI). In this mode, it can be used with either gaseous or aqueous samples. The system consists of a membrane module used to extract the analyte from the sample, generally a hollow fiber membrane. Aqueous sample is pumped through the membrane while an inert gas (stripping gas) flowed counter currently with the sample. In this technique, aqueous sample can be flows inside the hollow fiber membrane while stripping gas flows outside (Figure 2.12) (Kou *et al.*, 2001) or in reverse direction where aqueous sample flow outside the hollow fiber membrane while stripping gas flow inside (Figure 2.13) (Matz *et al.*,

1999). Analyte permeate from the liquid phase across the membrane and flow into the gas phase. This module is connected to a sorbent trap where extracted analyte from membrane module is preconcentrated. The adsorbed analyte was thermally desorbed and flow through analytical system (Luo *et al.*, 1997; Segal *et al.*, 2000). Table 1 shows the summary of membrane extraction techniques.

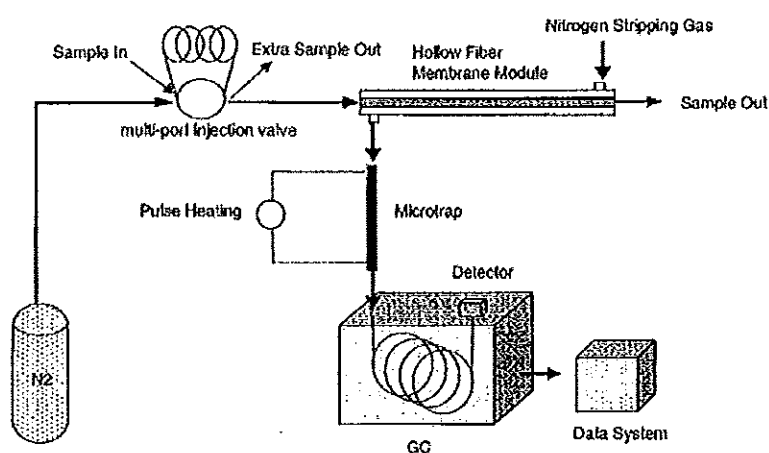


Fig. 2.12 Membrane extraction with sorbent interfaces (MESI) where the sample flows inside the hollow fiber membrane (Kou *et al.*, 2001).

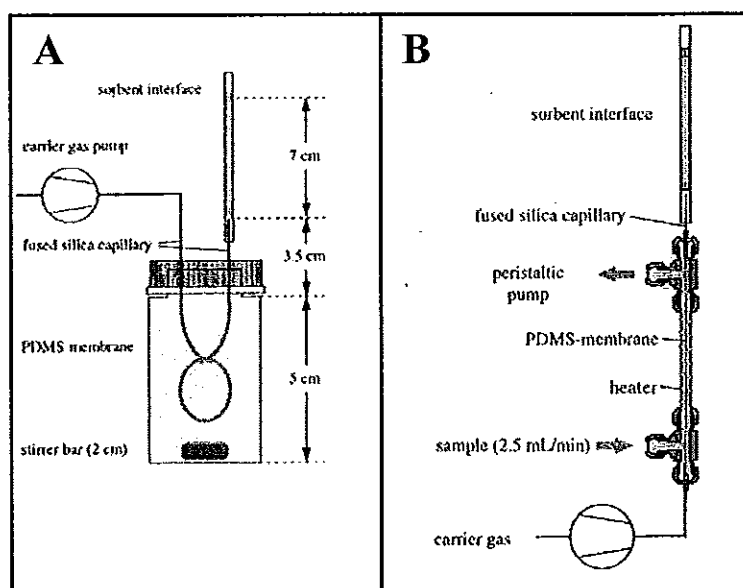


Fig. 2.13 Membrane extraction with sorbent interfaces (MESI) where the sample is outside the hollow fiber membrane (A) Aqueous sample is placed in the vial (B) Aqueous sample flow outside the hollow fiber membrane (Matz *et al.*, 1999).

Table 2.1 Summarization of membrane extraction techniques

Membrane extraction system	Phases (Donor-membrane-acceptor)	References
Supported liquid membrane extraction (SLM)	Aqueous-organic-aqueous	Jönsson and Mathiasson, 2000 and Lui and Shi, article in press
Microporous membrane liquid-liquid extraction (MMLLE)	Aqueous-organic-organic or organic-organic-aqueous	Jönsson and Mathiasson, 2000 and Zorita <i>et al.</i> , 2007
Polymeric membrane extraction (PME)	Aqueous-polymer-aqueous or organic-polymer-aqueous or aqueous-polymer-organic	Creaser <i>et al.</i> , 1998 and Li <i>et al.</i> , 2004
Membrane extraction with sorbent interface (MESI)	Gas-polymer-gas or liquid-polymer-gas	Kou <i>et al.</i> , 2001, Matz <i>et al.</i> , 1999, Luo <i>et al.</i> , 1997 and Segal <i>et al.</i> , 2000

2.2.4.5 Enrichment in membrane extraction

The concentration enrichment factors in SLM are not limited by the partition coefficient. Instead, the trapping conditions in the acceptor phase need to be considered. In the case of SLM extraction of a basic compound, the maximum enrichment factor $E_{e(\max)}$ depends on the acceptor pH_A and the dissociation constant of the analyte (pK_a) (Equation 2.2) (Jönsson and Mathiasson, 2000):

$$\log E_{e(\max)} = pK_a - pH_A \quad (2.2)$$

With an acidic acceptor, it is easy to predict large values for the maximum enrichment factor of strong bases. For example, the maximum enrichment factor for aniline derivatives with $pH_A = 1$. For aniline itself with $pK_a = 4.6$, this leads to a maximum enrichment factor of about 4000 times (Jönsson and Mathiasson, 2000).

Extraction for all membrane extraction techniques is usually evaluated in terms of extraction efficiency (E), which is the fraction of analyte that is collected in the acceptor (Jönsson and Mathiasson, 2000):

$$E = \frac{n_A}{n_s} \quad (2.3)$$

where n_s and n_A are the number of moles input from the sample during the extraction and those collected in the acceptor, respectively. The concentration enrichment factor (E_e) can be calculated from the relation of the extraction efficiency as shown in equation 2.4 (Jönsson and Mathiasson, 2000).

$$E_e = \frac{C_A}{C_s} = E \frac{V_s}{V_A} \quad (2.4)$$

where V_s and V_A are the volumes of the extracted sample and the acceptor channel, respectively.

It can be seen that if E approaches 1, the concentration enrichment factor is the volume ratio between sample and acceptor phase. In SLM the extract volume is kept small because of the trapping and at the same time giving relatively

high extraction efficiencies and this leads potentially to high enrichment factors. To obtain high enrichment factors with limited sample volumes, small acceptor volume have to be used.

In MMLLE and PME, the maximum value of E_e is obviously equal to the distribution coefficient between the donor and the acceptor phases. Therefore, in those techniques, large distribution coefficients are needed to obtain high enrichment factors. However, in MMLLE and PME, the acceptor is pumped continuously leading to larger V_A and consequently, a smaller E_e will be obtained. This limitation can be overcome by introducing a secondary focusing step which is MESI technique (Jönsson and Mathiasson, 2000).

2.2.5 Headspace techniques

Headspace techniques have been widely used in the determination of VOCs in water or solid sample since it is a “green chemistry” technique and easy to use. Headspace technique can be divided to static and dynamic headspace techniques.

2.2.5.1 Static headspace technique

Static headspace technique refers to the analysis of gas phase of target analyte from a heterogeneous system in equilibrium (Kolb and Ettre, 1997) therefore it is also known as equilibrium headspace extraction or headspace (Mitra, 2003).

Headspace is a widely used technique for VOCs analysis in various matrices. There are two options for headspace operation. It can be done by manual injection or by automatic sampler headspace where a sample is placed into a vial, typically 10 or 20 mL. After applying heat for a period of time, the analyte will diffuse in the headspace and reach equilibrium. The headspace is injected to the analysis system by autosampler (Mitra, 2003). A variety of extraction techniques was developed by combining headspace with the extraction techniques such as headspace-single drop microextraction (HS-SDME), headspace-solid phase microextraction (HS-SPME) as mention previously in section 2.2.2 and 2.2.3.

2.2.5.2 Dynamic headspace technique (purge and trap)

Purge-and-trap is the method for extracting and preconcentrating of VOCs from several matrices. The procedure involves purging an inert gas, such as nitrogen or helium, through an aqueous sample resulting in transferring of analyte to the gas phase and flow to a trap containing a suitable adsorbent. Finally, the trap is heated to desorb the analyte. The trap is then held at the desorbed temperature for an optimal time to achieve completely desorption. The vaporized contents are swept into the analysis system. Figure 2.14 is an example of purge and trap system consists of a purging (sparging) gas which used to purge analyte from aqueous sample to the vapor phase. A dry purge gas is used to reduce the water vapor condensation on the adsorbent trap. Glass-lined stainless steel desorption tube containing the adsorbent (TenaxTM TA) which adsorb the vapor of analyte. (www.sisweb.com). This procedure is particularly useful for insoluble or poorly soluble VOCs in water that has a boiling point below 200°C. However, for polar compound longer purging time while applying the heat to the sample can increase the purging efficiency of water soluble compounds.

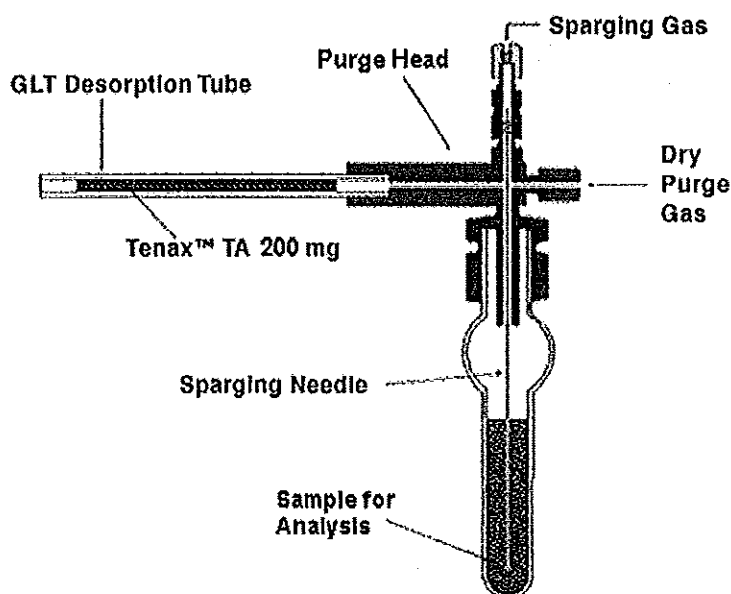


Fig 2.14 Purge and trap system (www.sisweb.com)

2.3 Sample preparation methods for VOC analysis in air

Sample preparation for VOC in air primarily aims at preconcentration to enhance the analytical sensitivity. Generally, VOCs contaminated is at very low concentration, air sample collection and transfer to laboratory for analysis is difficult therefore effective preconcentration device in the field is needed. In this section, preconcentration of VOCs in air sample using adsorbent and membrane extraction coupled with sorbent tube is focused.

2.3.1 Enrichment using immobilized sorbents

Solid sorbent is widely used technique for the enrichment and measurement of VOCs in air sample. Samples collected on sorbents can be introduced by thermal or solvent desorption. In this section thermal desorption is reviewed since it is widely used, easy to operated which can be either offline or online system and solventless technique.

2.3.1.1 Adsorption on solid sorbent

Adsorption on a solid sorbent is a very important technology and widely used in trace analysis. The desorption of the analytes can be preformed by solvent and thermal desorption. However, the latter is solvent free and completely desorbs. In addition, direct transferring of analytes into the gas chromatographic system could be operated. Therefore, thermal desorption and types and guide for selection of adsorbent is reviewed in this section.

Breakthrough volume is one very important parameter for solid sorbent and defined as the volume of gas that causes a compound to migrate through an adsorbent bed of one gram at a specific temperature (Figge *et. al.*, 1987). Generally, breakthrough volume can be investigated experimentally by frontal technique or elution technique. In the experiment, adsorbent is packed into the tube, placed into a GC-oven, one end connects to injection and another connects to detector. In the

frontal mode, a gas containing model analyte is passed continuously through the adsorbent bed at a defined temperature, and a frontal chromatograms is recorded (Figure 2.15A). The breakthrough can be caused by a migration of analytes and by a capacity overload at high analyte concentrations. In the elution technique, a model substance is applied as a pulse onto the adsorbent bed, and the elution chromatogram at a defined temperature is recorded (Figure 2.15B). The assumption of this technique is that the dilution analyte is applied therefore the breakthrough is caused by a migration of the analyte through the adsorbent bed (Dettmer and Engewald, 2002).

The specific retention volume can be calculated using the reduced retention time (elution technique) or the point of inflection (frontal technique). These values are used for the calculation of the specific breakthrough or retention volume according to equations 2.5, 2.6 and 2.7 (Dettmer and Engewald, 2002)

$$V_{g(B)}^{\theta} = \frac{t'_B}{m_A} \times F_c \quad (2.5)$$

$$V_g^{\theta} = \frac{t'_R}{m_A} \times F_c \quad (2.6)$$

$$F_c = F_a \frac{T_c}{T_a} \times \frac{3 \left(\frac{P_i}{P_o} \right)^2 - 1}{2 \left(\frac{P_i}{P_o} \right)^3 - 1} \quad (2.7)$$

Where $V_{g(B)}^{\theta}$ is the specific breakthrough volume, V_g^{θ} is the specific retention volume, t'_B is the reduced breakthrough time ($t_B - t_M$), t'_R is reduced retention time ($t_R - t_M$), t_B is the breakthrough time, t_R is retention time, t_M is hold-up time, F_c is adsorbent tube gas flow rate, F_a is the measurement gas flow rate at the end of adsorbent tube, T_a is temperature at the end of adsorbent tube, T_c is adsorbent tube temperature, P_i is pressure P_o is pressure at the end of adsorbent tube and m_A is mass of adsorbent (Dettmer and Engewald, 2002).

For breakthrough volume study, some research used a back-up tube (another adsorbent tube) placed behind the adsorbent tube. This technique is similar to frontal technique where model analyte is continuously flow through the adsorbent tube. Back-up tube works as a guard to adsorb the analyte from the first tube until its

concentration at the outlet reaches 5% of its inlet concentration. The acceptable percentage found in the back-up tube should be less than 15% of the total concentration. This can then be combined to the concentration obtained from the front section and used as the results. The sampling using both front and back-up beds is limited and inefficient when the sample found in back-up section exceeds 20-25% of the total sample when this is more than 33%, saturation has occurred (Figure 2.16) (Harper, 2000).

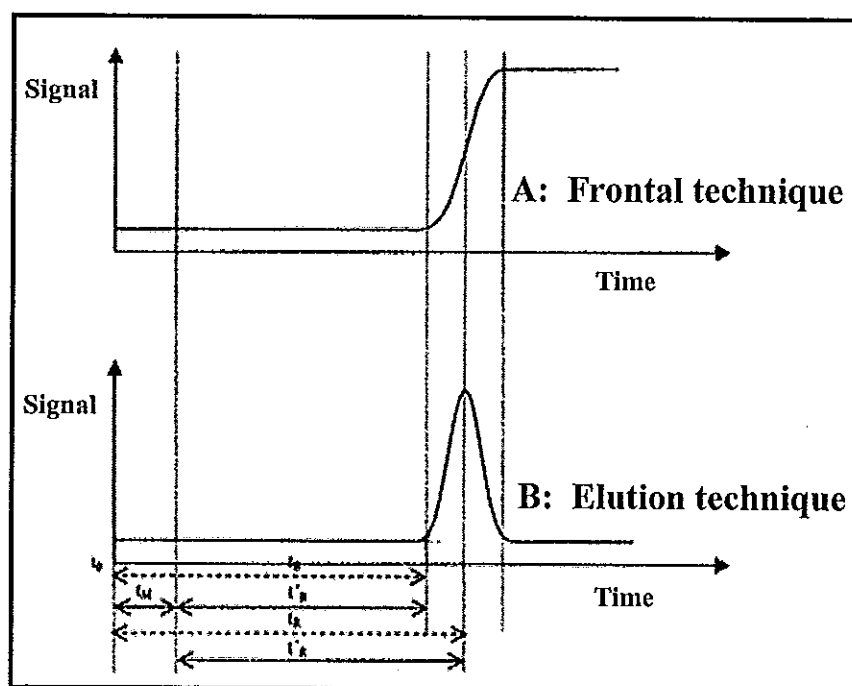


Fig. 2.15 Chromatographic techniques used for the determination of the specific breakthrough/retention volume (A) Frontal technique (B) Elution technique (Dettmer and Engewald, 2002).

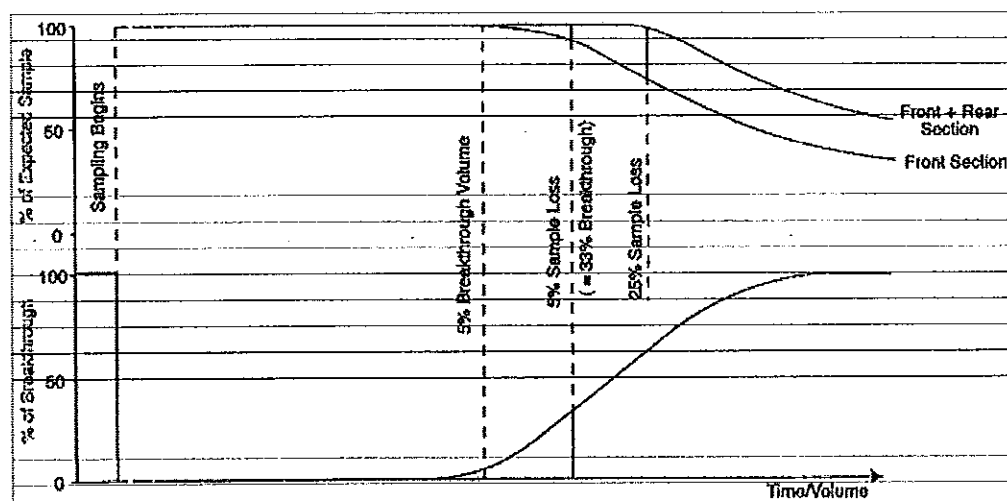


Fig. 2.16 Relationship of breakthrough to sample loss in a typical two-section sample tube sampling an atmosphere of constant sorbate concentration, showing the difference between 5% breakthrough volume and 5% sample loss to the back-up section. Actual shape of the curves will vary with sorbent, sorbate, concentration, temperature and the presence of other sorbates (Harper, 2000).

2.3.1.2 Thermal desorption and type of adsorbent

The criteria for thermal desorption to guarantee accurate determinations of VOCs are (Dettmer and Engewald, 2002).

- Complete adsorption and desorption of the analytes.
- Homogenous and inert surface.
- Low affinity to water to eliminate displacement and hydrolysis reactions and to minimize disturbances of the gas chromatographic analysis, for example, damage of the stationary phase or retention time shift.
- Low adsorption capacity for other inorganic constituents of air, for example, nitrogen oxide, sulfur dioxide, carbon dioxide, or ozone.
- High mechanical and thermal stability which can repeat using.

There are various types of commercially available adsorbents that can be used for trace analysis of volatile organic compounds. They are divided into 2 categories, carbon adsorbent and organic polymers.

Carbon adsorbents

Carbon adsorbent materials could be classified into activated carbon, carbon molecular sieves and graphitized carbon blacks.

Activated carbon

Activated carbons are micro-porous carbon materials with a broad pore size distribution and high specific surface areas ($800\text{--}1500\text{ m}^2\text{ g}^{-1}$). Activated carbons are thermally stable materials allowing the application of thermal desorption (Dettmer and Engewald, 2002; Harper, 2000). Activated carbons are often used for monitoring work place air. For example, multisorbent tubes packed with Carbopack B, Carbopack C, and Carbosieve SIII were used to adsorb VOCs such as acetone, isopropyl alcohol, 2-heptanone, and toluene in work place air (Wu *et al.*, 2003). Using thermal desorption, % recoveries were 94-101%.

Carbon molecular sieve

Carbon molecular sieves are micro-porous adsorbents with a sharp pore size distribution and high specific surface areas. Due to the defined micro-porous structure, carbon molecular sieves can act as molecular sieves which are commercially available as Carboxen, Carbosphere, Carbosieve, or Amborsorb materials (Dettmer and Engewald, 2002; Harper, 2000). Carboxens are hydrophobic which has a high porosity but it is not inert at high temperature (Harper, 2000).

Graphitized carbon blacks

Graphitized carbon blacks for analytical purposes are non-polar adsorbents with a physically and chemically homogeneous surface. The specific surface area varies between $5\text{ and }260\text{ m}^2\text{ g}^{-1}$ for commercial materials (Dettmer and Engewald, 2002; Harper, 2000).

Porous organic polymers

Porous organic polymers are a large group of adsorbents with different surface areas and polarities which can be classified to Tenax, Chromosorb, Porapak, Amberlite and XAD. A serious drawback is the limited temperature stability of several adsorbents restricting the application of thermal desorption. Tenax is a very hydrophobic material which is characterized by a high thermal stability. Due to its low specific surface area ($35\text{ m}^2\text{ g}^{-1}$), it is not suitable for sampling highly volatile organics (Dettmer and Engewald, 2002). Chromosorb 106 a higher specific surface

area but a lower temperature stability could replace Tenax for sampling more volatile and polar compounds in workplace air however it has a higher blank level which difficult for trace analysis (Harper, 2000; Sunesson *et al.*, 1995).

2.3.2 Membrane extraction

The advantages of membrane extraction are the improved selectivity and enrichment power, the minimized solvent use and the automation potential (Jakubowska *et al.*, 2005). Typically, analytes are transferred from a donor to an acceptor phase through a single or multi-membrane device, where distinction can be made between non-porous and (solvent impregnated) porous membranes. Mostly, membrane techniques for VOC sampling out of air are membrane inlet mass spectrometry (MIMS) (Ciucanu *et al.*, 2003; Creaser *et al.*, 2003; Moxom *et al.*, 2003) and membrane extraction with a sorbent interface (MESI) (Segal *et al.*, 2000), silicone membranes are widely used.

In MIMS, volatile organic compounds (VOCs) analytes from air sample permeate selectively through the membrane into the ion source of a mass spectrometer. The extraction process is the same as mentioned previously. The extracted analyte can either directly flow to the mass spectrometer vacuum system or into a stream of inert gas which transports the analyte to the ion source (Creaser *et al.*, 1998). Figure 2.17 illustrate that (A) the extracted analyte from hollow fiber membrane module directly flow to MS and (B) the extracted analyte from hollow fiber membrane module flow through the cryotrap to preconcentrate before carrying to MS.

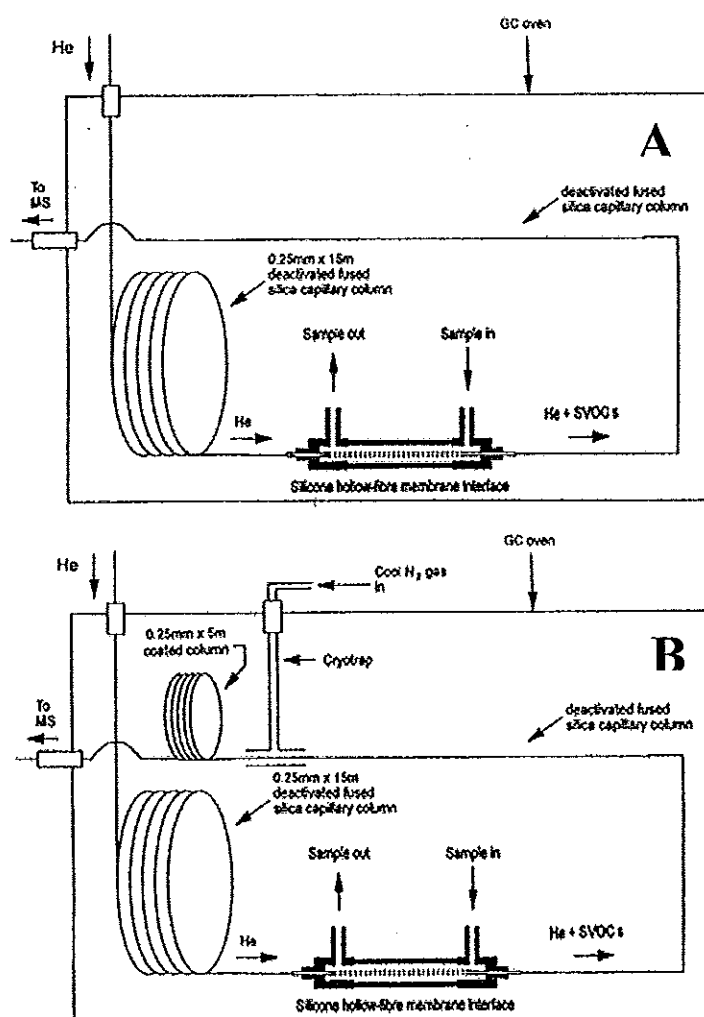


Fig 2.17 Schematic diagram of membrane inlet mass spectrometry (MIMS) (A) the extracted analyte from hollow fiber membrane module directly flow to MS and (B) the extracted analyte from hollow fiber membrane module flow through the cryotrap to preconcentrate before carrying to MS (Creaser *et al.*, 1998).

In MESI, gaseous analytes are extracted in a membrane module usually silicone rubber membrane is used. A stream of inert gas flow one side of the membrane module and carry the extracted compounds to sorption trap. After thermal desorption (apply voltage from power supply in Figure 2.18), analytes are detected by analytical instrument usually gas chromatography technique (Segal *et al.*, 2000).

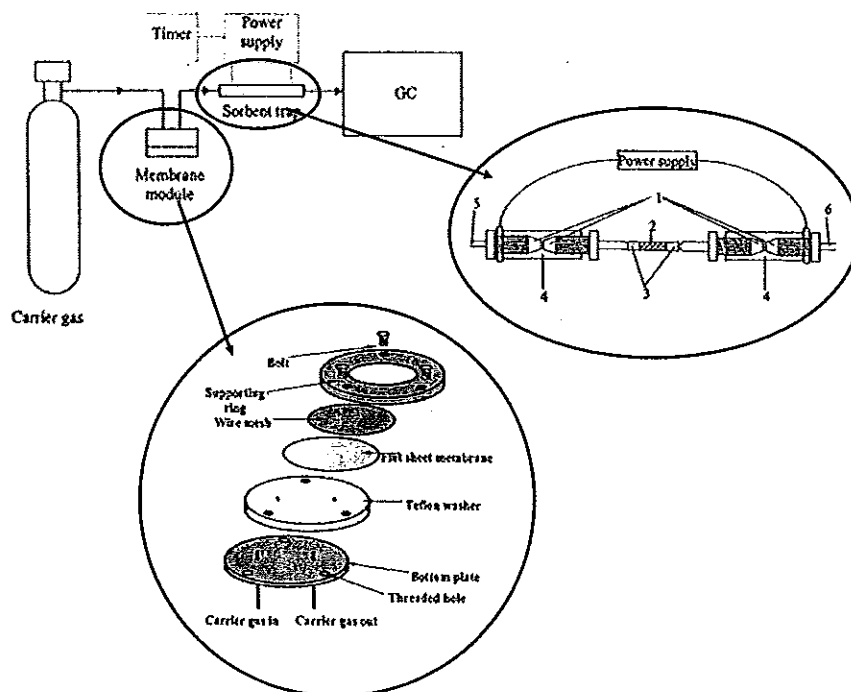


Fig 2.18 Schematic diagram of membrane extraction with a sorbent interface (MESI), flat membrane was used in this work (Segal *et al.*, 2000).

2.4 Conclusions

Sample preparation is often a time consuming and challenging step, particularly for VOC contaminated at trace levels (pg L^{-1} to ng L^{-1}) in air and water matrices. Main purposes of sample preparation are enhancement of sensitivity allowing low LODs, elimination of interferences and providing a robust and reproducible method.

For VOC analysis in water, high preconcentration factors are needed for trace analysis. Conventional LLE is not fit for green analytical chemistry. Therefore, solvent microextraction techniques, *i.e.*, SDME, (HF)-LPME and DLLME were developed. In addition, solvent-free sorptive enrichment, *i.e.*, SPME and SBSE is used in general. Membrane extraction offers fast, on-line and high capacity is also popular technique. For VOC enrichment in air sample, adsorptive enrichment is well-

established methods since it allows on-line automation and is easy to use. Membrane extraction techniques such as MIMS and MESI are emerging. Due to their automation potential and high sample throughput, they have large merit for passive sampling. Overall, it may be concluded that the state-of-the-art in sample preparation and analytical methods to provide reliable results, robust and highly sensitive method for trace analysis of VOC in both air and water matrices is progressive. Trend is still toward miniaturization, green chemistry, fast and cost effective system.

CHAPTER 3

Electrochemical analysis of organic compounds

3.1 Introduction

Electrochemistry is concerned with the relationship of electrical and chemical effects. A huge area of this field involved with the study of chemical change caused by applying an electric current or voltage and the production of electric energy by chemical reactions (Bard and Faulkner, 2001). Electrochemical techniques are widely used to study the kinetic and mechanisms of chemical reaction including electron transfer at the electrode. When an electric potential is applied to the system the current is generated proportional to the amount of chemical (Wang, 2006). Thus, different electrochemical methods can be applied to the analysis system and this is called electrochemical analysis. Electrochemical analysis is the technique based on the electrical quantities such as current, potential or charge which is related to the chemical in the sample. Here we focused on the potential-controlled technique which studied the charge transfer processes at the electrode-solution interface and the application of electrochemical methods for organic compound analysis.

3.2 Electrochemical detection technique

3.2.1 Voltammetry

Voltammetry is one of the techniques in electrochemical analysis which current is studied as a response to a scanned potential. This technique has a broad range of applicability in analytical chemistry and provides chemists with information about the thermodynamics and kinetics of chemical reactions, and they can be used to identify quantitative different species in solution effectively. In this chapter, some techniques used for detection of organic compounds are reviewed.

Cyclic voltammetry is a widely used technique to study the electrochemical reaction at the electrode surface. This can be performed by linearly scanning the potential in an unstirred solution with single or multiple cycle waveforms to meet special needs. It can be used to investigate the interfacial behavior of electroactive compounds (Wang, 2006). For example, the real surface area of copper electrode was studied via the integral of adsorption peak of Pb (Lukomska and Sobkowski, 2004). The peak current obtained is related to the surface coverage (Γ , mol cm⁻²) and potential scan rate which is shown below (Wang, 2006);

$$I_p = \frac{n_2 F_2 \Gamma A \nu}{4RT} \quad (3.1)$$

where ν is the scan rate, A is the surface area of the electrode (cm²), n is the number of transferred electron, F is the Faraday' constant (96,485.4 C), R is the gas constant (8.314 J K⁻¹ mol⁻¹) and T is the temperature. The saturation peak area can be used to calculate the surface coverage which correlated to the area of the surface occupied by the adsorbed molecule as follows.

$$Q = nFA\Gamma \quad (3.2)$$

In addition, cyclic voltammogram can be applied for quantitative analysis via the measured peak current. For example, the irreversible oxidation peak of ephedrine, norephedrine and n-methylephedrine can be observed by single anodic peak using carbon past electrode (CPE) modified with cobalt phthalocyanine (CoPC) (Figure 3.1A) (Cookeas and Efstathiou, 2000). Electrochemical reduction of two nitroso compounds, *i.e.*, ortho- and meta-nitrosotoluene derivatives has been carried out using cyclic voltammetry (Núñez-Vergara *et al.*, 2001).

Other voltammetric techniques are based on current/potential-step and differ in their potential waveforms and current sampling regime. For example, square wave voltammetry was used to measure the current response of the electrochemical reduction of 2, 4, 6 trinitrotoluene and 2, 4-dinitrotoluene (Bozic *et al.*, 2008). In this technique, the surface of a gold electrode was modified with alkanethiols to improve the resolution of the reduction peaks from both compounds and interference from background current. The results showed a good resolution between these two peaks with the potential of -0.48 and -0.62V for DNT and TNT, respectively (Figure 3.1B).

As comparing background, it is clearly observed that modified electrode with SAM layer can suppress of the interfering background currents effectively. Mackie and co-worker have also reported the usage of Triton-X-100 in cathodic stripping voltammetry (CSV) for pyrrithione detection. Triton-X-100 can separate the peak of pyrrithione from other interfering thiol compounds (Mackie *et al.*, 2004).

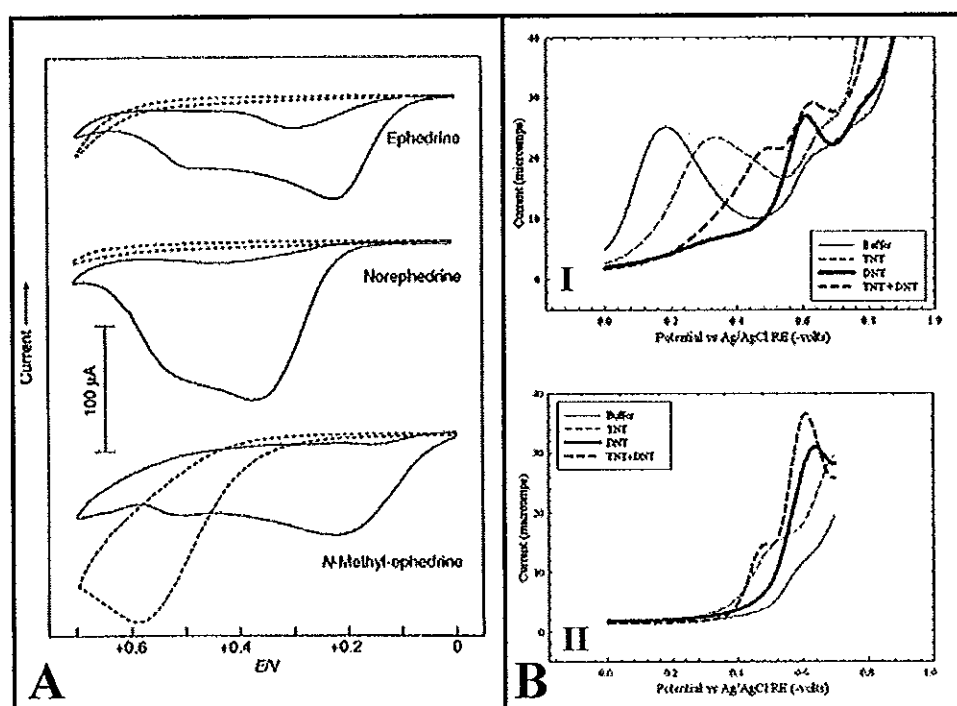


Fig. 3.1 Cyclic voltammograms for quantitative analysis, (A) CoPC/CPE (solid line) and the CPE (broken line) of 1.0 mmol L^{-1} solutions of ephedrines in 0.10 mol L^{-1} NaOH. Scan rate: 100 mV s^{-1} (Cookeas and Efsthathiou, 2000) (B) Square wave voltammograms for 4 ppm TNT analyte only, 4 ppm DNT analyte only, and for a 4 ppm DNT+ 4 ppm TNT mixture. I: The working electrode was bare gold, II: The working electrode was gold modified with an MCP monolayer (Bozic *et al.*, 2008).

3.2.2 Amperometry

In this technique, a fixed potential is applied and the resulting current response was measured. This section will be reviewing some of amperometric

techniques for organic compound detection. The widely used technique is chronoamperometry. This technique involves with the current resulting from given potential at working electrode. The resulting current-time related to the change of the concentration gradient of the electrode surface (Bard and Faulkner, 2001; Wang, 2006). The peak current at a macroelectrode for one electron reduction is given by the Randles-Ševčík equation (Bard and Faulkner, 1982);

$$I_{peak} = 2.69 \times 10^5 n^{3/2} D^{1/2} C_{bulk} \nu^{1/2} A \quad (3.3)$$

where I_{peak} is the peak current in amperes, n is the number of electrons transferred in the rate determining step, D is the diffusion coefficient in $\text{cm}^2 \text{s}^{-1}$, C_{bulk} is the bulk concentration of active species in solution in mol cm^{-3} , ν is the scan rate in V s^{-1} and A is the surface area in cm^2 . Therefore, chronoamperometry can also be used for measuring the diffusion coefficient of electroactive species or the surface area of working electrode.

Chronoamperometry is a useful technique for measuring the adsorbed reactant. For example, ephedrine and ethylamine were determined using cobalt phthalocyanine modified carbon paste electrode with amperometric detection (Cookeas and Efstathiou, 2000). To improve limit of detection, integrated pulsed amperometric detection (IPAD) was applied for the detection of thiourea in flow injection analysis (Lee and Yeo, 2001). The pulse waveform used in the integrated pulsed amperometry consisted of three steps: detection potential, oxidation potential, and reduction potential (Figure 3.2). In this technique, better signal to noise was obtained which could improve the limit of detection (Lee and Yeo, 2001).

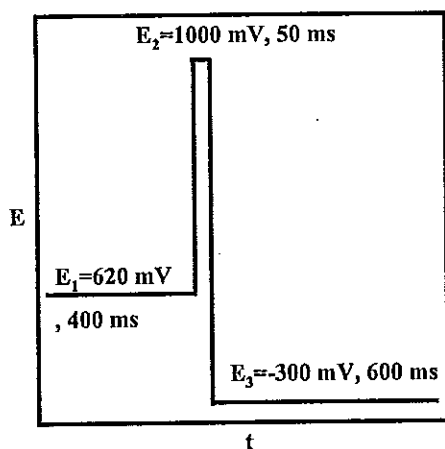


Fig. 3.2 Triple-step potential waveform for the integrated pulsed amperometry for the analysis of thiourea in 0.1 M NaOH.

3.3 Electrode material

3.3.1 Mercury electrode

Mercury electrode is an attractive choice for electrode material due to high hydrogen overvoltage property resulting in wide cathodic potential window. However, the drawbacks of this electrode are its limited anodic range and high toxicity (Boening, 2000; Economou and Fielden, 1997; Page *et al.*, 1962; Wang, 2006). There are several types of mercury electrode such as dropping mercury electrode (DME), hanging mercury drop electrode (HMDE) and mercury film electrode (MFE). Among these HMDE is the popular working electrode for stripping analysis and cyclic voltammetry (Economou and Fielden, 1997; Page *et al.*, 1962). However, using mercury can cause environmental problems. Therefore, another material was introduced instead of mercury such as bismuth which will be discussed in section 3.5.3.

3.3.2 Solid electrode

Because of the limitation of the anodic range of mercury electrode, many types of solid electrode was developed such as gold (Giacomino *et al.*, 2008), platinum (Kyriakou *et al.*, 2006), silver (Liang *et al.*, 2005), nickel (Kerr and Mike, 1998), bismuth (Romann *et al.*, 2008), palladium (Grdeń *et al.*, 2008) and copper electrodes (Chen and Hibbert, 1997). Some of these were developed for specific purposes. For example, bismuth microelectrodes with the in situ renewable surface have been developed and applied to capillary electrophoresis in flow injection analysis for pyridine and Pb^{2+} and Cd^{2+} detection (Romann *et al.*, 2008). Copper wire electrode was used for carbohydrate and carboxylic acid detection in flow injection analysis (Chen and Hibbert, 1997). In addition, to enhance the electrode performance metal solid amalgam electrodes has also been successfully introduced. The example is either silver or copper solid amalgam electrode for cathodic stripping voltammetry of cysteine (Yosypchuk and Novotný, 2002). Silver or copper solid amalgam electrodes were prepared by packing silver or copper powder into a glass capillary which electric contacted to a platinum wire inserted into the powder then amalgamated by liquid mercury (Yosypchuk and Novotný, 2002). A new type of copper solid amalgam electrode was also investigated by the same group for phytochelatins detection (Yosypchuk *et al.*, 2003).

3.3.3 Chemically modified electrodes

Chemically modified electrodes (CMEs) have been developed over the past two decades. The ability to modify electrode surface has led to a wide range of analytical applications and created powerful opportunities for electroanalysis. The manipulation of the electrode surface aims to improving sensitivity, selectivity and/or stability for tailoring and the response in order to meet analytical needs. Chemically modified electrode can be reformed by immobilization of modifier agent onto the electrode surface via chemical reactions, chemisorptions, composite formation or polymer coating. Since physicochemical properties of the modifier are transferred to the electrode, therefore, electrode characteristics and reactivity could be controlled via

surface modification. Many applications of CMEs have been reported and are summarized here.

Carbon nanotubes modified electrodes

Carbon nanotubes (CNTs) were discovered in 1978 by Peter Wiles and John Abrahamson at the University of Canterbury in Christchurch, New Zealand. They observed carbon fiber ranging in diameter from 4 nm up to 100 nm with lengths up to 15 micrometers. Then, the properties and applications of CNTs were introduced by Ijima in 1991 (Gong *et al.*, 2005). Their unique properties have led them to be employed in significant applications in many fields such as electronics, medicine, aerospace and industry. Multiwall carbon nanotubes successes in electrochemical applications due to the ability of this nanomaterial to improve electron transfer in electrochemical reactions. In particular, CNTs are excellent electrode materials due to their good electrical conductivity and mechanical strength, chemically inertness, high surface activity and a wide potential window (Agüí *et al.*, 2008; Wildgoose *et al.*, 2006). The CNTs were modified to adjust the properties in some researches. The methods for modifying the surfaces of CNTs can be classified into two ways;

1) Covalent bonding or chemisorption of the modifier to the CNTs. For example, covalently derivatization of carbon powder via the chemical reduction of aryl diazonium salts with hypophosphorous acid (Heald *et al.*, 2004). This allows the covalent derivatisation of MWCNTs by anthraquinone-1-diazonium chloride (Figure 3.3A) and 4-nitrobenzenediazonium tetrafluoroborate (Figure 3.3B). This can be used for a variety of applications such as the possibility of sensor miniaturisation.

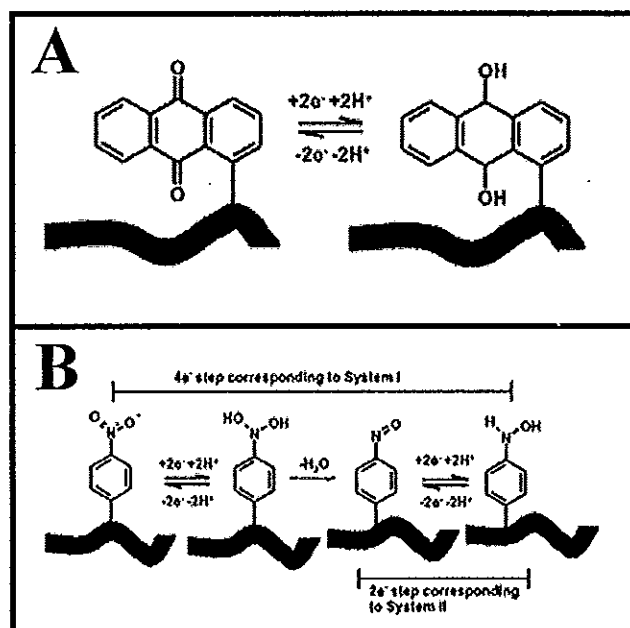


Fig. 3.3 Modification of CNTs via covalent bonding (A) The redox reaction for 9,10-anthraquinone covalently attached to MWCNTs (B) The proposed reduction mechanism for nitrobenzene covalently attached to MWCNTs (Heald *et al.*, 2004)

2) Miscellaneous methods of modification via incorporation CNTs with others materials such as polymer film and intercalation of the modifier into the CNTs. For example, the nanocomposite films of polypyrrole (PPy) and multiwalled carbon nanotubes (MWCNTs) were electrochemically synthesized by direct oxidation of pyrrole in 0.1 M aqueous solution of dodecylbenzene sulfonic acid containing MWCNT as shown in Figure 3.4A (Han *et al.*, 2005). This material could be used in a sensor system. In addition, a 10–40 nm diameter Pt–Pb alloy nanoparticle/multiwalled carbon nanotube (Pt–Pb/MWCNT) nanocomposite was prepared by electrodepositing Pt–Pb alloy onto MWCNTs that were vertically aligned on Ta plates (Cui *et al.*, 2006). From the result Pt–Pb alloy nanoparticles were mainly deposited at the tips, and sparsely dispersed on the sidewalls of the bamboo-like MWCNTs (Figure 3.4B). This electrode was developed for nonenzymatic glucose sensor.

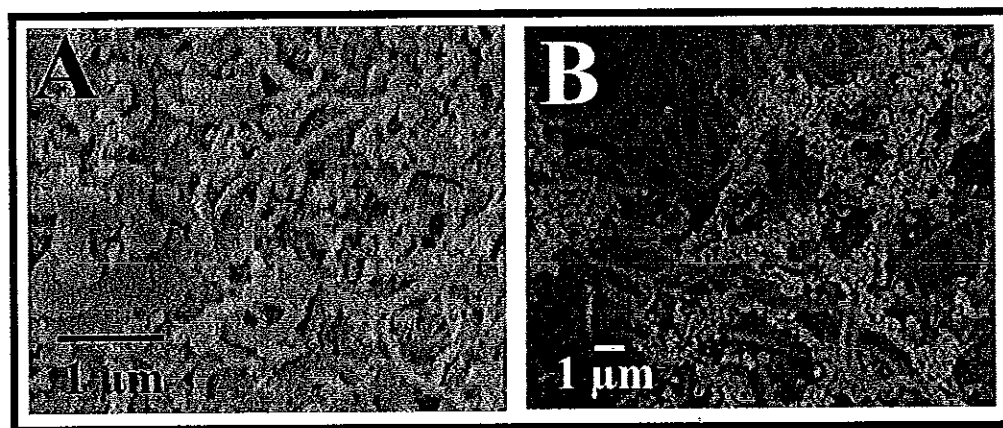


Fig. 3.4 SEM images of composite CNTs modified electrode (A) Ppy-MWCNTs (Han *et al.*, 2005) (B) Pt-Pb/MWCNT (Cui *et al.*, 2006).

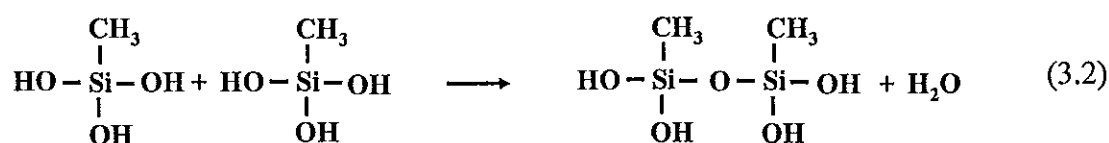
The sol-gel technique is another choice to synthesize composite electrodes due to the combined benefit of sol-gel and electrochemistry of CNTs. This can be prepared by adding CNTs into a silica gel matrix. The formation of silicate gel can be performed via hydrolysis, condensation, polycondensation and drying using methyltrimethoxysilane as a precursor, following these reactions (Gong *et al.*, 2005).

Hydrolysis



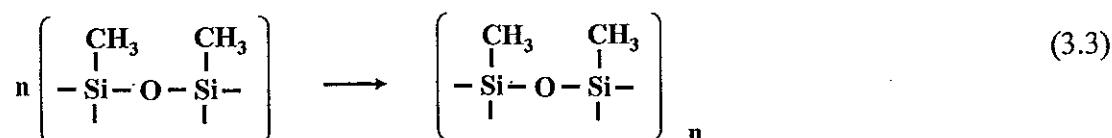
This reaction provides the formation of silanol groups.

Condensation



The silanol groups further react to produce siloxane polymers.

Polycondensation



Siloxane polymers further react to produce polysiloxane polymer.

This polymer is hydrophobic which could interact with CNTs via hydrophobic sidewalls. The CNTs covered with silicate particle are not electrochemically assessable therefore could not be used for electrode reaction (Gong *et al.*, 2005). In contrast, the open part could work as nano-electrode for electrochemical reaction.

Nanomaterials modified electrode

In recent years, the electrode development has focused on the miniaturization of nanotubes, nanoballs, nanodots and in particular nanoparticles. The benefits to the use of a nanoparticle modified electrode when compared to a macroelectrode are high effective surface area, improved mass transport and catalysis. For example, gold nanoparticles were electrodeposited onto planar gold electrode (Figure 3.5A). The assembly structure and property of mercaptopropionic acid self-assembled monolayers on gold nanoparticle modified electrode (nanogold electrode) was developed. This modified electrode was used to study electron transfer by cyclic voltammetry (Liu *et al.*, 2005).

Pd nanowire arrays (NWAs) with the diameter of 50 nm and length of 850 nm were prepared using a porous aluminum oxide template by pulse electrodeposition (Cheng *et al.*, 2008). The SEM image was used to characterize the obtained PdNWAs structure (Figure 3.5B). The electrocatalytic activity of electrodes for methanol and isopropanol oxidation in alkaline media was investigated and found that PdNWAs provide excellent catalytic activity for alcohol electrooxidation.

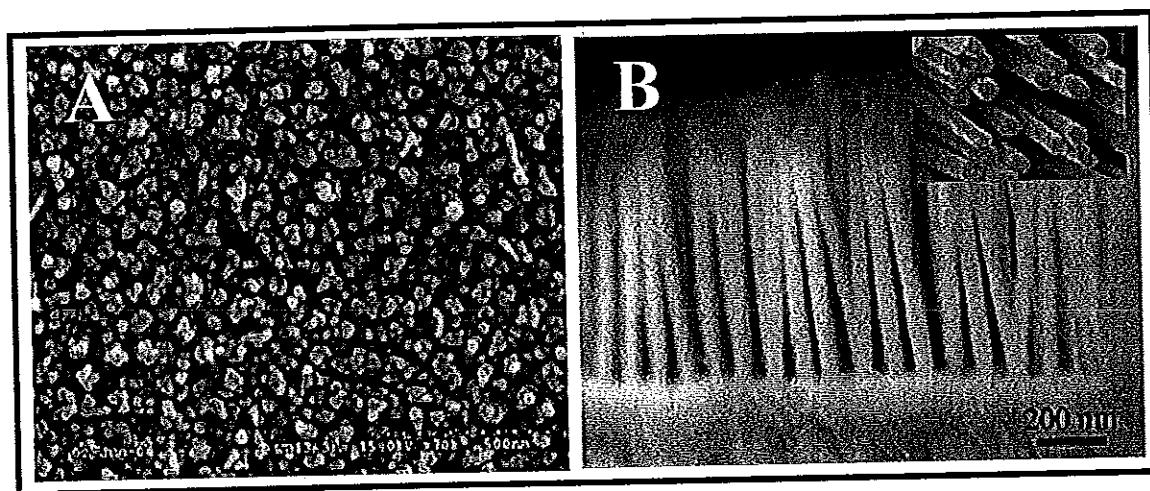


Fig. 3.5 SEM image of nanowires modified electrodes (A) Gold nanoparticles (Liu *et al.*, 2005) (B) Pd nanowire arrays (PdNWAs) (Cheng *et al.*, 2008).

Thin film modified electrode

Recently, Hou and coworkers (Hou *et al.*, 2008) reported on using a film of 3,5-dihydroxy benzoic acid, polymerized on the surface of a glassy carbon electrode (GCE) in neutral solution by cyclic voltammetry. The voltammogram was shown in Figure 3.6, a cathodic peak appeared in the first cycle with a potential at -0.55 V. Then larger peaks were observed on continuous scanning, reflecting the continuous growth of the film. These facts indicated that DBA was deposited on the surface of GCE by electropolymerization. The poly(DBA) film-coated GCE provided excellent electrocatalytic activity toward the oxidation of dopamine (DA).

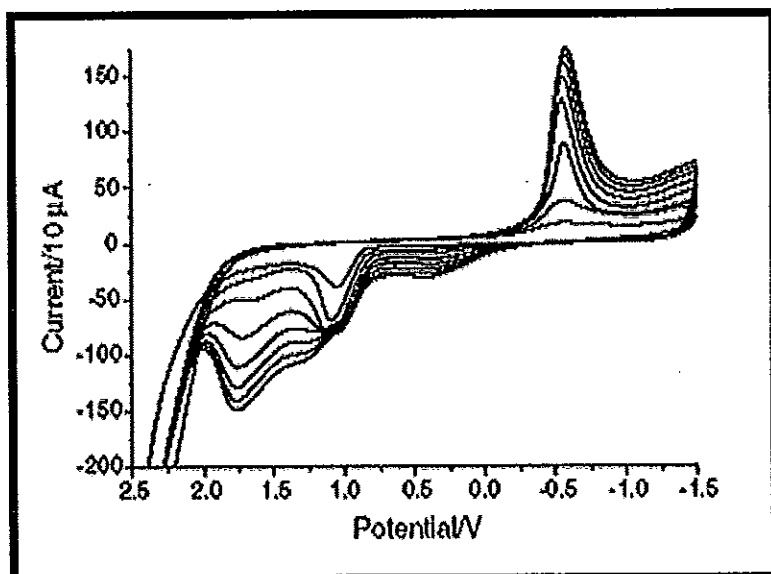


Fig. 3.6 Repetitive cyclic voltammograms of 2.0×10^{-2} M DBA in 0.1 M NaCl solution. Initial potential: -1.5 V; terminal potential: +2.5 V; scan rate: 100 mV s^{-1} (Hou *et al.*, 2008).

Another interesting work on polymer modified electrode is the usage of conducting polymer organic electrodes modified with phage host cells (*Salmonella Newport*) (Dadarwal *et al.*, 2008). In this work, the polypyrrole conducting polymer was modified into microporous polycarbonate membranes (Figure 3.7). Then, *S. Newport* host cells were deposited on the surface of a polypyrrole polymer electrode and placed under vacuum to draw the cells into the membrane pores followed by transferring to the electrode housing assembly. It is successfully employed to detect bacteriophage by monitoring their infectivity of host cells immobilized on the surface of polypyrrole organic electrodes.

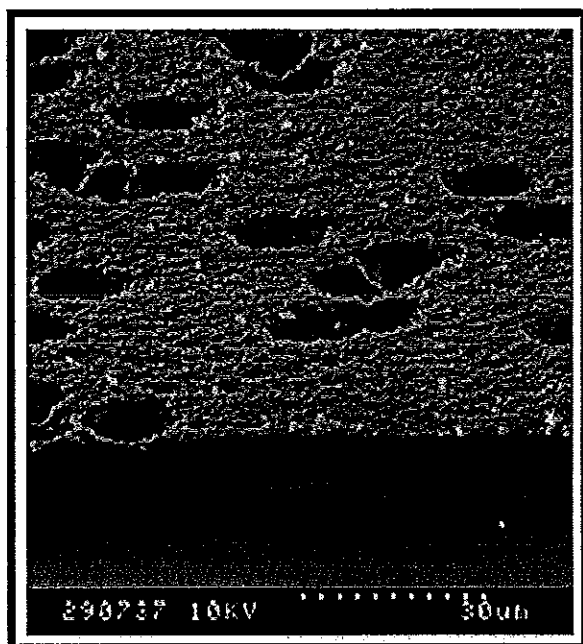


Fig. 3.7 Polypyrrole film deposited onto microporous polycarbonate membranes to form conducting polymer organic electrode (Dadarwal *et al.*, 2008).

Another type of thin film electrode is amalgams electrode, demonstrated by Kapturski and Bobrowski (Kapturski and Bobrowski, 2008). The application of the silver amalgam film electrode (Hg(Ag)FE) prolonged analytical applicability to the determination of cobalt and nickel by adsorptive stripping voltammetry. Silver and copper solid amalgam electrodes have been successfully tested for cathodic stripping voltammetry of cysteine (Yosypchuk and Novotný, 2002).

3.4 Other electrodes

3.4.1 Microelectrodes

Electrodes of different materials have been miniaturized in many geometrical shapes to develop small dimension devices. Generally, the term “microelectrode” is defined for electrodes which at least one dimension not greater than 25 μm (Wang, 2006). Microelectrodes provide attractive properties which could

be applied in various electrochemistry systems. The very small current at the microelectrode making it possible to use this electrode in highly resistive solution, reduced double layer capacitance allowing high speed voltammetric experiments. Microelectrodes can also increase rates of mass transport of electroactive species.

Replacable microelectrode has been applied to microchip capillary electrophoresis system. This electrode could be prepared in laboratory from carbon fiber and could be used for dopamine and epinephrine detection as shown in Figure 3.8A (Zeng *et al.*, 2002). Recently, column and row microelectrodes on two different glass substrates were arranged for electrochemical detection (Lin *et al.*, 2008). This device provided 10×10 detection points on a single chip (Figure 3.8B). The present device was used for imaging the spots of alkaline phosphatase on the array substrate indicating that the device can be applied to comprehensive and high-throughput detection and imaging of biochemical species.

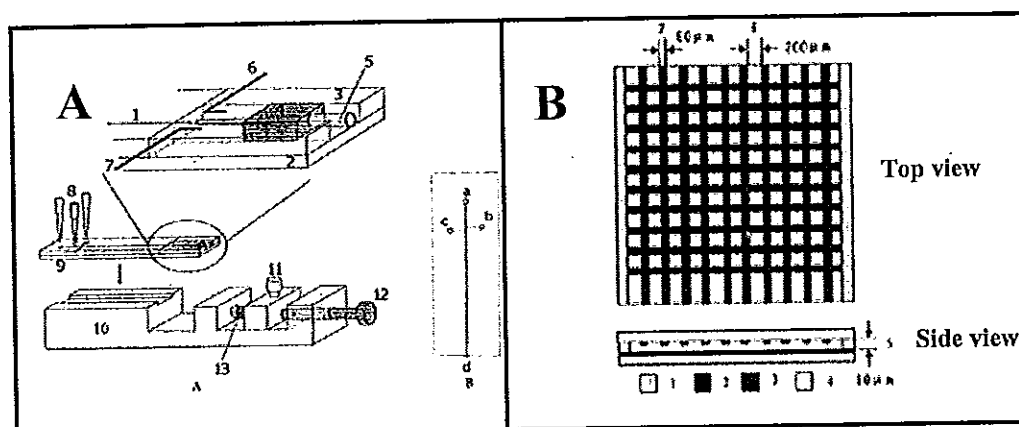


Fig. 3.8 (A) Capillary electrophoresis chip for carbon fiber microelectrode assembly 1 separation channel; 2 glass plate; 3 plexiglass block; 4 epoxy; 5 guide tube; 6 Pt wire; 7 Ag/AgCl wire reference electrode; 8 pipet tips; 9 capillary electrophoresis chip; 10 plexiglass body; 11 electrode holder; 12 precision screw; 13 spring. B. Layout of the chip: (a) buffer reservoir, (b) sample reservoir, (c) sample waste reservoir, (d) detection reservoir (Zeng *et al.*, 2002) (B) Scheme of the working area of the device; 1 double-sided adhesive paper; 2 row electrode; 3 column electrode; 4 glass substrate; 5 gap of the substrate; 6 gap between the two microelectrodes; 7 width of the microelectrode (Lin *et al.*, 2008).

3.4.2 Screen printed electrodes

The demand for easy to use, portable, cost effective electrodes led to the development of screen printed electrodes. For example, an electrode coated with nafion layer was prepared on PVC pad with the screen-printing technique containing a pair of working and reference electrodes (Figure 3.9A). This screen printed electrode was modified with CNTs (Figure 3.9B) for hydrogen peroxide detection (Wang and Musameh, 2004). The thick-film of CNT sensor strips can improve electrochemical properties and analytical performance. The fabrication and characterization of screen printed electrodes modified with polyaniline polymer nanoparticle films produced via inkjet printing were also investigated (Morrin *et al.*, 2008). Both conductive and

electroactive of the film was studied. The redox peak of leucoemeraldine, emeraldine salt, p-benzoquinone and hydroquinone was also characterized. The film morphology was presented by SEM (Figure 3.9C).

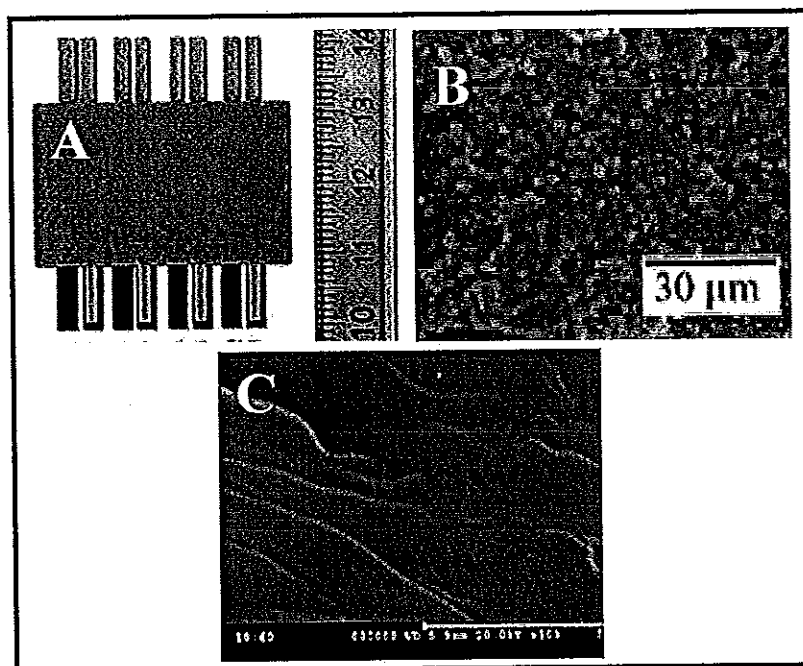


Fig. 3.9 Screen printed electrode (SPE) (A) SPE coated with nafion layer for cholinesterase biosensor design (Gogol *et al.*, 2000) (B) SEM image of multiwall carbon nanotubes (CNTs) modified screen-printed (SP) electrochemical sensors (Wang and Musameh, 2004) (C) SEM of polyaniline polymer nanoparticle films modified on screen printed electrode (Morrin *et al.*, 2008).

3.5 Flow injection system with electrochemical detection

Flow injection is the technique that the liquid analyte is injected into a flowing stream of carrier solution and flow through working electrode. Electrochemical reaction occurred at working electrode can be measured at different mode such as current or potential. Applications of electrochemical detections in flow injection systems have gained popularity in recent years, in particular it is useful for organic compounds detection (Tóth *et al.*, 2004; Wang, 2006). Electrochemical

detection under hydrodynamically controlled conditions reveals special features as follows (Tóth *et al.*, 2004):

- The shear forces of the flowing liquid continuously clean the surface of the working electrode therefore the fresh of working electrode surface is generated with intensive washing, solution or solvent switching and potential cycling compared to batch system.
- The continuously flowing of carrier solution can remove reaction products (voltammetric electrodes) and impurities can condition of the working electrode.
- The convective transport of an analyte reduces response time and improves the detection limit compared to batch system with diffusion transport.
- Reference electrode can be selected and designed.
- The usage of microelectrodes provides operating condition in solutions with very low conductivity, suppressed signal dependence on the liquid flow rate.

In flow injection systems, a wide range of flow cell has been designed for electrochemical detection. Each type is characterized by the length, diameter, and shape of its detection channel and electrode geometry. Generally, the flow is either parallel to the electrode surface (Pingarrón *et al.*, 2001), perpendicular to the electrode surface (wall-jet cells) (Alden *et al.*, 1999) or the liquid passes through a tubular electrode. These parameters determine the character of the liquid flow under the experimental conditions and the predominant mode of the mass transport within the cell (Tóth *et al.*, 2004).

Amperometric detection is usually performed by controlling the potential of the working electrode using a constant value. The current is monitored as a function of time. The magnitude of the peak current measured is related to the concentration of analyte that passes through the detector. For example, carbon fiber microelectrodes (CFMEs) modified with rhodium (Rh) via electrodeposition technique for amperometric detection of hydrazine under flow-injection conditions was studied (Pingarrón *et al.*, 2001). The comparison between the amperometric responses to hydrazine injections of Rh-CFME and Rh-modified glassy carbon electrode was presented in Figure 3.10. A stable baseline and a reproducible response

were obtained with CFMEs, whereas less stability, high background current and decrease of the peak current with consecutive injections were accomplished when glassy carbon electrode was used.

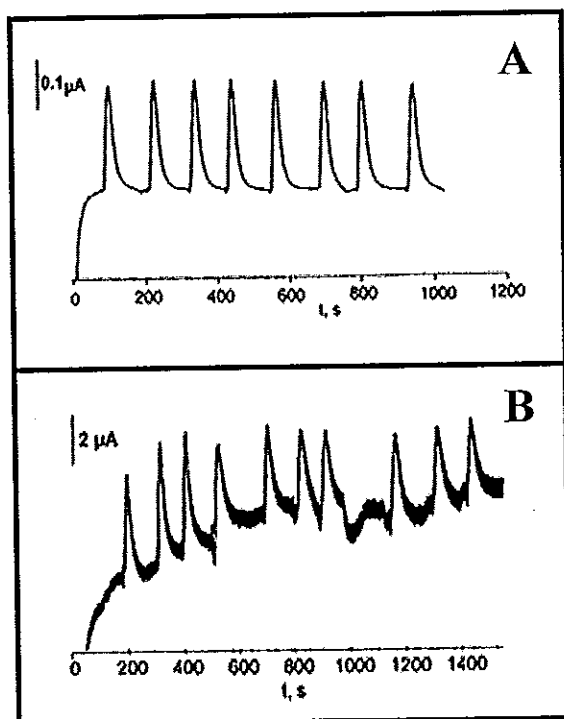


Fig. 3.10 The comparison between the amperometric responses to hydrazine injections using (A) Rhodium-modified carbon fiber microelectrodes (Rh) (B) Rhodium-modified glassy carbon electrode in a flow injection system (Pingarrón *et al.*, 2001).

The detection limit in flow injection systems is determined by the signal-to-noise (S/N) ratio which can be improved by electronic and hydrodynamic. In voltammetry techniques, the waveform of the excitation signal and the sampling pattern of the measured current determine the sensitivity and detection limit. The different potential pulse techniques generally can improve the detection limit by decreasing the noise, *i.e.*, the detrimental effect of charging current. In addition, increasing mass transfer rate by the hydrodynamic approach and flow rate increasing can also improve the detection limit since the background current changes less while the signal improves significantly (Tóth *et al.*, 2004).

3.6 Conclusions

The interest in electrochemical analysis for organic compounds detection is the wide range of potential applications and the possibility to enhance the analytical signal by using different detection methods such as voltammetry and amperometry or modifying of electrode with various materials. Main objectives of modified electrode are to enhance sensitivity providing low LODs, specificity, eliminating of interferences and providing a robust and reproducible method. Various materials were taken to be electrode modifier such as thin film of metal and polymer, nanomaterials which are carbon nanotubes, nanoparticle and nanowires. To achieve high speed voltammetric experiments microelectrode was then developed. In addition to the demand for ease of use, portability and cost effectiveness screen printed electrodes were introduced. The incorporation of flow injection and electrochemical detection was also emphasized. Overall, it may be concluded that the state-of-the-art in electrochemical analysis to provide low LODs, high specificity, elimination of interferences and providing a robust and reproducible method is progressive and still be the challenge for researchers.

CHAPTER 4

Electrochemical synthesis of nanowires

4.1 Introduction

Nanotechnology is the technology that makes it possible to create functional materials, devices and systems through the controlling of matter on the nanometer length scale (1-100 nanometers) and exploitation of novel phenomena and properties such as physical, chemical, biological, mechanical and electrical at that length scale (Klabunde, 2001). Nanomaterials have influence on huge area which could change our industries and finally our lives. For instance, at present it is possible to create medicines in nanoparticle form which can dissolve in bloodstream where larger particle can not do (Roco *et al.*, 1996) or coating gold nanoparticle with DNA stands for DNA detection (Wang, 2003). In environmental role, there are successfully developments of porous metal powder-sand membranes for ground water decontamination (Belyakovaa *et al.*, 1998), semiconductor nanoparticles for more efficient solar cell (Günesa *et al.*, 2007), metal oxide nanoparticle for acidic gases (Leva *et al.*, 2007) and polar organics compound adsorption (Grasset *et al.*, 2003). Nanoparticle can also improve security systems (Strem Chemicals, 2005). Therefore, it is quite clear that these nanomaterials are useful in health, environment and industries world wide.

The definition of nanomaterials is that one of their dimensions should be less than 100 nanometers which is around a thousandth of a single strand of human hair. These nanomaterials can be classified into nanoparticle, cluster, colloid, nanocrystal, quantum dot and nanoscale material (nanowire) (Klabunde, 2001). Nanowires are a specific type of nanoparticle that has cylindrical shape and it is one of the most attractive nanomaterials because of their unique properties leading to various applications. However, in the nanoworld the aspect ratio (length to diameter ratio) is the parameter used to classify the type. For example, wires with large aspect

ratio greater than 20 are called nanowires, whereas the one with smaller aspect ratio is called nanorod (He and Tao, 2003).

The objective of this chapter is to give an introduction of nanowires, their production, characterization technique and finally applications.

4.2 Nanowires fabrication

Nanowires can be produced from different materials such as metals and polymers. Different methods such as sol-gel and deposition could be performed resulting in different properties of nanowires. In this chapter two typical synthesizing techniques of nanowires are reviewed, *i.e.*, top down and bottom up.

4.2.1 Top down technique

In the top down approach, amounts of material in specific locations are removed revealing a nano structure where the original size is much larger than the obtained material (Yogeswaran and Chen, 2008). Top down technique is generally used for making solid state integrated circuitry devices that can have features down to tens of 1 nanometers, or even microfluidic devices where the working fluid has a total volume in nanoliters (Yogeswaran and Chen, 2008).

The main top down technique is lithography. The general idea with lithography is that a pattern is traced onto a photosensitive material by selective exposure to a radiation source such as light. A photosensitive material is a material that can change its physical properties when exposed to a radiation source. If photosensitive material is selectively exposed to radiation (e.g. by masking some of the radiation) the pattern of the radiation is traced to the material. When exposed to radiation at specific wavelength the properties of photosensitive material can be changed therefore the removal of exposed or unexposed photosensitive material can be performed. This process can be applied to make a pattern of microfluidic chip and may also be used as a template for depositing another material (Figure 4.1A). Schematic diagram showing photosensitive material used as a template for nanowires synthesis is shown in Figure 4.1B. Once the pattern or nanowires have been

deposited, the photoresist is stripped and the nanowire is pattern on the substrate (Darling, 2005). The top-down approach can be used to synthesize nanowires and also nanoelectrodes. For example, combination of multiple lithographic steps and anisotropic chemical etching processes or deposition of other materials can produce GaAs nanowires with controlled properties along their longitudinal dimension (Sun *et al.*, 2005).

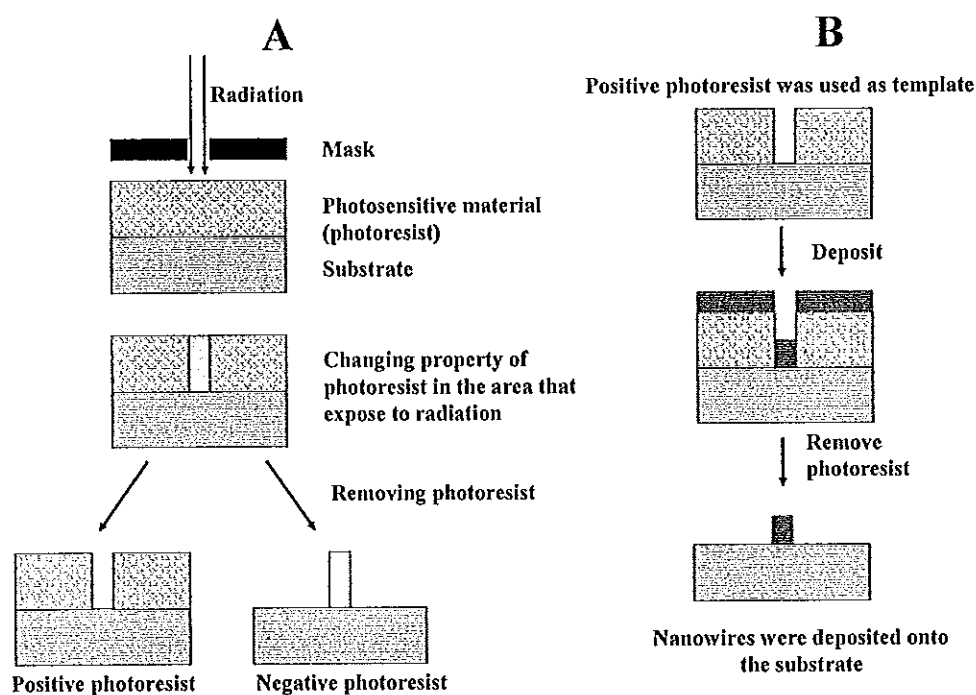


Fig. 4.1 Schematic diagram of photolithography, (A) Photosensitive material was exposed to the radiation resulting changing its property (B) Positive material was used as template for nanowires synthesis (Darling, 2005).

To make a microfluidic device, metal nanoelectrode structures were produced by blending traditional top-down lithography with nanogaps in the 10–50 nm regime, this would enable reliable measurement of the conducting properties of single molecules, nanoparticles and other low-dimensional materials (Srinivasana *et al.*, 2006). In addition, a microfluidic device was made by soft lithography for the fabrication of microchannels. The patterned energy responsive material such as polydimethylsiloxane (PDMS) and poly-methyl methacrylate (PMMA) is often used for pattern casting (Vlachopoulou *et al.*, 2005). This technique is powerful and widely

used, however making of nanowires with this technique is not very practical since it is very labor intensive.

4.2.2 Bottom up technique

The other type of nanofabrication is bottom up technique. Generally, this process involves the reduction of metal and electropolymerization of the polymer from the solution into the pore of the template. Either soft or hard template can be used in this approach (Leach *et al.*, 2007; Yogeswaran and Chen, 2008).

4.2.2.1 Soft template

This synthetic route is used to make common colloidal gold and various other nano-sized materials including magnetic, and semiconductor types. The basic procedure is to precipitate the ionized materials from a solution into a soft surfactant template by chemical reduction of the material. The shape and size of the material reduced out of solution can be controlled by varying the surfactant type and concentration, the material type and concentration, and the reducing agent type and concentration (Shankar and Raychaudhuri, 2005).

Generally, the above procedure can produce both spherical particles and rod-shape nanostructures. For example, when spherical micelles were used (Figure 4.2a) spherical particles were synthesized. In case of rod-shape nanostructure, it could be synthesized using cylindrical micelles shown in Figure 4.2b. There is report on the usage of gold with certain aqueous media surfactants such as hexadecyltrimethyl-ammonium bromide where rod-shaped nanoparticles were produced (Nikoobakht and El-Sayed, 2003), Pluronic 123 (P123) surfactant was used as a template to produce silver nanowires (Habib, 2006) and sodium dodecylbenzene sulfonate was used to synthesize Se/Te alloy nanowires with the length ranges from 300 nm to several μm (Qin *et al.*, 2006).

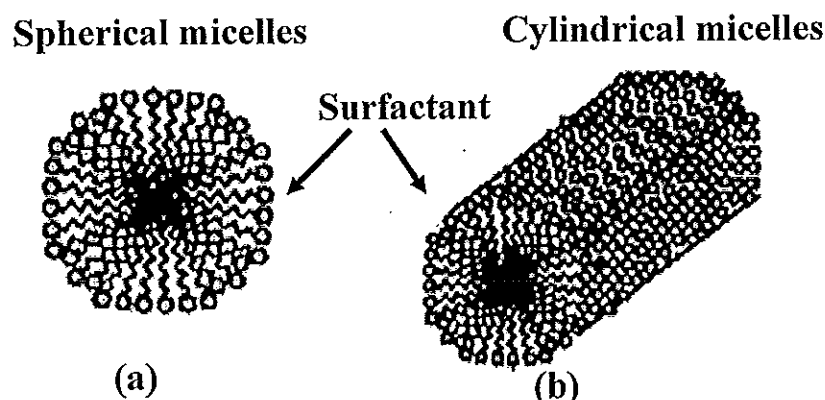


Fig. 4.2 Schematic illustrated of micelle soft template used for nanowires synthesis (a) spherical micelles for spherical particles (b) cylindrical micelle for rod-shape nanowires (Shankar and Raychaudhuri, 2005).

4.2.2.2 Hard template

In hard template synthesis, the material or template used for the growth of nanowires is acting as a working electrode. After the potential is applied, the nanowires start to grow inside the pore of the template. Generally, hard templates are rigid and non conducting. This means that the templates used for the electrochemical synthesis need a conductive layer on one side of the template. Therefore, the bottom-up synthesis can begin. The hard templates used for fabrication of nanowires include track etched membranes, alumina membrane and anodized aluminum oxide (AAO) membranes.

4.2.2.2.1 Track etched membranes

The technique is based on a heavy charge particle from nuclear radiation resource passes through a certain material such as mica film and leaves behind a track of radiation damage (Figure 4.3), called “Coulomb Explosion” phenomenon (He and Tao, 2003; Price and Walker, 1962). The minimum pore size of the track is only 2.5 nm. The track can be selectively etched in a suitable reagent, such

as hydrofluoric acid and the diameter of the pores can be controlled by controlling the etching time (Price and Walker, 1962).

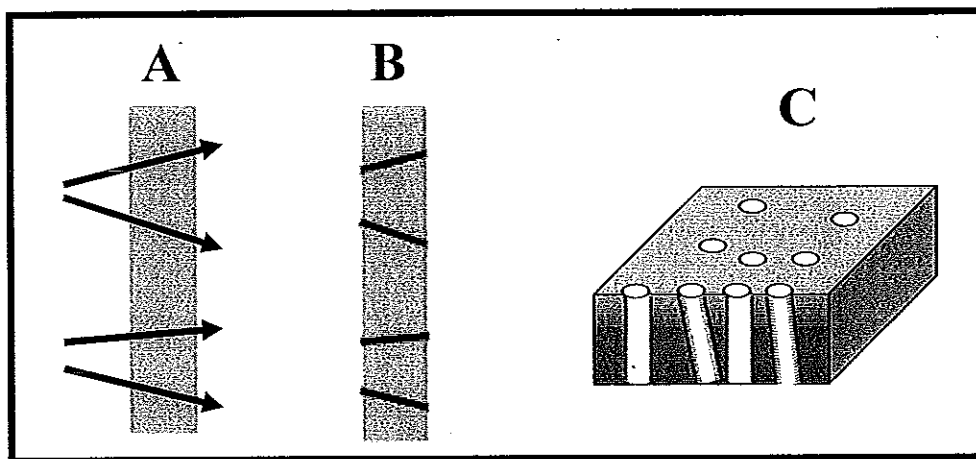


Fig. 4.3 Track-etch process for nanoporous membranes. A) heavy-charged particle pass through substrate B) Cylindrical pore in a mica C) Top view of nanomembrane

This technique can be applied to various substrates such as plastic membrane including polycarbonate membrane and polyester. Track etched polycarbonate membranes are merely thin pieces (standard thickness range from 6 to 20 μm) of polycarbonate that are bombarded with ions accelerated in a high potential gradient. Typical pore diameters for polycarbonate membranes can range from ten nanometers to several microns (Cao and Liu, 2008). An important advantage of these plastic templates over the mica films is that their surface wettings properties can be adjusted which is important for some applications. Some drawbacks of polycarbonate membranes include pores crossing paths inside the polymer and pore density (10^9 pores cm^{-2}). Pores tend not to be perfectly parallel to each other which is tolerable in many applications and complicate the interpretations of measured properties could be achieved. Membrane must be dissolved with an organic solvent to free the nanowires. The membranes are very flexible and somewhat hard to work with (He and Tao, 2003). They are however commercially available and inexpensive (Figure 4.4).

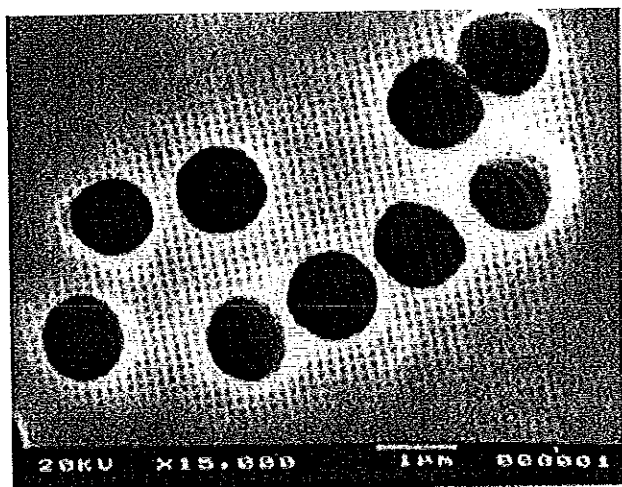


Fig 4.4 Electron micrograph of polycarbonate template membrane with 1 μm diameter pores (Hulteen and Martin, 1997).

4.2.2.2.2 Porous alumina membranes

Alumina membrane templates are the most common hard template used for nanowires synthesis (Figure 4.5). These templates are very rigid and have a very regular porous structure with pores ranging from 20 nanometers to a maximum of 200 nanometer (<http://www.whatman.com>, 2007). The benefits of these membranes are that they are commercially available and relatively inexpensive, rigid and slightly easier to handle although fragile, stable in slightly acidic to slightly basic solutions and have regular and cylindrical pores.

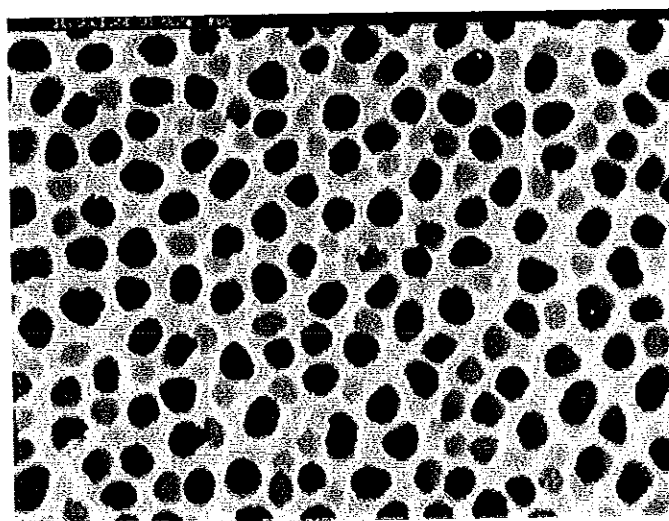
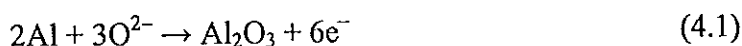
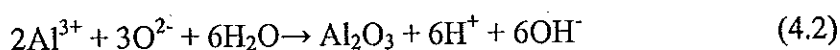


Fig 4.5 Electron micrograph of alumina membrane with 200 nm diameter pore (<http://www.whatman.com/PRODAnoporeInorganicMembranes.aspx>, 2007).

Another type of porous alumina template can be prepared via the anodization of aluminum film in acidic solution (Shankar and Raychaudhuri, 2005). This type of template can be fabricated easily. Before anodization the surface of Al sheet needs to be cleaned in acetone to remove impurities. The surface impurities can then be removed using 1% HF, 10% HNO₃, 20% HCl, and 69% H₂O by volume (Caffarena *et al.*, 2006). The diameter, depth of the pores and the space between each pore can be controlled by adjusting the anodization conditions *i.e.*, anodization voltage, time and electrolyte (He and Tao, 2003). During the anodization process, a voltage is applied to the Al sheet (anode). Oxidation occurs at the metal/oxide interface by the movement of oxygen ions (O²⁻ or OH⁻) from the electrolyte as shown in this reaction (Caffarena *et al.*, 2006);



This Al₂O₃ layer is called “barrier layer” (Saedi and Ghorbani, 2005). After the formation of Al₂O₃, the hydration reaction occurs causing the dissolution of the oxide layer as shown below (Caffarena *et al.*, 2006);



The occurrence of electrons at the anode is then ejected to the solution and forming hydrogen gas with hydrogen ion at the cathode as shown below (Sarkar *et al.*, 2007);



O^{2-} moves toward the Al sheet and the porous alumina oxide layer form. When Al^{3+} is ejected into the solution at the oxide/electrolyte interface the pores are formed. These porous alumina structures are separated from Al substrate by barrier layer (Saedi and Ghorbani, 2005).

The individual nanopores in the alumina can be ordered into a close-packed honeycomb structure (Figure 4.6). The pore density could be up to 10^9 - 10^{11} pores cm^{-2} which allows large scale nanowire production, the pore diameter ranges from 4–200 nm and pore length from 1–50 μm (Sarkar *et al.*, 2007). Therefore, various sizes of nanowires can be synthesized. The anodized alumina oxide templates are easily dissolved with alkaline solutions most commonly sodium hydroxide (NaOH) (reaction 4.4) (Cao and Liu, 2008) to obtain free-standing nanowires (Caffarena *et al.*, 2006).

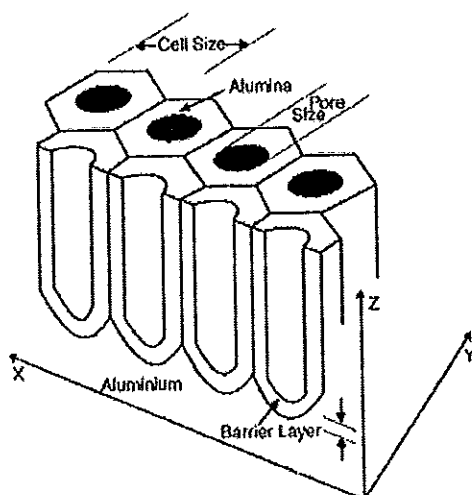
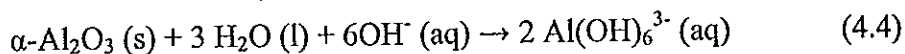


Fig. 4.6 Schematic diagram of a porous anodic alumina film on aluminum, showing honeycomb pores structure in cross-section (Saedi and Ghorbani, 2005).

4.3 Electrochemical deposition

There are several ways to fill the nanopores with metals or other materials to form nanowires, but the electrochemical method is a general and versatile method. Electrochemical deposition or electrodeposition is the technique that external electric field was applied, to diffuse charged reactive species to be deposited at the electrode. In general, this method is suitable for electrical conductive materials such as metal, alloys, semiconductor and conductive polymers. Electrochemical deposition can be accomplished by coating one side of the membrane with conductive layer. In this process, at the initial deposition, the electrode was separated from the depositing solution. The electrical current must go through the deposit to allow the deposition process to continue. The electrode potential was described by Nernst equation (Bard and Faulkner, 2000; He and Tao, 2003);

$$E = E^{\circ} + \frac{RT}{n_i F} \ln(a_i) \quad (4.1)$$

Where E° is the standard electrode potential, a_i the ion activity, F the Faraday's constant, R the gas constant and T the temperature. When the electrode potential is more negative (higher) than the energy level of vacant molecular orbital in the electrolyte solution, electron transferred from electrode to the solution as shown in Figure 4.7a. In this stage the reduction process occurs. When electrode potential is more positive (lower) than the energy level of the occupied molecular orbital the electron transferred from the electrolyte solution to electrode (Figure 4.7b) the oxidation process occurs and the reaction stops when the equilibrium is reached (Bard and Faulkner, 2000).

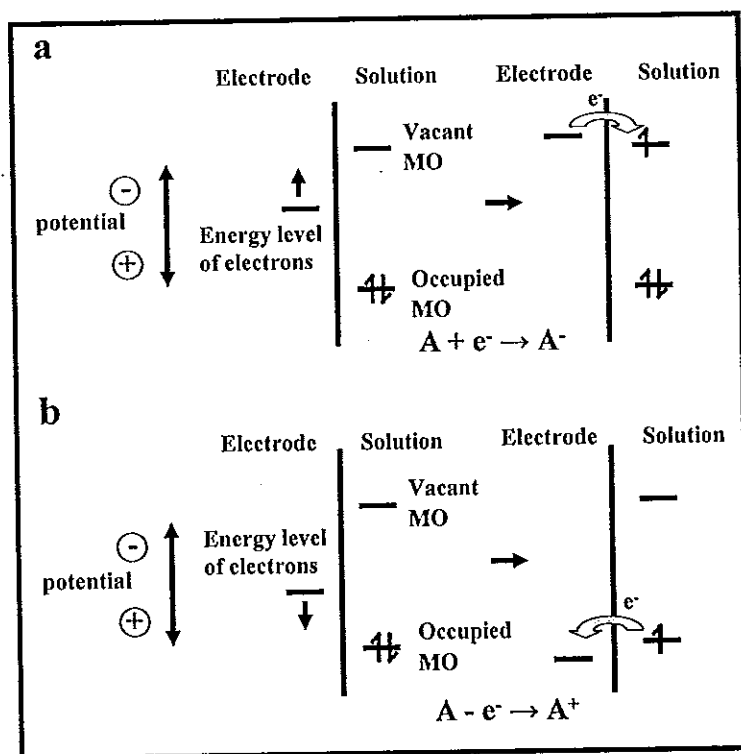


Fig. 4.7 Schematic diagram showing a reduction (a) and oxidation (b) process of a species A in solution. MO: molecular orbital (Bard and Faulkner, 2000).

In the electrodeposition technique the membrane with conductive layer was set up as shown in Figure 4.8. The conducting layer contacted with the working electrode therefore, the template acted as a working electrode. On the other side is the plating solution (Figure 4.8A). The deposition process starts from the bottom of the membrane and proceeds to the top. The current during the electrodeposition step is presented in Figure 4.8B. Since the membrane pores are very small, at the beginning the solution moves slowly into the pores and electrodeposition gradually takes place. This can be observed from the gradually increase of current (I) until the bottom of the pores are completely filled with metal. Then the current increase rapidly since the contact area with the electrolyte increases (II). Finally, the current is constant showing that the pores are completely filled with nanowires (III) (Cao and Liu, 2008).

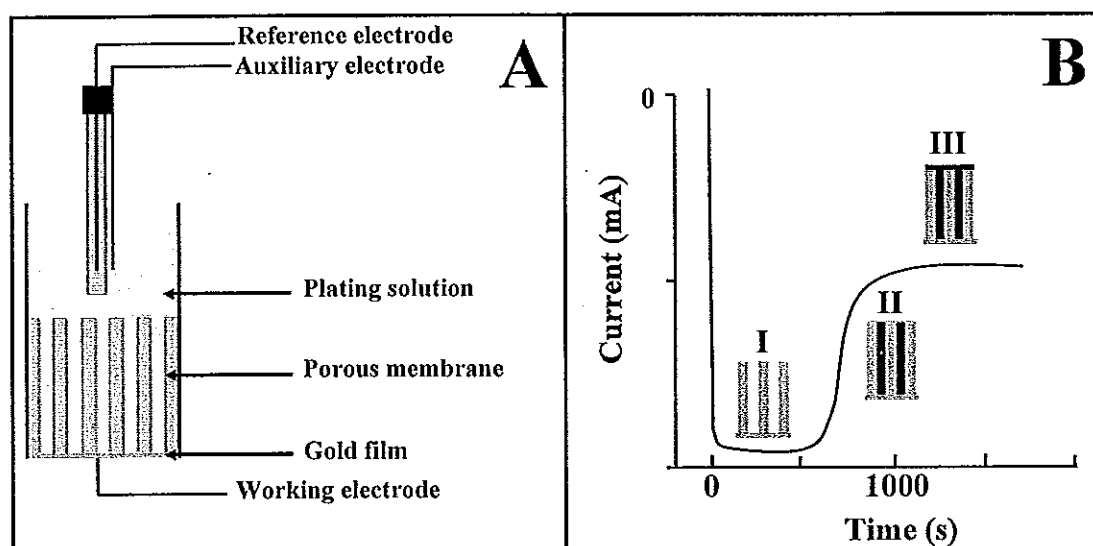


Fig. 4.8 Experimental set up of (A) the template-based assist electrodeposition technique (B) Current-time for the electrodeposition of Ni nanowires into a polycarbonate membrane with 60 nm diameter pores at -1.0 V (Whitney *et al.*, 1993).

The growth of nanowires using conductive material in electrodeposition technique can be divided into metals and alloy, metal oxide, semiconductors, conductive polymers and composite nanowires (He and Tao, 2003; Hulteen and Martin, 1997; Meenach *et al.*, 2007).

4.3.1 Metals and alloy

Various metals and alloys have been used to synthesize nanowires. For example, Bi nanowires with diameter of 40, 70 and 100 nm have been synthesized by electrochemically depositing Bi into porous polycarbonate membrane. Figure 4.9A shows TEM image of Bi nanowires (Tian *et al.*, 2006). In another work, Pd nanowire arrays were prepared by pulsed electrodeposition (PED) method using anodic alumina oxide (AAO) template. The diameter of prepared Pd nanowires was 80 nm. The SEM image of free standing Pd nanowires is shown in Figure 4.9B (Kim *et al.*, 2006). In addition to solid nanowires, porous Au was also fabricated via electrodeposition of Ag/Au alloy followed by acid etching of Ag component using alumina membrane

template with 200 nm pore size. SEM imaging was used to study the characteristic and pore size of porous gold nanowires as presented in Figure 4.9C (Liu and Searson, 2006). To obtain more functional nanowires, multisegment nanowires were also synthesized by electrodeposition method. The mixture of metals plating solution was used to obtain strip nanowires of Fe/Au. TEM image of these nanowires is as shown in Figure 4.9D (Lee *et al.*, 2007).

Besides pure metal, alloy nanowires could also be generated. Two-metal alloy nanowires, Fe-Pd, has been fabricated by alternating current electrodeposition into nanoporous anodic alumina and then TEM image is presented in Figure 4.9E (Fei *et al.*, 2007). Alloy nanowires employing three types of the metal have also been prepared, for example, Ni-Fe-Co alloy nanowire was grown by electrodeposition method using anodic aluminum oxide as a template. The SEM images of such nanowires were presented in Figure 4.9F (Saedi and Ghorbani, 2005).

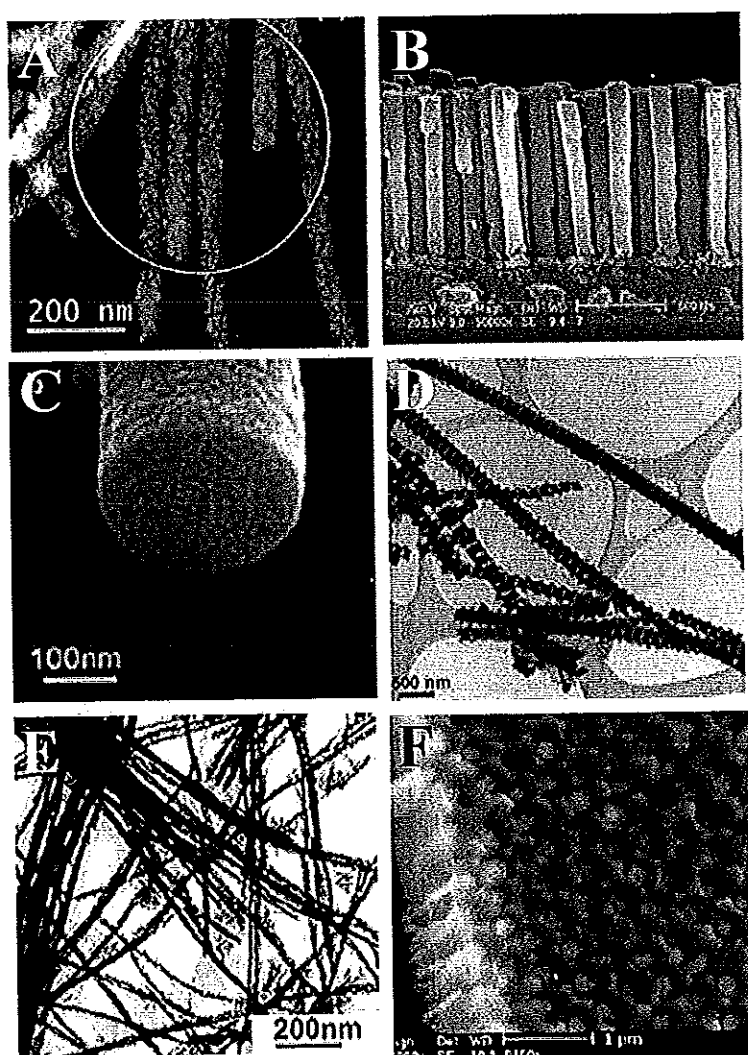


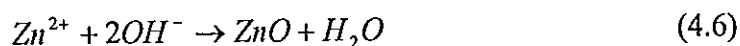
Fig. 4.9 Images of metal nanowires using electrodeposition technique (A) TEM image of Bi nanowire (Tian *et al.*, 2006) (B) SEM image of free standing Pd nanowires (Kim *et al.*, 2006) (C) SEM image of porous gold nanowires (Liu and Searson, 2006) (D) TEM image of Fe/Au nanowires (Lee *et al.*, 2007) (E) TEM image of the Fe-Pd alloy nanowires (Fei *et al.*, 2007) (F) SEM image of Ni-Fe-Co alloy nanowires (Saedi and Ghorbani, 2005).

4.3.2 Metal oxide nanowires

Metal oxide nanowires can be synthesized either by electrodeposition of metal into the membrane pores or electrodeposition of metal followed by oxidation method. For example, MnO_2 nanowires were fabricated on anodized aluminum oxide membrane (Kim *et al.*, 2008). In this work, 1 M MnSO_4 and 0.5 M H_2SO_4 plating bath was used then anodic electrodeposition was performed following with dissolution of the template. In another work SnO_2 nanowire arrays were fabricated by electrochemical deposition and thermal oxidizing methods (Zheng *et al.*, 2001). Sn nanowires were electrodeposited into the porous of the membrane. A plating solution contain 7 g L^{-1} $\text{SnCl}_2 \cdot 2\text{H}_2\text{O}$, and 25 g L^{-1} $\text{Na}_3\text{C}_6\text{H}_5\text{O}_7 \cdot 2\text{H}_2\text{O}$ solution at room temperature. After Sn nanowire array was synthesized, the systems were annealed in the air at different temperatures resulting in oxidization of Sn to form SnO_2 nanowire array. The prepared SnO_2 nanowires are equal in height and uniformly embedded in the alumina membrane (Figure 4.10A). ZnO nanowires were also synthesized by electrochemical deposition within a porous polycarbonate membrane (Leprince-Wang *et al.*, 2005). The sizes of pores were 10 to 90 nm in diameter. ZnO electrodeposition involves in two steps, first generating hydroxide ions at the electrode surface by reducing hydrogen peroxide (oxygen precursor) at the cathode, reaction 4.5, then deposition of zinc ion in the pore of working electrode.



The overall deposition reaction of ZnO in the presence of H_2O_2 can be written as reaction 4.6:



4.3.3 Semiconductors

In case of semiconductor nanowires only co-deposition was performed. For example, CdS nanowires were prepared by template-electrodeposition in aqueous solution of Cd^{2+} from CdSO_4 and $\text{S}_2\text{O}_3^{2-}$ from $\text{Na}_2\text{S}_2\text{O}_3$ solution following reaction 4.7 and 4.8 (Yang *et al.*, 2006).



Ag₂Se nanowire arrays had also been prepared by electrodeposition from non-aqueous dimethyl sulfoxide solutions (Chen *et al.*, 2003). This nanowire was synthesized from the reduction of Ag⁺ to Ag and Se⁴⁺ to Se and then further reduction to Ag₂Se (Reaction 4.9). SEM image of Ag₂Se was presented in Figure 4.10B.

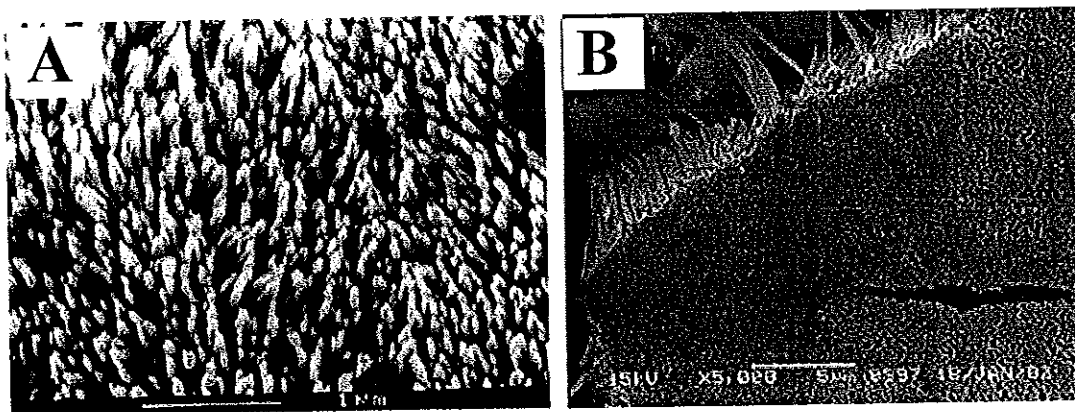
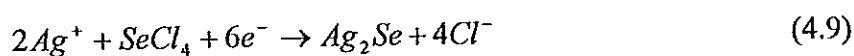


Fig. 4.10 SEM image of (A) SnO₂ nanowires (Zheng *et al.*, 2001) (B) Ag₂Se nanowire arrays

4.3.4 Conductive polymers

Conducting polymers such as polypyrrole (Jérôme *et al.*, 2004; Wang *et al.*, 2006), poly(methyl pyrrole) (Ramanathan *et al.*, 2007) and polyaniline (Wang *et al.*, 2006) have many advantages since they exhibit electrical, magnetic and optical properties. Conducting polymer nanowires have a promise potential for electronic and sensor applications. A mechanism of the formation of polypyrrole nanowire onto the surface of an electrode using the anodic electropolymerization process after electrografting a poly(alkylacrylate) film was proposed (Jérôme *et al.*, 2004). The experimental conditions for the pyrrole oxidation, type of solvent, concentrations of

monomer and supporting electrolyte, have been investigated. The characteristic of polypyrrole was investigated by SEM (Figure 4.11A). A new approach for the in situ electrochemical fabrication of an array of conducting polymer nanowires (CPNWs), polypyrrole and polyaniline, positioned within an integrated microfluidic device (Figure 4.12B) was introduced by using spatially localized, template-free electrochemical polymerization and also demonstrate that such an integrated device can be used as a NH_3 sensor immediately after its construction (Wang *et al.*, 2006). In the case of poly(methyl pyrrole) nanowires, they were in-situ synthesized by electrochemical polymerization of 1-methyl pyrrole with chloride and p-toluene sulfonate dopants in nanochannels for microfluidic device shown in Figure 4.11C (Ramanathan *et al.*, 2007). This type of nanowire was prepared in between microfabricated gold electrodes and used for biomolecule entrapment.

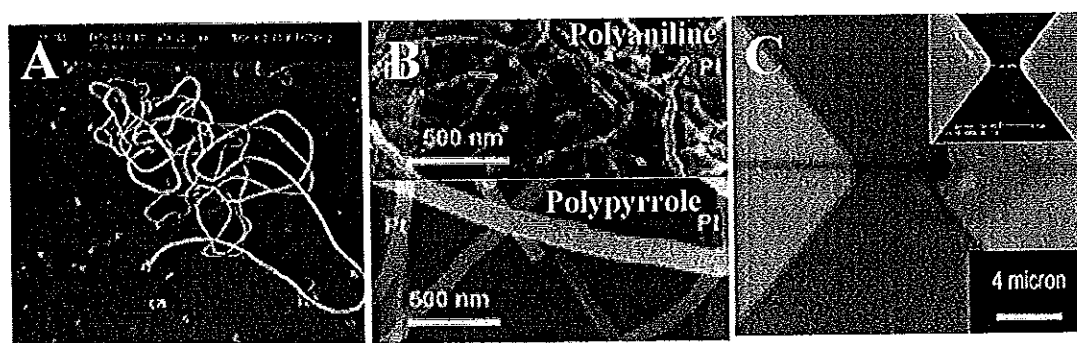


Fig. 4.11 SEM image of conducting polymer nanowires prepared by electrochemical technique: (A) Polypyrrole (B) Polyaniline and polypyrrole (C) Poly(methyl pyrrole) nanowires

4.3.5 Composite nanowires

Similar to metals, semiconductors and conductive polymers, composite nanowires can grow directly from solution using template-based electrochemical deposition. For example, polyaniline/ Bi_2Te_3 nanowires have been prepared by chemical and electrochemical reactions on a porous alumina template (Xu *et al.*, 2005). In this research, polyaniline was electropolymerized at room temperature. Polyaniline preferentially nucleates and grows on the pore walls resulting in a tubular

structure. However if longer polymerization was allowed solid fibril was formed. This tubule structure of polyaniline could be used as second-order template to electrochemically deposit bismuth telluride (Bi_2Te_3) into its pore. SEM image of polyaniline/ Bi_2Te_3 nanowires are shown in Figure 4.12A. In another approach, polypyrrole/porous gold nanowires have been developed by electrochemical deposition of Ag/Au alloy nanowires followed by chemical etching of silver component to obtain porous gold structure, then back filling of polypyrrole was performed. This resulted in polymer surrounding porous gold nanowires therefore the composite nanowires was obtained (Figure 4.12B) (Meenach *et al.*, 2007). Hybrid nanowires, nickel/3,4-ethylene-dioxythiophene, have been also developed using alumina membrane as a template (Lallemmand *et al.*, 2008). Nickel nanowires were electrodeposited and changed to another electrochemical plating cells where 3,4-ethylene-dioxythiophene (PEDOT) was electropolymerization in the pores on top of nickel. Therefore hybrid nanowires of PEDOT/Ni, clearly distinguishing the metal part from the polymer part, could be obtained (Figure 4.12C).

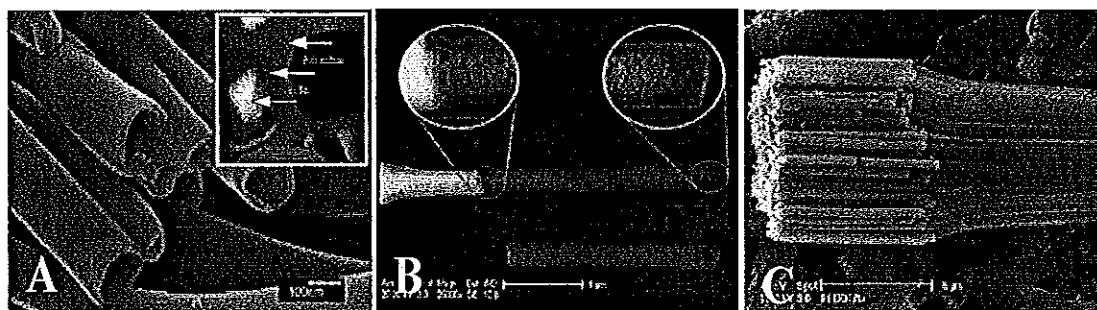


Fig. 4.12 SEM image of composite nanowires (A) Polyaniline deposited inside alumina membrane and work as a second-order template, inset show Bi_2Te_3 nanowires surrounded by polyaniline (Xu *et al.*, 2005) (B) Polypyrrole/porous gold nanowires (Meenach *et al.*, 2007) (C) Nickel/3,4-ethylene-dioxythiophene nanowires (Lallemmand *et al.*, 2008).

4.4 Characterization of nanowires

4.4.1 Optical microscopy

Optical microscopy provides information about the physical characteristic of nanomaterials. However, when the object is small, some limitation due to the equipment resolution will occur. The resolution of the image is limited by diffraction of the wavelength of the light (λ), the smallest distance (d_{\min}) between two points for the resolution is derived from;

$$d_{\min} = \frac{\lambda}{2NA} \times 1.22 \quad (4.2)$$

where NA is the numerical aperture of the objective lens. This should be as large as possible since it can improve either resolution or collective efficiency (Günzler and Williams, 2002). Typically, a high value of NA would be ca. 1.4. This gives the resolution limit of an objective in violet light ($\lambda=400$ nm) to be 142 nm. Practically, the resolution limit is greater than 200 nm due to non ideal systems, and even when an object on that size scale may not be able to be resolved and it may be blurred.

4.4.2 Electron microscopy

The electron microscope is the equipment that uses a beam of highly energetic electrons to examine objects on a very small scale to sub-nanometers. The investigation can yield surface features, shapes and size of the object, also the composition and crystallographic information. This instrument was developed due to the limitations of light microscopes which are limited by the physics of light to 500x or 1000x magnification and a resolution of 200 nanometers. Electron microscopes (EMs) use a focused beam of electrons instead of light to "image" the specimen and gain information as to its structure and composition. The basic steps involved in all electron microscopes are that electrons produced by the electron source are accelerated toward the sample using a positive electrical potential. This stream is confined and focused using metal apertures and magnetic lenses into a thin, focused, monochromatic beam. This beam is focused onto the sample using a magnetic lens.

Interactions occur inside the irradiated sample, affecting the electron beam. These interactions and effects are detected and transformed into an image (Amelinckx *et al.*, 1997).

4.4.2.1 Scanning electron microscopy (SEM)

The scanning electron microscope is a type of electron microscope that images the sample surface by scanning with a high-energy beam of electrons in a raster scan pattern. SEM has a magnification range from 15x to 200,000x and a resolution of 5 nanometers (Amelinckx *et al.*, 1997).

The SEM requires conductive objects for the electron beam to scan the surface and that the electrons have a path to ground. All samples must also be prepared to an appropriate size to fit in the specimen chamber and generally mounted on some sort of holder. Nonconductive materials are needed to coat with a layer of conductive material such as, gold, gold/palladium alloy, platinum, tungsten or graphite by low vacuum sputter coating or by high vacuum evaporation. This is done to prevent the accumulation of static electric charge on the sample during electron irradiation. Another reason for coating, even when there is more than enough conductivity, is to improve contrast and resolution (Günzler and Williams, 2002).

4.4.2.2 Transmission electron microscope (TEM)

Transmission electron microscope is a microscopy technique whereby a beam of electrons is transmitted through an ultra thin specimen, the electron which passes through the object will be recorded, and this provides the high resolution image. However, there are some drawbacks to the TEM technique in which many samples require a sample preparation step to produce a sample thin enough to be electron transparent, which makes TEM analysis a relatively time consuming process with a low throughput of samples (Günzler and Williams, 2002).

4.4.3 Atomic force microscopy (AFM)

Although optical microscopy and electron microscopy can provide two-dimensional magnified images of an object's surface, the images obtained are typically in the plane horizontal to the surface of the object. Such microscopes do not readily supply the vertical dimensions of an object's surface, the height and depth of the surface features. To gain such information, atomic force microscopy is now readily applied. Unlike traditional microscopes, the AFM does not rely on electromagnetic radiation such as photon or electron beams to create an image. An AFM is a mechanical imaging instrument that measures the three dimensional topography as well as physical properties of a surface with a sharpened probe or AFM tip. This tip is positioned at the end of a cantilever beam. When the tip is attracted to the object's surface, the cantilever beam is bent. The magnitude of the bend is detected by a laser that reflects at an oblique angle. A plot of the laser deflection versus tip position on the sample surface provides the surface characteristics that constitute the topography of the surface (Figure 4.13). AFM can operate on both conducting and non-conducting surfaces (Birdi, 2003). Atomic force microscopy is a very high resolution type of scanning probe microscopy to the nanometer scale. The AFM is one of the most important tools for imaging, measuring and manipulating matter at the nanoscale which uses piezoelectric elements for accurate and precise movements (Günzler and Williams, 2002).

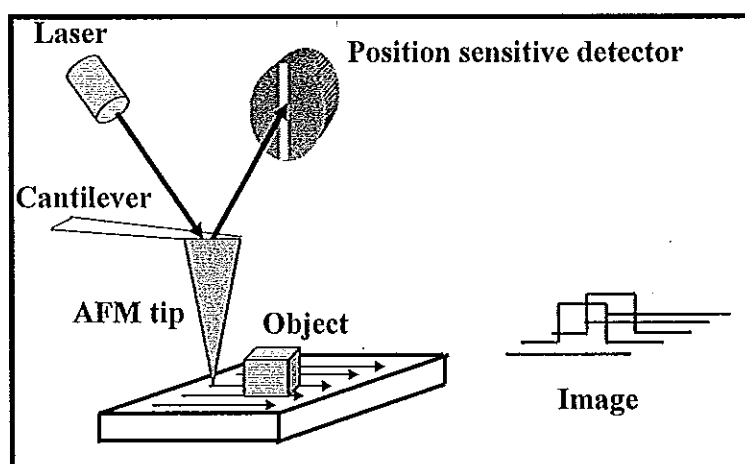


Fig. 4.13 Schematic diagram of atomic force microscope (AFM)

4.4.4 X-ray Fluorescence (XRF)

X-ray fluorescence spectrometry is the technique that used the primary x-ray excitation source from an x-ray tube to bombard the matter, when the atom is bombarded. An electron from the inner shell is ejected resulting in a vacancy. At this stage the atoms are not stable and try to return to its stable condition by transferring the electron from the outer shell to the inner shell and this process give off a characteristic x-ray fluorescence. Each metal has unique energy levels, therefore x-rays at a unique set of energies could be achieved (Günzler and Williams, 2002). This technique provides the information of an element by measuring the x-ray emission wavelength and energy including the qualitative and quantitative analysis data by measuring the emitted characteristic line intensity. Then the relation of the peak intensity with peak energy and metal concentration could give the qualitative and quantitative information (Christian and O'Reilly, 1986).

4.5 Applications

Nowadays, nanowires become interesting for research since they provide great promised applications in many fields such as sensor device and security systems. Some of these applications are summarized as follows.

4.5.1 Nanowires for bioapplications

In bioapplications, nanowires are widely used to functionalize for multiplexed biodetection due to the large surface area-to-volume ratio of nanowires. In addition, their properties can be designed for specific biological applications. Multiplexed bioapplication is the method to investigate multiple reactions in a single sample. There is reported on the formation of bimetallic nanostructures through chemical synthesis. For example, an Ag-Au bimetallic nanowire was synthesized by sequential electrochemical deposition of metal within a porous membrane template (Keating and Natan, 2003). The basic concept of novel route for multiplex biodetection is that the introduction of different metals allows for the selective

functionalization of portions of the nanowires. In order to achieve successful functionalization, each reaction needs to correspond to the unique properties of the metal. For example, gold nanowires are most often functionalized with thiols, while nickel is most often functionalized with carboxylic acids, which bind to the native oxide layer on the metal (Birenbaum *et al.*, 2003). Keating and Natan proposed that biomolecules (antibodies) can be functionalized on the bimetallic nanowires surface which can further bind with the analyte in the solution then another fluorescent tag secondary antibody was added for detection. In this work, reflectivity of bimetallic nanowires of different sequential and length of Au-Ag (different functionalized antibody) was investigated (Figure 4.14A). Therefore, different reflectivity pattern was achieved. Then, three simultaneous sandwich immunoassays can be performed, reflectivity and fluorescence was measured for each nanowire as shown in Figure 4.14B (Keating and Natan, 2003). From the fluorescence study then the information of analyte presented in the sample could be interpreted.

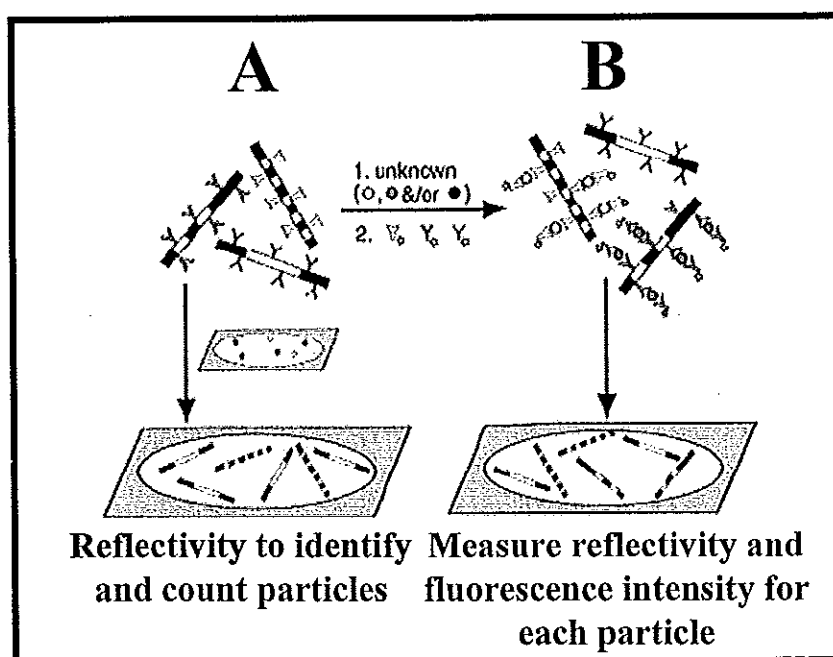


Fig. 4.14 Barcode nanowires for bioanalysis (A) reflectivity can be used to identify and quantify particles (B) Reflectivity and fluorescence intensity is measured for each particle (Keating and Natan, 2003).

A nanowire used as an alternative substrate for sandwich immunoassays was also reported (Tok *et al.*, 2006). Strip nanowires of Au and Ag were prepared by electrodeposition within a porous alumina template. An optical reflectance image provides the identify stripe pattern of nanowires, while fluorescence images report information on the binding between the antibody-conjugated nanowires and a fluorophore-tagged antigen target. In this study the capability of directly detecting potential biological warfare agents in both clinical and environmental samples was investigated. Three nonpathogenic simulates used are *Bacillus globigii* (Bg) spores to simulate *Bacillus anthracis* and other bacterial species, RNA MS2 bacteriophage to simulate Variola (virus for smallpox) and other pathogenic viruses, and ovalbumin (Ova) protein to simulate protein toxins such as ricin or botulinum toxin were used. The detection process is illustrated in Figure 4.15. The identity of the antigen present can be identified from the stripe pattern of the nanowires. For example, the fluorescently labeled antibody-Bg attached to nanowire to which antigen-Bg spore was attached and has a stripe pattern of 011110 (0=Au, 1=Ag). Therefore, this strip pattern 011110 nanowire gave fluorescence (Figure 4.15C). This indicates that Bg spores are present in the test sample mixture. Nanowires with the stripe patterns 010000 (functionalized with antibody-Ova) or 010100 (functionalized with BSA; negative control) are not fluorescent, thus indicating that the test sample does not contain Ova proteins.

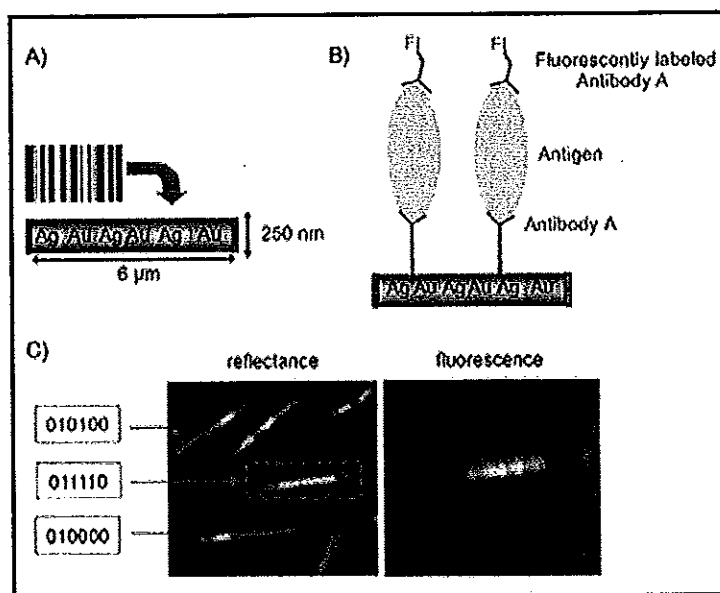


Fig. 4.15 Schematic diagram illustrated the encoding process of strip nanowires for biological detection. A) Analogy between a conventional barcode and a metallic stripe encoded nanowire. B) Schematic of the sandwich immunoassay performed on a nanowire. C) Reflectance and fluorescence readout of the nanowires (Tok *et al.*, 2006).

4.5.2 Nanowires for non-bioapplications

Nanowires for non-biological applications such as product tracking, inventory and library are widely studied. They play an important role not only for the security system but also chemical sensor since they are small, robust, and provide uniquely identifiable. The applications of nanowires for non-biological samples are focused in the following sections.

4.5.2.1 Security systems

The role of nanowires in security systems, for example, strips of nanowires of gold and silver prepared from sequential deposition was synthesized and provide a great promise to be used as a product tracking (Figure 4.16) (Lee *et al.*, 2007; Nicewarner-Peña *et al.*, 2001; Reiss *et al.*, 2002; Walton *et al.*, 2002).

Reflectivity was used to identify the pattern of nanowires strip and was demonstrated to use as a barcode system.

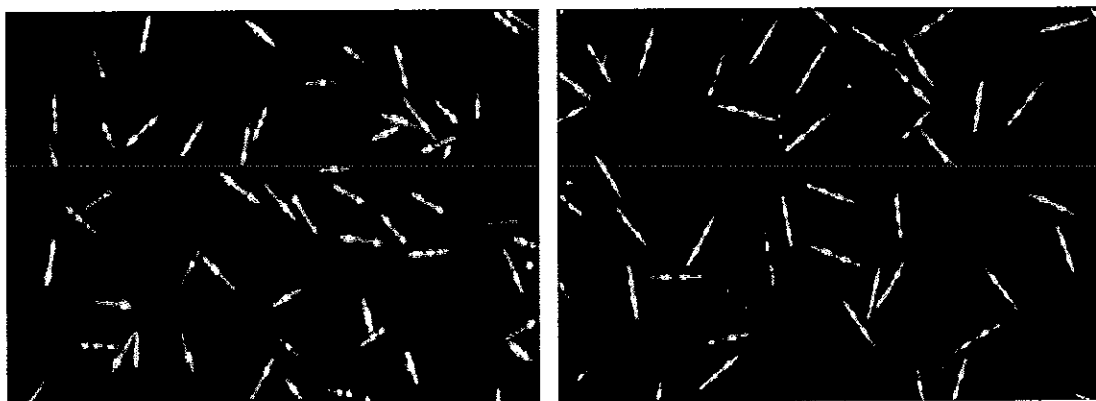


Fig. 4.16 Optical images of different strip pattern nanowires prepared from sequential electrodeposition of gold and silver (Nicewarner-Peña *et al.*, 2001; Reiss *et al.*, 2002).

However, the preparation of multisegment nanowires is time-consuming, and requires careful control of the growth process along with replacement of the metal solutions. In addition, optical readout is not a convenient tool for studying the level of the corresponding metal compositions. Therefore, a single step preparation of barcode alloy nanowire using template-assisted electrodeposition was proposed (Wang and Liu, 2006). In this technique, indium-lead-bismuth nanowires were prepared and dissolved in HNO_3 . Square-wave voltammetric (SWV) were performed for measurements of metal composition and concentration (Figure 4.17). The SWV resulting signatures correlated with composition of the metal mixture in plating solution, indicating reproducible plating processes and suitable to be used as barcode.

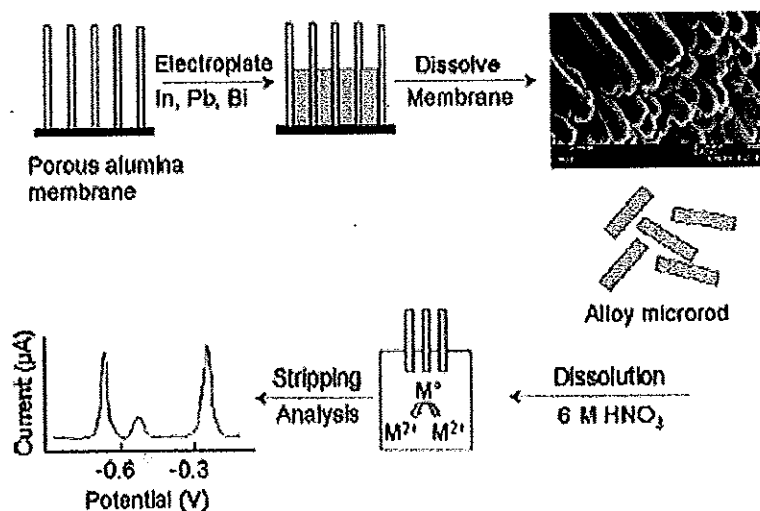


Fig. 4.17 Alloy nanowires barcodes prepared from chemically electrodeposition following with SWV measurement. SEM image shows alloy nanowires prepared (Wang and Liu, 2006).

4.5.2.2 Chemical sensors

In chemical sensor applications, nanowires modified electrode was proposed. For example, Li and Lin (Li and Lin, 2007) used Au-nanoparticle/polypyrrole composite nanowires to modify glassy carbon electrode. At the beginning polypyrrole nanowires were prepared and electrochemically deposited onto glassy carbon electrode following electrochemical deposition of gold nanoparticle onto polypyrrole nanowires (Figure 4.18). This electrode was used for hydrazine and hydroxylamine detection (Li and Lin, 2007). In addition, metal nanowires with enzyme modified electrodes were widely studied. For example, gold nanowires have been prepared by electrodeposition process whereas polycarbonate membrane was used as a template (Lu *et al.*, 2007). These nanowires were functioned with glucose oxidase. The functionalized gold nanowires were then dispersed in chitosan solutions and dropped onto the glassy carbon electrode surface. This electrode has been used for H_2O_2 determination. Gold nanowires were not only used for electrode modification but also used for micro-fluidic chips. For example, gold

nanowires prepared from electrodeposition onto 200 nm alumina membrane template were fabricated onto micro-fluidic platform (Aravamudhan *et al.*, 2007). This modified micro-fluidic platform was fabricated onto silicon substrate using photolithography. This device was developed for cholesterol detection. The systematic set up is shown in Figure 4.19. Similar to gold nanowires, platinum nanowires were also prepared from electrodeposition technique (Qu *et al.*, 2007). Then, platinum nanowires were mixed with carbon nanotubes and chitosan for casting onto the glassy carbon electrode surface. Finally, the glucose oxidase was functionalized onto this modified electrode for H_2O_2 determination.

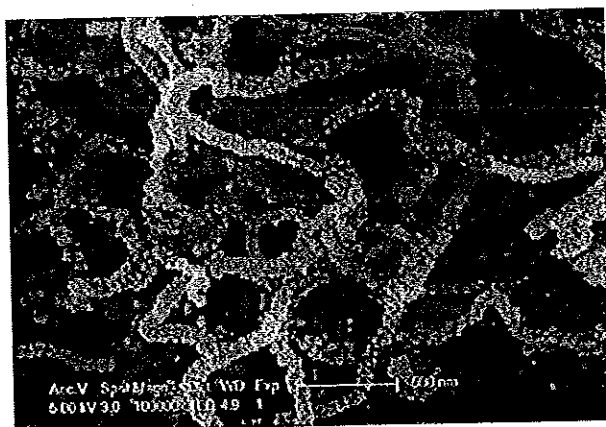


Fig. 4.18 Au-nanoparticle/polypyrrole composite nanowires modified glassy carbon electrode for hydrazine and hydroxylamine detection (Li and Lin, 2007)

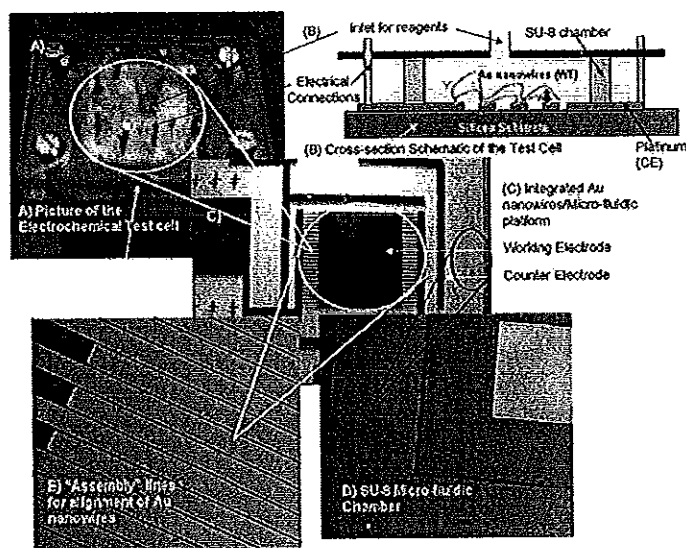


Fig. 4.19 (A) Electrochemical test set up (B) Cross-sectional schematic of the test cell, with nanowires aligned on the platinum (C) Micro-fluidic platform in silicon with electrodes/gold nanowires and SU-8 chamber. (D) Platinum “assembly” lines for nanowire alignment. (E) Hard-baked SU-8 micro-fluidic chamber (Aravamudhan *et al.*, 2007).

4.6 Conclusions

Electrochemical methods for nanowires synthesis via template-assisted have been widely used due to its simplicity and flexibility. Size (diameter and length) of the nanowires can be made as thin as a single atom to μm by controlling the deposition conditions. Various conducting materials can be used to synthesize nanowires including metals, polymers and semiconductors. In addition, composite material is possible to generate in order to develop the properties of nanowires. Several techniques were brought to study and characterization of nanowires properties such as optical microscope SEM, TEM and AFM. Due to the unique properties of nanowires, mechanical stability, light weight, enhancement in the current, therefore various applications of nanowires were investigated such as chemical and biological sensors including nanowires functionalization. Also, their electrical, thermal,

magnetic and optical properties are prominent therefore it is possible to use nanowires for development of optical and nano-electronic devices. From the review in this chapter, in a few more years nanowires will become even more prominent among researchers and in the market.

CHAPTER 5

On-Line System for Trace Organic Compounds by Gas Injection Membrane Extraction

5.1 Introduction

Volatile organic compounds (VOCs) are commonly used in manufacturing or industries with various functions, including degreasing, lubricating, fueling, stripping or thinning paint and cleaning (Rafson, 1998). The widely used VOCs can cause contamination of the environment which may have an adverse effect to human health (Rafson, 1998). Due to their high toxicity, it is necessary to monitor VOCs.

A priority for the determination of contaminated VOCs in water is sample preparation, to separate analytes from the matrices. The frequently used sample preparation techniques are liquid-liquid extraction (LLE) (Golfinopoulos *et al.*, 2001; Keller and Bierwagen, ; Santos and Galceran, 2002), purge and trap (P&T) (Golfinopoulos *et al.*, 2001; Lara-Gonzalo *et al.*, 2008; Santos and Galceran, 2002), headspace analysis (HS) (Golfinopoulos *et al.*, 2001) and solid phase microextraction (SPME) (Lara-Gonzalo *et al.*, 2008; Santos and Galceran, 2002). However, those methods have some disadvantages such as long analysis time, using toxic solvents and exhibiting high cost (Golfinopoulos *et al.*, 2001; Kou *et al.*, 2001). To solve these problems, membrane extraction is now being applied for sample preparation to provide faster, easier, cheaper and more efficient analysis than other separation techniques (Peng *et al.*, 2003; Pinto *et al.*, 1999).

Most research on membrane-based separation technique for VOCs in water were done by continuously passing the sample through the hollow fiber membrane (Hasanoglu *et al.*, 2005) or using deionized water as carrier stream to deliver the sample to the membrane (Bishop and Mitra, 2004). However, a boundary layer is formed between membrane and aqueous sample resulting in higher resistance to mass transfer, longer extraction time and lower response (Bishop and Mitra, 2004;

Keller and Bierwagen, 2001; Melcher and Morabito, 1990). To overcome this problem, gas injection membrane extraction (GIME) was introduced (Kou *et al.*, 2001). In this technique, the liquid sample is placed direct contact to the hollow fiber. A nitrogen stream is used to inject the liquid sample through the hollow fiber in order to reduce the boundary layer between the membrane surface and liquid sample, which can reduce the analysis time and increase the diffusion.

In this study, the use of GIME was investigated for trace organic compounds focusing on methanol, ethanol, 1-propanol, MIBK and MTBE. These were selected as representative compounds because they are widely used in industrial application and their contaminations are found in various matrices such as wastewater and biosolids sample. In this work, three types of sample were studied, *i.e.*, ground water, wastewater and biosolids.

5.2 Experimental

5.2.1 Chemical and reagent

Stock standard solutions were prepared from methanol (99.8%, AR grade, Lab Scan, Thailand), ethanol (99.8%, AR grade, Carlo Erba), 1-propanol (99.5%, AR grade, Lab Scan, Thailand), methyl-isobutyl ketone (MIBK) (99.5%, ACS-for analysis, Carlo Erba) and tert-butyl methyl ether (MTBE) (99.5%, Fluka, Switzerland). Ultra pure water was used in all aqueous sample preparation (Millipore water system, USA).

5.2.2 Instrumentation

Figure 5.1 shows a schematic diagram of the system. A peristaltic pump (Miniplus 3, Gilson Co. Inc., USA) was used to deliver the aqueous sample to a 10-port valve (Valco Instruments Co. Inc., Houston, TX, USA), where a known volume of sample was injected. Nitrogen (99.995% purity, Thai Industrial Gases Public Company Limited, Thailand) was used as carrier stream to deliver the aqueous sample through the hollow fiber membrane module where the analyte permeated and

transported by carrier gas to be adsorbed in a microtrap (μ -trap) as shown in Figure 5.2 (see 5.2.5). It was then thermally desorbed, transported to another 10-port valve before being injected into a gas chromatograph with flame ionization detector (FID). All analytes were separated using HP-FFAP fused silica capillary column (30 m \times 0.32 mm i.d. film thickness 0.25 μ m, Agilent Technology, USA). The results were integrated by CR-4A Chromatopac integrator (GC-15A and CR-4A Chromatopac, Shimadzu, Japan). Gas chromatograph conditions *i.e.*, carrier gas flow rate, make up gas flow rate, column and detector temperature were optimized to obtain the best performance.

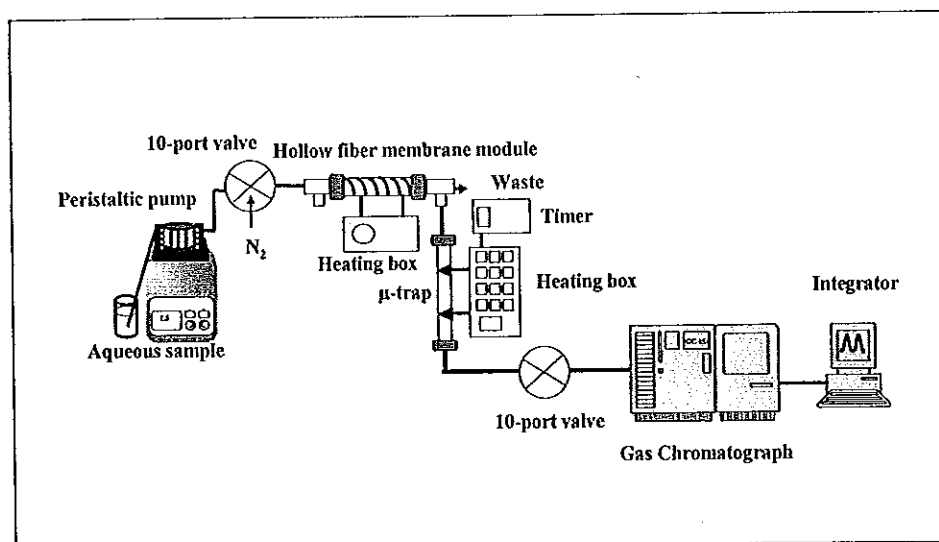


Fig. 5.1 Schematic diagram of the gas injection membrane extraction (GIME) system for trace organic compounds analysis.

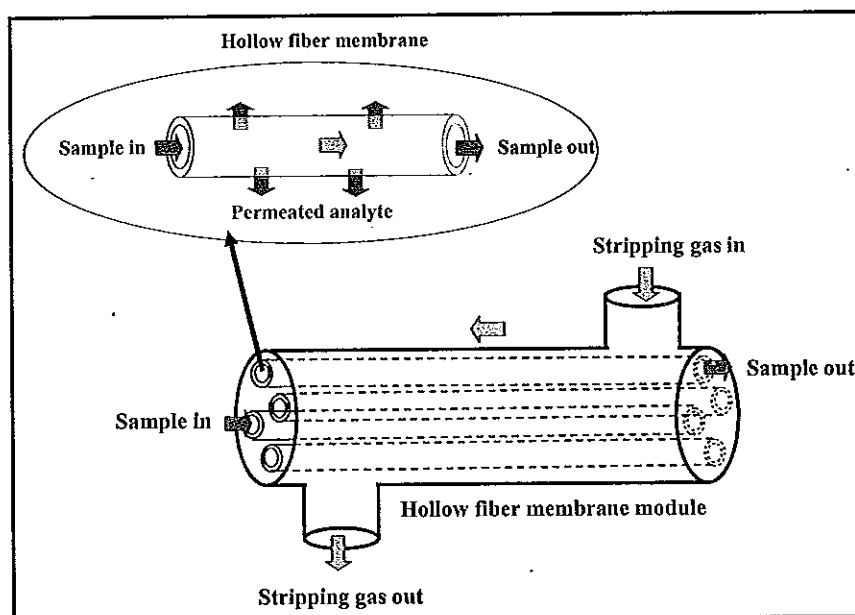


Fig. 5.2 Pervaporation process through the hollow fiber membrane

5.2.3 Extractor module

A hollow fiber membrane (HFM) used to construct the extractor module consisted of 290 μm o.d. and 240 μm i.d. polypropylene membranes coated with silicone (Apply Membrane Technology (AMT), Minnetonka, MN, USA). This module was made by insertion of the HFM inside a teflon tube. Two Swagekok®T-union (Alltech Associates, Inc., PA) were connected to the ends of the teflon tube and sealed with epoxy to make the inlet and outlet of the stripping gas and prevent the mixing of the stripping gas and aqueous sample.

Two 10-port valves were employed, one was to inject standard solution into the hollow fiber membrane module and another one was to inject analyte to the gas chromatograph. The analyte, from aqueous sample passing through the lumen of the hollow fibers, permeated through the membrane. Stripping gas, flowing on the outside the hollow fibers, carried the permeated compounds to the μ -trap. Standard solution containing 1 mg L^{-1} MTBE, 500 mg L^{-1} methanol, 500 mg L^{-1} ethanol, 500 mg L^{-1} 1-propanol and 20 mg L^{-1} MIBK were used to optimize the affecting parameter *i.e.*, sample flow rate and membrane temperature. Sample flow rate was

investigated between 0.6 to 1.4 mL min⁻¹ whereas the membrane temperature was studied in the range 25 to 55 °C due to the thermal limitation of the membrane.

5.2.4 Preconcentrator

A μ -trap is a 12 cm long, 1.02 mm i.d., and 1.59 mm o.d. siliconsteel tubing (Restek Co., Bellefonte, PA, USA) packed with a mixture of Carboxen B 80/100 mesh and Tenax TA 80/100 mesh (Alltech, IL, USA). It was placed between the extractor module and the gas chromatograph inlet to preconcentrate the compounds and injected to GC. A laboratory-built heating box was used to apply the heat (voltage) to the μ -trap, a microprocessor-based timer (Gra Lab 451, OH, USA) was used to control the interval of heating time. When a fixed potential was applied to the μ -trap, the adsorbed compounds were desorbed and collected in the sampling loop of the second 10-port valve prior to injection to the gas chromatograph. Optimization of the μ -trap operating conditions was carried out by using standard solution containing a mixture of 1 mg L⁻¹ MTBE, 500 mg L⁻¹ methanol, 500 mg L⁻¹ ethanol, 500 mg L⁻¹ 1-propanol and 20 mg L⁻¹ MIBK. Permeated analytes from the hollow fiber membrane module were passed through the μ -trap at a flow rate of 2.0 mL min⁻¹. Parameters investigated included adsorption, desorption, sampling and injection time. Adsorption time was investigated in the range 5 to 13 min while desorption, sampling and injection time were set at 1 s, 10 s and 15 s, respectively. At the optimum adsorption time the desorption time was optimized between 1 to 3 s. At the optimum adsorption and desorption times, loading and injection times were studied in the range 5 to 30 s and 10 to 25 s.

5.2.5 Sample mixture

To study the effect of mixed analytes in the sample, the response of ethanol was first studied by passing 100-700 mg L⁻¹ ethanol standard solution to the hollow fiber membrane module. Next, 1 mg L⁻¹ of MTBE standard solution was added to this ethanol standard solution and the response of ethanol and MTBE were recorded. Then, 20 mg L⁻¹ of MIBK was added to ethanol standard solution and again

the standard solution was passed through the hollow fiber membrane. The responses of these two mixtures were compared with the response of ethanol. The same processes were repeated by replacing ethanol with methanol.

5.2.6 System performance

A series of 25-2500 mg L⁻¹ of methanol and ethanol, 50-2500 mg L⁻¹ of 1-propanol, 4-160 mg L⁻¹ of MIBK and 0.5-10 mg L⁻¹ MTBE standard solution were prepared and passed through the system to study the linear dynamic range of an analytical system. Linearity was determined from the plot between the responses and concentration by considering from correlation of determination (r^2). Limit of detection (LOD) was investigated by IUPAC method (Long and Winetordner, 1983). Average peak area from 20 blank injections (\overline{X}_B) were performed and standard deviation (S_B) was calculated by the following equations;

$$S_B = \sqrt{\frac{\sum_{j=1}^{n_B} (X_{Bj} - \overline{X}_B)^2}{n_B - 1}} \quad (5.1)$$

$$\overline{X}_B = \frac{\sum_{j=1}^{n_B} X_{Bj}}{n_B} \quad (5.2)$$

The smallest signal that can be detected (X_L) can be expressed as;

$$X_L = \overline{X}_B + kS_B \quad (5.3)$$

Where k is constant factor with the confidence level desired and in this research is 3 at the confidence level of 99.86%. Therefore, the smallest concentration that can be detected (C_L) can be calculated by;

$$C_L = \left(\frac{X_L - \overline{X}_B}{m} \right) \quad (5.4)$$

Where m is the sensitivity or slope of the calibration curve and C_L is the smallest concentration that can be detected. Substituting equation 5.3 into 5.4 C_L becomes;

$$C_L = \frac{kS_B}{m} \quad (5.5)$$

The stability of the system was also tested by consecutive injection of standard solution containing a mixture of 1000 mg L⁻¹ of methanol, 500 mg L⁻¹ of ethanol and 1-propanol, 20 mg L⁻¹ of MIBK and 1 mg L⁻¹ of MTBE. The responses were plotted as a function of concentration. The stability was considered from 10% reduction of the response.

5.2.7 Real sample analysis

Three types of sample, *i.e.*, wastewater, biosolids and ground water, were selected since they equally contain these VOCs.

5.2.7.1 Wastewater sample

Samples were collected from wastewater ponds of Songklanakarin Hospital and a garage in Hat Yai, Songkhla, Thailand. The samples were filtered by stainless steel slip-on inlet filter with the porosity 10 and 2 µm (Alltech Associates, Inc.) before passing through the extractor module. The matrix effect was studied by adding a known concentration and appropriate volume of standard solution containing a mixture of 200-1000 mg L⁻¹ methanol, 200-1000 mg L⁻¹ ethanol, 200-1000 mg L⁻¹ 1-propanol, 20-100 mg L⁻¹ MIBK and 0.5-10 mg L⁻¹ MTBE to the wastewater samples. The response was investigated and compared with standard solutions at similar concentration range. The percentage of relative recovery was also calculated.

5.2.7.2 Biosolids sample

Biosolids are the product of the wastewater treatment process. Sample was collected from rubber industry wastewater pond in Hat Yai, Songkhla, Thailand and was filtered by stainless steel slip-on inlet filter with the porosity 10 and 2 µm.

The solution was passed through the extractor module by using a peristaltic pump. To study the matrix effect, a known concentration and appropriate volume of standard solution containing a mixture of 200-1000 mg L⁻¹ methanol, 200-1000 mg L⁻¹ ethanol, 200-1000 mg L⁻¹ 1-propanol, 20-100 mg L⁻¹ MIBK and 0.5-10 mg L⁻¹ MTBE were spiked to the sample. Biosolids samples were left for 2 hours to achieve complete mixing, before filtered and passed through the extractor module. The response was investigated and compared with standard solutions. The percentage of relative recoveries was also calculated.

5.2.7.3 Ground water sample

Ground water sample was collected from Singhanakron District, Songkhla, Thailand. They were analyzed by passing through the extractor module without prior filtration. Then a standard solution containing a mixture of 200-1000 mg L⁻¹ methanol, 200-1000 mg L⁻¹ ethanol, 200-1000 mg L⁻¹ 1-propanol, 20-100 mg L⁻¹ MIBK and 0.5-10 mg L⁻¹ MTBE were spiked to the sample to investigate the matrix effect and % recoveries.

5.3 Results and discussion

5.3.1 Optimum conditions of gas chromatograph

The mixtures were separated using HP-FFAP fused silica capillary column (30 m × 0.32 mm I.D. film thickness 0.25 µm, Agilent Technology, USA). GC-15A coupled with FID, all effective parameters were optimized by injecting standard solutions through the system, responses were investigated and the results are shown in Table 5.1.

Table 5.1 Optimum conditions of the gas chromatograph; 5 mL of standard solution mixture was used, *i.e.*, 1 mg L⁻¹ MTBE, 500 mg L⁻¹ methanol, 500 mg L⁻¹ ethanol, 500 mg L⁻¹ 1-propanol and 20 mg L⁻¹ MIBK.

Studied parameters	Studied range	Optimum
Column temperature (°C)	50-60	50
Detector temperature (°C)	100-280	260
Make up gas flow rate (mL min ⁻¹)	10-50	20
Hydrogen flow rate (mL min ⁻¹)	10-40	20
Oxidant gas flow rate (mL min ⁻¹)	100-400	200

5.3.2 Pervaporation

Seven strands, 26 cm long, hollow fiber membrane (HFM) were packed inside a teflon tube to construct the extractor module. This system provided an effective mass transfer area of $1.4 \times 10^{-3} \text{ m}^2$ and each strand provide a high surface area to volume up to $1.7 \times 10^4 \text{ m}^{-1}$. The sample flow through the hollow fiber membrane module was optimized by passing 5.0 mL of standard solution containing a mixture of 500 mg L⁻¹ methanol, ethanol, 1-propanol, 1 mg L⁻¹ MTBE and 20 mg L⁻¹ MIBK at sample flow rates of 0.6-1.4 mL min⁻¹; while stripping gas which flowed outside the HFM and directly to the column was kept constant at 2 mL min⁻¹ (measured at the end of the column) since this is the optimum flow rate of carrier gas in GC. The results showed that lower sample flow rate provide higher response due to longer contact time between sample and hollow fiber membrane. However, decreasing the flow rate brought lower amounts of analytes into the membrane per unit time, resulting in a lower permeate flux rate and a longer lag time. In this work the sample flow rate was studied from 0.6 to 1.4 mL min⁻¹ and 0.8 mL min⁻¹ was the optimum flow rate since it provided the highest response. At 0.6 mL min⁻¹, the injection gas pressure is not high enough to carry sample through the fiber.

HFM extraction is based on pervaporation process and the liquid sample was in indirectly contact to the hollow fiber membrane and diffused through the membrane in a vapor phase. Diffusion coefficient can be determined by measuring the lag time, the time required by the gas to establish a state of equilibrium in the degassed membrane, by equation (Schmidt, 2003);

$$\theta = l^2 / 6D \quad (5.1)$$

Where θ is the lag time, l is the membrane thickness, and D is the diffusivity. In the experiment, l is constant at 50×10^{-6} m and lag times of methanol, ethanol, 1-propanol, MTBE and MIBK were 10, 10, 8, 5, 7 minutes respectively. The diffusivity were calculated to be, methanol and ethanol $6.9 \times 10^{-9} \text{ cm}^2 \text{ s}^{-1}$, 1-propanol $8.7 \times 10^{-9} \text{ cm}^2 \text{ s}^{-1}$, MTBE $1.4 \times 10^{-8} \text{ cm}^2 \text{ s}^{-1}$ and MIBK $1.0 \times 10^{-8} \text{ cm}^2 \text{ s}^{-1}$. That is, silicone hollow fiber membrane provided the highest diffusivity for MTBE and the lowest diffusivity for methanol and ethanol. This is probably because silicone is non polar, similar to MTBE, therefore, MTBE can dissolve in silicone hollow fiber membrane much better than other compounds and when considering the vapor pressure MTBE has the highest value hence it can rapidly diffuse from the membrane (Schmidt, 2003).

5.3.3 Membrane Temperature

Temperature effect on VOC separation was studied in the range of 25 to 55 °C (Figure 5.3). The temperature was limited to 55 °C since higher temperature than 55 °C could cause membrane degradation. As the temperature increased, the response also increased due to the increased diffusion coefficient (Schmidt, 2003). In this study, 55 °C gave the highest response but also the highest standard deviation, therefore, 45 °C was selected as the optimum temperature. The high standard deviation at 55 °C was probably due to the fact that at high temperature, water could also permeate through to the outside of the hollow fiber. The moisture coated on the membrane surface could prohibit the diffusion of analytes resulting in a different diffusion surface for each injection, hence, the high standard deviation.

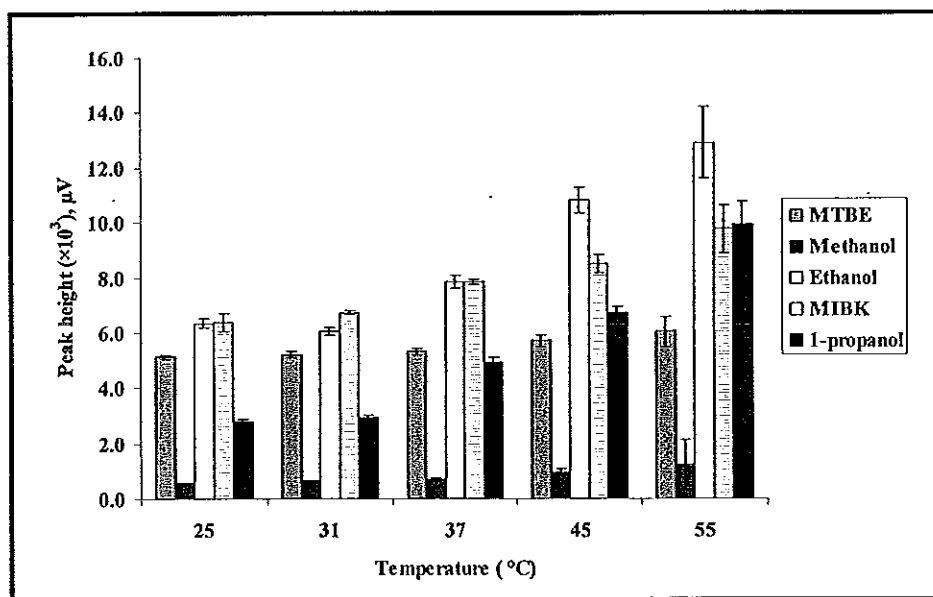


Fig. 5.3 Effect of membrane temperature to the response of the analytes

5.3.4 Extraction time

To obtain the complete extraction step, extraction time of every compound was studied. This is the time that allows all analyte to permeate from the membrane surface to the carrier stream and μ -trap. Standard solution containing a mixture of 500 mg L⁻¹ methanol, ethanol, 1-propanol, 1 mg L⁻¹ MTBE and 20 mg L⁻¹ MIBK was extracted between 5 to 13 minutes (Figure 5.4). The results indicated that as the extraction time increased from 5 to 11, the responses of every compounds increase except MTBE. The response of MTBE was constant after 6 min, this is probably due to the high diffusion coefficient of MTBE. Consequently, the optimum extraction time for determination of all compounds is 11 minutes.

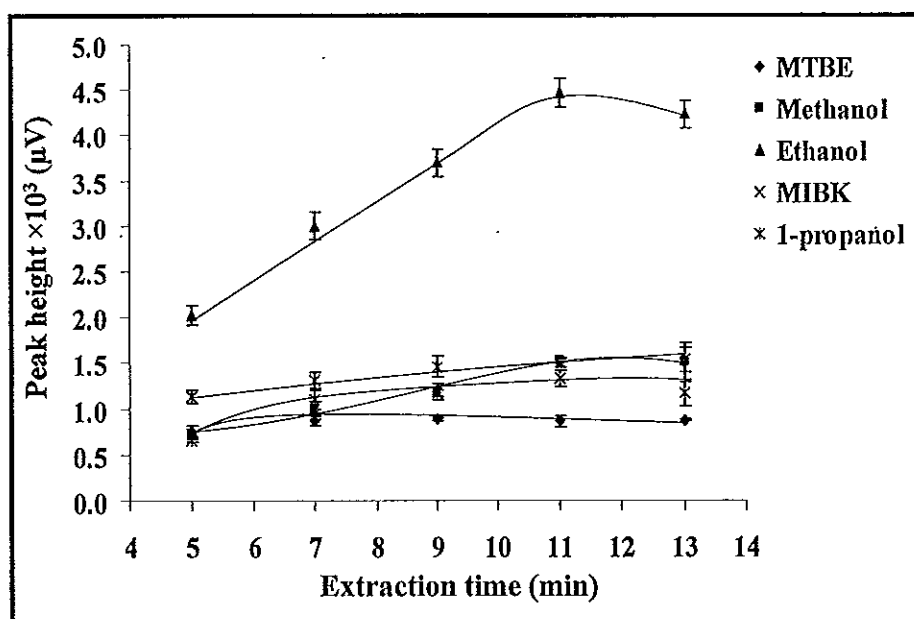


Fig 5.4 Effect of extraction time to the response of the analytes; 0.8 mL min^{-1} sample flow rate and 2 mL min^{-1} of stripping gas, and 45°C of membrane temperature.

5.3.5 Preconcentrator

A μ -trap was used as a preconcentrator. Since there is no single adsorbent that can trap all analytes, Tenax TA and Carbopack B were selected and used as a binary-bed. Each μ -trap can take 40.8 mg of Carbopack B or 25.1 mg of Tenax TA and these are taken as 100% for the adsorbents. Different ratios between the two adsorbents, Carbopack B: Tenax TA, were also investigated *i.e.*, 20:80, 40:60, 50:50, 60:40 and 80:20 and these corresponded to the weight 8.9:18.9 mg, 16.3:15.3 mg, 24.4:10.8 mg, and 33.5:5.7 mg, respectively were studied and the results indicated that the best ratio of the binary mixture was Carbopack B 16.0 – 16.3 mg and Tenax TA 15.0 – 15.3 mg (40:60). At this optimum ratio, Carbopack B adsorbed the non polar compounds and large molecules, *i.e.*, MTBE and MIBK, while alcohols were adsorbed by Tenax TA. Afterward, desorption voltage (heating) and time were optimized to achieve the suitable desorption conditions. The desorption voltage was studied in the range 5 to 10 V using 1 s desorption time (Figure 5.5). At the optimum desorption voltage, desorption time was optimized in the range 1-3 s (Figure 5.6). As desorption voltage increased the responses were also increased from 5 to 8 V. The

results indicated that all analytes were completely desorbed at 8 V. After 8 V the responses were constant but the standard deviations were also higher due to the deterioration of adsorbent.

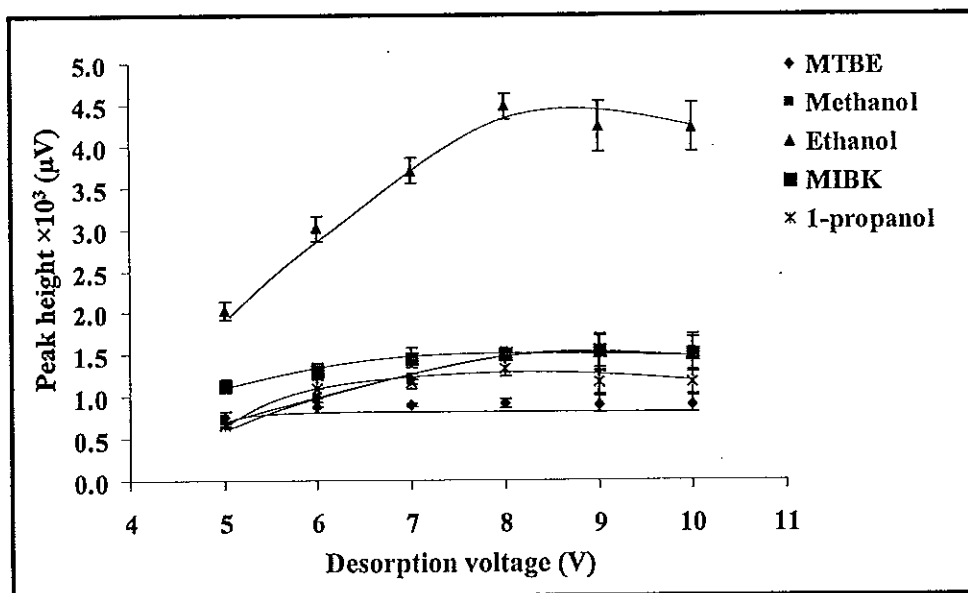


Fig. 5.5 Effect of desorption voltage to the response of the analytes; 0.8 mL min^{-1} sample flow rate and 2 mL min^{-1} of stripping gas, and 45°C of membrane temperature.

The desorption time was optimized in the range 1 to 3 s, the results showed that the optimum desorption time was 1.5 s. After 1.5 s the responses were constant but the standard deviations were increased due to the deterioration of adsorbent from the heat.

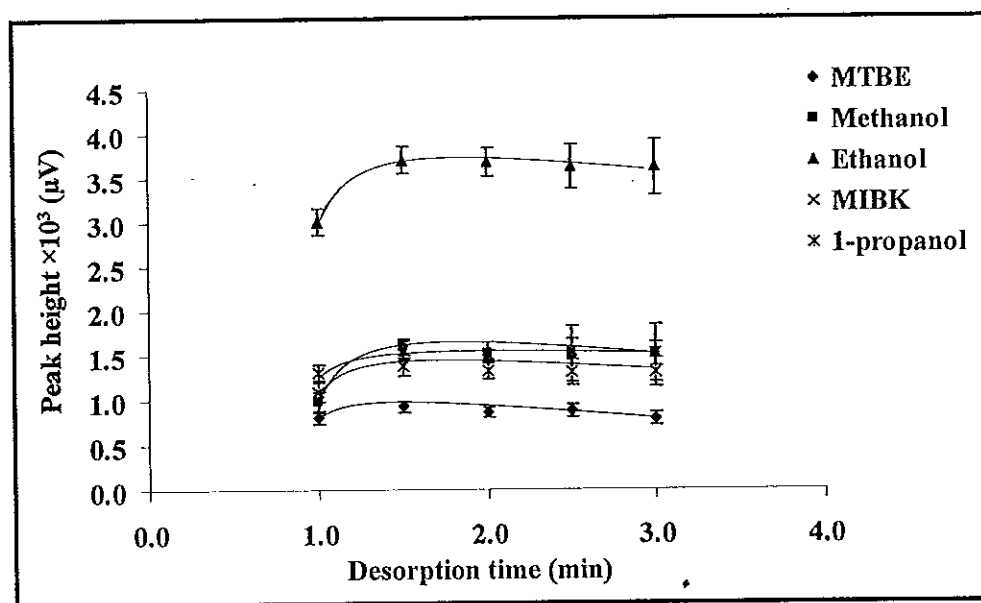


Fig. 5.6 Effect of desorption time to the response of the analytes; 0.8 mL min^{-1} sample flow rate and 2 mL min^{-1} of stripping gas, and 45°C of membrane temperature.

5.3.6 Injector

In most works the μ -trap was used as a preconcentrator and an injector. (Tarkiainen *et al.*, 2005; Thammakhet *et al.*, 2005; Yang *et al.*, 1994). However, in this work, μ -trap was only used as a preconcentrator and the second 10-port valve was used to focus the analyte and used as the injector. If this second 10-ports valve is not used, then a μ -trap is generally used as an injector. High voltage is required to obtain sharp peaks depending on the affinity between adsorbent and analytes. This causes adsorbent deterioration and the lost of adsorption capacity. Then a new μ -trap is required, that is, re-calibration is needed and this will hinder the analysis process. This second 10-ports valve is, therefore, used to prolong the life time of the μ -trap while still providing sharp chromatograms and high response. In this valve, a $250 \mu\text{L}$ sample loop was used to collect the desorbed analyte from the μ -trap. Loading time which is the time allowing desorbed analytes collected in the sample loop and injection time which is the time being injected desorbed analyte the GC were optimized in the range 5 to 30 s and 10 to 25 s, respectively to obtain the highest

response. From the results (Figure 5.7), as loading time increased from 5 to 25 s, the signals increased, after optimum loading time the signal decreased due to the loss of analytes.

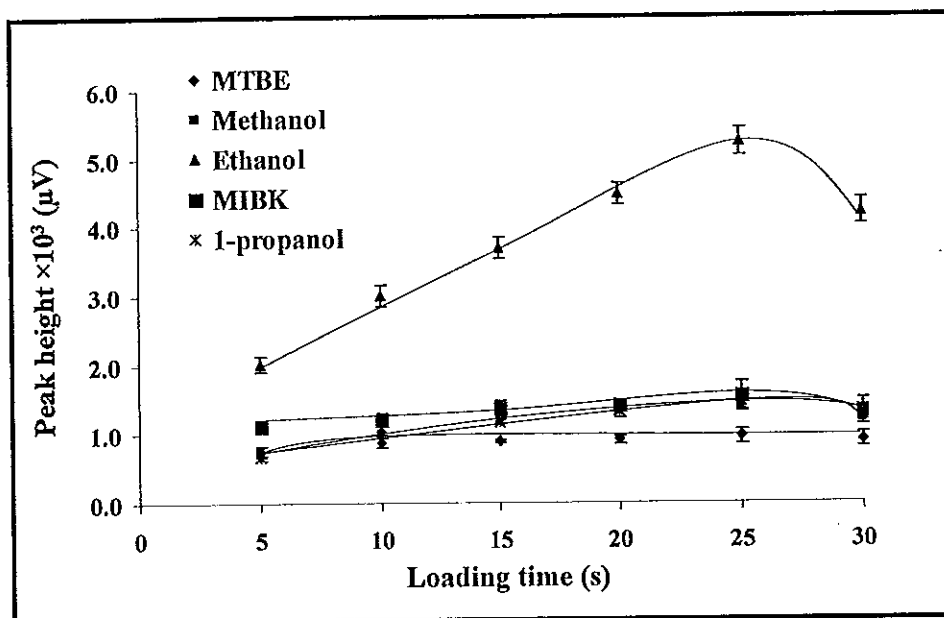


Fig. 5.7 Effect of loading time to the response of the analytes; 0.8 mL min^{-1} sample flow rate and 2 mL min^{-1} of stripping gas, and 45°C of membrane temperature.

Injection time was also investigated (Figure 5.8) since it is the time allowing analyte to flow to the analytical system. The results indicated that 15 s provided the highest signal, *i.e.*, the analytes completely flow to analytical system within this time.

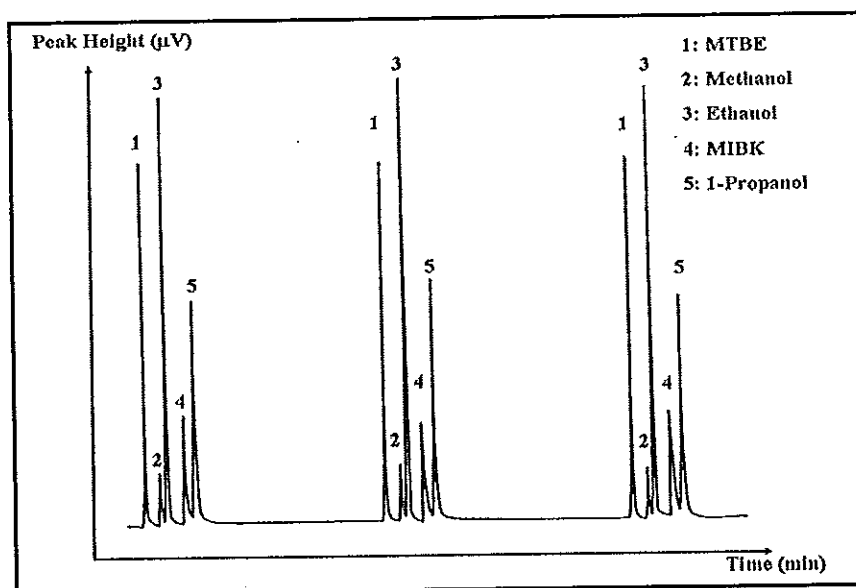


Fig. 5.9 Chromatograms of an on-line system at the optimum conditions for trace organic compounds analysis. A 5-mL of 1 mg L^{-1} MTBE, 20 mg L^{-1} MIBK, 500 mg L^{-1} methanol, ethanol and 1-propanol were used.

5.3.7 Sample mixture

In the case where a sample contains several compounds, the permeation of all analytes would become more complicated due to the effect of the analytes to the membrane called “plasticizing effect” (Feng and Mitra, 2000). Therefore, the responses of standard mixture were investigated. Figure 5.9 shows the responses of ethanol (A) and methanol (B) increased in the presence of MTBE due to the plasticizing effect. This could possibly due to membrane swelling (plasticizing effect), consequently, the dissolved compounds in membrane can diffuse to the permeated side easier. For the effect of MIBK to the response of ethanol and methanol, MIBK only affected the responses of ethanol while the response of methanol was not changed. This indicated that MIBK can cause the changing of the responses of ethanol only. Therefore, from this study can be concluded that standard addition technique is required to obtain the same effect for analyte response.

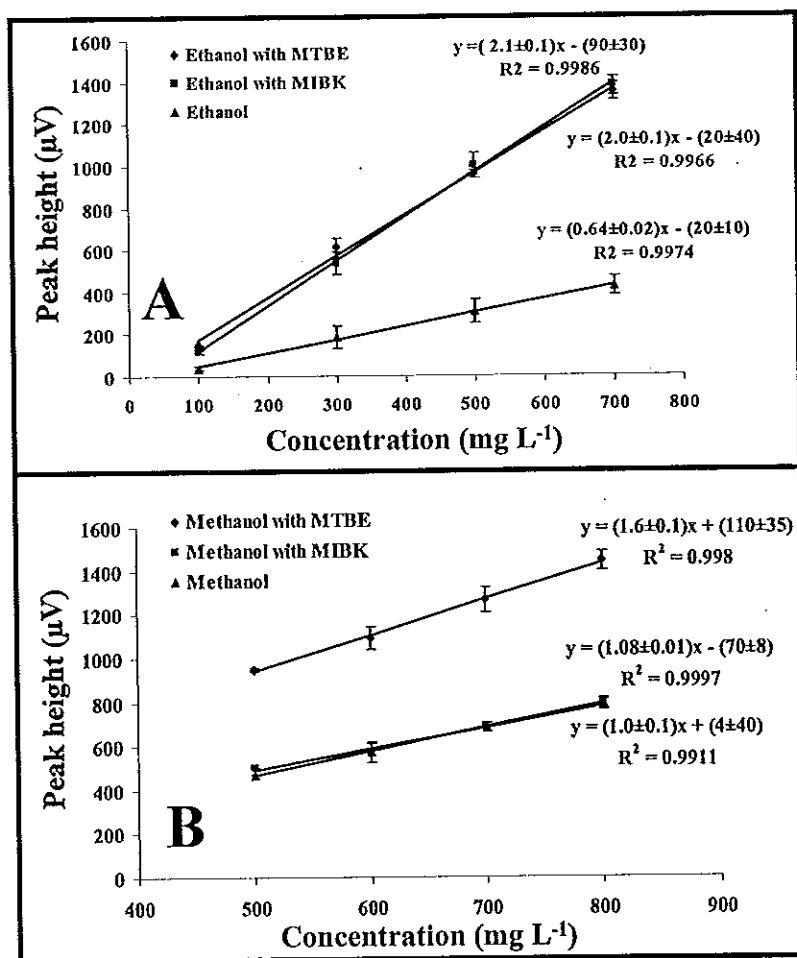


Fig. 5.10 Effect of 1 mg L⁻¹ MTBE and 20 mg L⁻¹ MIBK to the response of (A) 100- 700 mg L⁻¹ Ethanol (B) 500-800 mg L⁻¹ Methanol

5.3.8 Linearity and limit of detection

Limit of detection and linear dynamic range were determined for ethanol, methanol, 1-propanol, MIBK and MTBE. The results are presented in Table 5.3. MTBE gave the lowest detection limit of 1 μg L⁻¹ because it is non-polar and is suitable with silicone hollow fiber membrane that is also non-polar. In addition, MTBE has the highest vapor pressure making it possible to permeate through the hollow fiber membrane rapidly. The highest detection limit is methanol followed by ethanol and 1-propanol since these compounds preferably dissolve in water (considering from K_{oc}) rather than silicone hollow fiber membrane resulting in low

sensitivity and high detection limit. However, linear dynamic range and limit of detection for all of these compounds are within the range that could be used for detection of contaminated sample.

Table 5.3 Linear dynamic range and limit of detection of GIME system

Compounds	Linear dynamic range (r^2)	Limit of detection (LOD)
	(mg L ⁻¹)	(mg L ⁻¹)
Methanol	50-1750 (0.9909)	5.0 ± 0.2
Ethanol	50-1750 (0.992)	1.00 ± 0.04
1-Propanol	200-1500 (0.9935)	7.0 ± 0.3
MIBK	20-80 (0.9953)	0.60 ± 0.03
MTBE	0.05-10 (0.997)	0.010 ± 0.001

5.3.9 Stability

The stability of this system was studied by consecutive injection of the mixture of 1 mg L⁻¹ of MTBE standard solution, 1000 mg L⁻¹ of methanol, 500 mg L⁻¹ of ethanol, 20 mg L⁻¹ of MIBK and 500 mg L⁻¹ of 1-propanol. The obtained responses were plotted versus concentration. The results show that this system can be used up to 70 times before the response rapidly decreased due to the deterioration of adsorbent from the heat (Figure 5.5). The average response obtained were $(7.6 \pm 3.6) \times 10^3$ (%RSD = 4.7), $(2.3 \pm 1.1) \times 10^3$ (%RSD = 4.8), $(4.3 \pm 2.3) \times 10^3$ (%RSD = 5.3), $(1.28 \pm 0.06) \times 10^3$ (%RSD = 4.7), and $(9.0 \pm 0.4) \times 10^3$ (%RSD = 4.5) for MTBE, methanol, ethanol, MIBK and MTBE, respectively.

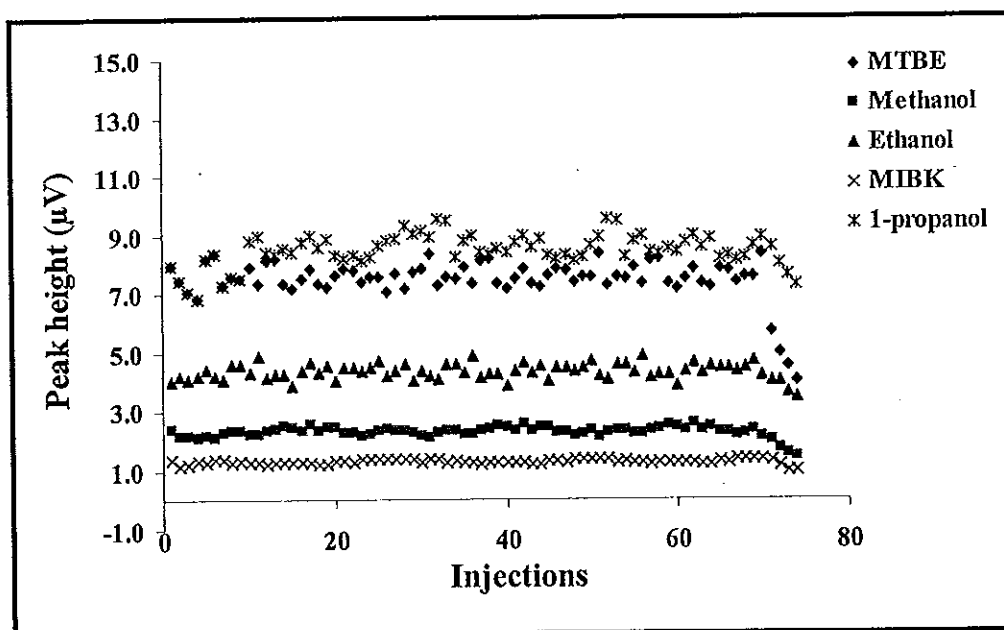


Fig. 5.11 Stability of the extraction and preconcentration systems

5.3.10 Real sample analysis

5.3.10.1 Wastewater

Wastewater samples were collected from Songklanakarin Hospital wastewater pond and garage. However, none of the studied compounds was detected in both samples. To study the matrix effect, known concentrations of standard solutions were then spiked to these samples and pass through the separation and analytical system. The signal obtained was plotted as a function of concentration. The analytical sensitivity of spiked sample was compared to analytical sensitivity of standard curve using two-way ANOVA (analysis of variance). Probability (P) value used to test was calculated by R software (R development Core Team, 2006). The null hypothesis (H_0) made that is the interaction of spike curve and standard curve is not significant and H_1 is the interaction of spike curve and standard curve is significant. From the test, the slope of spike curve and standard curve was significantly different ($P < 0.05$). Therefore, it can be concluded that the matrix in both wastewater sample

(Songklanakarin Hospital and garage) have an effect to the response of target analytes. Therefore, standard addition is needed for sample analysis.

The percentages of relative recoveries of these compounds were calculated and the results are shown in Table 5.4.

Table 5.4A The percentages of relative recoveries of spiked sample from Songklanakarin Hospital wastewater pond.

Analyte Sample	Methanol	Ethanol	1-Propanol	MTBE	MIBK
1	90 ± 7	96 ± 6	91 ± 8	87 ± 2	102 ± 4
2	96 ± 6	96 ± 4	91 ± 2	95 ± 3	101 ± 5
3	92 ± 3	105 ± 6	90 ± 2	90 ± 2	96 ± 2

Table 5.4B The percentages of relative recoveries of spiked sample from garage wastewater.

Analyte Sample	Methanol	Ethanol	1-Propanol	MTBE	MIBK
1	95 ± 7	106 ± 6	97 ± 8	90 ± 2	92 ± 4
2	96 ± 6	96 ± 4	91 ± 2	95 ± 3	91 ± 5
3	92 ± 3	105 ± 6	95 ± 2	93 ± 2	96 ± 2

5.3.10.2 Biosolids sample

For the determination of contaminated compounds, biosolids sample was filtered by stainless steel slip-on inlet filter with a porosity 10 and 2 µm and passed through the hollow fiber membrane. However, the deposition of biosolids

cake layer on the hollow fiber membrane surface caused membrane fouling (Feng and Mitra, 2000; Winston and Sirkar, 2001) and decreased the responses of all analytes. To eliminate this problem, the sample was filtered for several times in a close system to prevent the loss of analyte, and the results were much improved. To study the matrix effect, known concentrations of standard solution were spiked into the biosolids samples, after complete mixing the samples were filtered for 3 times and passed through the system. The analytical signals were plotted as a function of concentration. The analytical sensitivities of spiked sample were compared to analytical sensitivities from standard curve. Two-way ANOVA (analysis of variance) was used. From the test, the slope of spike curve and standard curve was significantly different ($P < 0.05$). Therefore, standard addition is needed for sample analysis.

The %relative recoveries were calculated and the results are shown in Table 5.5. For all compounds, extraction efficiency was in the range 79.0-86.0%. This can be explained that thin cake layer still occurred and blocked the membrane surface resulting in lower extraction efficiency. Moreover, life time of the membrane was also reduced, a new extractor module is required.

Table 5.5 The percentages of relative recoveries of spike biosolids sample.

Analyte Sample	Methanol	Ethanol	1-Propanol	MTBE	MIBK
1	87 ± 2	87 ± 2	86 ± 3	88 ± 1	90 ± 1
2	83 ± 2	83 ± 2	80 ± 6	80 ± 1	81 ± 1
3	78 ± 2	78 ± 2	85 ± 4	90 ± 2	83 ± 1

5.3.10.3 Ground water sample

Ground water was collected for analysis however none of the studied compounds was detected. To study the matrix effect, known concentrations of standard solutions were then spiked to ground water sample and passed through the separation and analytical system. The signal obtained was plotted as a function of

concentration. The analytical sensitivity of spiked sample was compared to analytical sensitivity of standard curve using two-way ANOVA (analysis of variance). From the test, the slope of spike curve and standard curve was significantly different ($P < 0.05$). The %relative recoveries of these compounds were calculated (Table 5.6). This system provides % relative recoveries in the range 87.3-100%.

Table 5.6 The percentages of relative recoveries of spike ground water sample.

Analyte Sample	Methanol	Ethanol	1-Propanol	MTBE	MIBK
1	89 ± 5	87 ± 6	87 ± 2	87 ± 2	101 ± 4
2	87 ± 6	93 ± 2	91 ± 1	95 ± 3	101 ± 5
3	96 ± 5	106 ± 6	86 ± 2	90 ± 3	96 ± 2

In summary, the target analyte in real samples could not be detected, *i.e.*, either there were no VOCs in the samples or the amount of VOCs was lower than the detection limit. However, this system provides good % relative recovery between 79-100% which was still within the acceptable range, 70-130%, set by EPA method 515.3 (EPA, 1996).

5.4 Conclusion

The proposed gas injection membrane extraction on-line system for monitoring of trace organic compounds was achieved. Both hollow fiber membrane module and μ -trap were constructed in the laboratory and tested with methanol, ethanol, 1-propanol, MIBK and MTBE, with different polarities. The results showed that that this technique could provide wide linear dynamic range for all of compounds and a low detection limit for MTBE and MIBK since these two compounds have non-polar properties, the same as hollow fiber membrane. MTBE showed lower detection limit than MIBK since MTBE has higher vapor pressure. For effluent mixture it has

been shown that different concentrations of analyte presented in the solution can affect the response to other compounds. The effect of the matrix was found in both wastewater and biosolids samples. The latter has a more profound effect since it contains higher amount of particles, because these particles can coat on the membrane surface, reducing the response of analyte. Moreover, the analyte can also adsorb on these particles and, hence was filtered out. From the results, this system is suitable for liquid sample but not suitable for the samples that have large amount of particles.

CHAPTER 6

High Efficiency Coating Film for Preconcentration Device for VOCs

6.1 Introduction

Volatile organic compounds (VOCs) are significant indoor air contaminants. They are contributed by a number of indoor sources such as personal care products (perfume and hair spray), cleaning agents, dry cleaning fluid, paints, lacquers, varnishes, hobby supplies, and from copying and printing machines (Forst and Conroy, 1998). VOCs can cause irritation, odoration, or reproductive hazards with short-term exposure and having mutagenic and carcinogenic properties with long-term exposure (EPA, 1995). To avoid its harmful effect indoor air monitoring of VOCs is necessary.

VOCs in indoor air are generally found in the range of ppb (v) to ppt (v) levels (Dettmer and Engewald, 2002) and a preconcentration step is generally required to improve the sensitivity and the limit of detection. Collection and preconcentration of VOCs is generally through the use of adsorbent with subsequent thermal desorption or solvent desorption following with gas chromatographic analysis (Dettmer and Engewald, 2002; Harper, 2000; Thammakhet *et al.*, 2006). Generally, the desorption method is mainly dependent on the choice of adsorbent materials, sampler design and analytical task. However, thermal desorption is faster and simpler for on line analysis of VOCs. Adsorbents materials commonly used for VOCs analysis are activated carbon, carbon molecular sieve, graphitized carbon black and porous organic polymer (Dettmer and Engewald, 2002; Harper, 2000; Sunesson *et al.*, 1995; Thammakhet *et al.*, 2006; Volden *et al.*, 2005). However, no single adsorbent can trap all VOCs. Although multibed adsorbent has been introduced to improve the performance but it still lacks adsorption capacity and requires long desorption time to avoid carryover (Kuntasal *et al.*, 2005; Wu *et al.*, 2004; Yamamoto *et al.*, 1998). Therefore, a more suitable adsorbent for VOCs preconcentration is still needed.

To improve the sensitivity and limit of detection one possible material,

based on sol-gel technique, is sol-gel polyethylene glycol (PEG). This material has earlier been developed as solid phase microextraction (SPME) for VOCs preconcentration (Basheer *et al.*, 2005). Since sol-gel PEG has a porous structure it will provide high surface area, high adsorption capacity, can adsorb both polar and non-polar VOCs and is suitable for thermal analysis (Bigham *et al.*, 2002; Silva and Augusto, 2005; Wang *et al.*, 2000). Therefore, it is possible to develop sol-gel PEG as an adsorption material for on-line analysis of VOCs

Carbon nanotubes (CNTs), due to its porous graphite and graphene sheet structure, have also been used as adsorbent to preconcentrate VOCs (Li *et al.*, 2004) and semi-volatile organic compounds (SVOCs) (Cai *et al.*, 2005; Zhou *et al.*, 2006). However, in these applications off-line systems were applied and needed large amount of CNTs, leading to very costly systems. A preconcentration device was subsequently developed and used as an on-line system where a thin film of CNTs was grown inside steel tubing and directly connects to a gas chromatograph but the preparation process of CNTs film is rather complicated (Wu *et al.*, 2004). Therefore, a simpler technique for preparation of VOCs preconcentration device would be useful.

Based on the good quality of sol-gel PEG we investigated its application in a preconcentration device, in the form of a trapping tube, aiming for on-line application by coating sol-gel-PEG inside a silico-steel tube. This was compared to the trapping tube coated with sol-gel PEG and MWCNTs. It is possible to make a composite material by combining the sol-gel porous structure, MWCNTs porous structure and planar π -moiety of MWCNTs which could interact with aromatic molecules. This composite material could be a good candidate to adsorb and, hence, preconcentrate both polar and non polar VOCs from indoor air such as aliphatic and aromatic compounds. Tested analytes are dichloromethane, (DCM), dichloroethane (DCE), trichloromethane (TCM), trichloroethane (TCE) benzene, toluene and xylene (BTX), selected due to their adverse affects an human health (Forst and Conroy, 1998). The developed trapping tubes were validated and compared to a commercial, Carboxen B. These trapping tubes were then applied to monitor indoor air.

6.2 Experimental

6.2.1 Materials

Chemicals used to generate standard gases were benzene, xylene (Merck KGaA, Darmstadt, Germany, 99.7%), toluene (Lab Scan Asia Co., Ltd, Patumwan, Bangkok, Thailand, 99.5%), 1, 2-dichloroethane, DCE (BDH Chemical Ltd, Poole, England), dichloromethane, DCM (Merck KGaA, Darmstadt, Germany, 99.5%), trichloroethene, TCE (Scharlau Chemie S.A. Barcelona, Spain) and trichloromethane, TCM (BDH Chemical Ltd, Poole, England).

Silico-steel tubing (15 cm long, 0.53 mm i.d., and 0.74 mm o.d.), used as a trapping device, was purchased from Restek Company (Bellefonte, PA, USA). Methyltrimethoxysilane (MTMOS) and polyethylene glycol (PEG) were purchased from Fluka (Fluka Chemie GmbH, Germany). Trifluoro acid (TFA) was purchased from Baker Analyzed Reagent (J.T. Baker, 100%) and acetone was purchased from BHD Analar® (Poole, BH15 1 TD, England, 99.5%). Multi-walled carbon nanotubes (MWCNTs, 95% purity, 5-15 μm length, 20-40 nm i.d.) were kindly provided by Shenzhen Nanotech Port Co., Ltd. (Nanshan, Shenzhen, China). Carbowack B (Supelco, Bellefonte, PA, USA), a commercial adsorbent, was used to compare with the developed trapping tube.

6.2.2 Instrumentation

The system was composed of a custom-built gas generator (diffusion tube) where the generated standard gases were carried by nitrogen (99.995% purity, Thai Industrial Gases Public Company Limited, Thailand) (see 6.2.3). When the gas mixture flowed through the trapping tube held by a 10-port valve (Valco Instruments Co. Inc., Houston, TX, USA) the analytes were adsorbed (Figure 6.1A). A custom-built heating box, with a microprocessor-based timer (Gra Lab 451, OH, USA) to control the desorption time which was used to desorb the analytes from the trapping tube and injected into a gas chromatograph (Figure 6.1B). Affecting parameters were optimized, *i.e.*, desorption time and desorption voltage, to obtain the best desorption

conditions. The analytes were then separated and detected by a gas chromatograph - flame ionization detector (GC-FID, GC-15A, Shimadzu, Japan) equipped with an HP-FFAP fused silica capillary column (30 m \times 0.32 mm I.D. film thickness 0.25 μ m, Agilent Technology, USA).

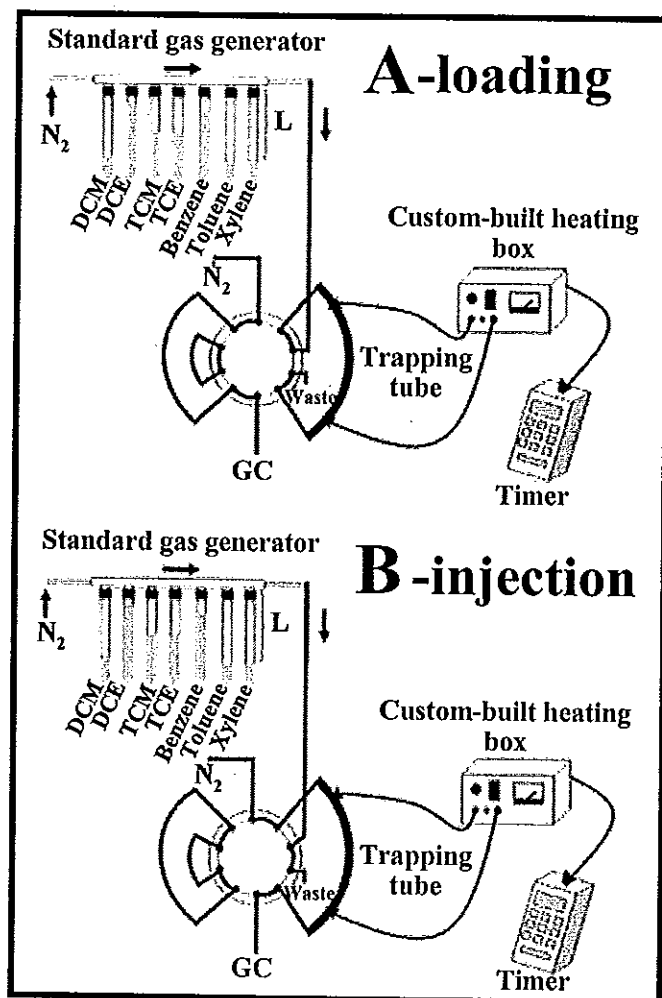


Fig. 6.1 Schematic diagram showing (A) the loading position of the 10-port valve where the analytes generated by a standard gas generator were flowed and adsorbed inside the trapping tube held in the 10-port valve and (B) the injection position where the analytes were thermally desorbed and injected into a gas chromatograph. Adsorption and desorption time was controlled by a custom-built heating box and timer.

6.2.3 Standard gas (vapor) generator

Standard gases mixture containing DCM, DCE, TCM, TCE and BTX were prepared by diffusion method (Barratt, 1981; Grob, 1985; Savitsky and Siggia, 1972) where concentrations of the gases were varied by changing the level of standard solution within the diffusion tube while nitrogen gas (dilution gas) flow rate and temperature were kept constant as mentioned in 6.2.2. The diameters of the diffusion tubes affecting the concentration was calculated using equation 6.1 (Barratt, 1981; Savitsky and Siggia, 1972).

$$\frac{CF2l}{KX\rho} = A \quad (6.1)$$

where C is the concentration of analyte (ppmv), F is the flow rate of dilution gas (mL min^{-1}), l is the length of diffusion path (cm), K is $24.45/\text{molecular weight of analyte}$ (nL ng^{-1}), X is the diffusion coefficient ($\text{cm}^2 \text{s}^{-1}$), ρ is the analyte density (g mL^{-1}) and A is the surface area of the diffusion tube (cm^2). For example, if we would like to prepare 0.5 ppmv of benzene using 100 mL min^{-1} dilution gas flow rate and the length of tube is 20 cm, the values of K , X and ρ of benzene are 0.3 nL ng^{-1} (molecular weight of benzene is 78 g mol^{-1}), 0.88 g mL^{-1} and $9.8 \times 10^{-6} \text{ cm}^2 \text{s}^{-1}$, respectively (Forst and Conroy, 1998). Substituting these values, equation 6.1 becomes

$$\frac{0.5}{1,000,000} \times \frac{100 \text{ mL}}{60 \text{ s}} \times 2 \times 20 \text{ cm} \times \frac{\text{ng}}{0.3 \text{ nL}} \times \frac{1,000,000 \text{ s}}{9.8 \text{ cm}^2} \times \frac{\text{mL}}{0.88 \text{ g}} = 3.14 r^2 \quad (6.2)$$

From equation (6.2), the diameter of the diffusion tube for benzene is calculated to be approximately 0.06 cm. Similar calculation was done for other compounds, and the diameters of the diffusion tubes were found to be 0.060 cm for DCM, 0.200 cm for DCE, 0.200 cm for TCM, 0.200 cm for TCE, 0.060 cm for benzene, 0.200 cm for toluene and 0.200 cm for xylene. The diffusion rates of standard gas using these diffusion tubes were also studied by placing them in a thermostat chamber, the length of diffusion path (reduction of the level of standard solutions in each tube) were then measured every 2 h while N_2 gas (dilution gas) was flowed through the diffusion tube (Savitsky and Siggia, 1972). The square of the length of diffusion path was then

plotted versus time, the diffusion coefficient were obtained from the slope of these plots and used to calculate diffusion rate.

To study whether the position of each standard solution tube affected the responses, a reverse of sequence of the standard solution tubes was tested, *i.e.*, instead of DCM, DCE, TCM, TCE and BTX from left to right (Figure 6.1A), the tubes were XTB, DCM, DCE, TCM and TCE. Stability of standard gases was also studied by directly injecting the standard gases from the diffusion tubes to gas chromatograph at the optimum conditions. The responses were recorded and plotted versus the injection times. This process was repeated for five concentrations with %RSD less than 4.

6.2.4 Trapping tube preparation

The silico-steel tube was cleaned by modifying the procedure described by Basheer and co-worker (Basheer *et al.*, 2005). This was done by flowing 0.1 mL min^{-1} of 0.1 M NaOH for 60 min, to form silanol group on the inside surface of the tube, and water for another 30 min. To neutralize the excess NaOH, 0.1 mL min^{-1} of 0.1 M HCl was passed through the tube for 30 min followed by 30 min of water. The tube was dried under the slow N_2 stream at 120°C for 2 h.

Sol solution was prepared following the method described by Wang and co-workers (Wang *et al.*, 2000) by mixing 400 μl of methyltrimethoxysilane (sol-gel precursor), 200 mg of polyethylene glycol (PEG: sol-gel active organic polymer), 200 μl of acetone (solvent) and 150 μl of 95% trifluoroacetic acid (TFA) (sol-gel catalyst) in a 15.0 mL plastic centrifuged tube then centrifuged for 20 min. The clear sol solution (500 μl) from the top layer was purged by N_2 to coat the silico-steel tube (Figure 6.2). The filled tube was left at room temperature ($25 \pm 1^\circ\text{C}$) for 30 min where the sol-gel network was formed via chemical bond by condensation reaction with the silanol group to the silico-steel wall inside the tube (Wang *et al.*, 2000). Nitrogen gas was then flowed through the silico-steel tube again to remove the excess sol solution. The sol-gel PEG trapping tube was conditioned using program temperature modified from Bigham and co-workers (Bigham *et al.*, 2002), starting

from 40 °C, increased with a ramp rate of 1 °C/min to 300 °C then held at 300 °C for 2 h. The program temperature was performed under slow nitrogen stream (2 mL min⁻¹). To remove all residual monomer, the trapping tube was rinsed with methylene chloride and methanol followed by drying under nitrogen stream using the same temperature program as conditioning step except for the hold time of the final temperature (300 °C) which was 30 min (Bigham *et al.*, 2002). However, this holding time was also investigated in order to achieve complete cleaning in the range 30 to 90 min.

For sol-gel PEG combined with MWCNTs (sol-gel PEG/MWCNTs), sol solution was prepared as described above and 4.0 mg of MWCNTs was added. The mixed solution was sonicated for 40 min to disperse MWCNTs in the sol solution before purged it through the silico-steel tube and conditioned as previously described. The sol-gel PEG and sol-gel PEG/MWCNTs trapping tubes were used to adsorb standard gas vapors. The reproducibility of prepared trapping tube (sol-gel PEG and sol-gel PEG/MWCNTs) in three different batches was investigated.

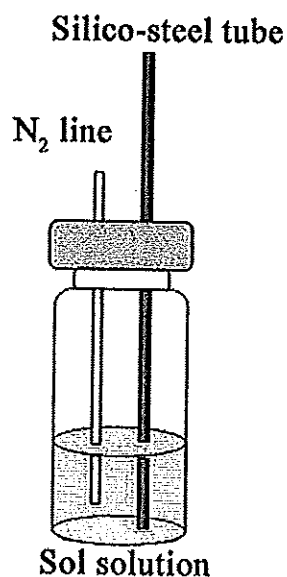


Fig. 6.2 Coating of sol-gel PEG inside silico-steel tube using N₂ gas to purge the sol solution through the silico-steel tube

6.2.5 Analytical procedure

Vapors of standard gases generated from diffusion tube were carried by 100 mL min⁻¹ of dilution gas and flowed through the trapping tube (Figure 6.1A) where the analytes were adsorbed for 10 min. The 10-port valve was then switched to injection position (Figure 6.1B) where the analytes were thermally desorbed and carried by nitrogen into the GC. Three time spans were investigated in this position. First is the delayed time between the switching and before analytes were thermally desorbed to prevent the loss of analyte. Next is the desorption time or heating time required to release all analyte. Finally, is another delayed time which will be called "injection time" to allow all the desorbed analyte to be injected into the GC. These three time spans and the heating voltage were optimized to obtain the highest response. The chromatograms were integrated by CR-3A Chromatopac (CR-3A Chromatopac, Shimadzu, Japan). Gas chromatographic conditions *i.e.*, carrier gas flow rate, column temperature, detector temperature, oxidant and fuel gas flow rate were optimized to obtain the highest sensitivity and the best separation.

6.2.6 System performance

System performances of the developed trapping tubes *i.e.*, linear dynamic range, sensitivity and limit of detection (Restek, 2003) were studied and compared to Carbopack B, a commercial adsorbent. Carbopack B packed inside the silico-steel tube was used to adsorb target analytes. The desorption time and voltage were also optimized to obtain the best conditions. Limit of detection (LOD) was investigated using signal to noise ratio ($LOD = 3 \frac{S/N}{b}$) where b is the slope of analytical sensitivity (Grob, 1985). Noise (N), the average distance between the highest point and lowest point, is taken as a peak to peak measurement.

6.2.7 Real sample analysis

Real samples, indoor air in a laboratory at Department of Chemistry, Faculty of Science, Prince of Songkla University, Hat Yai, Songkhla, Thailand was sampled using a vacuum pump (Gast Manufacturing Inc., USA) at 100 mL min^{-1} . Air sample was allowed to pass through a trapping tube for 10 min. The sample was thermally desorbed using optimum conditions and then analyzed by gas chromatography at the optimum conditions.

6.3 Results and discussion

6.3.1 Gas chromatograph optimum conditions

Standard gases obtained from diffusion tubes were used to optimize gas chromatographic conditions to accomplish the highest response, good resolution, sharp peak and short analysis time.

Initially, trapping tube without sol-gel coating was used as a sample loop to retain the standard gases from diffusion tubes and injected by 10-port valve to GC. Therefore, there is no need to use the custom-built thermal desorption unit. The optimized parameters studied composed of carrier gas flow rate, fuel, oxidant and make up gas flow rate, column temperature and detector temperature. Five replications were performed for each parameter with % RSD lower than 4 and the optimum condition was selected as the one providing the highest signal. Using these criteria, the optimum conditions were obtained as shown in Table 6.1 and they were used for further studies.

Table 6.1 Optimum gas chromatographic conditions for DCM, DCE, TCM, TCE and BTX

Parameters	Investigated values	Optimum
Carrier gas flow rate (N ₂) (mL min ⁻¹)	1.0, 2.0, 3.0, 4.0, 5.0	3.0
Fuel gas flow rate (H ₂) (mL min ⁻¹)	10, 20, 30, 40	30
Oxidant gas flow rate (Air) (mL min ⁻¹)	100, 200, 300, 400	300
Make up gas flow rate (N ₂) (mL min ⁻¹)	10, 20, 30, 40, 50	30
Program column temperature		
Initial temperature (°C)	40, 50, 60, 70	50
Initial holding time (min)	2.0, 3.0, 4.0, 5.0	3.0
Ramp rate 1 (°C min ⁻¹)	10, 15, 20, 25, 30	15
Final temperature 1 (°C)	90, 100, 110, 120, 130	100
Final holding time 1 (min)	0.0, 1.0, 2.0, 3.0	0.0
Ramp rate 2 (°C min ⁻¹)	10, 20, 30, 40	40
Final temperature 2 (°C)	120, 130, 140, 150	140
Final holding time 2 (min)	0.0, 1.0, 2.0, 3.0	0.0
Detector temperature (°C)	180, 190, 200, 210, 220	210

6.3.2 Standard gas vapor generator validation

6.3.2.1 Calculation of diffusion rate and concentration

The preparation of standard gas mixture was performed using the diffusion method. In this system the diffusion tubes of the test compound was prepared. The relationship between the lengths of diffusion path (the reduction of the level of standard gas solution in diffusion tube, l) and time (t , sec) were measured. (Goldup and Westaway, 1966; Lugg, 1968; Savitsky and Siggia, 1972). By plotting l^2 versus time this should give a straight line and the diffusion coefficient, X , could be obtained from the slope (Barratt, 1981; Savitsky and Siggia, 1972). The diffusion rate (S , ng min⁻¹) is then calculated by:

$$S = \frac{X\rho A}{2l} \quad (6.3)$$

where l is the length of diffusion path (cm), X is the diffusion coefficient (cm² s⁻¹), ρ is the analyte density (g mL⁻¹) and A is the surface area of the diffusion tube (cm²) (Savitsky and Siggia, 1972). These values are presented in Table 6.2.

Table 6.2 Effective values used for diffusion rate calculation (equation 6.6) X is the diffusion coefficient obtained from the experiments, ρ is the density of analyte and A is the cross sectional area of the diffusion tube

Analyte	X ($\times 10^{-5}$, $\text{cm}^2 \text{s}^{-1}$)	ρ (kg L^{-1})	A (cm^2)
DCM	2.4 ± 0.4	1.33	0.00281 ± 0.0001
DCE	0.43 ± 0.04	1.25	0.0314 ± 0.0001
TCM	1.07 ± 0.07	1.48	0.0314 ± 0.0001
TCE	0.71 ± 0.04	1.34	0.0314 ± 0.0001
Benzene	0.57 ± 0.04	0.88	0.00281 ± 0.0001
Toluene	0.19 ± 0.01	0.87	0.0314 ± 0.0001
Xylene	0.092 ± 0.004	0.87	0.00281 ± 0.0001

The concentration of standard gas can then be calculated by:

$$C = \frac{SK}{F} \quad (6.4)$$

where C = concentration (ppm, v/v), F = diluent gas flow rate (mL min^{-1}), K = $24.45/\text{MW}$ (nL/ng) at 25°C and 760 torr and S = diffusion rate (ng min^{-1}) (Barratt, 1981). From equations 6.3 and 6.4, concentration of the analytes can be varied by changing the length of diffusion path (Barratt, 1981; Grob, 1985; Savitsky and Siggia, 1972).

6.3.2.2 Stability

The stability of standard vapor gases was studied. They were collected using a sampling valve with a $33 \mu\text{L}$ sample loop and injected to the GC where the response was monitored for 35 injections (Figure 6.3). Results obtained from

consecutive injections showed that each concentration level of generated standard gases can be injected up to 30 times with $\%RSD \leq 4.0$ after that the signal gradually decreased due to the reduction of standard solution level in the diffusion tubes. Hence, if the generated standard gases are used within 30 injections it can provide reliable results.

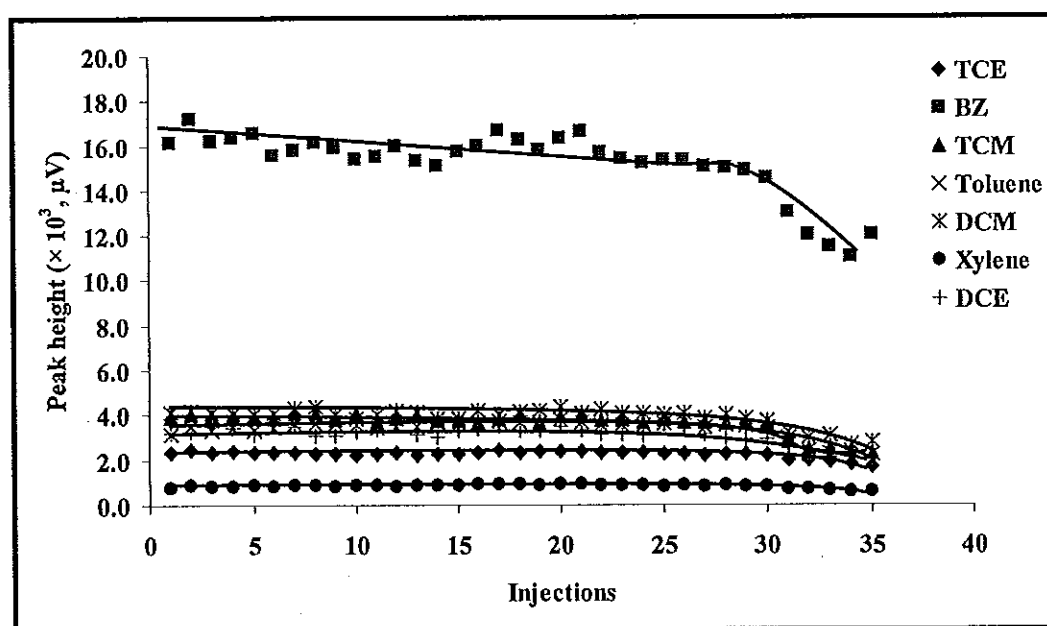


Fig. 6.3 Stability of standard gases vapor from 35 injections

6.3.2.3 Effect of diffusion tube position

The effect of the position of the diffusion tube to the responses of each analyte generated from custom-built standard gas generator was also studied. The responses obtained from reversing the position of analytes are presented in Figure 6.4. The percentage difference between the responses of the two positions was calculated by equation 6.5;

$$\% \text{ difference} = \left| \frac{\text{response from position 1} - \text{response from reverse of position 1}}{\text{response from position 1}} \right| \quad (6.5)$$

The % difference was between 0.6% and 7.4% and these were within the acceptable criteria (10%) (Green, 1996).

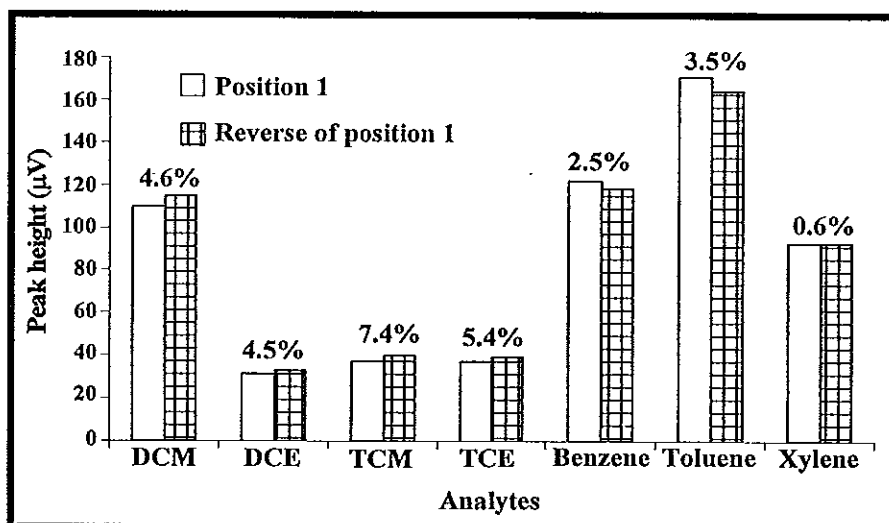


Fig. 6.4 Responses obtained from changing the position of standard solutions in the diffusion tube. Position 1 is DCM, DCE, TCM, TCE and BTX, the reverse of the position 1 is XTB, TCE, TCM, DCE and DCM. The percentage differences of the response between position 1 and the reverse of position 1 were shown above the columns.

6.3.3 Optimization of desorption conditions

Before use, the developed trapping tube was cleaned with methylene chloride and methanol followed by drying under nitrogen stream using program temperature starting from 40 °C, increased with a ramp rate of 1 °C/min to 300 °C then held at 300 °C for 30, 60 and 90 min, respectively. However, using longer holding time for final temperature can cause low response due to deterioration of coating polymer from the heat. Therefore, the hold time at 300 °C was set at 30 min. After the cleaning step, the sol-gel PEG trapping was used to optimize the delayed time and injection time.

A custom-built heating unit coupled with a timer was used to desorb the analytes from the developed trapping tubes and Carbopack B packed tube. The delay time between switching and before analytes were thermally desorbed was first investigated in the range of 5-20 s while the injection time, heating voltage and time were fixed at 10 s, 5 V and 1 s. The results showed the highest response was

accomplished at 10 s then the response decreased due to the loss of analyte before the valve was switched to inject position (Figure 6.5).

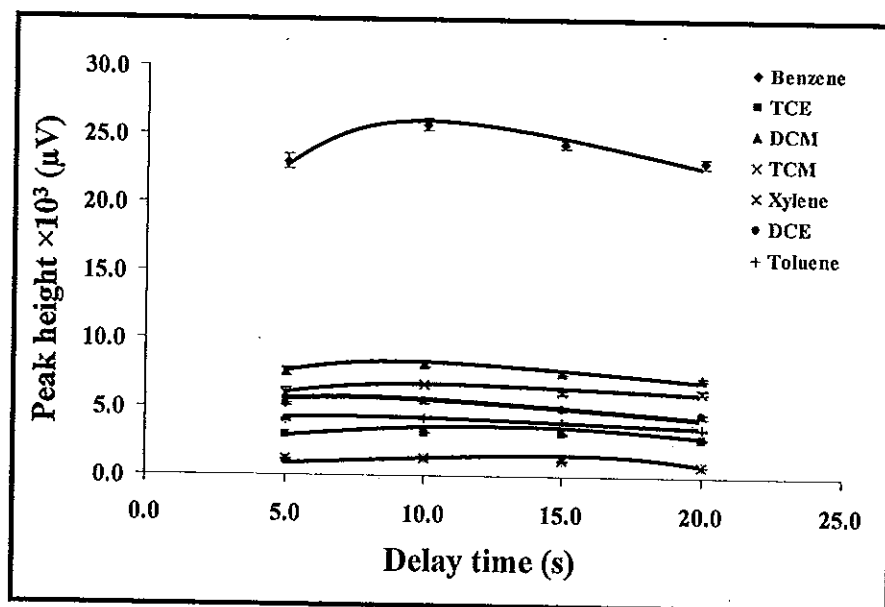


Fig. 6.5 Delay time of injection valve between switching and before analytes was thermally desorbed.

The optimum delay time was used for further studies of other parameters, the injection time was then optimized between 5 and 20 s. The response increased from 5 to 15 s since this is the time allowing analyte to flow to analytical system. Therefore, analytes were completely passed through GC at 15 s then became constant at 20 s (Figure 6.6).

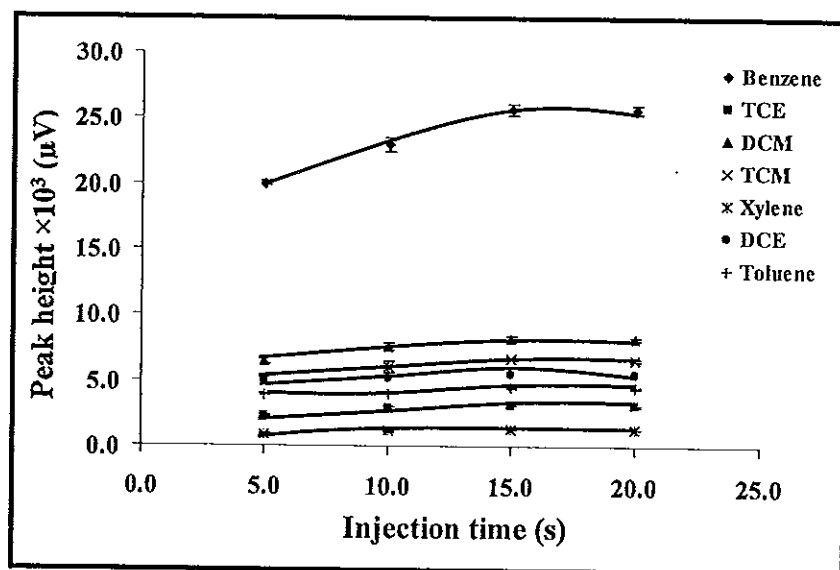


Fig. 6.6 Effect of injection time to the response of analyte.

These optimum delay and injection times (10 s and 15 s) were used to optimize other parameters for sol-gel PEG, sol-gel PEG/MWCNTs and Carbopack B, the applied heating voltage was then varied between 3.0 and 8.0 V by fixing heating time at 1 s for all trapping tubes as shown in Figure 6.7. The response increased with voltage from 3.0 to 5.0 V and then leveled off. When the desorption voltage was higher than 6 V the responses showed some fluctuation, this can be attributed to the deterioration of polymer coating and adsorbent packed tube by thermal desorption (Dettmer and Engewald, 2002; Harper, 2000).

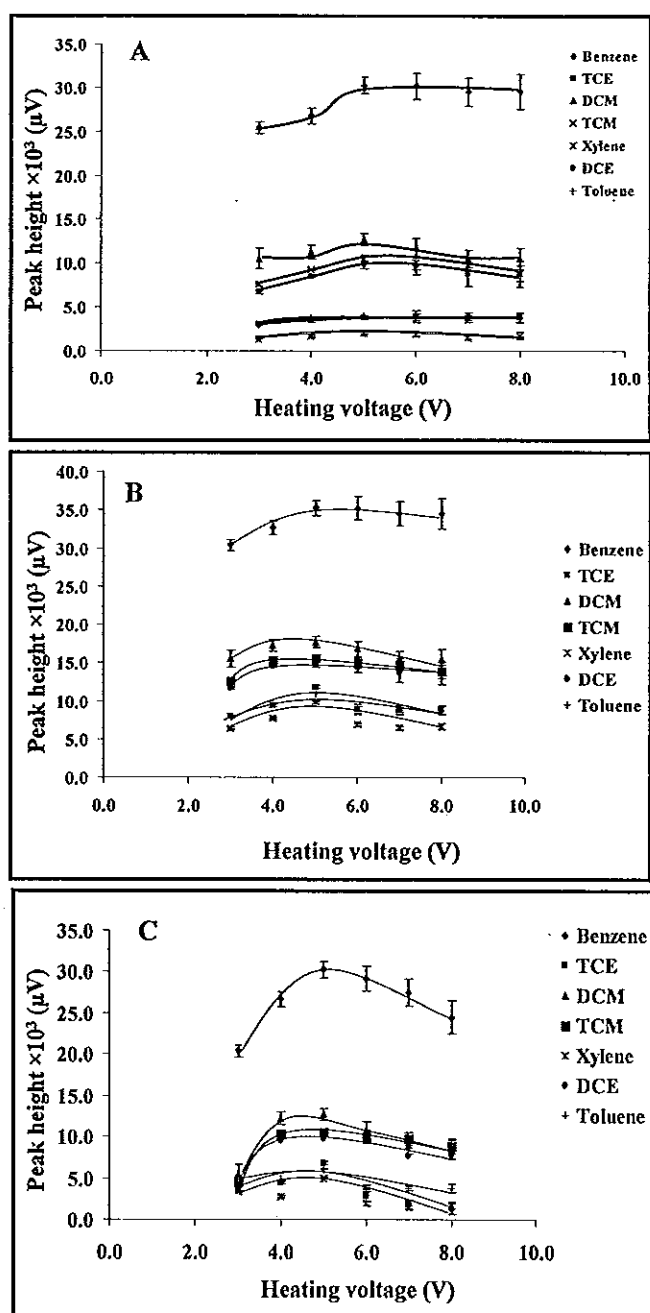


Fig. 6.7 Effect of heating voltage to the response of analyte using (A) sol-gel PEG (B) Sol-gel PEG/MWCNTs (C) Carbopack B.

Finally, the desorption time was varied between 1 to 3 s for sol-gel PEG, Sol-gel PEG/MWCNTs, Carbopack B using desorption voltage 5 V and the results showed that at 1 s the best response was obtained (Figure 6.8). The desorption time in this research was advantageous over some earlier report by less than 300 times

(Kuntasal *et al.*, 2005). In summary, the delay time between switching and desorption is 10 s and injection time 15 s. The optimum conditions for desorption are a desorption voltage of 5 V and a desorption time of 1 s.

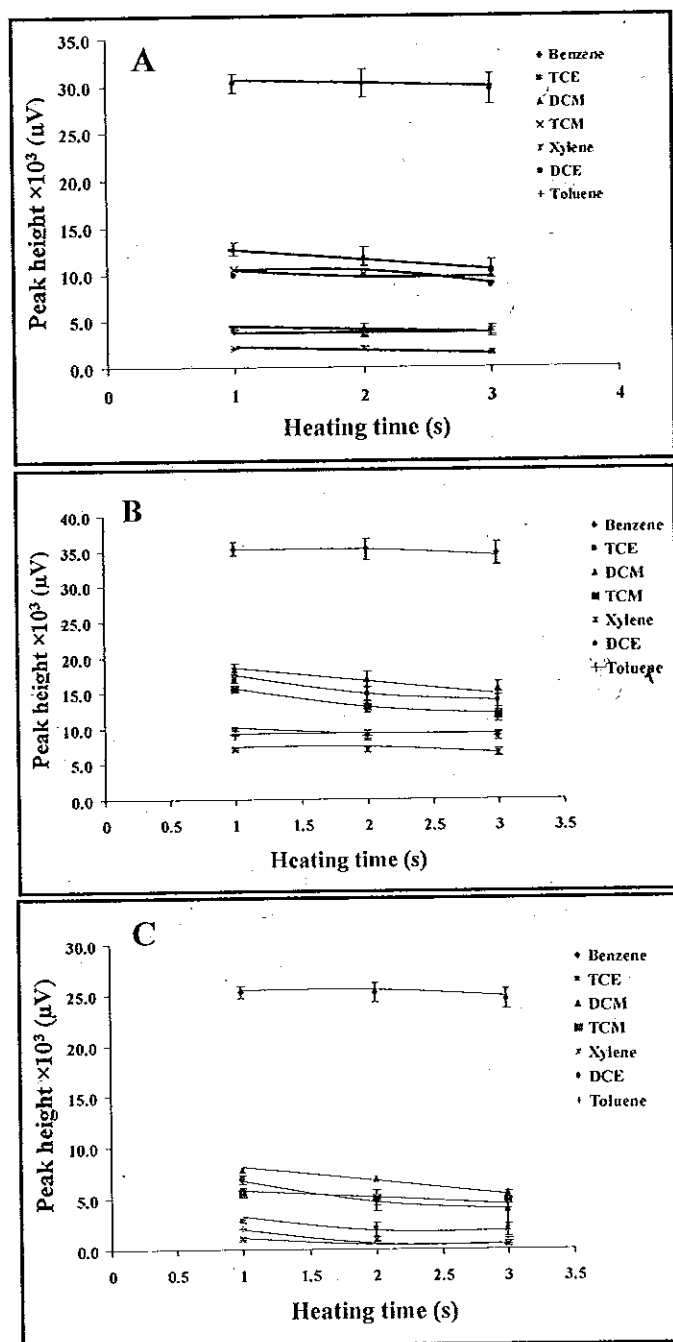


Fig. 6.8 Effect of heating time to the response of analyte using (A) sol-gel PEG (B) Sol-gel PEG/MWCNTs (C) Carbopack B.

6.3.4 Validation of trapping tube

At the optimum conditions, the chromatogram obtained using developed trapping tube (MWCNTs/PEG) as an injector is shown in Figure 6.9. All compounds can be separated and detected within 10 min.

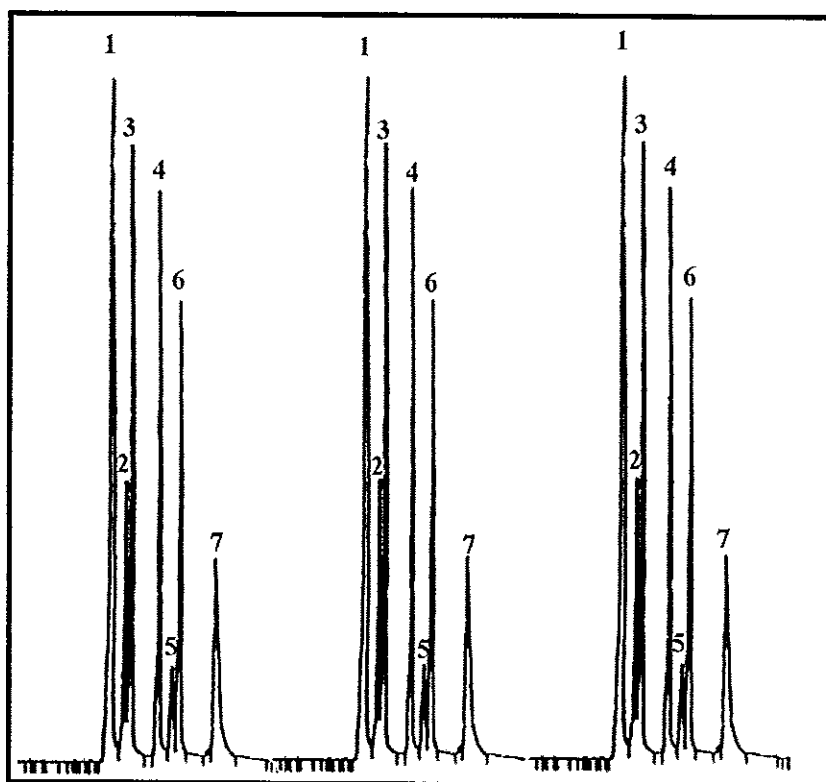


Fig. 6.9 Chromatogram obtained from MWCNTs/PEG trapping tube injection where 1: TCE ($t_R = 3.4$ min), 2: DCM ($t_R = 3.9$ min), 3: Benzene ($t_R = 4.2$ min), 4: TCM ($t_R = 5.2$ min), 5: Toluene ($t_R = 5.7$ min), 6: DCE ($t_R = 6.0$ min) and 7: Xylene ($t_R = 7.3$ min).

6.3.4.1 Reproducibility

Reproducibility was studied by preparing the trapping tubes in three different batches. Toluene was selected as a testing compound since it is widely used in the laboratory. Standard gas of toluene at a concentration of 2.4 ppmv was passed

through the trapping tube, desorbed and analyzed with GC-FID. The average responses from the three different batches of sol-gel PEG and sol-gel PEG/MWCNTs were $(2.4 \pm 0.1) \times 10^4 \mu\text{V}$ (%RSD = 3.8) and $(2.8 \pm 0.1) \times 10^4 \mu\text{V}$ (%RSD = 1.8), respectively. These results indicate that the preparation processes provide excellent reproducibility (%RSD<4).

6.3.4.2 Stability

The developed trapping tubes were compared to commercial adsorbent, 2.4 ppmv of toluene was tested. Carbopack B was chosen since it is a strong adsorbent that can be used to trap all kind of volatile organic compounds and has high thermal desorption temperature (400 °C) (Dettmer and Engewald, 2002; Harper, 2000). The results showed that both sol-gel PEG and sol-gel PEG/MWCNTs trapping tube can be used up to 160 times before the response decreased from 100% to 90% while Carbopack B can be used only 70 times. That is the developed trapping tubes provide higher thermal stability than Carbopack B. These results also showed a slight advantage over previous report where sol-gel PEG can be used up to 150 times at 300 °C (Wang *et al.*, 2000). The average response obtained from developed trapping tubes were $(2.2 \pm 0.1) \times 10^4 \mu\text{V}$ with % RSD 1.4 for sol-gel PEG and $(2.9 \pm 0.1) \times 10^4 \mu\text{V}$ with % RSD 1.7 for sol-gel PEG/MWCNTs. These were higher than Carbopack B ($(0.70 \pm 0.02) \times 10^4 \mu\text{V}$ with % RSD 2.9) by about 3 and 4 times, respectively.

6.3.5 Performance of trapping tubes

Linear dynamic ranges were studied by passing analytes at various concentrations to the trapping tube, adsorption and desorption was performed. The responses from analytical system were plotted versus concentrations. Linearity was considered from coefficient of determination (r^2) greater than 0.99 (Figure 6.10). Limit of detection (LOD) were investigated based on signal to noise ratio (S/N) of 3

(Green, 1996). Table 3 illustrates the experimental data where linearity, sensitivity and LOD of developed trapping tube and Carbopack B packed tube were compared.

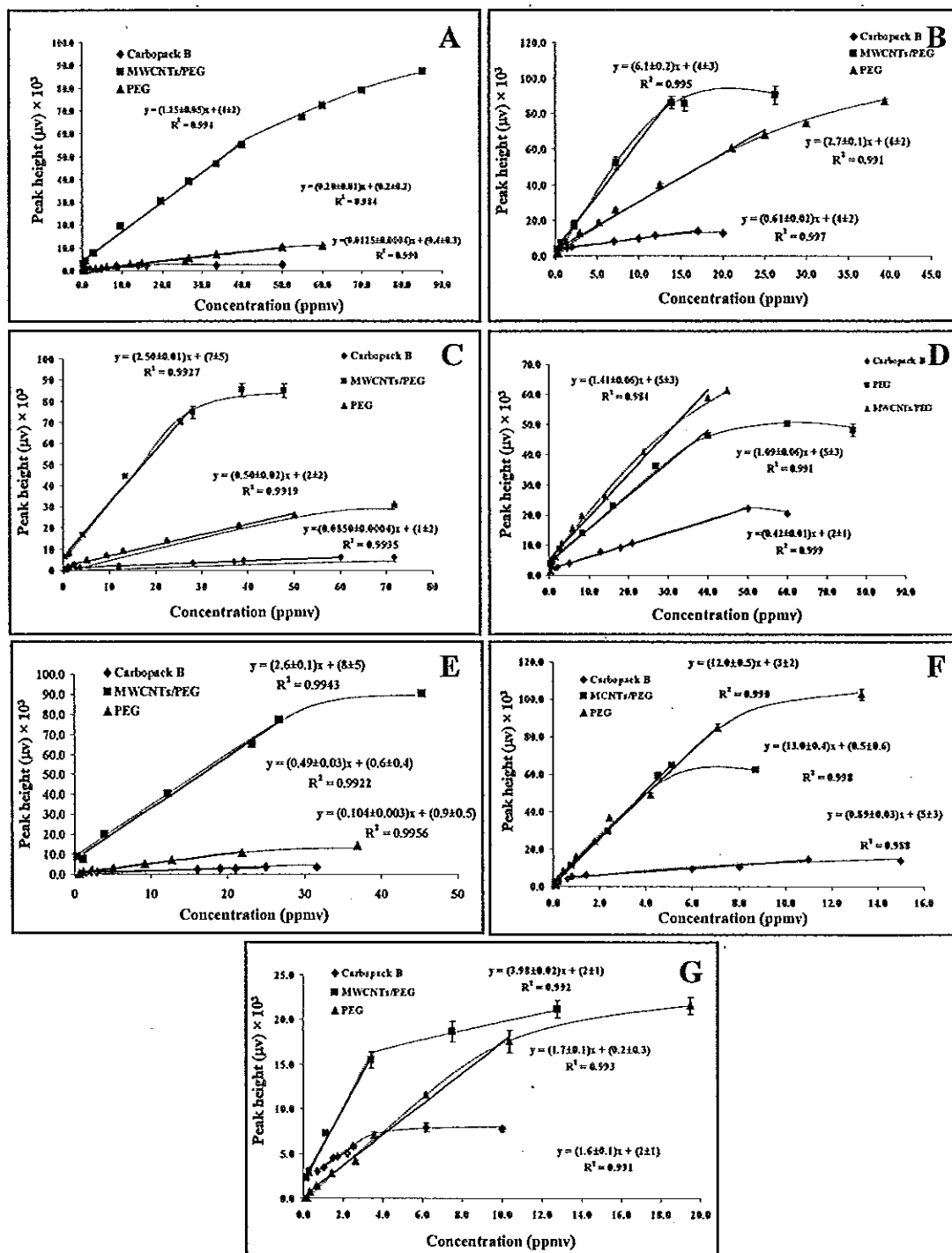


Fig. 6.10 Linear dynamic range and sensitivity of (A) DCM (B) DCE (C) TCM (D) TCE (E) Benzene (F) Toluene (G) Xylene.

Table 3

Performances of sol-gel polyethylene glycol (sol-gel PEG) and sol-gel polyethylene glycol/multiwall carbon nanotubes (sol-gel PEG/MWCNTs) trapping tubes compared to Carbopack B for determination of selected VOCs in indoor air

	DCM	DCE	TCM	TCE	Benzene	Toluene	Xylene
Linearity ($\times 10^2$, ppmv), r^2							
- Carbopack B	0.1-15	0.01-17	0.03-60	0.01-50	0.02-25	0.01-11	0.01-2
(r^2)	0.996	0.997	0.999	0.999	0.996	0.998	0.991
- PEG	0.04-50	0.01-25	0.01-50	0.01-40	0.01-13	0.001-8	0.002-10
(r^2)	0.994	0.991	0.992	0.984	0.992	0.990	0.993
- PEG/MWCNTs	0.03-40	0.004-14	0.01-30	0.01-40	0.004-27	0.001-5	0.001-3
(r^2)	0.994	0.995	0.993	0.991	0.991	0.998	0.992
LOD (ppmv)							
- Carbopack B	0.01 \pm 0.2	0.002 \pm 0.001	0.011 \pm 0.001	0.002 \pm 0.001	0.0020 \pm 0.0003	0.0011 \pm 0.0004	0.006 \pm 0.004
- PEG	0.006 \pm 0.003	0.004 \pm 0.002	0.002 \pm 0.001	0.001 \pm 0.001	0.001 \pm 0.001	0.00010 \pm 0.00004	0.00070 \pm 0.0004
- PEG/MWCNTs	0.008 \pm 0.004	0.002 \pm 0.001	0.0010 \pm 0.0002	0.001 \pm 0.003	0.0004 \pm 0.0002	0.00008 \pm 0.00002	0.0003 \pm 0.0001
Sensitivity ($\times 10^2$, μV ppmv$^{-1}$)							
- Carbopack B	0.125 \pm 0.004	6.1 \pm 0.2	0.850 \pm 0.004	4.2 \pm 0.1	1.04 \pm 0.03	8.9 \pm 0.3	16 \pm 1
- PEG	2.0 \pm 0.1	27 \pm 1	5.0 \pm 0.2	11.0 \pm 0.6	4.9 \pm 0.3	120 \pm 5	17 \pm 1
- PEG/MWCNTs	12.5 \pm 0.5	61 \pm 2	25.0 \pm 0.1	14.0 \pm 0.6	26 \pm 1	130 \pm 4	39.8 \pm 0.2

From the results, sol-gel PEG and sol-gel PEG/MWCNTs trapping tube provided higher sensitivity than Carbopack B. This could be explained by the structure of Carbopack B which is the graphitized carbon black which provides non-specific adsorption. It can adsorb various organic compound by London dispersion (Dettmer and Engewald, 2002; Harper, 2000) while sol-gel PEG are highly porous structure and this help increase the available surface area. It can adsorb both polar and non polar compounds (Wang *et al.*, 2000) hence by using sol-gel PEG trapping tube the analytical sensitivity was improved. In the case of MWCNTs incorporated with sol-gel PEG, since MWCNTs provide the adsorbent with a planar π -moiety hence it could strongly interact with an aromatic molecule and hydrophilic compound via π -stacking (Chen *et al.*, 2007). For hydrophobic compounds, it can adsorb through capillary condensation in the MWCNTs pores (Chen *et al.*, 2007; Shih and Li, 2008). Therefore, MWCNTs can possibly enhance the analytical sensitivity. From the results, the sensitivity of trapping tube increase from Carbopack B to Sol-gel PEG and Sol-gel PEG/MWCNTs. When considered the adsorption properties of MWCNTs, the analytical sensitivity of aromatic compounds which are benzene, toluene and xylene and polar compound (TCM, DCM and DCE) should be enhanced more than the others. However, the enchantments of sensitivity showed the same trend as other compounds, similar to the trend when using sol-gel PEG. Therefore, it is likely that sol-gel- PEG is the major component that plays an important role in the adsorption process.

When considering LOD, the results indicated that the LOD from the developed trapping tube was much better than Carbopack B. The trapping tube using sol-gel PEG/MWCNTs can provide LOD down to ppb (V) level. Both of the developed trapping tubes can provide high enough sensitivity and low LOD which can be used to preconcentrate all analytes and work as an injection device effectively.

6.3.6 Measurements of VOCs in indoor air

The developed trapping tubes and also Carbopack B were applied to a real sample. To calibrate the system five concentrations of standard gases (0.2-2 ppmv) were first passed through the trapping tube. Indoor air in a laboratory at

Department of Chemistry, Faculty of Science, Prince of Songkla University, Hat Yai, Songkhla, Thailand was sampled and monitored by drawing the air through the trapping tube at a rate of 100 mL min^{-1} for 10 minutes. The optimum heating voltage and time were applied to the trapping tube. The desorbed analytes were then flowed directly to GC with the carrier gas. Sampling was done for 5 times continuously using Carbopack B packed tube and developed trapping tube. The samples were sampling for 5 days however toluene and xylene were found only on one day. For the other days no interesting compounds were detected.

From the results, the concentrations of toluene detected from 5 replications are shown in Table 6.4 while the concentrations of xylene detected in indoor air are presented in Table 6.5

Table 6.4 Concentration of toluene detected in indoor air from 5 replications using 3 types of trapping tube

Trapping tube \ Concentration of toluene (ppmv)	Sampling time				
	1	2	3	4	5
Carbopack B	2.9	3.0	2.9	2.9	2.9
Sol-gel PEG	3.3	3.2	3.1	3.1	3.1
Sol-gel PEG with MWCNTs	2.9	2.9	3.0	3.2	3.2

Table 6.5 Concentration of xylene detected in indoor air from 5 replications using 3 types of trapping tube

Trapping tube \ Concentration of xylene (ppmv)	Sampling time				
	1	2	3	4	5
Carbopack B	0.5	0.8	0.9	1.0	0.8
Sol-gel PEG	0.6	0.7	0.9	1.0	0.7
Sol-gel PEG with MWCNTs	0.6	0.7	0.8	1.1	0.9

The levels of toluene and xylene were lower than the recommended exposure limit (NIOSH, recommended time-weighted (TWA) average 10 h, was set at 100 ppm) (NIOSH, 1994; Periago and Prado, 2005).

To confirm that the concentration obtained from these three types of trapping tube, Carbopack B, sol-gel PEG and sol-gel PEG/MWCNTs, were not significantly different, analysis of variance (two-way ANOVA) were calculated (James and Jane, 2000). Table 6.6 and Table 6.7 show two-way ANOVA of analysis results of toluene and xylene. *F*-test was used to see whether the variance estimates differ significantly ($P < 0.05$).

Table 6.6 Two-way ANOVA of toluene

Source of variation	Sum of squares	degree of freedom	Mean square	<i>F</i>
Between sampling time	0.031	4	0.008	2.667 ($F_{crit}=4.120$)
Between trapping tube	0.007	2	0.004	1.333 ($F_{crit}=4.737$)
Residual	0.024	7	0.003	
Total	0.139	14		

Table 6.7 Two-way ANOVA of xylene

Source of variation	Sum of squares	degree of freedom	Mean square	<i>F</i>
Between sampling time	0.287	4	0.072	1.756 ($F_{crit}=4.120$)
Between trapping tube	0.001	2	0.001	0.012 ($F_{crit}=4.737$)
Residual	0.286	7	0.041	
Total	0.400	14		

From the statistical test, *F* calculation was lower than *F* critical for both toluene and xylene indicated that the results from three trapping tubes were not significant differently ($P < 0.05$) (James and Jane, 2000). Therefore, the developed trapping tubes (sol-gel PEG and sol-gel PEG/MWCNTs) can be effectively used to detect volatile organic compounds in indoor air.

6.4 Conclusions

The developed trapping tubes based on sol-gel techniques showed that they can effectively be used as preconcentration device for on-line monitoring of VOCs. The trapping tube can be easily prepared by purging the sol solution (with or

without CNTs) through silico steel tube. Both sol-gel PEG and sol-gel PEG/MWCNTs can trap all analyte effectively. Desorption using a custom-built heating device is fast and can effectively be used as an injection device for on-line VOCs detection. Comparing to a commercial adsorbent, Carbopack B, all system performances of the developed trapping tube were much better. They provided good thermal stability, *i.e.* can be used up to 160 times, making them suitable for online monitoring of VOCs. They provide a wide linear dynamic range, high sensitivity and low detection limit, in the order of ppb (v), meaning that the system can effectively be used to quantify VOCs for a wide range of concentrations. That is, the developed sol-gel PEG and sol-gel PEG/MWCNTs trapping tubes offered an alternative technique to commercial adsorbents with higher operational temperatures, better analytical performance and longer lifetimes.

CHAPTER 7

Bismuth Film Electrode for Analysis of Tetracycline in Flow Injection System

7.1 Introduction

Mercury electrodes, mercury film and mercury drop, have often been used for electrochemical measurements because mercury has high hydrogen over voltage that greatly extends the negative potential window (Hutton *et al.*, 2001) and their usages have recently been reviewed (Barek *et al.*, 2001). However, the high toxicity of mercury has led to a search for alternative materials that can replace these electrodes. Although a wide range of non-mercury electrodes such as gold (Achterberg and Braungradt, 1999) and iridium (Nolan and Kounaves, 1999) has been investigated, the performance of these electrodes has not approached that of mercury. Recently bismuth film electrode (BiFE) has been proposed as an alternative to mercury film electrode (MFE) due to its environmental friendly nature (Wang *et al.*, 2000).

BiFE can be prepared by depositing thin bismuth film on a suitable substrate material such as glassy carbon (Charalambous and Economou, 2005; Economou, 2005; Hutton *et al.*, 2003; Hutton *et al.*, 2001; Kefala *et al.*, 2006; Kefala *et al.*, 2003; Morfobos *et al.*, 2004; Wang *et al.*, 2001a; Wang *et al.*, 2006; Wang *et al.*, 2000; Yang *et al.*, 2006), carbon paste (Kefala *et al.*, 2006; Królicka *et al.*, 2002; Švancara *et al.*, 2006), pencil-lead (Demetriades *et al.*, 2004), copper (Legeai and Vittori, 2006) and carbon fiber (Hutton *et al.*, 2005; Hutton *et al.*, 2006; Wang *et al.*, 2000). It has been widely applied for trace metal analysis by anodic stripping voltammetry, adsorptive stripping voltammetry, voltammetry and potentiometric stripping analysis. The analysed metals included nickel (II) and cobalt(II) (Legeai and Vittori, 2006), cadmium(II) (Charalambous and Economou, 2005; Hočevár *et al.*, 2002; Hutton *et al.*, 2005; Kefala *et al.*, 2003; Królicka *et al.*, 2002; Legeai and Vittori, 2006; Švancara *et al.*, 2006; Wang *et al.*, 2001a; Wang *et al.*, 2001b), zinc(II)

(Demetriades *et al.*, 2004; Kefala *et al.*, 2003; Królicka *et al.*, 2002; Legeai and Vittori, 2006) and lead(II) (Charalambous and Economou, 2005; Demetriades *et al.*, 2004; Hočevár *et al.*, 2002; Hutton *et al.*, 2005; Kefala *et al.*, 2003; Królicka *et al.*, 2002; Švancara *et al.*, 2006; Wang *et al.*, 2001a; Wang *et al.*, 2001b). However, only a few reports used BiFE and bismuth bulk electrode (BiBE) to determine organic compounds. These included amperometric detection of 2-nitrophenol and bromofenoxim (Hutton *et al.*, 2001), adsorptive stripping voltammetry of daunomycin (Bučárová *et al.*, 2005), and for trace analysis of several metals by forming a complex with dimethylglyoxime (DMG) such as cadmium (II) (Hutton *et al.*, 2004), lead (II) (Hutton *et al.*, 2003), cobalt (II) (Hutton *et al.*, 2006; Kefala *et al.*, 2003; Morfobos *et al.*, 2004), nickel (III) (Hutton *et al.*, 2006; Morfobos *et al.*, 2004), molybdenum (Wang *et al.*, 2006) and vanadium (Wang *et al.*, 2006). It was also used to detect aluminum by forming intermetallic compound with cupferron (Kefala *et al.*, 2006). Recently, BiFE has been applied to detect metallothionein (protein with low molecular weight) (Yang *et al.*, 2006). Therefore, it would be interesting to apply BiFE for the analysis of some other organic compounds in a flow system.

Tetracycline is an important antibiotic that has been used for a long time to control bacteria of many different infections in both human and animals such as respiratory tract infections and is still commonly used in veterinary medicine (Grayson, 1982). Many methods have been described for the determination of tetracycline such as liquid chromatography (Alfredsson *et al.*, 2005), high performance liquid chromatography (Cai *et al.*, 2005) coupled with different detection techniques such as mass spectrometer (Alfredsson *et al.*, 2005) and UV detection (Cai *et al.*, 2005). However, these are time consuming and high cost techniques.

An interesting detection principle is electrochemical, since it is a simple, low cost and high sensitive technique. Tetracycline has been detected by mercury film micro-electrode with fast cyclic voltammetry detection (Zhou *et al.*, 1999). However, the problem is still the toxicity of mercury. Therefore, other materials have been studied. For example, gold rotating disk electrode with pulse amperometric detection (Palaharn *et al.*, 2003) and anodized boron-doped diamond

thin film electrode (Wangfuengkanagul *et al.*, 2004) but the cost of these electrodes was relatively high.

In this research, to achieve low cost and environmental-friendly detection system, BiFE was prepared and used to determine tetracycline, which was selected as a test organic compound, in a flow injection system with amperometric detection.

7.2 Experimental

7.2.1 Chemical and reagents

$\text{Bi}(\text{NO}_3)_3 \cdot 5\text{H}_2\text{O}$ (Fluka, Switzerland) was dissolved in 0.5 M HNO_3 (Carlo Ebra Reagent, France) to obtain 2.0 mM of bismuth solution. Sodium acetate buffer, 100.0 mM pH 4.5 (Hutton *et al.*, 2005; Hutton *et al.*, 2004; Kefala *et al.*, 2003; Wang *et al.*, 2006), was used for the deposition of bismuth film on glassy carbon electrode (GCE). Sodium tetraborate buffer (25.0 mM pH 8.7) was prepared from sodium tetraborate (Sigma-Aldrich, USA) and HCl and used to prepare standard and running buffer solutions in all experiments. Stock standard solution of tetracycline (Sigma-Aldrich, Germany) was prepared in running buffer solution and stored at -20°C . Working standard solution was diluted from stock standard solution, stored at -4°C and used within three days (Zhou *et al.*, 1999).

7.2.2 Preparation of BiFE

An electrochemical cell composed of a 3 mm diameter GCE working electrode, a Ag/AgCl (3M KCl) reference electrode and a platinum wire (Metrohm, Netherlands) counter electrode. GCE was polished with 5.0 μm , 1.0 μm and 0.3 μm alumina powder (Metkon Instruments Ltd., Turkey), respectively, to mirror-like and then sonicated for 15 minutes in deionized water before use. Anodic stripping voltammetry technique was performed using a μ -Autolab type III (Metrohm, Netherlands) connected to a personal computer and driven by GPES 4.9 software

(Eco Chemie, Switzerland) to optimize the deposition of bismuth film onto GCE. Cyclic voltammetry was performed to investigate the reduction and oxidation potential of Bi(III). The reduction potential was further studied for bismuth film deposition whereas oxidation was used for cleaning GCE surface (stripping bismuth film) for next preparation. The parameters investigated include concentration of bismuth solution, deposition potential and time. At the beginning, concentration of bismuth was optimized in the range 0.2 to 1.7 mM while deposition potential and time were -0.3 V and 6 min. Then, deposition potential was optimized in the range -0.2 to -0.7 V using optimum concentration of bismuth solution and deposition time 6 min. Finally, the deposition time was investigated from 1 to 6 min using optimum condition of bismuth concentration and deposition potential. After each optimization, bismuth film was removed using oxidation potential at 0.25 V then new bismuth film was deposited and used for further study.

The reproducibility of bismuth film preparation was investigated from the current value of bismuth stripping peak from ten different batches where the % relative standard deviation was calculated. Then, three electrodes were tested with 1.0, 4.0 and 6.0 mM tetracycline standard solution. The current responses were plotted versus the concentration. The % relative standard deviation of the slope from these plots was studied. Finally, the slope of each curve was statistically compared using two-way ANOVA (analysis of variance).

7.2.3 Flow injection system for tetracycline

A flow injection system for tetracycline analysis is shown in Figure 7.1. A peristaltic pump (Miniplus 2, Gilson, France) was used to deliver buffer solution via a six-port valve (Valco, Houston, TX, USA), used as an injector of a controlled sample volume. A bare GCE (3 mm) or bismuth coated GCE (BiFE) served as a working electrode with a Ag/AgCl (3 M KCl) and a stainless steel tube acting as the reference and counter electrode, respectively. All electrodes were held in a custom-built flow cell with a dead volume of 10 μ L. Detection potential, carrier flow rate and sample volume were optimized. The detection potential of tetracycline using

BiFE was investigated between -1.0 and -1.4 V while the detection potential of tetracycline using GCE was studied in the range -1.0 to -1.3 V. During this study the carrier flow rate and sample volume were set constant at 0.2 mL min^{-1} and $200 \text{ }\mu\text{L}$. Then, the carrier flow rate was optimized between 0.1 and 0.4 mL min^{-1} using the optimum value of detection potential and $200 \text{ }\mu\text{L}$ sample volume. Finally, sample volume was studied using the optimum value of detection potential and carrier flow rate. Moreover, in order to increase the signal of the system, concentration of supporting electrolyte, $0.05\text{--}1.0 \text{ M KCl}$, was also studied to decrease the resistance of the buffer solution and enhance sensitivity of the system. The optimum value was considered from the one providing the highest response.

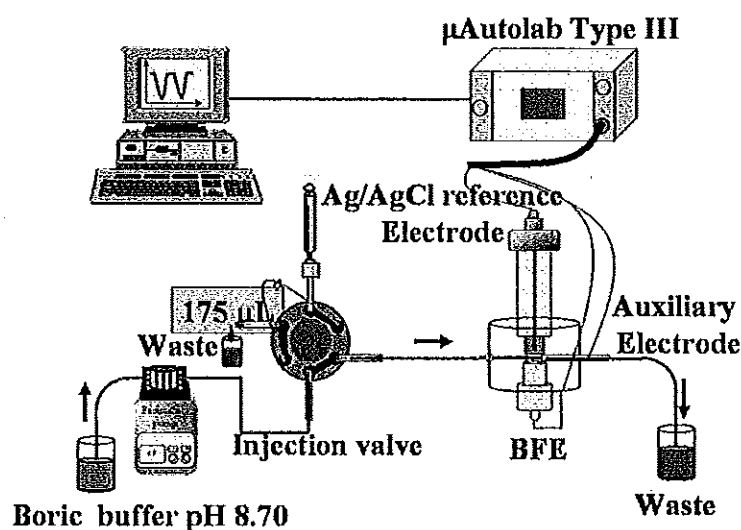


Fig. 7.1 Schematic diagram of the flow injection system for tetracycline detection

7.2.4 System performances

Stability of BiFE was investigated by continuously injecting $200 \text{ }\mu\text{L}$ of 2.0 mM tetracycline to the flow injection system with amperometric detection. All parameters were set at the optimum values. Amperometric responses of tetracycline using GCE and BiFE in the flow injection system were also compared. Linear

dynamic range, limit of detection and correlation coefficient were studied. Real samples were tetracycline capsules (250 mg) purchased from a local drugstore in Hat Yai, Songkhla, Thailand.

7.3 Results and discussion

7.3.1 Reduction and oxidation of Bi(III) on GCE

Cyclic voltammogram of 1.5 mM Bi (III) performed on GCE with potential between -1.2 V to 0.2 V showed a cathodic and an anodic peak (Figure 7.2). The reduction potential of bismuth was between -0.10 and -0.70 V. This is the range of potential where bismuth film is deposited onto GCE surface, therefore, this potential range was used for further optimization of deposition potential of bismuth film. From the same voltammogram oxidation potential was shown to be between 0.0 and 0.25 V and this is the stripping potential of bismuth film from the electrode surface. Therefore, 0.25 V was used to strip bismuth film from electrode surface (cleaning electrode surface) since this potential is high enough to strip bismuth film for all deposition potentials. After stripping new bismuth film can be deposited without polishing the electrode surface.

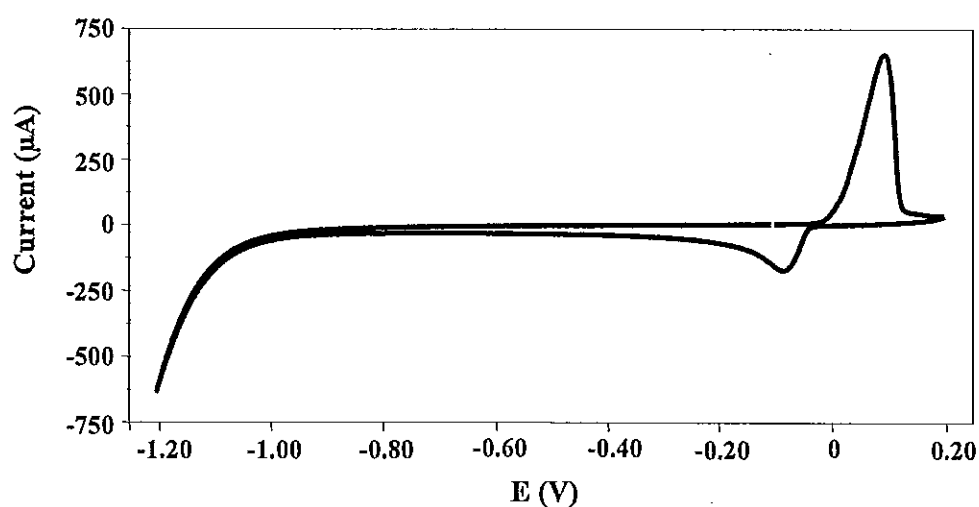


Fig. 7.2 Cyclic voltammogram of 1.5 mM Bi(III) on GCE using 1.0 M, pH 4.5 sodium acetate as a running buffer, scan rate 0.1 V s^{-1} .

7.3.2 Optimization of BiFE preparation

BiFE was prepared by depositing Bi(III) onto the GCE surface. Concentration of the bismuth solution, deposition potential and time was optimized by using anodic stripping voltammetry technique. Five replications were performed for each parameter where the % RSD was obtained at less than 4.0.

The concentration of bismuth was varied in the range 0.2 to 1.7 mM. After each deposition, the potential was increased to 0.25 V to strip the bismuth film from GCE surface and the current peaks of stripping bismuth were recorded. This peak current indicates the deposited amount of Bi (III) and generally, it is proportional to deposited molecule onto electrode surface (Wang, 2006). Figure 7.3 illustrates the increasing of anodic stripping peak current with the concentration of Bi(III) solution which reached a steady value at 1.5 mM. This indicated that at this stage the surface of the electrode was completely covered with Bi hence after this concentration the current was constant. Therefore, the optimum concentration of Bi(III) was 1.5 mM.

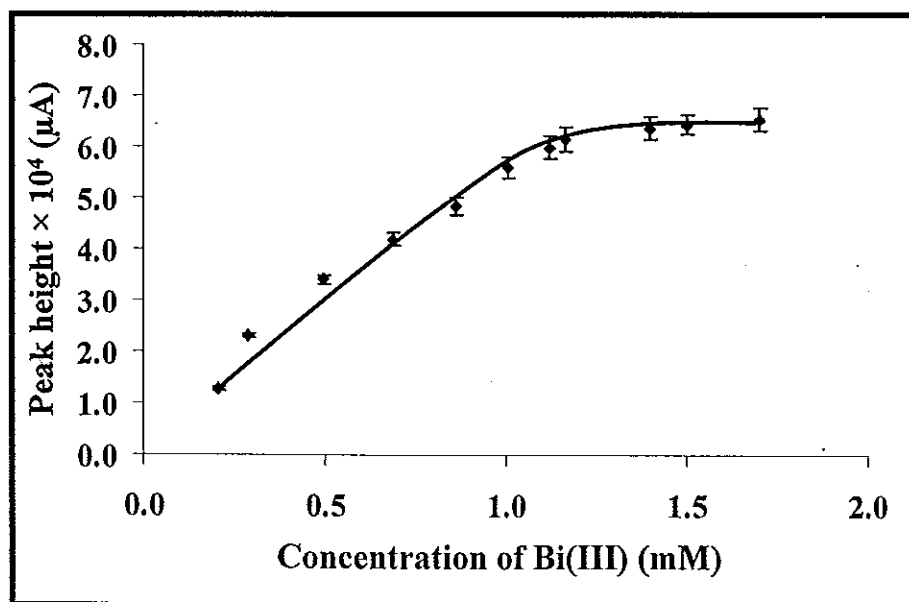


Fig. 7.3 The relationship between anodic stripping peak current of Bi(III) and concentration of Bi(III). 0.1 M, pH 4.5 sodium acetate buffer was used for deposition and stripping bismuth film.

The deposition potential was then investigated in the range of -0.2 to -0.7 V. At a potential more negative than -0.3 V the stripping peak current decreased (Figure 7.4). This is probably because of the faster reduction rate of Bi(III) (Wang, 2006) that can cause non-uniformity of the film hence the amount of Bi(III) deposited which corresponding to stripping peak current was reduced. Since -0.3 V provided the highest response it was selected as the optimum deposition potential and used for further study.

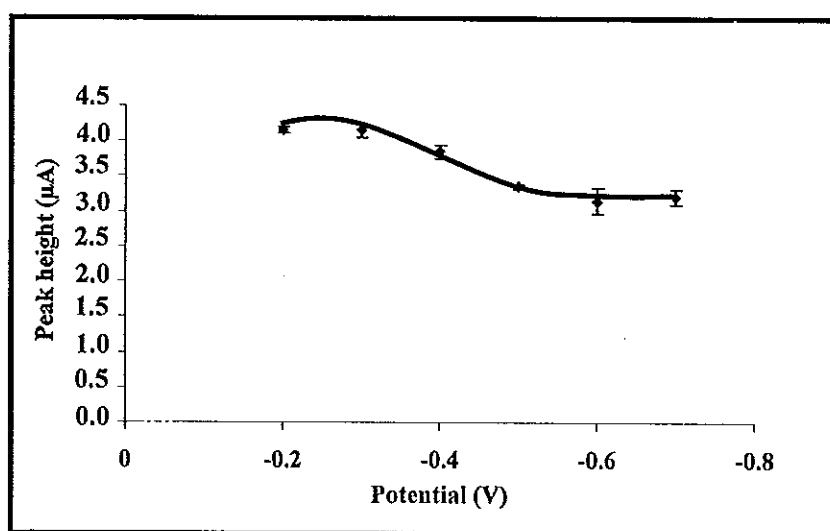


Fig. 7.4 Effect of deposition potential of 1.5 mM Bi(III) onto GCE. 0.1 M, pH 4.5 sodium acetate buffer was used for deposition and stripping bismuth film.

For the deposition time, the results showed stripping peak current increased with deposition time from 1 up to 6 minute (Figure 7.5) and becomes constant. That is, 6 minutes is the optimum condition for this parameter.

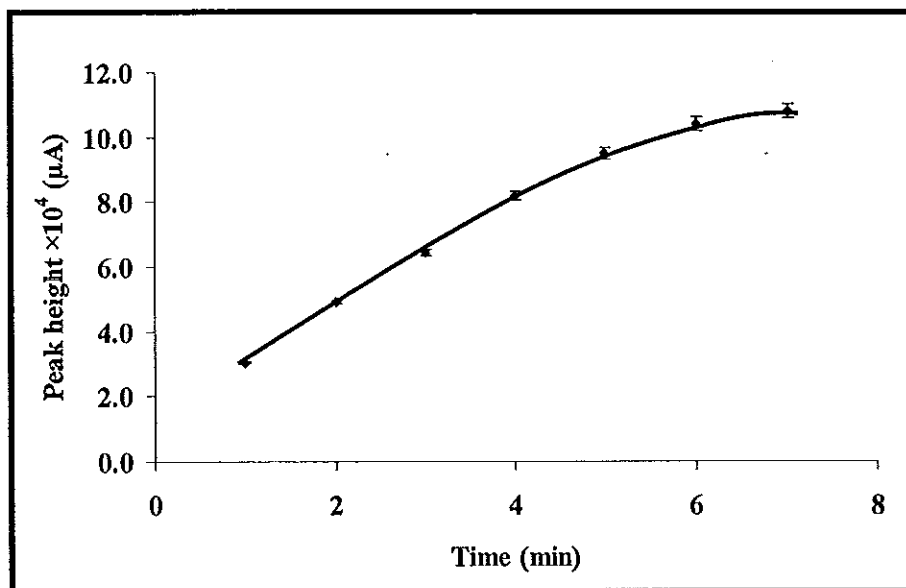


Fig. 7.5 Effect of deposition time of 1.5 mM Bi(III) onto GCE. 0.1 M, pH 4.5 sodium acetate buffer was used for deposition and stripping bismuth film.

Using optimum preparation bismuth film conditions (concentration of bismuth 1.5 mM, deposition potential -0.3 V and deposition time 6 min), 10 different preparations of BiFE were investigated. Anodic stripping peak currents of Bi(III) from GCE surface of these preparations provided the stripping current of $10.1 \pm 0.5 \mu\text{A}$ with a relative standard deviation of 4.7%. That is, the process provided good reproducibility.

7.3.3 Working potential of BiFE

When study tetracycline, borate buffer was used as a running buffer because basic solution was needed to provide the reduction reaction of tetracycline at negative potential and provide a wide potential window suitable for reduction potential of tetracycline. The potential window of BiFE and GCE (working electrode) were tested in 25.0 mM borate buffer pH 8.7 in a batch system, using a Ag/AgCl (3M KCl) reference electrode and a platinum wire counter electrode. They were found to be between -0.9 and -1.5 V for BiFE and in the range -1.0 to -1.3 V for GCE (Figure

7.6). Although, the potential windows of GCE and BiFE are narrower than that of mercury film micro electrode (-0.6 to -2.0 V) (Zhou *et al.*, 1999), they were wide enough for tetracycline detection (see 7.3.4).

7.3.4 Reduction potential of tetracycline

The reduction potential of tetracycline was studied by adding 1.0 mM tetracycline into the system. The cyclic voltammogram was scan between -0.9 to -1.5 V for BiFE and -1.0 to -1.3 V for GCE. Ten scans were performed in each run. The first voltammogram of tetracycline scan of each injection was used since subsequent scans provided lower peak current due to rapid desorption of tetracycline from the electrode surface. Reduction reaction of 1.0 mM tetracycline occurred at -1.25 V (Figure 7.6) which is slightly less than mercury film micro electrode where the reduction peak of tetracycline was found between -1.4 to -1.5 V (Zhou *et al.*, 1999). The shift of reduction potential is possible either from slightly higher electron transfer kinetics of tetracycline on BiFE than mercury film micro electrode or a difference in electrical double layer region of BiFE and mercury film micro electrode (Charalambous and Economou, 2005; Wang *et al.*, 2000). In the case of a bare GCE, although it has a potential window between -1.0 to -1.3 V, no current peak of tetracycline was obtained under the same condition probably because GCE is less sensitive to tetracycline than BiFE. To improve the sensitivity, supporting electrolyte, KCl, was added to increase the conductivity of the running buffer solution (Perrin and Dempsey, 1974). Using cyclic voltammetry the responses could be obtained from GCE but were still much less than BiFE (Figure 7.6). The cyclic voltammogram of tetracycline using BiFE shows good adsorption and rapid desorption of tetracycline. At 0.1 M KCl the response of 1.0 mM tetracycline obtained from BiFE increased by 50%. This supporting electrolyte was studied further in the flow injection system.

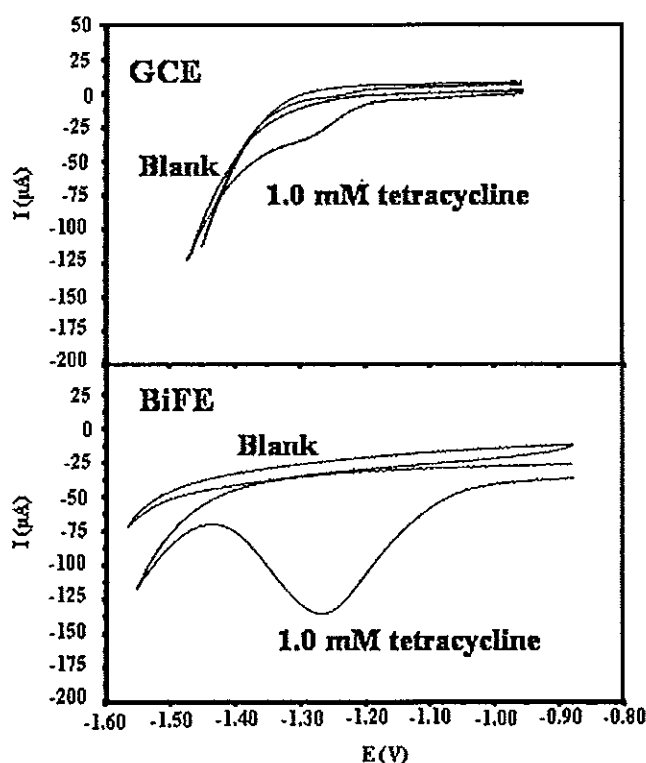


Fig. 7.6 Cyclic voltammograms of blank (25.0 mM borate buffer pH 8.7) and 1.0 mM of tetracycline in 25.0 mM borate buffer pH 8.7 containing 0.1 M KCl on GCE and BiFE at a scan rate of 50 mV s^{-1}

7.3.5 Optimization of flow injection system

7.3.5.1 Detection potential

Both GCE and BiFE were tested in the flow injection system. A constant potential of -1.0 V was applied until a stable baseline was obtained. The detection potential was then optimized to recheck the reduction potential of tetracycline in the flow injection system since the distance between working, reference and auxiliary electrodes were different from the batch system. In addition, auxiliary electrode in the flow and the batch systems were different (stainless steel and platinum wire). Tetracycline, $200 \mu\text{l}$ of 1.0 mM , was injected into the amperometric flow injection system. The detection potential was tested at -1.00 , -

1.20, -1.25, -1.30, -1.35 -1.40 V for BiFE (Figure 7.7A) and -1.00, -1.20, -1.25, -1.30 V for GCE (Figure 7.7B). Current peak of tetracycline provided the highest response at -1.30 V for both BiFE and GCE and this was used as the detection potential.

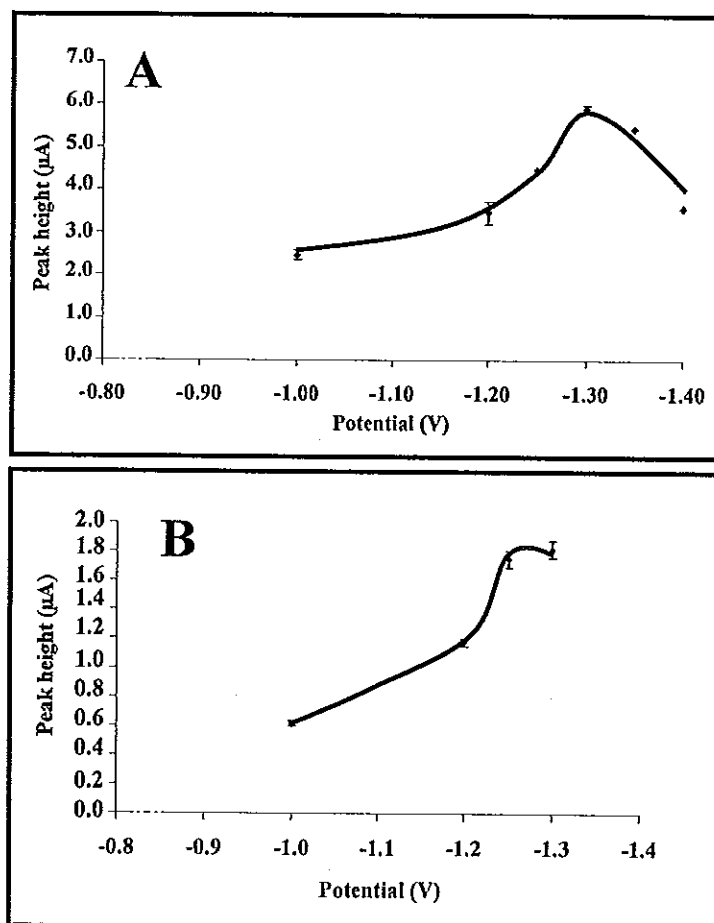


Fig. 7.7 Effect of detection potential on the response of 1.0 mM tetracycline using (A) BiFE and (B) GCE. System contains 25.0 mM borate buffer solution, 200 μ L of sample volume.

7.3.5.2 Carrier flow rate

The optimum carrier flow rate was then investigated from 0.1 to 0.4 mL min^{-1} using both GCE and BiFE. Between 0.2-0.4 mL min^{-1} the same value of current was obtained, however, at 0.1 mL min^{-1} the peak of 1.0 mM tetracycline was quite broad and the peak height was lower than the others (Figure 7.8). This was

probably caused by the dispersion of the sample in the flow system at a slow flow rate. Therefore, 0.2 mL min^{-1} was selected.

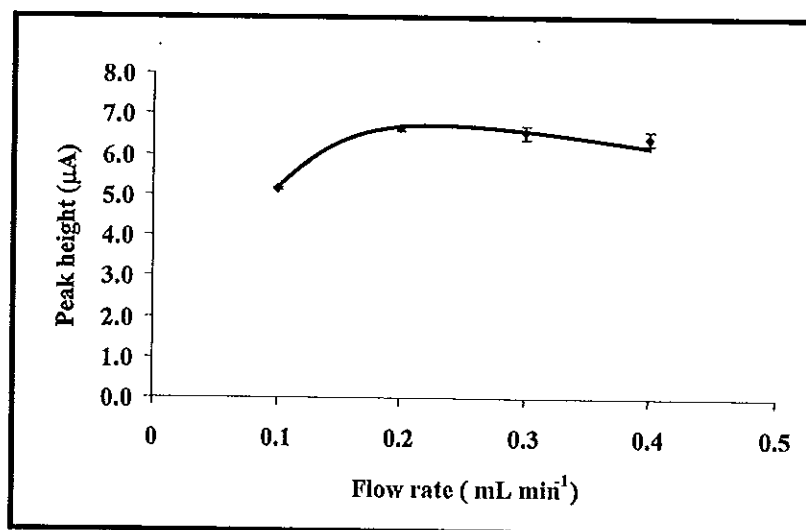


Fig. 7.8 Effect of carrier solution flow rate on the response to $200 \mu\text{L}$ of 1.0 mM tetracycline in 25.0 mM borate buffer, detection potential -1.3 V .

7.3.5.3 Sample volume

Since the dead volume inside the flow cell, which is dilution factor, could affect the response of the analyte thus it is necessary to optimize the sample volume. This was studied between 150 and $300 \mu\text{L}$. Since increase the sample volume would increase the amount of analyte resulting in higher response, the peak height increased with volume from 150 to $200 \mu\text{L}$. However, after $200 \mu\text{L}$ a constant response was achieved. Therefore, $200 \mu\text{L}$ was selected to be an optimum sample volume (Figure 7.9).

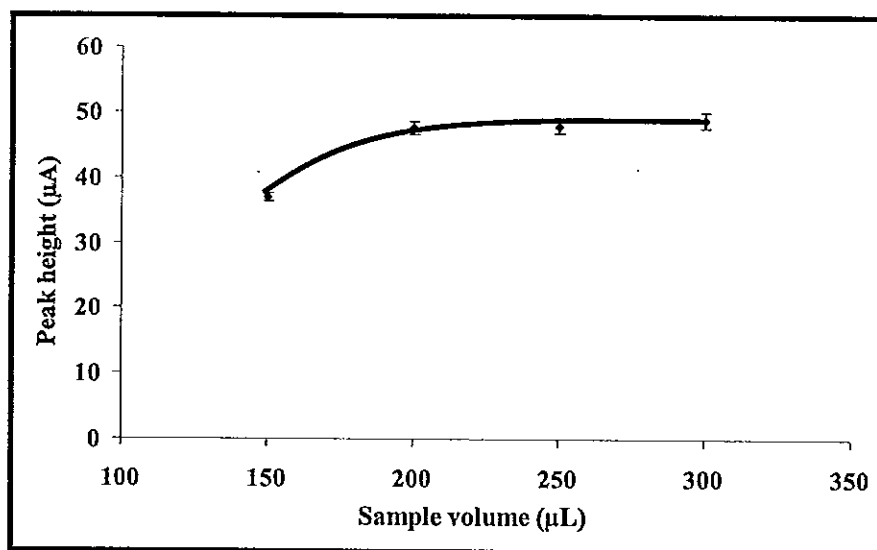


Fig. 7.9 Effect of sample volume on the response of 1.0 mM tetracycline in 25.0 mM borate buffer, detection potential -1.3 V.

7.3.5.4 Supporting solution concentration

To enhance the response of tetracycline, concentration of the added KCl was tested between 0.05–1.0 M. The current response of 1.0 mM tetracycline increased with KCl concentration from 0.05–0.1 M due to the reduction of the resistance of the solution. However, at higher concentration of 0.2, 0.3, 0.4, 0.5 and 1.0 M, the current of 1.0 mM tetracycline decreased because larger amount of KCl can shift the reduction potential of analyte to a more negative value resulting in the decrease of response in amperometric detection. Moreover, the baseline noise at high KCl concentration is also quite high. Therefore, 0.1 M was selected as the optimum value.

7.3.5.5 Concentration and pH of borate buffer

To obtain the best conditions, concentration and pH of borate buffer was investigated. The effect of borate buffer concentration to the response of tetracycline analysis using BiFE was studied between 12.5 and 100 mM (Figure 7.10).

The results showed the maximum peak current at 25 mM. Therefore, 25 mM was selected as an optimum condition.

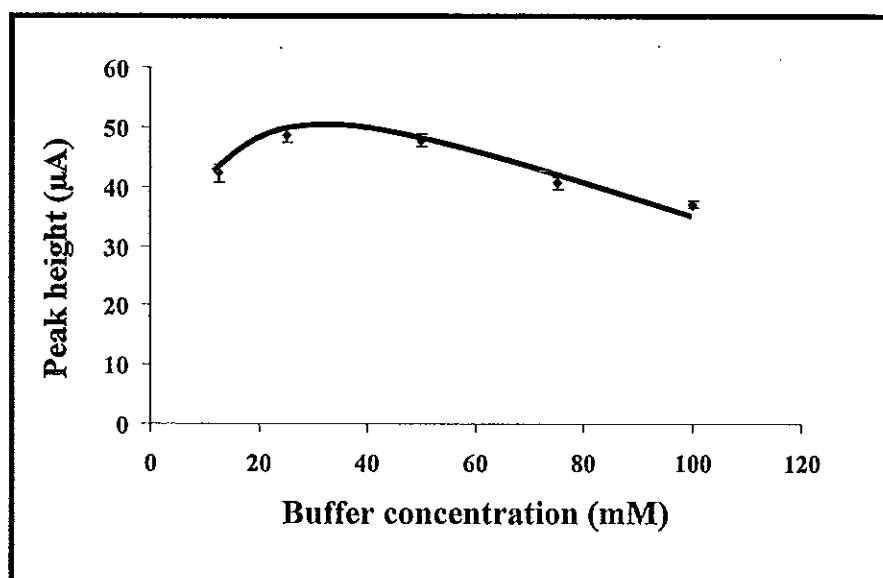


Fig. 7.10 Effect of buffer concentration on the response to 200 μL of 1.0 mM tetracycline in flow injection system; borate buffer solution, 0.2 mL min^{-1} flow rate and -1.3 V detection potential.

The effect of pH of borate buffer to the response of tetracycline was also investigated from 8.1 to 9.0. The responses of tetracycline were slightly increased in this range. However, the highest response was achieved at the pH 8.7 (Figure 7.11). Therefore, this pH was selected to be optimum value and used for further study (Zhou *et. al.*, 1999).

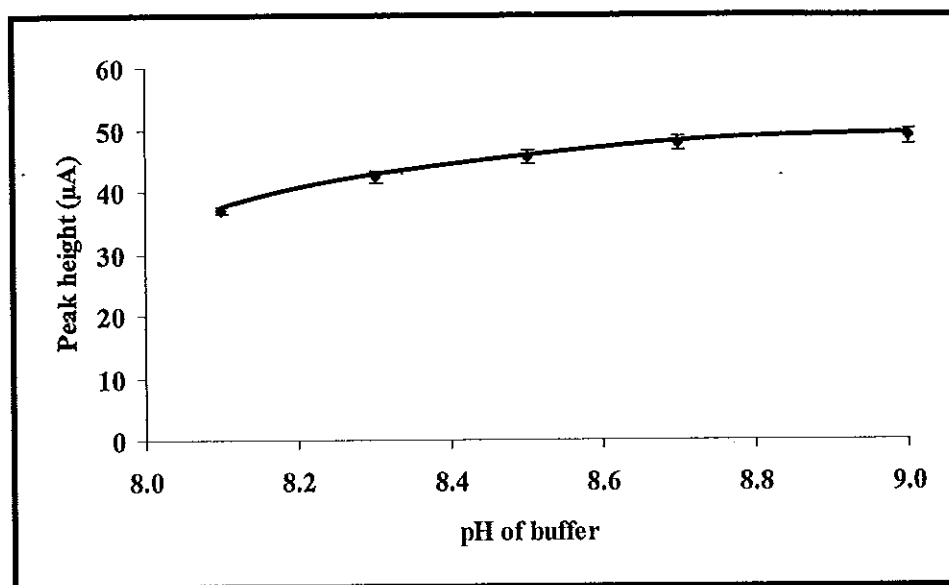


Fig. 7.11 Effect of pH of buffer on the response to 200 μL of 1.0 mM tetracycline in flow injection system; 25.0 mM borate buffer solution, 0.2 mL min^{-1} flow rate and -1.3 V detection potential.

The optimum conditions for both GCE and BiFE flow system are summarized in Table 7.1. These optimum conditions were used for system performance investigation and real sample analysis.

Table 7.1 The optimum conditions for GCE and BiFE in flow injection system

Conditions	Optimum values	
	GCE	BiFE
Detection potential (V)	-1.3	-1.3
Carrier flow rate (mL min^{-1})	0.2	0.2
Sample volume (μL)	200	200
KCl concentration (M)	0.1	0.1
Buffer concentration (mM)	25	25
pH of buffer	8.7	8.7

7.3.6 System performance

Borate buffer was used to prepared standard tetracycline in order to reduce the effect of background current and it can only dissolve tetracycline up to 6.0 mM. Therefore, tetracycline could only be tested up to 6.0 mM. However, this concentration is highly enough to detect tetracycline in real sample. At optimum conditions, system performance was investigated. Tetracycline standard solution (0-6.0 mM) was injected to the flow injection system. Figure 7.12 shows the actual amperometric responses of GCE and BiFE to 1.0, 2.0, 3.0 and 4.0 mM tetracycline in 25.0 mM borate buffer solution (pH 8.7) containing 0.1 M KCl where the peak height is proportional to the concentration of tetracycline.

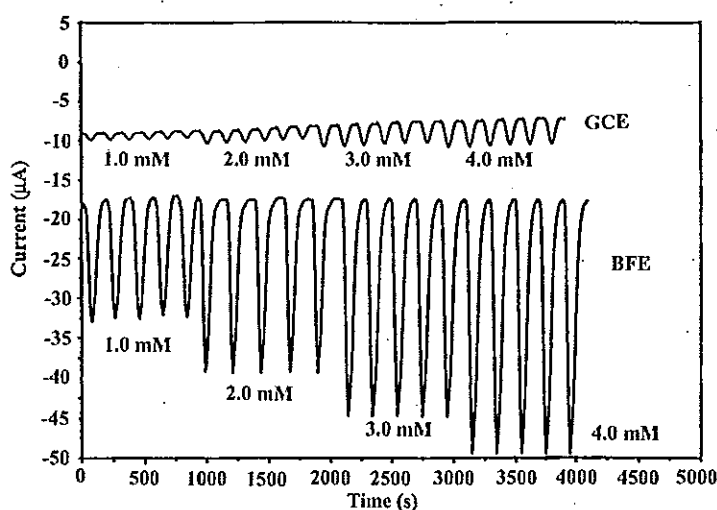


Fig. 7.12 The current responses of tetracycline obtained from GCE and BiFE at 1.0, 2.0, 3.0, 4.0 mM tetracycline at different concentrations; 25.0 mM borate buffer pH 8.70 containing 0.1 M KCl, applied potential -1.3 V.

The calibration curves are presented in Figure 7.13 showing the linearity of BiFE between 0 and 6.0 mM ($r = 0.999$). GCE gave the same linear range ($r = 0.999$) but was 4.5 times less sensitive (slope $1.7 \pm 0.3 \mu\text{A mM}^{-1}$) than BiFE ($7.9 \pm 0.2 \mu\text{A mM}^{-1}$). From the plot, the concentration of Bi(III) and peak current is linear in the study range (0-6 mM). The limit of detection was calculated following

IUPAC method (Long and Wineforder, 1983). Briefly, by injection of 20 blanks, standard deviation was calculated and multiplied with numerical factor chosen in accordance with the confidence level. In this research, the numerical factor selected was 3 allows a confidence level of 99.86%. Finally, to converse from measurement unit to concentration, the calculated value (numerical factor multiply by standard deviation of blank injection) was divided by analytical sensitivity. The related equations were presented on detail in chapter 5. The limit of detection obtained was 1.2 μM for BiFE and 7.0 μM for GCE, respectively. The linearity and detection limit of BiFE and GCE were in a higher concentration range than mercury film micro electrode used in capillary electrophoresis-end column detection with a small dead volume (linearity and detection limit were 1.0-500.0 μM and 0.7 μM for mercury film micro electrode) (Zhou *et al.*, 1999). However, this range of concentration is sufficient for the determination of tetracycline capsule in the market.

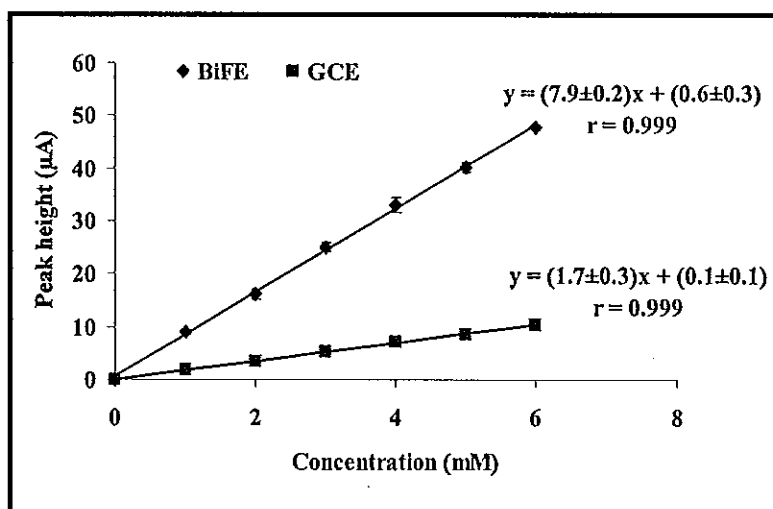


Fig. 7.13 Current responses of GCE and BiFE to tetracycline at different concentration in the flow injection system with 25.0 mM borate buffer pH 8.70 containing 0.1 M KCl.

7.3.7 Stability of bismuth film

The stability of BiFE was evaluated by injecting 2.0 mM of tetracycline 50 times into the amperometric flow injection system at optimum conditions. The results indicated that the cathodic peaks were relatively constant up to 40 injections ($16.3 \pm 0.9 \mu\text{A}$) and the peak currents decreased to about half thereafter (Figure 7.14). This is probably caused by the deterioration of bismuth film, similar to mercury film (Dinçkaya *et al.*, 2007). However, when this occurred, a new BiFE can be easily prepared by applying a potential of 0.25 V to strip off the bismuth film. The surface of GCE is then rinsed with deionized water and a new layer of bismuth can be deposited. The advantage of this technique is no mechanical polishing is needed to reactivate electrode surface prior to a new preparation because of the impurities on the electrode surface.

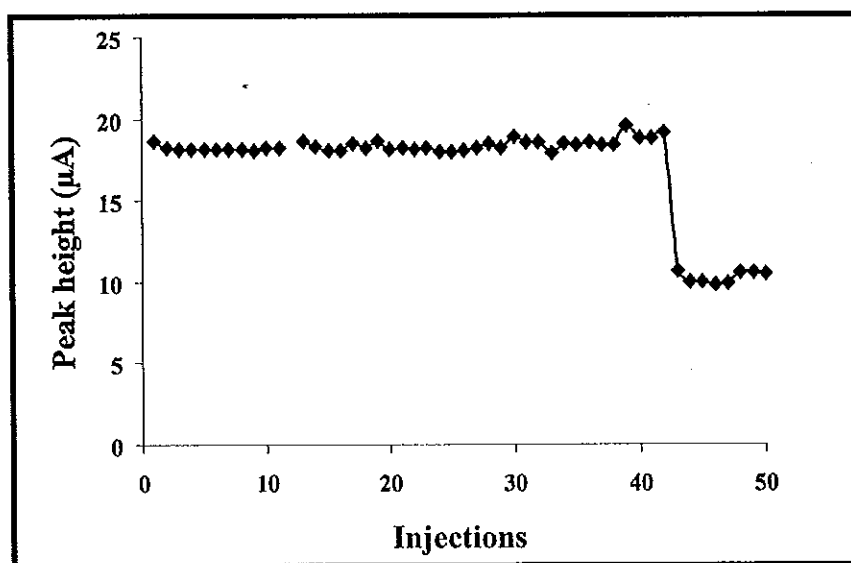


Fig. 7.14 Stability of the BiFE by injecting 2.0 mM of tetracycline for 50 times at the optimum conditions of flow injection system.

7.3.8 Reproducibility of bismuth preparation

To test the reproducibility of electrode responses three preparations of BiFE were used to analyze tetracycline at 1.0, 4.0 and 6.0 mM. By plotting the cathodic peak current as a function of tetracycline concentration then the relative standard deviation of the slopes were investigated and showed that each preparation of BiFE provided good reproducibility with %RSD 2.0 (Figure 7.15).

To confirm that the differences between the three different preparations of BiFE are not significant difference, the slopes of the three curves were also tested using two-way ANOVA (analysis of variance). Probability (P) value used to test was calculated by R software (R development Core Team, 2006). The hypothesis known as a null hypothesis, denoted by H_0 , is that the interaction of each pair of the slopes is not significant, and an alternative hypothesis (H_1), the interaction of each pair of the slopes is significant. If the P value is less than α (level of significance), then the null hypothesis was rejected at the significant level. In case of P value is higher than α , then the null hypothesis was retained showing that the slopes of the regression line is not significant different. The results from significant tests of the comparison of the three calibration curves are shown in Table 7.2. The results show that P value is higher than α (no significance code appear in the table). This indicates that the slope of regression line was not significantly different. Therefore, when the BiFE has reached its operation life a new film can be prepared and new calibration would not be required.

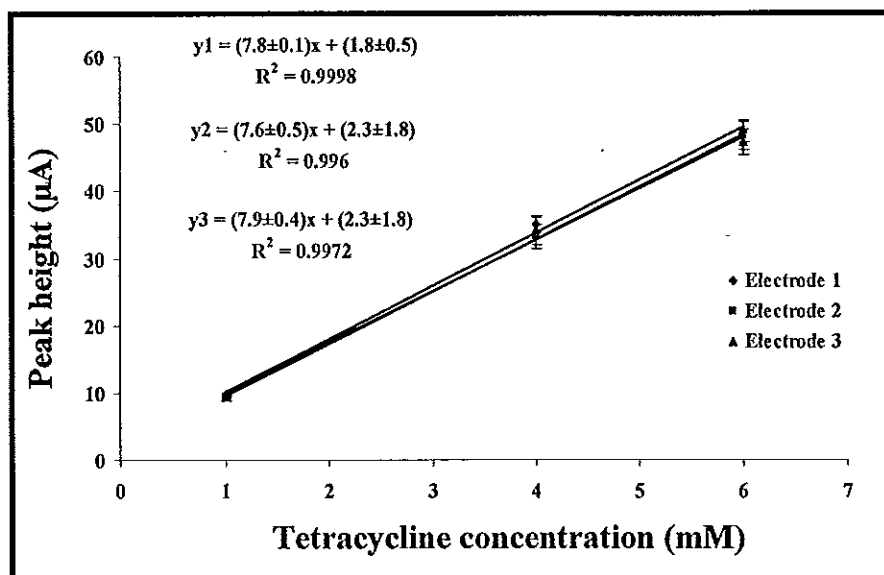


Fig. 7.15 The reproducibility of the responses from analysis of 1.0, 4.0 and 6.0 mM tetracycline using three new film modified electrodes.

Table 7.2 Statistical values for the comparison between the slopes of the regression line from three different BiFE using two-way ANOVA by R software.

Pair of electrode being tested	D_f	Sum Sq	Mean Sq	F	P
1 and 2	2	3.0	1.5	5.2×10^{-1}	6.1×10^{-1}
2 and 3	2	1.3	0.6	2.6×10^{-1}	7.8×10^{-1}
1 and 3	2	1.2	0.6	2.3×10^{-1}	8.0×10^{-1}

D_f : Degree of freedom

Sum Sq : Sum square

Mean Sq : Mean square

F : Ratio of two variances

P : Probability

7.3.9 Real sample analysis

Tetracycline contents of capsules obtained from a local drug store were determined by BiFE with amperometric flow injection system. Three different lot numbers were analyzed. For each lot, the content of twenty capsules of 250 mg

tetracycline were weighed and mixed. Then, 73.1 mg of the powder was dissolved in 25.0 mL of the running buffer solution (this would be equivalent to 4.0 mM) and injected to the amperometric flow injection system. Five replications were performed with $\% \text{RSD} \leq 4.0$ in all running. The responses were used to calculate the amount of tetracycline from the regression equation of the calibration graph. The results obtained for the three lots were 245 ± 5 mg, 260 ± 10 mg and 245 ± 10 mg of tetracycline per capsule. Relative recoveries were also studied by spiking 1.0 mM and 2.0 mM of tetracycline standard solution into each of the three lots of real samples. The results are shown in Table 7.3.

Table 7.3 % Relative recovery of spiked samples

Concentration of spiked tetracycline (mM)	% Relative recovery of 3 spiked samples		
	1	2	3
1.0	102 ± 5	86 ± 1	87 ± 1
2.0	106 ± 1	96 ± 1	93 ± 2

The results showed that the percentage relative recoveries were within the acceptance criteria (80-125%) providing sufficiently precise technique for medicine analysis (Bhattycharyya *et al.*, 2005).

7.4 Conclusions

A BiFE was applied to determine tetracycline in an amperometric flow injection system. The major advantages of BiFE are low toxicity of Bi(III), higher sensitivity when compared to bare GCE and simple to prepare. One preparation of bismuth film electrode can be used up to 40 times. When the responses have declined the bismuth layer can be easily stripped off and redeposited with good reproducibility. Therefore, analysis can be carried on without recalibration. When the system was applied for real sample analysis of tetracycline capsule, good agreement was obtained

between the value obtained from the flow injection analysis system and the labeled value. The system provided good recoveries and the analysis required only 3 minutes for each injection.

CHAPTER 8

Alloy Nanowires Barcodes

8.1 Introduction

Nanomaterial-based barcode system has attracted a lot of interest due to its potential applications ranging from product tracking to multiplexed biodetection (Finkel *et al.*, 2004; Han *et al.*, 2001; Nicewarner-Peña *et al.*, 2001). Widespread use of barcoded nanomaterials requires high coding capacity, a low-cost large-scale particle production, a portable and accurate detection system (Finkel *et al.*, 2004). In recent years, multi-striped metal nanowires, prepared by sequential templated electrodeposition of metal segments, such as gold and silver, of different lengths have been particularly useful for barcoding applications (Keating, 2003; Nicewarner-Peña *et al.*, 2001; Reiss *et al.*, 2002). However, the preparation of encoded multi-striped nanowires relies on a time-consuming synthesis involving multiple plating steps from different metal solutions and the encoding technique still take a long time (Reiss *et al.*, 2002).

Recently compositionally-encoded alloy nanowire tags were demonstrated. These alloy nanowires can be prepared by a single-step electrodeposition from a metal-mixture plating solution (Wang and Liu, 2006). A template-directed alloy preparation route obviates the need for sequential plating steps (from different metal solutions) common for the synthesis of multi-segment barcoded nanowires. This single-step preparation of one-segment alloy nanowires thus offers a substantial simplification and speed advantages over the multi-step preparation of multi-segment nanowires. However, a destructive and time-consuming readout electrochemical technique was performed, involving acid dissolution of the alloy nanowires (Wang and Liu, 2006).

In this chapter, two types of nanowires were investigated, i.e., multi- and single-segment alloy nanowires prepared from single plating solution. Multi-segment alloy nanowires were fabricated with different compositions of gold and

silver for each segment using single gold-silver mixture plating solution. It was expected that distinct optical reflectance of each segment, due to the different compositions, could provide distinctive stripping patterns and hence large coding capacity. This chapter also describes the possibility of synthesizing and usage of ternary alloy nanowires to develop single-segment alloy nanowires with non-destructive readout technique which is X-ray fluorescence (XRF).

For non-destructive readout method, X-ray fluorescence (XRF) has been widely used in various fields for rapid and accurate measurements of metal without sample preparation (Jurado *et al.*, 2006; Melquiades and Appoloni, 2004). The technique provides both qualitative and quantitative analyses and offers the simultaneous multi-element non-destructive readout of samples over a wide concentration range (Berendes *et al.*, 2006). XRF has thus been used for detecting the chemical composition of different alloys, ranging from steel (Ida *et al.*, 2005) to coins (Reiff *et al.*, 2001) and jewellery (Bonizzoni *et al.*, 2006). Portable (hand-held) XRF analyzers have been particularly useful for on-site non-destructive forensic or archeological analyses (Ida *et al.*, 2005) in which destructive sampling is not permitted. However, there are no early reports on XRF analyses of barcoded nanowires, in general, and of alloy nanowires, in particular.

In this study, a mixture of Ni, Co and Cu ions in an aqueous sulphate plating bath was used to prepare the alloy nanowires. These metals lead to well-resolved and close K_{α} XRF peaks and lead to a large coding capacity. Such coupling of one-step template synthesis of alloy nanowires with a non-destructive XRF readout (without dissolution of the encoded tags) greatly simplifies practical applications of bar coded nanomaterials, making the new strategy extremely attractive for different on-site tagging applications.

8.2 Experimental

8.2.1 Apparatus

Sputtering of the alumina membrane was accomplished with a Denton Vacuum Desk III TSC (Moorestown, NJ). Electroplating was accomplished using a

CHI 440 electrochemical analyzer controlled by CHI 2.06 software (CH Instruments, Austin, TX). The sputtered gold was removed from the membrane using a standard 8-inch SEM sample polishing machine (Model 900 Grinder/Polisher, South Bay Technology Inc., VA), along with 3 μm alumina powder (Fisher, Pittsburgh PA).

Optical images were acquired on a Nikon eclipse 80i microscope equipped with an X-Cite 120 fluorescence illumination system (EXFO, Mississauga, Ontario, Canada) as a light source and using a band-pass filter at 390 nm with a bandwidth 120 nm. Digital images from the microscope were acquired with a Photometrics CoolSnap CF camera (Roper Scientific, Duluth, GA) and MetaMorph 7 software (Molecular Devices Corp., Sunnyvale, CA).

X-ray fluorescence analyzer systems consisting of Kevex-ray 80800PSA and Kevex subsystem 0810A (Kevex, Foster City, CA) and a Kevex spectrometer (model 0810A, Kevex, Foster City, CA) were used to read the encoded alloy nanowires. Hand-held XRF measurements were performed with a NITON XLt 791 Thin Sample Analyzer (Thermo Fisher Scientific, NITON Analyzers, Billerica, MA). Scanning electron microscopy (SEM) images were obtained with the XL30 SEM instrument (FEI Co., Hillsboro, OR) equipped with an energy dispersive X-ray analyzer (Amatek Inc., Mahwah, NJ) using an acceleration potential of 30 kV.

8.2.2 Materials

The gold target (99.9+% pure) used for the sputtering of membrane was purchased from Denton Vacuum (Moorestown, NJ). Commercial gold and silver plating solutions (Orotemp 24 RTU RACK and 1025 RTU@4.5 Troy/Gallon, respectively) were obtained from Technic Inc. (Anaheim, CA). All standard solutions were prepared with ultra-pure (18.2 M Ω) water (ELGA-Ultra-Pure water polishing system model PURELAB ULTRA Scientific). Sodium hydroxide, cupric sulfate pentahydrate ($\text{CuSO}_4 \cdot 5\text{H}_2\text{O}$) and nickel sulfate hexahydrate ($\text{NiSO}_4 \cdot 6\text{H}_2\text{O}$) were obtained from Sigma (St. Louis, MO). Cobalt sulfate heptahydrate ($\text{CoSO}_4 \cdot 7\text{H}_2\text{O}$) was purchased from Alfa Aesar (Ward Hill, MA). Anodisc 25 alumina membranes (25-mm diameter, 200 nm pore size and 60 μm thickness) were received from Whatman (Maidstone, UK). For the application of single-segment alloy nanowires, cyclic olefin

copolymer (COC) sheets, 3 mm thickness, were obtained from Knightsbridge Plastic, Inc. (Fremont, CA), while the standard black inkjet ink was received from Hewlett Packard (Palo Alto, CA).

8.2.3 Preparation of multi-segmented (stripe) alloy nanowires barcodes

Alumina membranes were used as templates for the nanowires growth (Figure 8.1A). Before use, a gold layer was sputtered on one side of the membrane (where the pores are branched, Figure 8.1B) to serve as the working electrode during the electrodeposition (in connection to an aluminum foil contact). Ag/AgCl (3M KCl) and platinum wires were used as reference and counter electrodes, respectively. The sputtered membrane was placed at the bottom of a plating cell with the sputtered side contacting the aluminum foil (Figure 8.1C), acting as the working electrode.

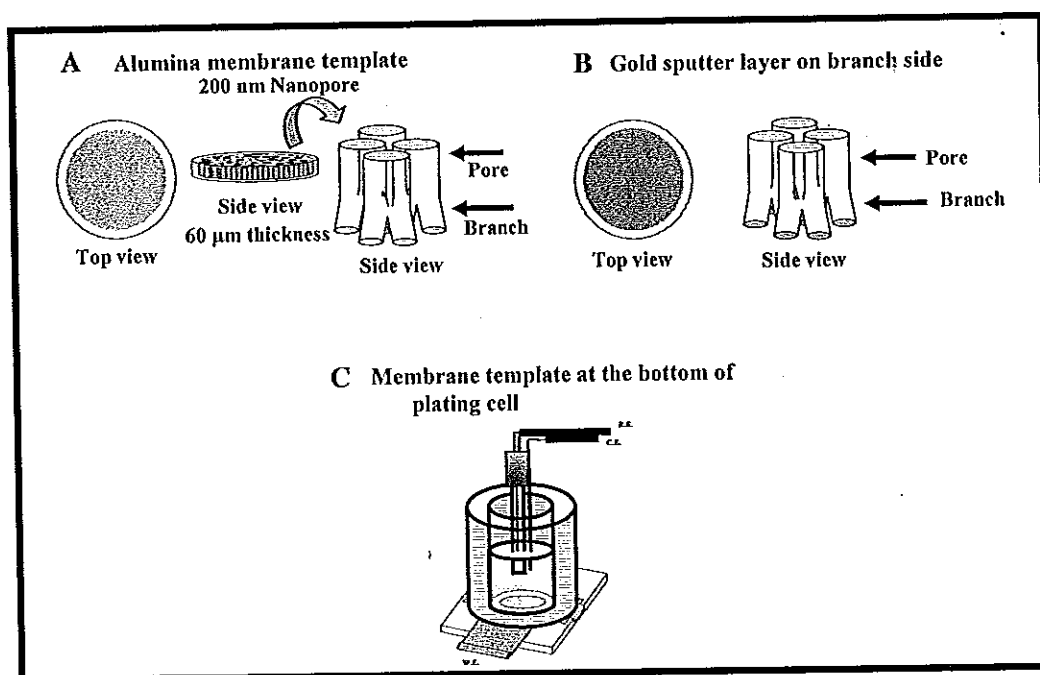


Fig. 8.1 Alumina membrane template (A) show a pore structure of the membrane (B) Gold was sputtered on the branch side of the membrane (C) Membrane was placed at the bottom of the plating cell.

Commercial gold plating solution (Orotemp 24RTU RACK) was added into the plating cell. Using deposition potential at -0.9 V gold was deposited into the branch of the membrane (Figure 8.2A). Then the mixture of commercial gold plating solution (Orotemp 24RTU RACK) was mixed with commercial silver plating solution (1025 RTU@4.5 Troy/Gallon) with the ratio of 85/15. This plating solution was introduced into the cell and then deposited using an amperometric technique (i-t curve) at a constant voltage, the length of the nanowires was controlled by the charge transferred. Three or four different potentials (-0.50 (Figure 8.2C), -0.85 (Figure 8.2D) and -1.20 V (Figure 8.2B) or -0.50, -0.73, -0.96 and -1.20 V) were applied sequentially in a pre-selected order and charge to deposit the individual alloy segments. The length of each segment was controlled by the total deposition charge.

After completing the deposition, the membrane was removed from the cell and a polishing step was performed, using the polishing machine combined with the alumina slurry to remove the sputtered gold layer and the membrane branches layer (Figure 8.2E). Nanowires were released from the template by dissolving the membrane in 3.0 M NaOH for 30 min (Figure 8.2F).

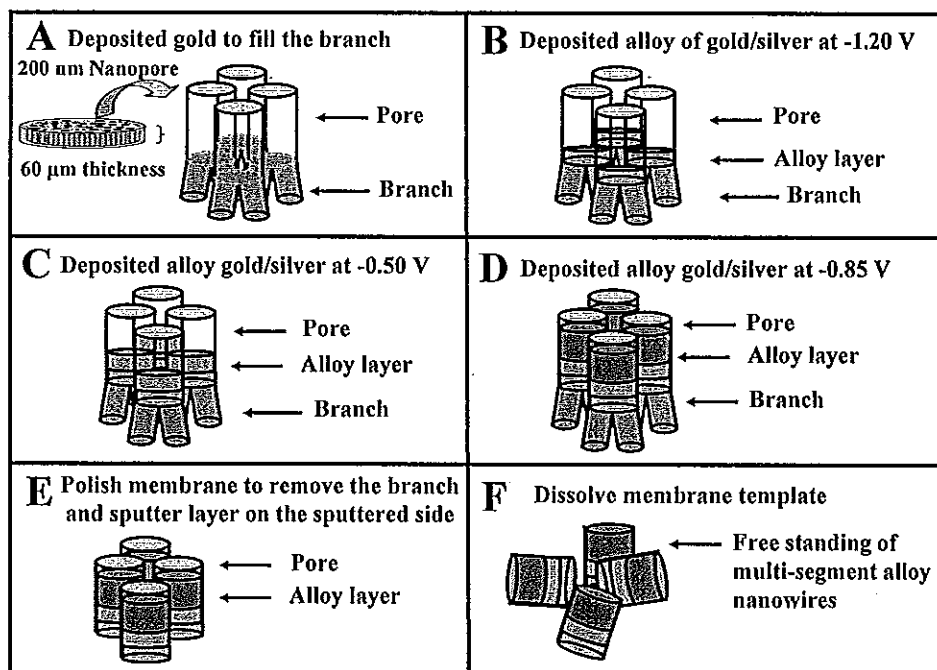


Fig. 8.2 Preparation of ternary alloy nanowires using alumina membrane as a porous template which have pore size 200 nm (A) Deposited gold into the branch (B) Deposited gold/silver at -1.20 V (C) Deposited gold/silver at -0.50 V (D) Deposited gold/silver at -0.85 V (E) Membrane was polished to remove sputtered metal and branch side of the template and (F) Dissolve membrane template to release alloy nanowires from template.

8.2.4 Optical barcode images processing of multi-segment alloy nanowires

Optical images were acquired using the 100x objective (LU Plan BD ELWD, Nikon Corp., Tokyo, Japan) on the Nikon 80i optical microscope, outfitted with the monochrome 12-bit dynamic range CoolSnap CF camera (previously mentioned). After the acquisition of the images, the optical pictures were processed using an internally developed protocol. First, using Photoshop CS2 (Adobe Systems Incorporated, San Jose, CA) the central part (along the axis of the nanowires) of the alloy nanowires barcode was selected (width of 4 pixels vs. different lengths), pasted

into a new 8-bit grayscale image and subsequently the auto-contrast filter built into Photoshop was applied on the nanowires strip image. The processed image was then fed to a Matlab (The Mathworks Inc., Natick, MA) program which averaged the pixel intensity across the 4 pixel columns and graphed this profile versus length of the wires. Using different plotting modes it is possible to quickly obtain the raw data or the normalized plots. The reflectance intensity was normalized using the highest intensity value corresponding to a predominantly silver segment deposited at -0.50 V. Normalization was performed with respect to the highest intensity value along the nanowires barcode. In order to obtain the dependency between the deposition potential and the reflectance intensity the above procedure was slightly modified. The same amount of pixels from each segment was selected and averaged to estimate intensity value of the segment. This segment intensity value was then plotted versus the corresponding plating potential. For normalizing the reflectance intensity, the brightest segment (pure silver) was assigned a value of 1.0, while the darkest segment (pure gold) was set to be 0.0. Every segment was measured 5 times (Figure 8.4).

8.2.5 Preparation of single-segment alloy nanowires

The plating system set up was as mentioned previously in section 8.2.3 (Figure 8.1). Silver plating solution (1025 RTU@4.5 Troy/Gallon) was used to deposit silver segment under amperometric mode at -0.9 V at a charge of 2.0 Coulomb (C) (Figure 8.3A). This was followed by deposition of gold, using commercial gold plating solution (Orotemp 24 RTU RACK), at -0.9 V using a charge of 1.0 C (Figure 8.3B). The metal-mixture plating solution was subsequently introduced to the cell. Plating solutions composed of 40.0 g L⁻¹ of H₃BO₃ with different concentrations of the metal salts [cobalt (CoSO₄·7H₂O), nickel (NiSO₄·6H₂O), and copper (CuSO₄·5H₂O)] (final pH ~3.8). Deposition from these plating solutions was carried out at a fixed potential of -1.4 V using a total charge of 15.0 C (Figure 8.3C). After completion, the membrane was removed from the cell and polished to remove the sputtered gold and branch side as previously stated (Figure 8.3D).

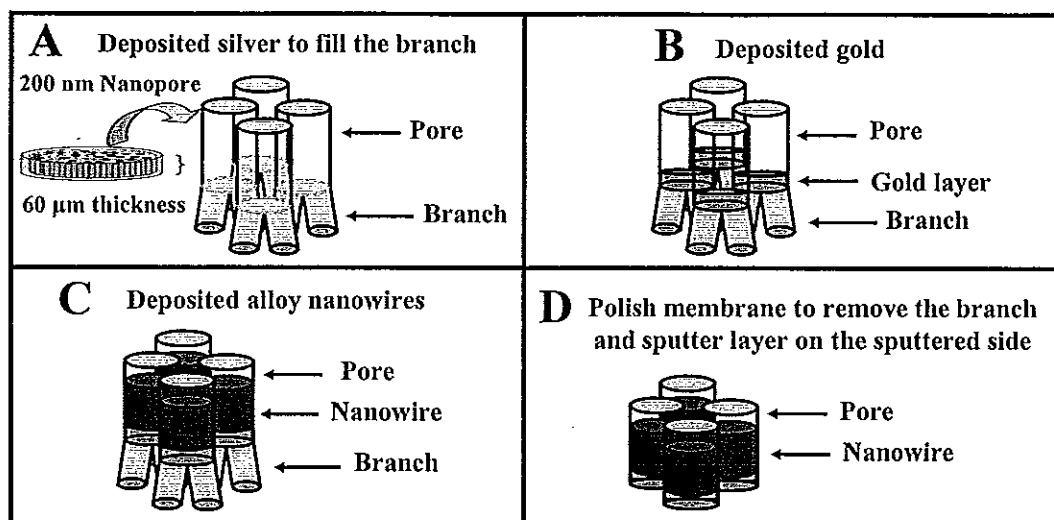


Fig. 8.3 Preparation of ternary alloy nanowires using alumina membrane as a porous template (A) Deposited silver into the branch at -0.9 V for 2.0 C (B) Deposited gold at -0.9 V for 1.0 C (C) Alloy nanowires was deposited at -1.4 V for 15.0 C and (D) Membrane was polished to remove sputtered metal and branch side of the template.

The alumina membrane was then rinsed with ultrapure water and divided into two equal pieces. One was placed in a 3.0 M NaOH solution for 30 min to allow complete dissolution of the membrane. Nanowires were separated magnetically from the NaOH solution and were rinsed with ultrapure water until a neutral pH was obtained (the final suspension volume was 2.0 mL). The other piece of the nanowire-containing membrane was kept intact for direct XRF analysis of the embedded nanowires.

To test their usages, ink containing the encoded nanowires was prepared by mixing 3.0 mg of the wires with 1.5 mL of a commercial black inkjet ink. Using a pipette a 30.0 μL droplet of the resulting ink was then dispensed dropwise onto standard white printing paper (Xerox, Business 4200, 20lb, Rochester, NY) and was allowed to dry prior to the XRF readout. Bar-coded nanowires were also embedded in cyclic olefin copolymer (COC) plastics by sandwiching and varying the amount of the encoded nanowires between the fused COC sheets.

8.2.6 Analytical procedure of single-segment alloy nanowires

XRF readouts of the nanowire composition profiles were performed on nanowires embedded in the membrane and those released after membrane dissolution. Most XRF spectra were obtained using the Kevex XRF system, with the high voltage power supply operated at 20.0 kV and 1.5 mA. X-rays that bombarded the nanowire samples were emanated from a Germanium secondary target with K_{α} and K_{β} lines at 9.89 and 10.98 keV, respectively. Some measurements were performed using a NITON handheld XRF analyzer which was operated at low power supply (1.0 W) at 20 kV and 5 μ A using X-ray tube germanium target to bombard samples. NITON handheld XRF provide similar K_{α} and K_{β} lines at 9.89 and 10.98 keV, respectively. The XRF spectra obtained from both instruments, Kevex XRF and NITON handheld XRF were compared. The XRF spectrum for each sample was acquired over 200 seconds with the Kevex XRF system and for 60 seconds with the NITON handheld unit. The XRF data (intensity) were normalized using Excel software, with respect to counts corresponding to a given K_{α} value of one of the unchanged metals.

8.3 Results and discussion

8.3.1 Multi-segment alloy nanowires

8.3.1.1 Multi-segment alloy nanowires synthesis

The multi-segment alloy nanowires preparation route via the mixture of plating solution greatly simplifies the code production when compared to the solution-changing sequential deposition of common bimetal nanowires barcodes (Nicewarner-Peña *et al.*, 2001; Reiss *et al.*, 2002; Walton *et al.*, 2002). The different deposition potentials are applied sequentially in a pre-determined order and for different durations to produce alloy segments of controlled length. This is followed by the template dissolution and optical readout of the reflectance patterns. Compared to recently developed single-segment alloy nanowires electrochemical barcodes (Wang

and Liu, 2006), the new striped alloy nanowires can be readily decoded on the basis of differences in optical reflectivity, which is a faster and cheaper diagnostic tool.

8.3.1.2 Alloy composition

The compositions of gold/silver, due to the different deposition potential from -0.50 to -1.20 V when using constant gold/silver ratio of 85/15, were studied using energy dispersive X-ray analyzer (EDX). The silver content decreased in a nearly sigmoidal fashion from 92 to 53 % (Table 8.1) upon raising deposition potential since increasing deposition potential provide faster reduction rate of gold, therefore, gold component increased while silver component decreased.

Table 8.1 Percentage of atomic silver at difference deposition potential using 85/15 of Au/Ag

No. of measurement	Deposition potential (V)		
	-0.50	-0.85	-1.20
1	91.5	76.0	55.3
2	92.0	75.0	51.0
3	92.5	77.0	53.0
Average	92.0	76.0	53.1
SD	0.5	1.0	2.2
%RSD	0.5	1.3	4.1

Optical microscope was then used to study the reflectivity of each segment which has different alloy composition resulting in different light reflectance (Figure 8.4).

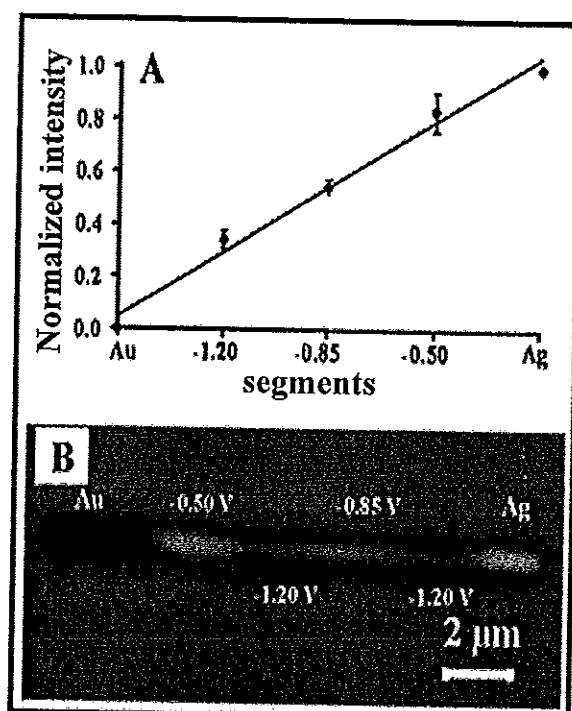


Fig. 8.4 (A) The relationship between normalized reflectance intensity and deposition potential (B) A reflectance microscopy image of a multi-segment nanowire deposited over the -0.50 to -1.20 V range and pure gold and silver segments (at the ends, deposited at -0.90 V).

8.3.1.3 Bar coding signature generation

The ability to tune the optical properties by adjusting the deposition potential and to generate multisegment alloy nanowires with distinct optical reflectance barcode patterns from a single plating solution are illustrated in Figure 8.5. In this study, three potentials were investigated, -0.50, -0.85 and -1.20 V. Pure solid silver presents the brightest segment while gold provide the darkest part. The brightest segment was used for normalization for the entire segment, therefore the brightness of silver segment was equal to 1 whereas gold's is equal to 0. Figure 8.5 shows reflectance images (top) and intensity lines (bottom) for three nanowires prepared by applying different potentials using different preset orders and charges. Such change in the deposition conditions results in distinct striping patterns involving three easily

distinguishable reflectance intensity levels (bright, dark and intermediate), corresponding to the individual alloy segments.

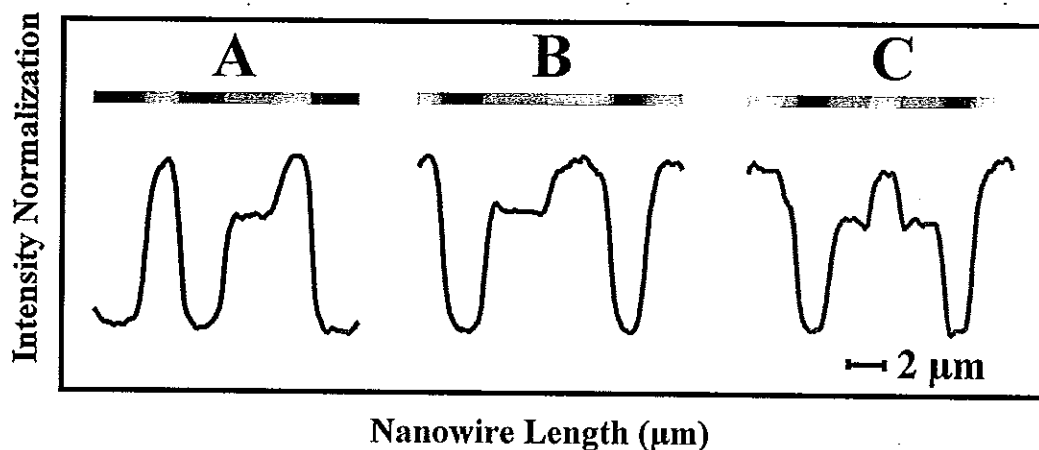


Fig. 8.5 Reflectance images (top) and intensity lines (bottom) for different multisegment alloy nanowire barcodes prepared from an 85/15 (v/v) Au/Ag plating solution. The sequences of the deposition potentials for each nanowire image are (from left to right) (A) -1.20, -0.50, -1.20, -0.85, -0.50 and -1.20 V (B) -0.50, -1.20, -0.85, -0.50, -1.20, and -0.5 V (C) -0.50, -1.20, -0.85, -0.50, -0.85, -1.20 and -0.50 V.

Also shown in Figure 8.6 is an SEM image of the corresponding nanowires (A) and optical reflectance image (B) of the same batch preparation of the wires. The individual segments are clearly visible for both SEM and optical reflectance image and as expected, four intensities of SEM are the opposite of the corresponding optical-reflectance intensities.

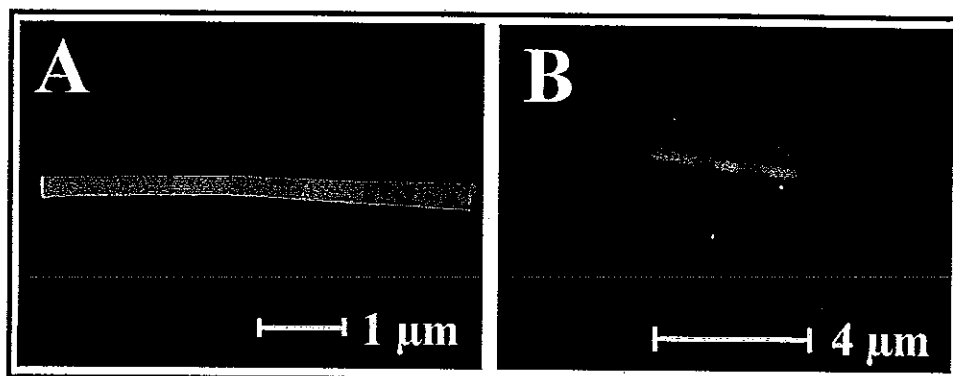


Fig. 8.6 (A) SEM and (B) optical reflectance images of multi-segment alloy nanobarcodes clearly show different color of each segment when changing plating potential. In optical microscopy technique, the most reflective is at -0.5 V (bright) and the least reflective is -1.2 V (dark) while -0.85 V provides intermediate color.

This concept can lead to a huge number of uniquely identifiable nanowires. Theoretically, varying the number of intensities, segment length and order can generate an unlimited number of codes. The coding capacity is effectively n^m where n is the number of intensity levels (i.e., alloy compositions) and m is the number of segments in the nanowires (assuming that the direction of the nanowires can be determined) (Wang, 2006 and Wang, 2003). In practice, however, given the current resolution, up to 5 intensity levels can be distinguished and up to 10 segments can be resolved within a typical 10 μm long nanowires. This combination corresponds to 9,765,625 (5^{10}) distinguishable nanowires. Such ability to generate 4-5 distinct alloy segments (and hence a huge coding capacity) using a single plating solution represents a major improvement over commonly used bimetal nanowires code ($n=2$) prepared by a solution-changing sequential deposition (Nicewarner-Peña *et al.*, 2001; Reiss *et al.*, 2002; Walton *et al.*, 2002). The plating process can be computer-controlled for the simultaneous synthesis of multiple striping patterns in different membranes.

8.3.2 Characteristic of single-segment alloy nanowires

8.3.2.1 Scanning electron micrographs of alloy nanowires

The single-segment alloy nanowires prepared from the deposition of the mixture of Co, Ni and Cu plating solution into a porous template called “ternary alloy nanowires” were studied by scanning electron microscope (SEM). Figure 8.7A shows alloy nanowires embedded in the membrane template and Figure 8.7B after the membrane template was dissolved. From the image only one color was observed indicating that preparation of “single segment” alloy nanowires was accomplished from the use of mixture of plating solution and constant deposition potential. For the nanowires shown in Figure 8.7, 30 g L⁻¹ of Co, 50 g L⁻¹ Ni and 10 g L⁻¹ Cu were used, nanowires were deposited at -1.4 V for a total charge of 15.0 C. At these conditions the lengths of alloy nanowires were 11.0±0.9 μm with a diameter of 200 nm, the same diameter as the pore size of the membrane template. Therefore, it is possible to control the size of nanowires through the pore size of the template and the deposition charge.

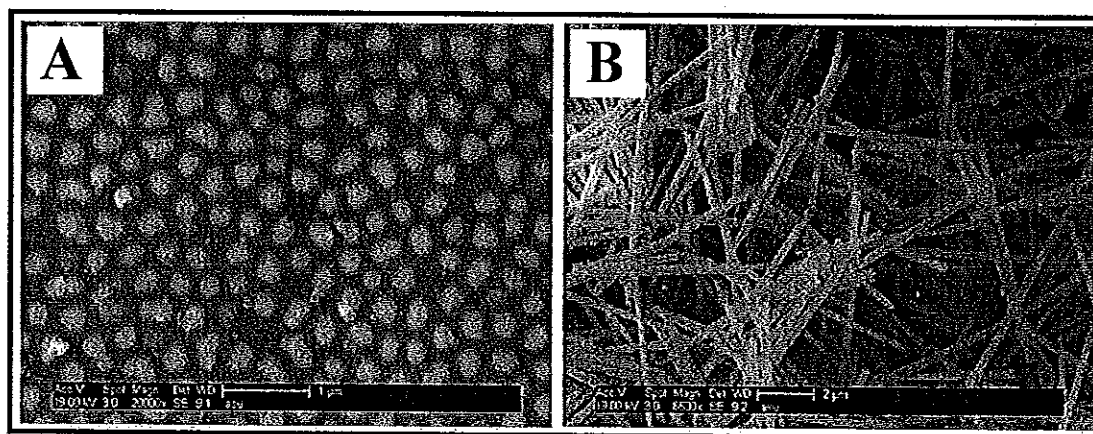


Fig. 8.7 Scanning electron micrographs of alloy nanowires deposited at -1.4 V for 15.0 C. (A) Alloy nanowires embedded in alumina membrane template and (B) after dissolve membrane template.

8.3.2.2 Non-destructive readout

X-ray fluorescence (XRF) was used to detect the compositions and amount of the deposited metal in the porous template. The readout of alloy nanowires yields a distinct multi-peak spectrum, reflecting the emission of K_{α} photons (Figure 8.8). The XRF spectra in Figure 8.8 show the peak energies for K_{α} lines at 6.9 keV for Co, 7.5 keV for Ni, and 8.0 keV for Cu. There are tiny shoulders on the nickel and copper peaks. Such shoulder reflects the emission of cobalt and nickel K_{β} photons at 6.8 keV and 8.1 keV. When the concentration of Cu increased from 5 (Figure 8.8A) to 10 mg L⁻¹ (Figure 8.8B) the peak intensity of copper K_{β} photon increased. That is, K_{β} spectra can provide added information for the content and distinct signature of the corresponding nanowires.

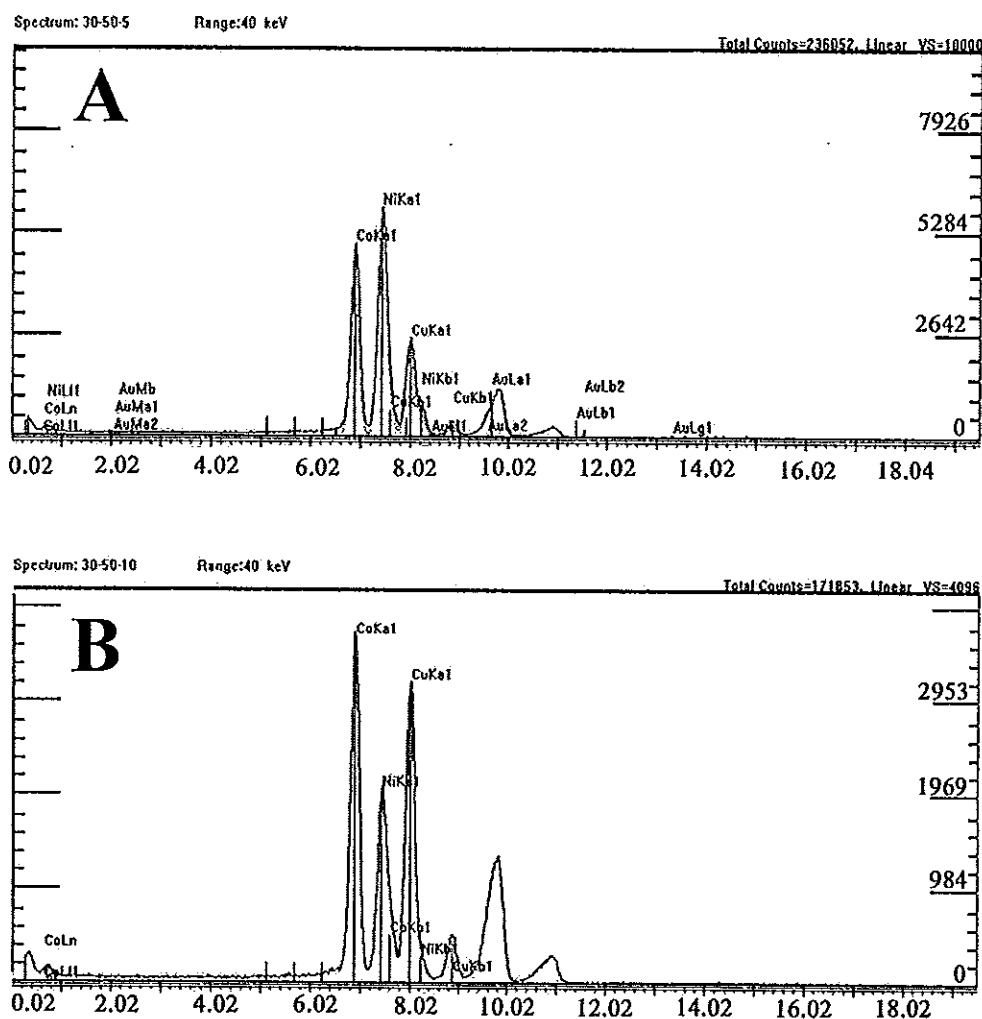


Fig. 8.8 XRF spectrum of alloy nanowires showing peak energies of K α and K β photons of Co, Ni and Cu (A) Co/Ni/Cu at the concentration of 30/50/5 mg L $^{-1}$ (B) Co/Ni/Cu at the concentration of 30/50/10 mg L $^{-1}$.

3.2.3 Two and three dimensional responses

Figure 8.9 compares XRF signatures of ternary alloy nanowires of both K α and K β (prepared from a 30/120/10 g L $^{-1}$ Co/Ni/Cu solution), obtained before (Figure 8.9A) and after (Figure 8.9B) dissolving the membrane template. Both cases yielded similar XRF signatures, with similar peak energies, intensities and peak intensity ratios, indicating the uniformity of alloy nanowires and that the barcodes are not affected by the membrane dissolution. The results also show that the XRF readout

of the alloy nanowires (K_{α}) can be accomplished while the wires are embedded in the membrane or after dissolving the membrane. Notice again the distinct Ni K_{β} shoulder peak on the copper signal that can provide additional identification capability.

The nanowires analyzed in the membrane represent a highly concentrated 2 dimensional array ($\sim 1 \times 10^9$ nanowires/cm²) and in the suspension, a dilute 3 dimensional scattering of nanowires. This figure shows that a relatively small sample of nanowires can produce the same normalized XRF response as a highly concentrated sample.

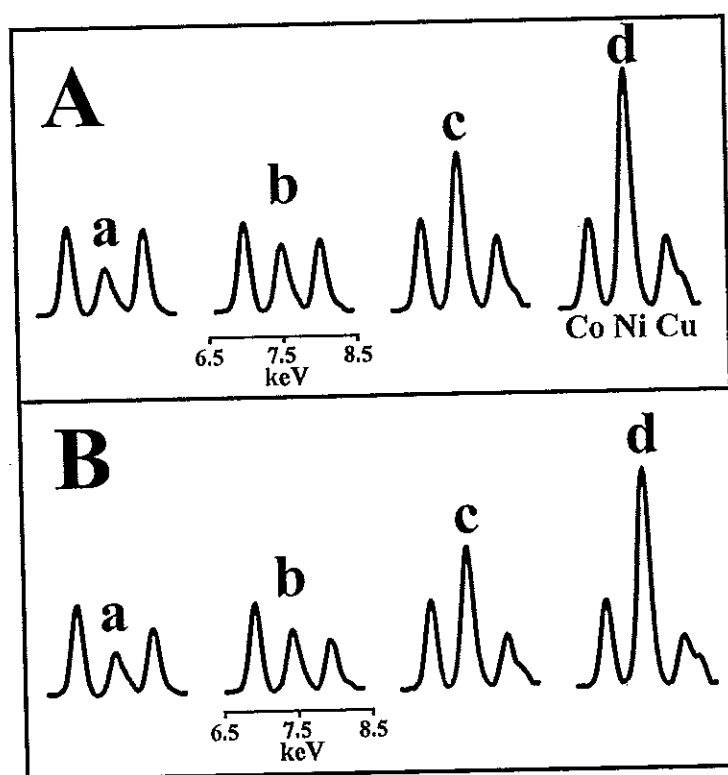


Fig. 8.9 Comparison of X-ray fluorescence readout of alloy nanowires obtained before (A) and after (B) dissolving the membrane template. The nanowires were prepared by electrodeposition at -1.4 V for a total charge of 15.0 C. The nanowires were prepared using plating solutions with different Co, Ni and Cu concentrations (in g L⁻¹): (a) 30Co/40Ni/10Cu (b) 30Co/60Ni/10Cu (c) 30Co/90Ni/10Cu (d) 30Co/120Ni/10Cu.

8.3.2.4 Generation of barcode signature

Since the aim of this research is to use alloy nanowires as a “nano-barcode” therefore the possibility to generate different coding patterns was investigated by varying the concentration of one metal while the other two were kept constant. For example, Co concentration was varied while Ni and Cu concentration were kept constant. The peak intensities of each metal were normalized with respect to the metal using constant concentration. Therefore, nanowires prepared from the same concentration provide the same signature even through the detected amount of nanowires is different.

The ability to tune the XRF peak intensities by controlling the composition of the alloy nanowires, through the composition of the plating solution, is illustrated in Figure 8.10. The figure shows XRF readouts of ternary wires with different composition patterns, obtained by changing the content of one metal (Co, Ni and Cu) while keeping the level of the other metals constant. The one-step template synthesis of Ni-Co-Cu alloy nanowires of different metal contents can lead to a large number of characteristic XRF bar coding patterns, reflecting the composition of the corresponding nanowires.

The resulting fluorescence signatures correlate well with the composition of the plating solution, with the corresponding peak intensities following the levels of the corresponding metal in the plating solution. A slight deviation from linearity of the corresponding intensity-concentration plots was observed at the lower concentration values (Figure 8.11). Linear intensity – concentration correlations were reported earlier for voltammetric signatures of alloy nanowires following their acid dissolution (Wang and Liu, 2006). The slight nonlinearity, observed at the lowest metal concentrations, is attributed to a potential composition gradient along the nanowires, associated with differences in the ion diffusion rates (Saedi and Ghorbani, 2005).

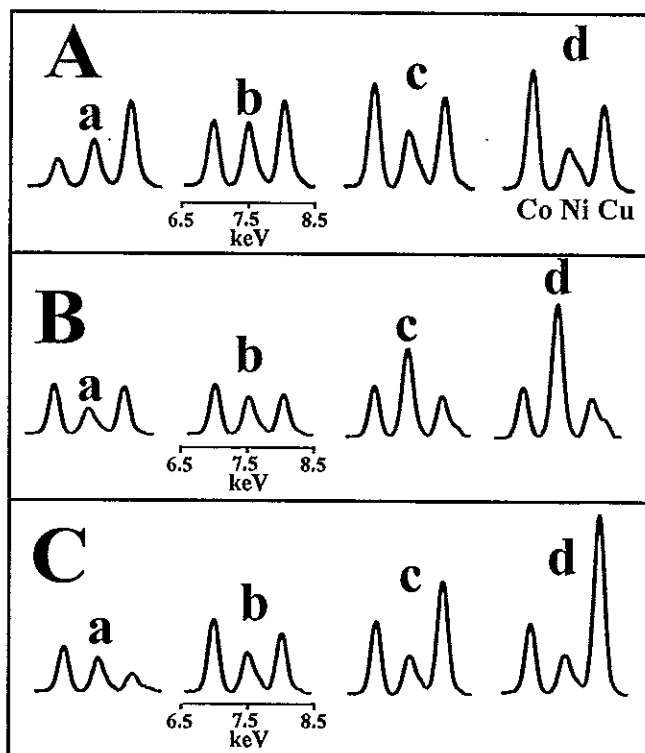


Fig. 8.10 X-ray fluorescence of single-segment alloy nanowires prepared by changing concentration of one metals (Co (A), Ni (B) and Cu (C)) while keeping the level of others constant. (A) Changing the Co concentration (a-d: 10, 20, 30, 40 g L⁻¹) with Ni and Cu at 50 and 10 g L⁻¹, respectively. (B) Changing the Ni concentration (a-d: 40, 60, 90, 120 g L⁻¹) with Co and Cu at 30 and 10 g L⁻¹. (C) Changing the Cu concentration (a-d: 5, 10, 15 and 20 g L⁻¹) with Co and Ni at 30 and 50 g L⁻¹. All alloy nanowires were electrodeposited at a potential of -1.4 V using a total charge of 15.0 C.

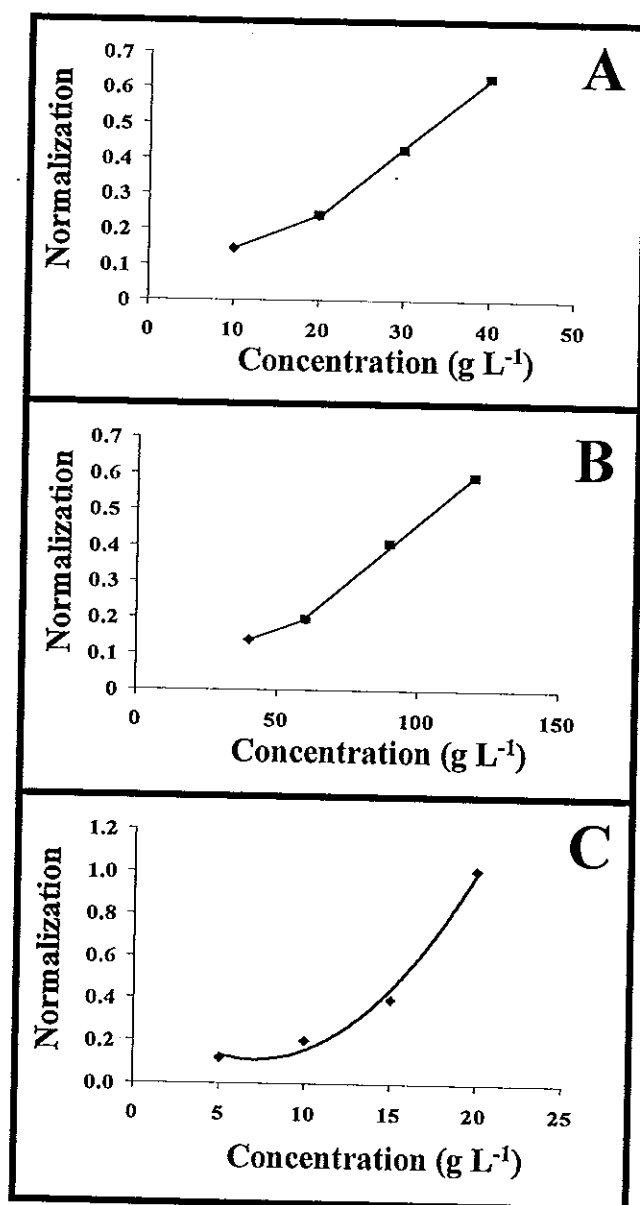


Fig. 8.11 Relationship between concentration and normalized intensity. (A) Changing Co concentration (10, 20, 30, 40 g L⁻¹) with Ni and Cu at 50 and 10 g L⁻¹, respectively. (B) Changing Ni concentration (40, 60, 90, 120 g L⁻¹) with Co and Cu at 30 and 10 g L⁻¹. © Changing Cu concentration (5, 10, 15 and 20 g L⁻¹) with Co and Ni at 30 and 50 g L⁻¹. All alloy nanowires were electrodeposited at a potential of -1.4 V using a total charge of 15.0 C.

8.3.2.5 Single-segment alloy nanowires validations

8.3.2.5.1 Reproducibility

Reproducibility of the plating process was investigated by divided one membrane template into 6 different sections; each section was detected using XRF. The peak intensity was recorded and the percentages of relative standard deviations of peak intensities were 4.7, 5.7 and 4.8 for Cu, Ni and Co, respectively (Table 8.2). This low %RSD indicated a reproducibility of the plating process. In addition, the reproducibility of the nanowires was also investigated by comparing three samples of the wires grown from different batch using the same solution. The XRF peak heights of these data (normalized as described earlier) yielded relative standard deviations ranging between 4.3 and 8.5% for the three metals.

Table 8.2 Reproducibility of 6 sections from one membrane template

Sections	Intensity (count s ⁻¹)		
	Co	Ni	Cu
1	374	342	272
2	370	366	282
3	347	334	275
4	339	310	246
5	377	322	263
6	382	342	271
Average	365	336	268
SD	17	19	12
%RSD	4.8	5.7	4.7

8.3.2.5.2 Uniformity

Uniform length-independent alloy compositions should greatly facilitate practical applications of the new bar-coded nanowires. Figure 8.12 examines the influence of the nanowire length (reflected by the deposition charge) upon the

corresponding XRF peak intensities for ternary Ni-Co-Cu nanowires prepared using charges ranging from 2.0 C to 15.0 C (a-d). As expected, the signals of the three metals increase linearly with the deposition charge over the entire 2.0 C to 15.0 C charge range. The peak intensity ratios for all study range were also constant (Table 8.3), indicating a uniform alloy composition along the length of the nanowires. The peak ratios in the corresponding fluorescence signatures, hence the overall nanowire signatures, are independent of the charge used during the plating process (i.e., length of the resulting nanowires).

Table 8.3 Normalized peak intensity of Co, Ni and Cu showing peak ratios of the fluorescence signature.

Total charge	Normalized peak intensity of		
	Co	Ni	Cu
2	0.22	0.13	1.0
5	0.24	0.19	1.0
10	0.29	0.17	1.0
15	0.26	0.15	1.0
Average	0.25	0.16	1.0
SD	0.03	0.02	0.0
%RSD	11.9	14.8	0.0

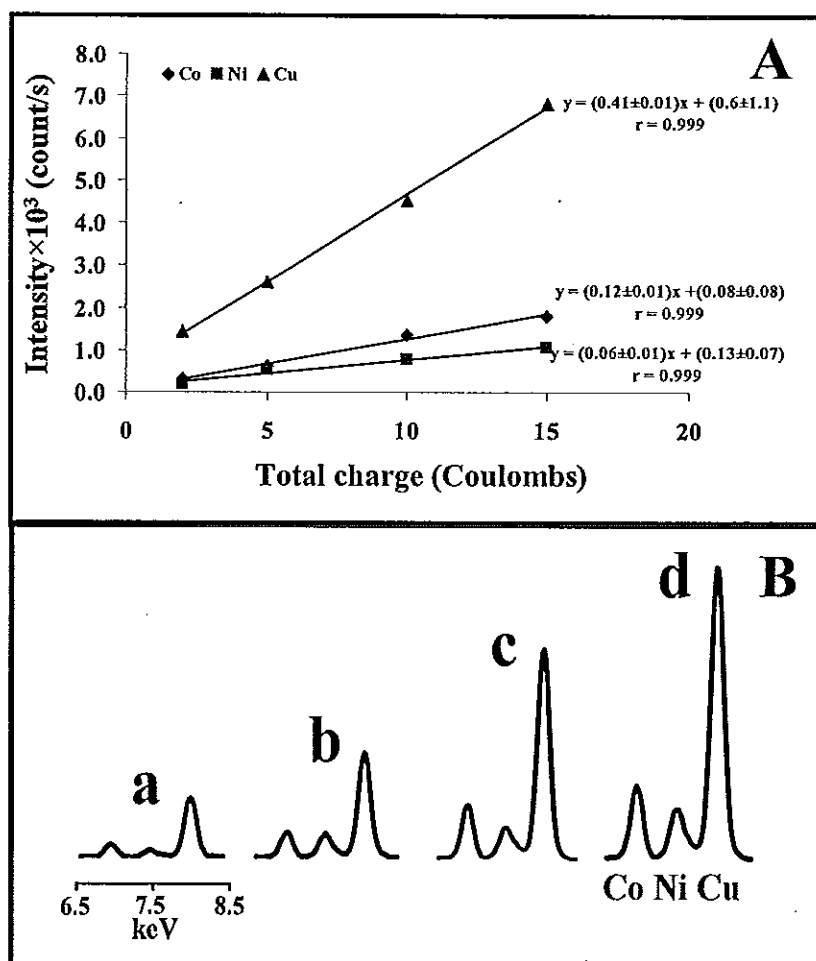


Fig. 8.12 XRF readout of Co-Ni-Cu alloy nanowires of different lengths (A) Linear relationship of deposition charge and peak intensity: (B) XRF signal obtained from various deposition charge 2.0 C (a), 5.0 C (b), 10.0 C (c), and 15.0 C (d) and a plating solution containing 5.0 g L⁻¹ of the corresponding metal salts.

8.3.2.5.3 Kevex XRF and hand-held XRF readout

There are some earlier reports that portable XRF analyzers have found extensive field applications (Ida *et al.*, 2005). Therefore, hand-held XRF could greatly facilitate numerous practical on-site applications of the encoded alloy nanowires. Accordingly, the XRF signatures obtained with an easy-to-use and compact hand-held XRF unit (shown in Figure 8.13) were compared with those recorded with a centralized large laboratory analyzer (Kevex XRF). These comparisons, shown in

Figure 8.14, indicated that both the Kevex XRF and portable systems yield similar XRF profiles. These studies could lead to the application of hand-held XRF for decoding of nano-barcode in real life.

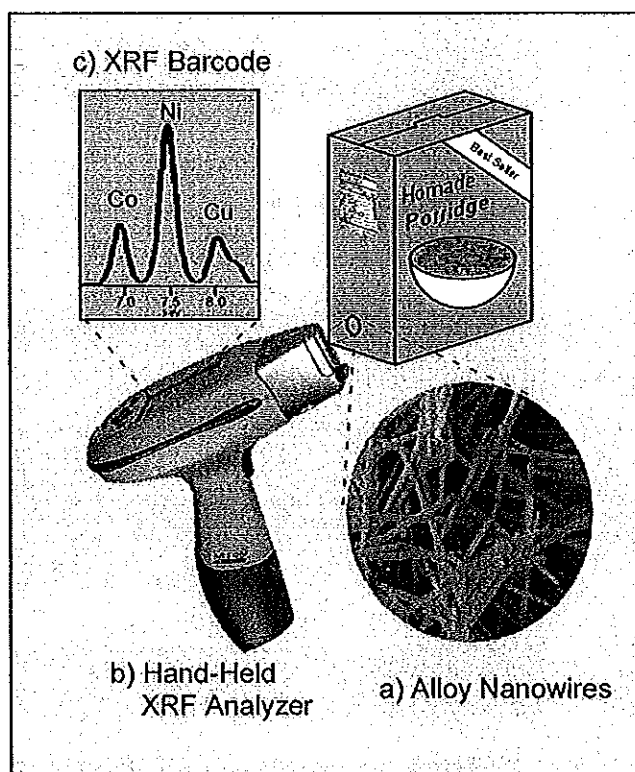


Fig. 8.13 Non-destructive XRF readout of barcoded alloy nanowires for the product identification. Barcoded nanowires (inset a) are embedded in packaging materials of a commercial product and detected with a hand-held XRF analyzer (b) The resulting XRF signature (c).

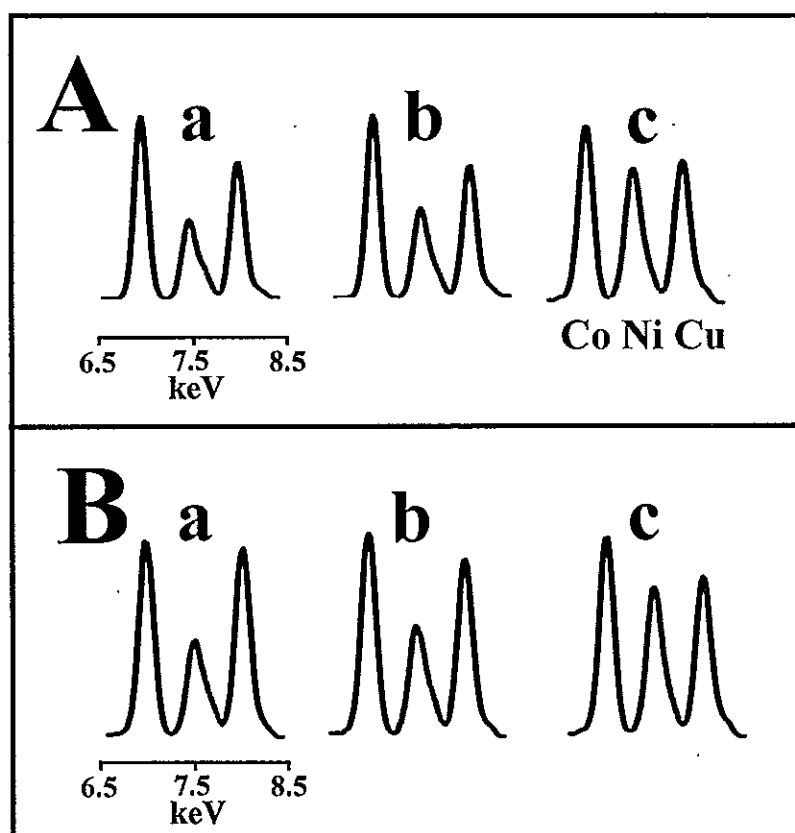


Fig. 8.14 Comparison of the nanowire XRF readout obtained with a handheld XRF (Niton) unit (A) and a laboratory-based (Kevex XRF) instrument (B). Alloy nanowires (in membrane) prepared using plating solutions with the following Co/Ni/Cu concentration ratios: (a) 30/45/10, (b) 30/50/10, (c) 30/65/10.

8.3.2.5.4 Limit of detection

Since the number of identifiable nanowires depends upon the number of distinguishable metals and the number of peak intensities, it is possible to obtain thousands of readable XRF signatures with three or four metals present at four to six loadings. In this study using three metals, a sample of wires grown from a solution containing equal amount 5 g L^{-1} of Co, Ni and Cu was used to evaluate the detection limit following the IUPAC method (Long and Wineforner, 1983 and Thomsen, 2003). Various concentration of nanowires were prepared by disperse different amount of

wires in nanopure water. Then, a 30.0 μL of dispersed nanowires was dropped on the printing paper. When dried, it provided an area of 0.28 cm^2 these dry nanowires were detected using XRF. The intensity versus amount of wires was plotted provided calibration curve (Figure 8.15). From analysis of 20 blanks, the background noise was measured from 6.9 to 8.4 keV (Table 8.4), the detection limits of Co, Ni and Cu were 2.4 ± 0.1 , 8.4 ± 0.3 and 3.2 ± 0.2 μg . These detection limits can be converted to be amount of wire per square centimeter (area) which is 8.6 ± 1.2 , 30.0 ± 1.2 and 11.4 ± 0.6 $\mu\text{g cm}^{-2}$. However, only at 30 $\mu\text{g cm}^{-2}$ that all these metals (Co, Ni and Cu) could be detected whereas at the level of 8.6 $\mu\text{g cm}^{-2}$ only Co can be analyzed and at the level of 11.4 $\mu\text{g cm}^{-2}$, Co and Cu can be investigated while Ni can not be detected. Therefore, at 30.0 $\mu\text{g cm}^{-2}$ was considered to be the detection limit in this research.

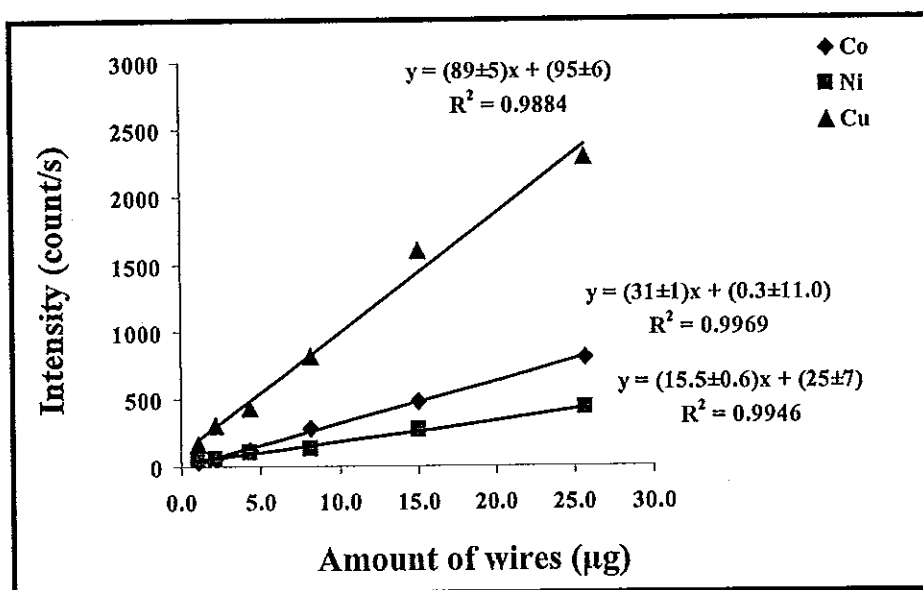


Fig. 8.15 Calibration curve of single-segment alloy nanowires dried on the paper with different amount of nanowires.

Table 8.4 The intensity of background noise measurement from 20 blanks

Number of measurement	Intensity of background (count s ⁻¹)		
	Co	Ni	Cu
1	19.5	65.0	203.5
2	62.8	61.4	305.6
3	37.6	66.1	75.2
4	45.1	109.0	113.9
5	51.6	102.0	93.8
6	45.1	27.1	113.9
7	37.0	45.0	147.3
8	24.3	55.0	110.1
9	23.6	67.8	103.1
10	44.0	76.8	77.0
11	22.7	88.0	113.3
12	55.9	28.9	108.5
13	55.9	76.0	28.9
14	22.7	77.0	113.3
15	35.2	65.9	102.7
16	38.1	98.0	131.4
17	45.7	87.0	139.0
18	30.8	78.0	122.9
19	33.5	66.0	131.6
20	39.9	71.1	73.7
Mean	38.6	70.0	120.4
SD	12	20	56
SD×3	37	60	168
LOD (µg)	2.4±0.1	8.4±0.3	3.2±0.2
LOD (µg cm ⁻²)	8.6±1.2	30.0±1.2	11.4±0.6

8.3.2.5.5 Tracking applications

To demonstrate potential tracking and authenticity (counterfeit) applications, the barcode nanowires were embedded within host materials relevant to product packaging. Figure 8.16 illustrates the ability to read XRF signatures of alloy nanowires incorporated in a printable ink (A) or within fused plastic (COC) plates (B). Well-defined XRF signals are observed for both the ink- and plastic-embedded nanowires. The resulting fingerprints are similar to those of the corresponding freshly-prepared nanowires (within the membrane template (i) versus incorporation within host material (ii)). Overall, the data of Figure 8.16 clearly indicated that compositionally-encoded alloy nanowires maintain their distinct XRF signatures upon incorporation in relevant host materials (with no apparent matrix effect) and that XRF leads to a convenient non-destructive readout of such fingerprints.

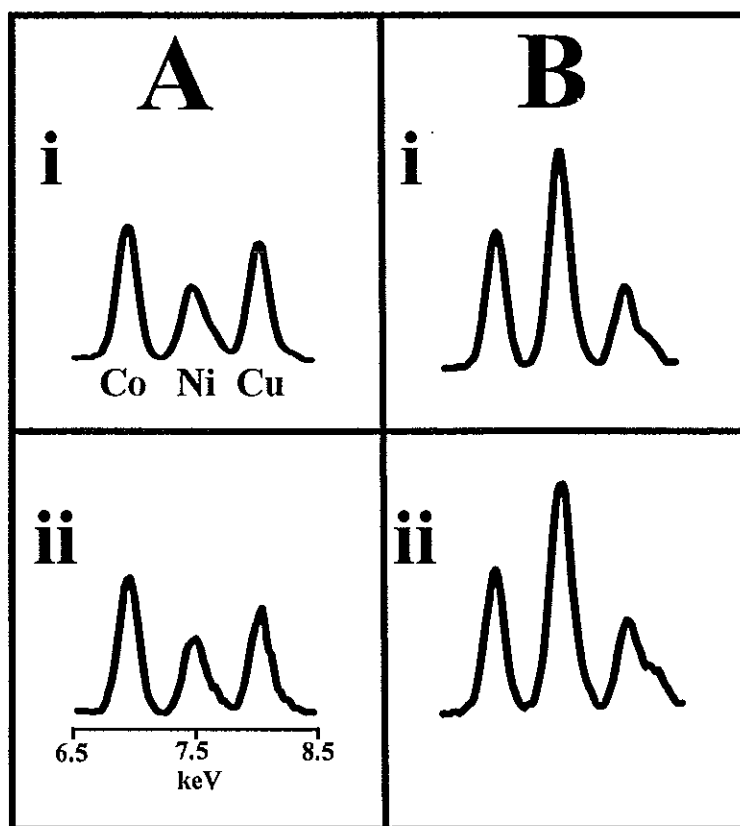


Fig. 8.16 XRF signatures of alloy nanowires. (A) Alloy nanowires incorporated within inks (i) Nanowires embedded in the membrane template (ii) Nanowires dispersed within an ink dispensed on a white printing paper. The nanowires were prepared using a plating solution containing 30-, 50-, 10- g L^{-1} of the Co, Ni and Cu salts. (B) Alloy nanowires incorporated within plastics (i) Nanowires nanowires embedded in the membrane template (ii) Nanowires embedded between fused plastic (COC) sheets. The nanowires were prepared using a plating solution containing 30-, 90-, 10- g L^{-1} of the Co, Ni and Cu salts.

Figure 8.17 shows a linear correlation between the amount of wires that is placed between sheets of COC plastic and the counts associated with the elements that constitute the wires. The results showed the linear relationship between intensity versus amount of wires.

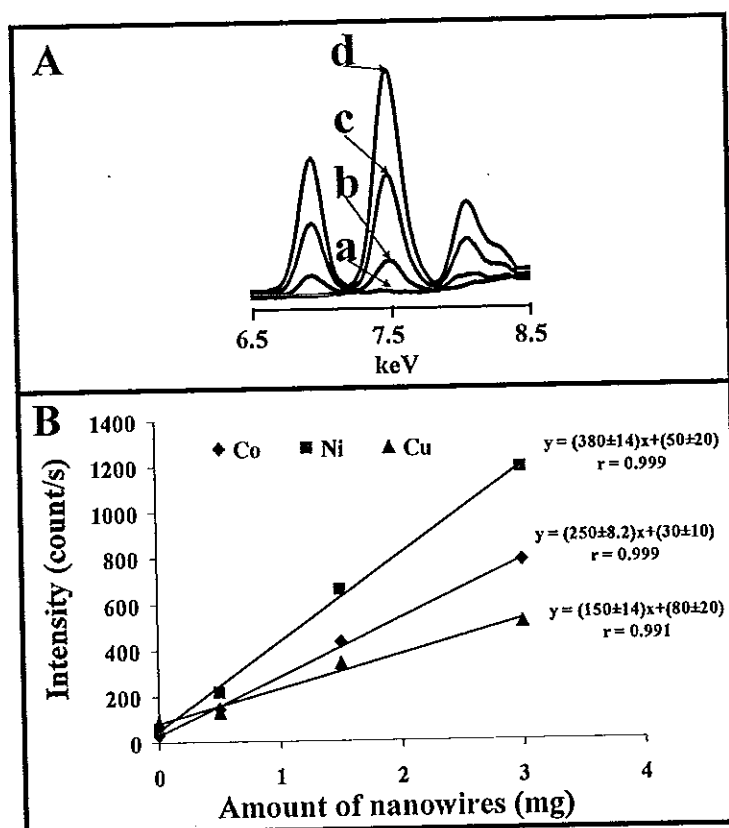


Fig. 8.17 Detection of increasing amounts of multi-metal nanowires that are imbedded between COC plastic sheets. The above was performed with 30-90-10 (g L^{-1}) multi-metal nanowires using the Kevex XRF. (A) XRF signature at various amounts of nanowires (a) Blank Plastic (b) 0.5 mg (c) 1.5 mg (d) 3.0 mg of multi-metal nanowires (B) linear relationship of amount of nanowires embedded in COC plastic sheet and counts.

From these two studies, the COC plastic sheet indicated similar profiles were obtained from standard ternary alloy nanowires and nanowires embedded in host material and as increasing amount of the wires in COC plastic sheet linear relationship still obtained with the same profile compared to standard multi-metal nanowires, therefore, it can be concluded that multi-metal nanowires can be applied to real samples effectively.

8.4 Conclusions

In this chapter, multi-segment alloy nanowires with different optical properties based on different composition were successfully prepared. The different reflectivity of adjacent alloy strips enables convenient identification and that can interpret to be coding pattern for product tracking. A new route for multi-segment alloy nanowires preparation coupled with decoding technique provided the simple and easy way to generate encoding nanowires with large coding pattern. The template-directed alloy co-deposition preparation route obviates the need for sequential deposition steps (from different metal solutions) common for the synthesis of multi-segment nanowire barcodes. Such coupling of one-step synthesis with a non-destructive readout (without prior dissolution) greatly simplifies practical applications of nanomaterial tags. Moreover, the possible usage of ternary alloy nanowires as barcodes were demonstrated where XRF provides an effective nondestructive readout of compositionally-encoded ternary alloy nanowires. The ability to prepare alloy nanowires with a large variety of compositions and visualize these compositions by XRF makes these alloy nanowires promising candidates for a wide variety of tagging applications ranging from product tracking and protection, counterfeit testing and bioaffinity assays.

CHAPTER 9

Shape-Tailored Porous Gold Nanowires

9.1 Introduction

Nanowires have become a more important part of nanotechnology in new era due to their high potential applications as nano-devices (Hurst *et al.*, 2006; Wanekaya *et al.*, 2006). An attractive and versatile route for preparing nanowires involves the electrodeposition of material into cylindrical nanopores of a host porous membrane template such as alumina (Shawn A. Sapp, 1999) and polycarbonate membranes (Schonenberger *et al.*, 1997), followed by dissolution of the template (Bentley *et al.*, 2005). This template-assisted electrochemical synthesis technique permits a convenient and reproducible preparation of nanowires of a variety of sizes, lengths and compositions. All materials that can be electroplated could be used for nanowires synthesis. In addition to solid metal nanowires, it is possible to prepare porous nanowires by a membrane-template electrodeposition of a bimetallic alloy followed by the selective dissolution (de-alloying) of the less noble component (Ji and Searson, 2003). The electropolymerization of polypyrrole within the resulting nanopores led to metal/ polymer composite nanowires of controllable composition (Meenach *et al.*, 2007). All of the above nanostructures have been characterized by a cylindrical shape of uniform diameter.

In this chapter, shape-tailored porous gold nanowires fabricated from gold and silver mixture plating solution followed by silver dissolution from multisegment silver-gold alloy nanowires were demonstrated. Each segment of this alloy nanowire composes of different Ag/Au compositions. Taking the advantages from earlier reports that the diameter of single-composition nanowires decreases upon the dissolution of the less noble component (Liu and Serson, 2006), in a new membrane template protocol, the different alloy composition ratio can be prepared from different plating composition of silver/gold or alternating of deposition potential. Subsequently by silver dissolution allowing free gold atom to diffuse to gold-rich

center providing different nanowires diameters. This versatile tailor-made result in nanoscopic objects with a wide range of shape and dimension.

9.2 Experimental

9.2.1 Chemical and reagents

The gold target used for sputtering the membrane (99.9+% pure) was purchased from Denton Vacuum (Moorestown, NJ). The commercial gold and silver plating solutions (Orotemp 24 RTU RACK and 1025 RTU@4.5 Troy/Gallon) were obtained from Technic Inc. (Anaheim, CA, USA). Sodium hydroxide was obtained from Sigma (St. Louis, MO). Anodisc 25 alumina membranes (25-mm diameter, 200 nm pore size and 60 μm thickness) were purchased from Whatman (Maidstone, UK) and used for all experiments. For porous gold nanowires, 1.0 M of cupric sulphate pentahydrate ($\text{CuSO}_4 \cdot 5\text{H}_2\text{O}$) solution was used to firstly plate into the branch area of the membrane. Pyrrole, 161 mM in 200 mM NaCl solution, was used for polypyrrole (PPy) electropolymerization. Other chemicals were of analytical grade purity and were used as received. All solutions were prepared using nanopure water (18 M Ω , ELGA purelab-ultra model, Ultra Scientific, Marlow, Buckinghamshire, UK).

9.2.2 Apparatus

Sputtering of the alumina membrane was accomplished with a Denton Vacuum Desk III TSC (Moorestown, NJ). Electroplating was accomplished using a CHI 440 electrochemical analyzer (CH Instruments, Austin, TX, USA). The sputtered gold was removed from membrane using a standard 8-inch SEM sample polishing machine (Model 900 Grinder/Polisher, South Bay Technology Inc.) along with 1 μm alumina powder (Struers, Cleveland, OH, USA). Scanning electron microscopy (SEM) images were obtained with the XL30 SEM instrument (FEI Co., Hillsboro, OR, USA) equipped with an energy dispersive X-ray analyzer (Amatek Inc., Mahwah, NJ) using an acceleration potential of 30 kV.

9.2.3 Preparation of nanowires

Alumina membranes were used as templates for the nanowires growth. Before use, a gold layer was sputtered on one side of the membrane (where the pores are branched) to provide an electrical contact and serving as the working electrode during electrodeposition (in connection to an aluminum foil contact) (Figure 9.1a). Ag/AgCl and platinum wires were used as reference and counter electrodes, respectively.

9.2.3.1 Porous gold nanowires

For all porous gold nanowires (step-like and not containing PPy), 10 coulombs (C) of copper was plated first into the branched section of the membrane using a 1 M cupric sulfate pentahydrate ($\text{CuSO}_4 \cdot 5\text{H}_2\text{O}$) solution (Figure 9.1b) followed by 0.2 C of gold from an Orotemp 24 plating solution (Figure 9.1c). Both plating steps were carried out at a potential of -0.9 V (vs. Ag/AgCl). Then, the asymmetric step-cone nanowires were prepared on top of the previously mentioned by sequentially depositing of 0.2 C of each segments (at -0.9 V vs. Ag/AgCl) from gold/silver plating solutions of different ratios: 9/1 (Figure 9.1d), 8.5/1.5 (Figure 9.1e), 8/2 (Figure 9.1f) and 7.5/2.5 (Figure 9.1g) (with rinsing in between). The nano-barbells were constructed by alternately depositing alloy segments from plating solutions with ratios of 9/1 and 7/3 for five segments of 0.2 C each (using the same reduction potential as step-cone) starting with 9/1. The alloy sections of the nanowires were then dealloyed the less noble silver component by placing approximately 1.0 ml of 35% nitric acid in the cell for 15 minutes (Figure 9.1h), then rinsing and repeating the process once. The membranes were then removed from the growth cells and rinsed with nanopure water. After rinsing, the membranes containing copper were swabbed (on gold sputtered side) with a cotton tipped applicator soaked in 0.1 M CuCl_2 in 20% HCl for ca. 2 minutes. This removed both the copper and the sputtered gold (Figure 9.1i, j).

To release the wires, the membrane was removed from the alumina membrane and rinse with nanopure water to remove any plating solution residue

before dissolve in 3.0 M NaOH for 15 minute with slight agitation (owing to the delicate nature of the wires). The resulting nanowire-containing NaOH solution was removed and dropped into 1.5 ml Eppendorf tubes for precipitation via centrifugation (for 3 min at 3000 rpm) and washed several times with nanopure water until a neutral pH was achieved. All nanowire solutions were stored in nanopure water at room temperature (20 °C) (Figure 9.1k).

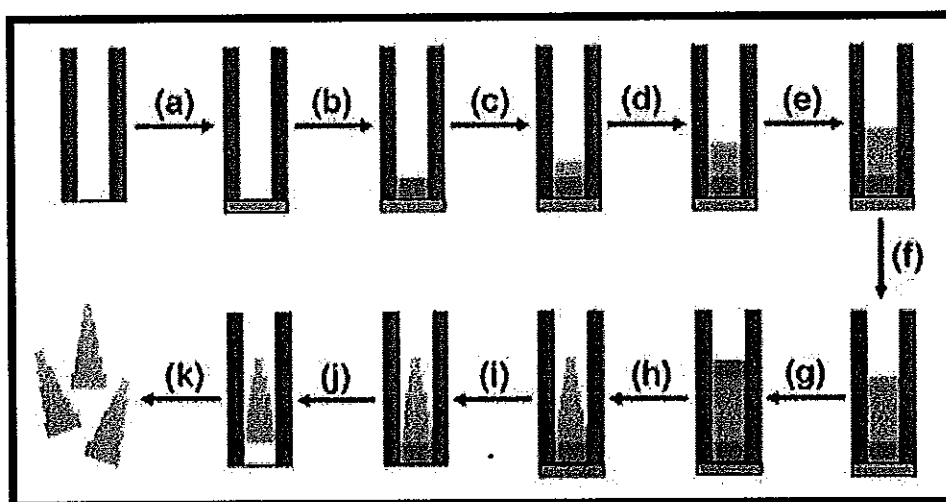


Fig. 9.1 Scheme illustrating the template-assisted electrochemical preparation of the porous gold nanowires: (a) Sputtering gold on alumina membrane; (b) copper deposition for a total charge of 10 C; (c) Au deposition (d) 9/1 (e) 8.5/21.5 (f) 8/2 (g) 7.5/2.5, all deposition steps were performed using a deposition potential of -0.9 V (vs. Ag/AgCl) for a charge of 0.2 C each; (h) dealloy the silver component using a 35% HNO₃ solution; (i) removal of the sputtered gold layer (j) removal of copper layer using 0.1 M CuCl₂ with 20% HCl; (k) dissolution of the membrane template.

9.3.2.2 Composite porous gold/polymer nanowires

Step-like gold nanowires with polypropylene (PPy) were grown; firstly, gold layer was sputtered on the alumina membrane (Figure 9.2 a) following with 10 coulombs (C) of copper was plated into the branched section of the membrane using a 1 M cupric sulfate pentahydrate (CuSO₄·5H₂O) solution (Figure 9.2 b) then a base of 1 C of gold was plated initially (at -0.9 V vs. Ag/AgCl) before plating Au/Ag

alloy nanowires (Figure 9.2 c). The asymmetric PPy-covered step-cone nanowires were prepared atop the porous gold. Porous gold nanowires were prepared from deposition of 7 ml of pure gold plating solution to generate a solid segment of gold followed by dilution of pure gold solution by adding 1 ml (Figure 9.2 d), 0.5 ml (Figure 9.2 e), and 0.5 ml (Figure 9.2 f) of silver plating solution to deposit alloy segment with different composition. The added silver plating solution provided the dilution the composition of Au/Ag plating solution at 8.8/12, 8.2/1.8 and 7.8/2.2, respectively. Each segment was grown for 0.3 C at -0.9 V vs Ag/AgCl. The silver was then removed from the alloy as aforementioned (Figure 9.2 g) and PPy was electropolymerized for 0.5 C at a potential of +1.0 V versus Ag/AgCl (Figure 9.2 h). After removing the membrane from the growth cell and rinsing, the gold side of the membrane was polished with a standard 8-inch SEM sample polisher (South Bay Technology, Inc., San Clemente, CA) using 1 μ m alumina powder and a polishing cloth. The membrane was polished until the gold color (from the solid gold segment) on the back of the membrane disappeared (Figure 9.2 i). The wires were then released from the alumina membrane as described above (Figure 9.2 j).

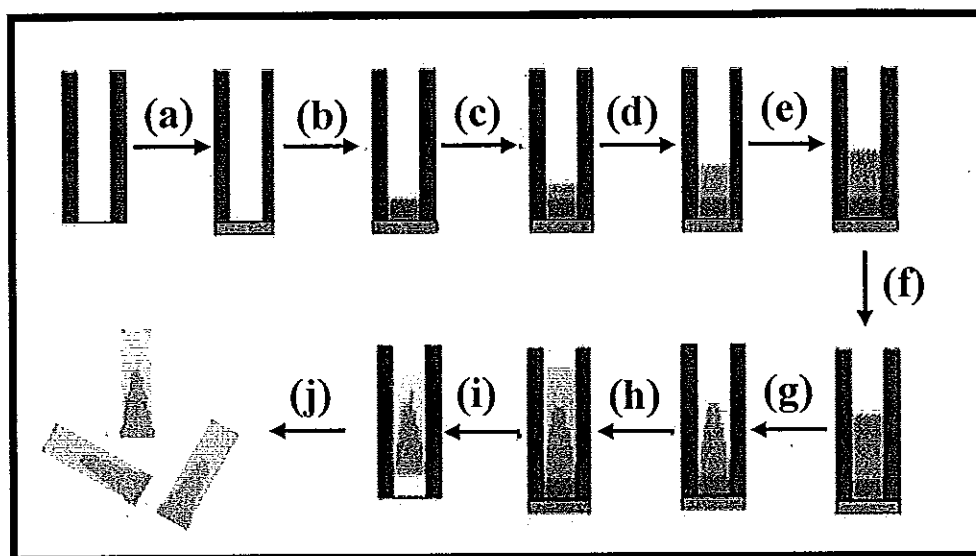


Fig. 9.2 Scheme illustrating the electrochemical preparation of the composite porous gold/polymer nanowires: (a) Sputtering gold on alumina membrane; (b) copper deposition for a total charge of 10 C; (c) Au deposition for a total charge of 1 C (d) 1.0 mL of silver plating solution was added into gold plating solution (e) 0.5 mL of silver plating solution was added into plating solution (f) 0.5 mL of silver plating solution was added into plating solution (g) dealloy the silver component using a 35% HNO_3 solution; (h) PPy was electropolymerized for 0.5 C (i) removal of the sputtered gold layer and removal of copper layer using 0.1 M CuCl_2 with 20% HCl ; (j) dissolution of the membrane template.

9.3 Results and discussion

9.3.1 Porous gold nanowires

9.3.1.1 Porous gold nanowires synthesis

Various shapes of porous gold nanowires, such as step-cone and nano-barbell were generated by sequentially depositing alloy segments from plating solutions of decreasing or alternating, gold/silver compositions using constant deposition potential. In addition, the porous gold shape can be synthesized by

changing the deposition potential while maintaining the composition of the plating solution constant. In this research, three deposition potentials were applied to the system, -0.9 V, -1.0 V and -1.1 V using the ratio of 85Au/15Ag.

Finally, the combination of porous metal and polymer was proposed. After porous step cone nanowires were prepared using a changing plating ratio with 0.3 C of each segment, polypyrrole was electropolymerized at +1.0 V, for 0.5 C.

9.3.1.2 Diameter characterization

The normalized diameter for each segment of porous gold nanostructure prepared at different alloy plating potentials and solutions (of different gold/silver ratios) was investigated (Figure 9.3A) and also the morphology of the pore was revealed (Figure 9.3B). Using a plating potential of -1.1 V (Figure 9.3a), normalized diameters of nanoporous wires were stable at 9/1 Au/Ag ratio and gradually decrease to ca. 78 % at an Au/Ag ratio of 6/4 upon increasing the silver content in the alloy plating solution. When different deposition potentials of -1.0 (Figure 9.3b) and -0.9 (Figure 9.3c) V were applied, the results show a decreasing trend of normalized diameters of the nanowires. The diameters were significantly decreased from 100 to 79%, 100 to 74% and 99 to 60% upon changing the Au/Ag from 9/1 to 6/4 using deposition potentials of -1.1, -1.0 and -0.9 V, respectively (Table 9.1). The greatest change in diameter of the porous gold segment was observed using a potential of -0.9 V. This behavior can be explained by considering the standard reduction potentials of silver cyanide ($\text{Ag}(\text{CN})_2^-$) and gold cyanide ($\text{Au}(\text{CN})_2^-$) which is the major component in silver and gold plating solution, respectively. The equilibrium potential of $\text{Ag}(\text{CN})_2^-$ and $\text{Au}(\text{CN})_2^-$ are -0.53 and -0.82 V, respectively (Matthias *et al.*, 2002). When plating at -0.9 V the rate of reduction of ionic silver is near its steady state current maximum as it is at a high overpotential; however, the reduction rate of ionic gold is relatively low as it is at a slight overpotential. Interestingly, when the potential increases to -1.0 V and above, the rate of silver reduction increases slightly, while the gold reduction rate increases dramatically. Such difference in reduction rates at varying plating potentials results in

a substantial increase in the amount of gold plated and in turn in the diameter of the same plated ratio nanoporous segments.

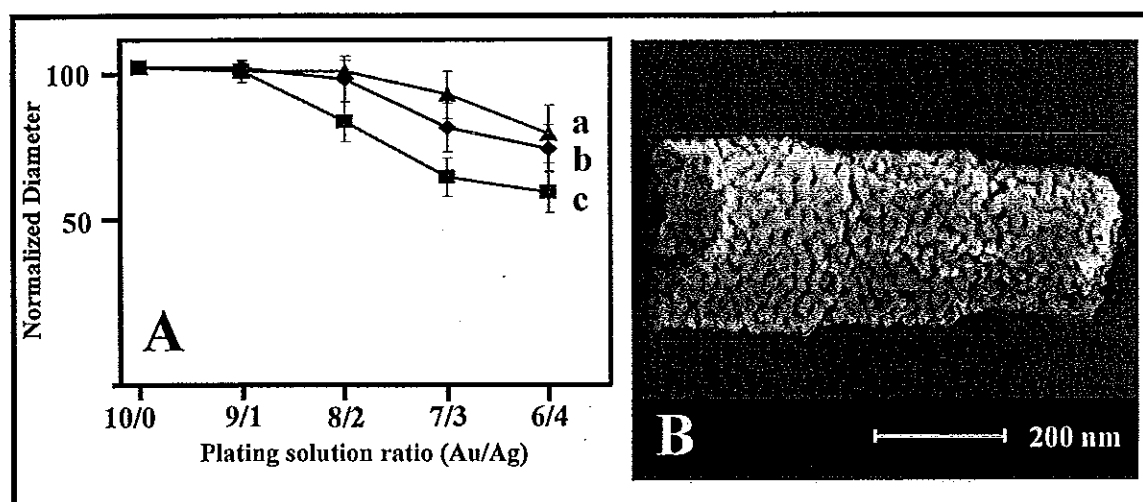


Fig. 9.3 Diameter characterization (A) Normalized diameters of porous gold nanowires at various plating ratio (Au/Ag) using of (a) -1.1 V; (b) -1.0 V, and (c) -0.9 V. (B) SEM image of a porous step-cone created by changing the potential from -1.1 to -0.9 V using plating solution ratio constant at 7/3.

Table 9.1 The percentage of reduction of normalization diameter at different deposition potential

Au/Ag ratio	% Reduction of normalization diameter at different potential		
	-1.1 V	-1.0 V	-0.9 V
100/0	100.0±0.0	100.0±0.0	100.0±0.0
90/10	99.2±3.5	99.6±2.4	98.9±2.3
80/20	98.3±3.8	96.3±7.2	82.7±6.2
70/30	88.7±7.6	80.7±7.7	65.0±6.0
60/40	78.7±9.1	74.1±7.6	60.2±6.6

The diameter of the porous nanowires decreased in a stepwise manner upon changing the gold/silver ratio in the plating solution from 9/1, 8/2, 7/3 to 6/4 for

each of three potentials. The normalized decreasing diameter for each potential is present in Table 9.1 (all potentials are with respect to Ag/AgCl reference). In our observations the segments made with low gold/silver alloy ratios seem to have the same size gold islands as the segments containing more gold (e.g. same final gold density). This observation is contrary to other work on nanoporous gold nanowires (Forty and Durkin, 1980). This means that the low gold/silver alloy ratio segments either exhibit a faster rate of reordering (gold surface diffusion) than that of the higher gold/silver plating ratio segments or the time scale for dissolution is large enough such that all segments reach the same asymptotic coarsening (Parida *et al.*, 2006). The fact that all segments appear to achieve the same final gold density (between 9/1 and 6/4 gold/silver plating solution ratio) explains why with lower gold composition the diameter is smaller.

9.3.1.3 Shape-tailored porous gold nanowires

The ability to generate different shapes of porous gold nanowires through the controlled plating of multi-segment gold/silver alloy composition and selective silver etching is illustrated in Figure 9.4 using the scanning electron microscopy (SEM) and transmission electron microscopy (TEM) technique. The images show well-defined step-cone (A, B) and nano-barbell (C, D) porous gold nanowires. The step-cone nanostructures were prepared by sequentially depositing binary alloy segments from plating solutions of decreasing gold/silver ratios (10/0, 9/1, 8.5/1.5, 8/2, 7.5/2.5, and 7/3) to yield alloy segments containing different compositions. In contrast, the nano-barbell configurations were synthesized by alternating between plating solutions with gold/silver ratios of 9/1 and 7/3. Etching the silver component from the corresponding alloy segment results in a significant change in the diameter of the porous gold nanowire section. Hence distinct step-cone and barbell nanostructures were generated. The normalized diameter of each segment of the porous gold nanostructure was calculated with respect to the diameter of the solid gold segment (bright segment in SEM and dark segment in TEM). The diameter of the step-cone porous nanowires decreased in a stepwise manner from 91% to 41% (of the pure gold segment) upon decreasing the gold/silver ratio in the plating solution

from 9/1 to 7/3, respectively. In contrast, the diameter of the nano-barbell alternates reproducibly between 100% and 64% upon switching between the 9/1 and 7/3 gold/silver solutions, respectively. The diameters of each segment of the nano-barbell structure are the same when the same composition of the Au/Ag plating solution was employed. Consequently, alternating between plating solutions of high-to-low Au/Ag ratios, or in an inverse fashion, does affect the diameter of the corresponding segments and the shape of the resulting nanostructures, in general. These images confirm the ability to create step-like porous nanostructures of different shapes based on the new synthesis protocol.

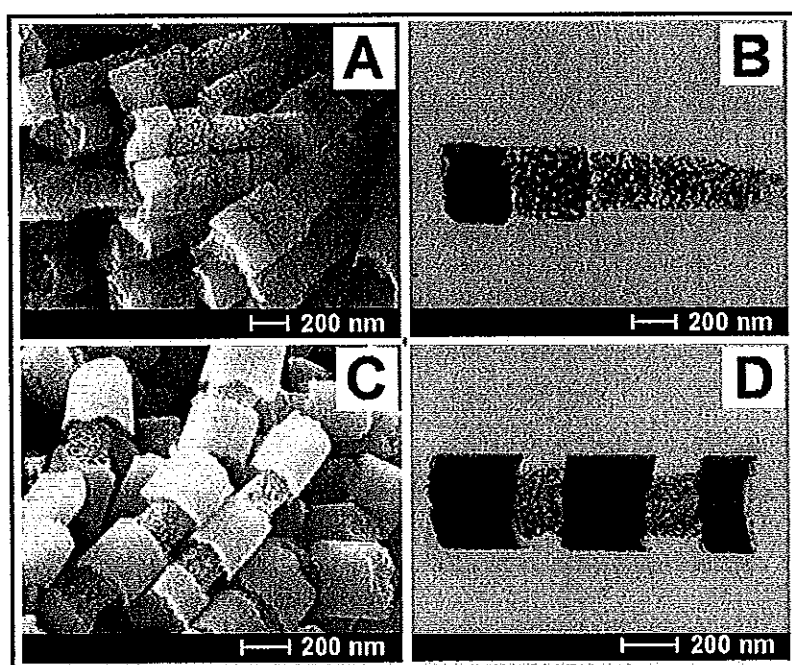


Fig. 9.4 SEM and TEM images of multisegment asymmetric porous gold nanowires prepared at a deposition potential -0.9 V and using plating solutions of different gold/silver composition ratios. SEM (A) and TEM (B) images of the porous step-cone nanostructure prepared by plating sequentially alloy segments from plating solutions with gold/silver ratios of 10/0, 9/1, 8.5/1.5, 8/2, 7.5/2.5 and 7/3. (C) SEM (C) and TEM (D) images of porous nano-barbell nanostructures prepared using plating solutions with gold/silver composition ratios 9/1 and 7/3.

9.3.2 Metal/Polymer composite material

The preparation of the new asymmetric porous gold nanowires can be coupled to an electropolymerization step as shown in previous work (Meenach *et al.*, 2007). The 'backfilling' of the porous gold voids results in the construction of versatile novel shaped conducting polymer and nanoporous gold composite wires. This is shown in Figure 9.5(A), (B) with SEM and TEM images of step-cone nanowires with the polymeric envelope and (C) SEM image of porous nano-barbell nanowires cover with Ppy. These images indicate that cylindrical composite nanostructures are formed with a defined internal porous gold step-cone but filled and surrounded with polypyrrole. This concept of metal/polymer composites can be extended to different shapes of porous gold and different polymers. Further dissolution of porous gold structure within the polypyrrole coverage could lead to porous polymer nanowires with pores reflecting the shape of the internal metal component.

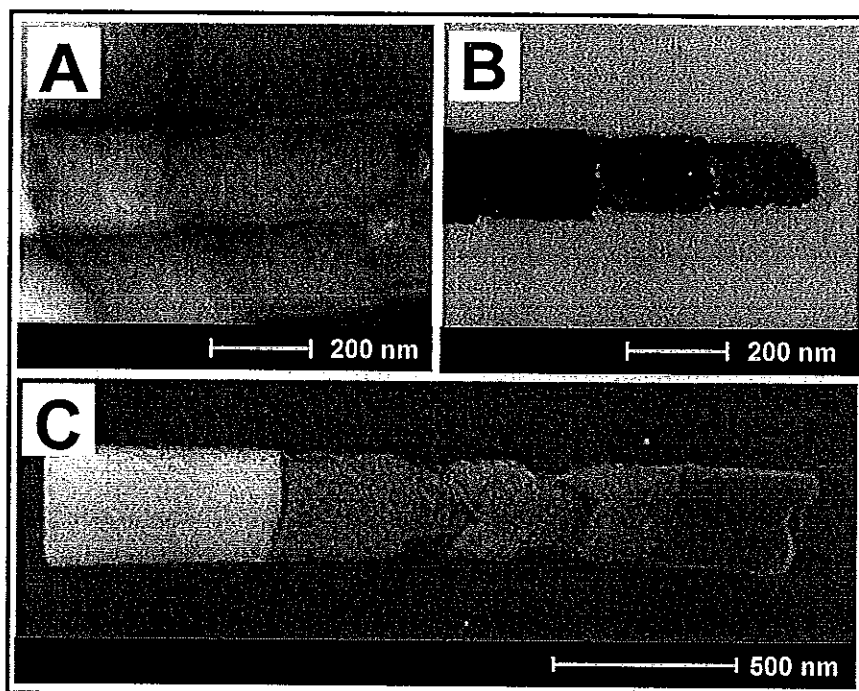


Fig. 9.5 SEM and TEM image of asymmetric porous gold/PPy composite by changing the ratio of the plating solution (Au/Ag ratios of 8.8/12, 8.2/1.8 and 7.8/2.2) while keeping the deposition potential constant at -0.9 V (A) SEM image of porous step cone/PPy composite (B) TEM image of porous step cone/PPy composite and (C) SEM image of nano porous gold/PPy composite wire grown with varying cross-section emulating “barcode” type wire. The five segments after the solid gold are plated from 7/3 Au/Ag alloy plating solution with the following recipe: -1.1 V for 0.3 C, -0.8 V for 0.2 C, -1.1 V for 0.15 C, -0.8 V for 0.15 C, and -1.1 V for 0.2 C all potentials are in reference to Ag/AgCl reference.

9.4 Conclusion

In this chapter, the template-assisted and electrochemical method of shape-tailored porous gold nanowires was described. Shape-tailored concept can be extended to nanowires of diverse configuration with variety of properties based on different metals and polymers, leading to an attractive arsenal of assorted nano-hardware. The production of such shape-tailored wires could lead to wide range of

potential applications, including barcoding/tagging, imaging, or delivery, and could have an impact in microelectronics and sensing devices. For example, the new nanomachining protocol can be used for generating barcode nanowires based on segments of different diameters and lengths, i.e., of distinct shape-dependent “signatures”, analogous to the much larger lithographically prepared diameter-modulated microwires leading to a wide range of tagging or multiplexed sensing applications. The tailoring of both diameter and porosity could possibly be used to tune the near-infrared absorbance of in vivo nanowires, aiding in pathological imaging and drug release.

CHAPTER 10

Conclusions

In this thesis, new analytical approaches based on thin film and nanomaterials were developed and evaluated. These include the usage of thin film and nanomaterials to develop and improve the performances of sample preparation techniques and electrochemical detection of organic compounds. Also, the preparation technique of nanomaterials (nanowires) was investigated to obtain a simple and fast method for versatile nanowires synthesis.

For the first study, hollow fiber membrane coupled to a microtrap was used as an extraction and preconcentration devices for on-line analysis of methanol, ethanol, 1-propanol, methyl-isobutyl ketone (MIBK) and tert-butyl methyl ether (MTBE) from water sample. This system provided a wide linear dynamic range and limit of detection of methanol, ethanol, 1-propanol, MIBK and MTBE were good and acceptable for the analysis. From the percentage relative recovery, this system showed very good results within the acceptable range. Table 10.1 shows the comparison of the analytical features of 4 different sample preparations for VOCs analysis. Method B provide the lowest detection limit since they used double preconcentration step which are headspace combined with liquid-liquid extraction however this technique is off line system. Although the technique developed here did not provide very low LOD, however, it was sufficient for the analysis. The main advantage of this system is the online analysis capability.

Table 10.1 Comparison of the analytical features of 4 different sample preparation for VOCs determination.

Analytical feature	Present work	Method A	Method B	Method C
Sample preparation technique	Gas injection membrane extraction	Membrane inlet mass spectrometric	Headspace liquid phase microextraction	Directed aqueous injection
Limit of detection (ppm)				
Methanol	5.0	-	0.097	-
Ethanol	1.00	5.0	0.067	-
1-propanol	7.0	0.5	0.020	-
MIBK	0.60	-	-	-
MTBE	0.010	-	-	1.0

Method A: On-line monitoring of continuous beer fermentation process using automatic membrane inlet mass spectrometric system (Tarkiainen *et al.*, 2005)

Method B: Dynamic headspace liquid-phase microextraction of alcohols (Saraji, 2005)

Method C: Analysis of methyl tert.-butyl ether and its degradation products by direct aqueous injection onto gas chromatography with mass spectrometry or flame ionization detection systems (Hong *et al.*, 1999).

To overcome the limitations of commercial adsorbents, a trapping tube was developed by coating inside a silico-steel tube with thin film of polymer (Polyethylene glycol, PEG) and thin film of polymer incorporated with nanomaterials (Multiwall carbon nanotubes, MWCNTs). These were used for the preconcentration of volatile organic compounds *i.e.*, dichloromethane (DCM), 1, 2-dichloroethane (DCE), trichloromethane (TCM), trichloroethene (TCE), benzene (B), toluene (T) and xylene (X). The performance of the developed trapping tube were investigated and compared to Carbopack B packed tube. Table 10.2 shows analytical features of this work compare to some methods used for VOCs analysis. The developed trapping tubes provided higher sensitivity and lower detection limit than Carbopack B trapping tube and can be used up to 160 times whereas Carbopack B can be used only 70 times. When comparing to the other methods, method D and method F provided lower detection limits than the developed trapping tube since cold trap injector was used in both techniques to preconcentrate analyte before being injected to analytical system. Particularly for method D, longer desorption times of 10 min, was needed to completely desorb the analyte. Comparing with method E which is sol-gel PEG

coated on fiber, our system provide better detection limit and shorter desorption time. Therefore, the developed sol-gel PEG and sol-gel PEG/MWCNTs trapping tubes offered an alternative adsorbent to commercial adsorbents with higher operational temperatures, better analytical performance and longer lifetimes.

Table 10.2 Comparison of the analytical features of 4 different adsorption tubes for VOCs determination.

Analytical feature	Present work			Method D	Method E	Method F
Adsorbed material	Carbopack B	Sol-gel PEG	Sol-gel PEG/MWCNTs	Carbopack C/ Carbopack B/ Carbosieve III	Sol-gel PEG	Carbotrap B
Limit of detection (ppbv)						
DCM	10	6	8	-	-	0.046
DCE	2	4	2	-	-	-
TCM	11	2	1	-	-	-
TCE	2	1	1	0.5	-	0.0056
Benzene	2	1	0.4	0.9	50	0.0048
Toluene	1.1	0.1	0.08	0.4	20	0.0047
Xylene	6	0.7	0.3	0.9	10	0.0045
Reusability (times)	70	160	160	-	150	-
Desorption time	1 s	1 s	1 s	10 min	20 s	-

Method D: Measurement of toxic volatile organic compounds in indoor air of semiconductor foundries using multisorbent adsorption/ thermal desorption coupled with gas chromatography-mass spectrometry (Tan *et al.*, 2005).

Method E: High-performance polyethylene glycol-coated solid phase microextraction fibers using sol-gel technology (Ji *et al.*, 1994)

Method F: A sensitive diffusion sampler for the determination of volatile organic compounds in ambient air (Uchiyama *et al.*, 1999)

Another technique studied in this thesis is an electrochemical detection of organic compounds. Electrodeposition technique of bismuth onto glassy carbon electrode (GCE) was investigated. A bismuth film electrode (BiFE) was used in a flow injection amperometric system to analyze tetracycline. System performances (BiFE) were compared to GCE. The linearity of BiFE was between 0 and 6.0 mM ($r = 0.999$) while GCE gave the same linear range ($r = 0.999$) but was 4.5 times less sensitive (slope $1.7 \pm 0.3 \mu\text{A mM}^{-1}$) than BiFE ($7.9 \pm 0.2 \mu\text{A mM}^{-1}$). The major

advantages of BiFE are low toxicity of Bi(III), higher sensitivity when compared to bare GCE and simple to prepare. One preparation of bismuth film electrode can be used up to 40 times. The system provided good recoveries and fast analysis time which required only 3 minutes for each injection. Table 10.3 shows the comparison of the analytical features of 4 different methods for tetracycline analysis. The limit of detection in this technique was higher than method H and I these two detection methods were coupled with separation system and this could preconcentrate the analyte before detection.

Table 10.3 Comparison of the analytical features of 4 different methods for tetracycline analysis.

Analytical feature	Present work	Method G	Method H	Method I
Electrode	Bismuth film electrode	Gold rotating disk electrode	Mercury film microelectrode	Gold electrode
Limit of detection (μM)	1.2	1.0	0.7	0.1
Reusability (times)	40	-	-	-
Detection technique	Amperometry	Pulse amperometry	Fast cyclic voltammetry	Integrate pulse amperometry

Method G: Flow injection analysis of tetracycline in pharmaceutical formulation with pulse amperometric detection (Palaharn *et al.*, 2003)

Method H: Capillary electrophoresis of some tetracycline antibiotics coupled with reductive fast cyclic voltammetric detection (Zhou *et al.*, 1999)

Method I: Optimizing the integrated pulsed amperometric multicycle step waveform for the determination of tetracycline (Cai *et al.*, 2005)

For the preparation technique of single and multi segment alloy nanowires to be used as a barcode system, the electrochemical synthesis with template-assist was investigated. A mixture of metal plating solution, cobalt, nickel and copper with different concentrations was used. A constant deposition potential was applied to synthesize single segment alloy nanowires. By changing metal concentrations various signatures could be generated. To demonstrate potential tracking applications, the barcode nanowires were embedded within host materials relevant to product packaging (plastic and printing ink). X-ray fluorescence (XRF) was used for metal identification and could interpret a coding pattern. It provided an

effective nondestructive readout of compositionally encoded alloy nanowires. For multi segment alloy nanowires, a mixture of gold and silver plating solution with constant concentration was used. By changing the deposition potential, different composition of Au and Ag could be obtained resulting in different reflectivity and this can be used as a tool for decoding alloy nanowire barcode with fast and reliable response. This concept can lead to a huge number of patterns of nanowires. In practice, 5 intensity levels can be distinguished and up to 10 segments can be resolved within a typical 10 μm long nanowire. This combination corresponds to 9,765,625 distinguishable nanowires.

A porous gold nanowires preparation was also studied by fabricating Au/Ag alloy nanowires and chemical etching of electro-active component (Ag) to obtain the porous structure of gold. Different composition of gold and silver can provide different diameters of pores, hence, different shape of porous gold nanowires could be synthesized range from nano barbell to nano step cones. This versatile shape-tailored concept can be extended to nanowires of diverse configurations with a variety of properties, based on different metals and polymers, leading to an attractive arsenal of assorted nano-hardware.

For the studies in this thesis, the results indicated that sample preparation technique using thin film and nanomaterial provide alternative technique for on-line analysis of organic compounds in liquid and air sample effectively (wide linear dynamic range and low detection limit to ppb level). In addition, they provide simple, cost effective and environmental friendly technique. For nanowires synthesis, the results showed that electrochemical synthesis with template-assist provide simple and fast technique which size, shape and composition controllable and adjustable for specific purposes.

References

- Abou-Nemeh, I., Das, A., Saraf, A. and Sirkar, K. K. 1999. A composite hollow fiber membrane-based pervaporation process for separation of VOCs from aqueous surfactant solutions. *Journal of Membrane Science* **158** (1-2): 187-209.
- Adams, J. M., Constable, J. V. H., Guenther, A. B. and Zimmerman, P. 2001. An estimate of natural volatile organic compound emissions from vegetation since the last glacial maximum. *Chemosphere - Global Change Science* **3** (1): 73-91.
- Agúf, L., Yáñez-Sedeño, P. and Pingarrón, J. M. 2008. Role of carbon nanotubes in electroanalytical chemistry: A review. *Analytica Chimica Acta* **622** (1-2): 11-47.
- Alden, J. A., Hakoura, S. and Compton, R. G. 1999. Finite Difference Simulations of Steady-State Voltammetry at the Wall-Jet Electrode. Effects of Radial Diffusion and Working Curves for Common Electrochemical Mechanisms. *Anal. Chem.* **71**: 827-836.
- Amelinckx, S., Dyck, D. v., Landuyt, L. v. and Tendeloo, G. v. 1997. ELECTRON MICROSCOPY: Principle and fundamental.
- Ann, S. and Wercinski, S. 1999. Solid phase microextraction :a practical guide New York, Marcel Dekker.
- Arai, S., Endo, M. and Kaneko, N. 2004. Ni-deposited multi-walled carbon nanotubes by electrodeposition. *Carbon* **42**: 641-644.
- Aravamudhan, S., Kumar, A., Mohapatra, S. and Bhansali, S. 2007. Sensitive estimation of total cholesterol in blood using Au nanowires based micro-fluidic platform. . *Biosen. Bioelectron.* **22**: 2289-2294.

- Audunsson, G. 1986. Aqueous/aqueous extraction by means of a liquid membrane for sample cleanup and preconcentration of amines in a flow system. *Anal. Chem.* **58** (13): 2714-2723.
- Banerjee, S., Dan, A. and Chakravorty, D. 2002. Review Synthesis of conducting nanowires. *Journal of Materials Science* **37** (20): 4261-4271.
- Bard, A. and Faulkner, L. 1982. Electrochemical methods: fundamentals and applicationsNew York, Wiley.
- Bard, A. J. and Faulkner, L. R. 2000. Electrochemical methods, JOHN WILEY & SONS, INC.
- Bard, A. J. and Faulkner, L. R. 2001. Electrochemical methods: fundamentals and applications. 2 New York, John Wiley & Sons, Inc.
- Barek, J., Fogg, A. G., Muck, A., Zima, J., rearon and iacute 2001. Polarography and Voltammetry at Mercury Electrodes. *Critical Reviews in Analytical Chemistry* **31** (4): 291 - 309.
- Barratt, R. S. 1981. The preparation of standard gas mixture. *The Analyst* **106** 817.
- Basheer, C., Jegadesan, S., Valiyaveetil, S. and Lee, H. K. 2005. Sol-gel-coated oligomers as novel stationary phases for solid-phase microextraction. *J. Chromatogr. A* **1087**: 252-258.
- Belyakovaa, L. A., Linkovb, V. M., Belyakovc, V. N. and Bulavina, T. V. 1998. New ceramic based membranes for catalytic membrane reactors Membranes modified by cobalt complexes with 1,3-diazoles *Separation and Purification Technology* **14**: 117-125.

- Bentley, A. K., Farhoud, M., Ellis, A. B., Listensky, G. C., Nickel, A. M. and Crone, W. C. 2005. Template Synthesis and Magnetic Manipulation of Nickel Nanowires. *J. Chem. Educ.* **82**: 765-769.
- Berendes, A., Neimke, D., Schumacher, R. and Barth, M. 2006. A Versatile Technique for the Investigation of Gunshot Residue Patterns on Fabrics and Other Surfaces: m-XRF. *Journal of Forensic Sciences* **51** (5): 1085-1090.
- Bhattacharyya, L., Dabbah, R., Hauck, W., Sheinin, E., Yeoman, L. and Williams, R. 2005. Equivalence Studies for Complex Active Ingredients and Dosage Forms. *The AAPS Journal* **7**: E786-E812.
- Bicchi, C., Cordero, C., Liberto, E., Sgorbini, B. and Rubiolo, P. 2008. Headspace sampling of the volatile fraction of vegetable matrices. *Journal of Chromatography A* **1184** (1-2): 220-233.
- Bigham, S., Medlar, J., Kabir, A., Shende, C., Alli, A. and Malik, A. 2002. Sol-Gel Capillary Microextraction. *Anal. Chem.* **74**: 752-761.
- Birdi, K. S. 2003. Scanning Probe Microscopes: Applications in Science and Tehnology, CR PRESS.
- Birenbaum, N. S., Lai, B. T., Chen, C. S., Reich, D. H. and Meyer, G. J. 2003. Selective noncovalent adsorption of protein to bifunctional metallic nanowire surfaces. *Langmuir* **19**: 9580-9582.
- Bishop, E. J. and Mitra, S. 2004. Hollow fiber membrane concentrator for on-line preconcentration. *Journal of Chromatography A* **1046**: 11-17.
- Bishop, J. D. and Klavins, E. 2007. An Improved Autonomous DNA Nanomotor. *Nano Lett.* **7** (9): 2574-2577.

- Blasco, C., Fernandez, M., Picó, Y. and Font, G. 2004. Comparison of solid-phase microextraction and stir bar sorptive extraction for determining six organophosphorus insecticides in honey by liquid chromatography-mass spectrometry. *Journal of Chromatography* **1030** (1-2): 77-85.
- Boening, D. W. 2000. Ecological effects, transport, and fate of mercury: a general review. *Chemosphere* **40**: 1335-1351.
- Bonizzoni, L., Maloni, A. and Milazzo, M. 2006. Evaluation of Effects of Irregular Shape on Quantitative XRF Analysis of Metal Objects. *X-ray Spectrometry* **35**: 390.
- Bozic, R. G., West, A. C. and Levicky, R. 2008. Square wave voltammetric detection of 2,4,6-trinitrotoluene and 2,4-dinitrotoluene on a gold electrode modified with self-assembled monolayers. *Sensors and Actuators B: Chemical* **133** (2): 509-515.
- Br'échignac, C., Houdy, P. and Lahmani, M. 2004. Nanomaterials and Nanochemistry, Springer.
- Brainina, K. Z., Ivanova, A. V. and Malakhova, N. A. 1997. Disposable thick film modified graphite electrodes for stripping voltammetry. *Analytica Chimica Acta* **349** (1-3): 85-91.
- Bu'caroková, M., Gründler, P. and Flechsig, G.-U. 2005. Adsorptive Stripping Voltammetric Detection of Daunomycin at a Bismuth Bulk Electrode. *Electroanalysis* **17** (5-6): 440-444.
- Burdick, J., Laocharoensuk, R., Wheat, P. M., Posner, J. D. and Wang, J. 2008. Synthetic Nanomotors in Microchannel Networks: Directional Microchip Motion and Controlled Manipulation of Cargo. *J. Am. Chem. Soc.* **130** (26): 8164-8165.

- Caffarena, V. d. R., Capitaneo, J. L., Simão, R. A. and Guimarães, A. P. 2006. Preparation of Electrodeposited Cobalt Nanowires. *Materials Research* **9**: 205-208.
- Cai, Y.-e., Cai, Y., Shi, Y., Mou, S. and Lu, Y. 2005a. Optimizing the integrated pulsed amperometric multicycle step waveform for the determination of tetracycline. *Journal of Chromatography A* **1118**: 35-40.
- Cai, Y.-q., Cai, Y.-e., Mou, S.-f. and Lu, Y.-q. 2005b. Multi-walled carbon nanotubes as a solid-phase extraction adsorbent for the determination of chlorophenols in environmental water samples. *J. Chromatogr. A* **1081**: 245-247.
- Campillo, N., Viñas, P., López-García, I., Aguinaga, N. and Hernández-Córdoba, M. 2004. Purge-and-trap capillary gas chromatography with atomic emission detection for volatile halogenated organic compounds determination in waters and beverages. *Journal of Chromatography A* **1035** (1): 1-8.
- Cao, G. and Liu, D. 2008. Template-based synthesis of nanorod, nanowire, and nanotube arrays. *Advances in Colloid and Interface Science* **136**: 45-64.
- Capannesi, C., Palchetti, I., Mascini, M. and Parenti, A. 2000. Electrochemical sensor and biosensor for polyphenols detection in olive oils. *Food Chemistry* **71** (4): 553-562.
- Chang, I.-S. and Kim, S.-N. 2005. Wastewater treatment using membrane filtration-- effect of biosolids concentration on cake resistance. *Process Biochemistry* **40** (3-4): 1307-1314.
- Chang, I.-S. and Lee, C.-H. 1998. Membrane filtration characteristics in membrane-coupled activated sludge system -- the effect of physiological states of activated sludge on membrane fouling. *Desalination* **120** (3): 221-233.

- Charalambous, A. and Economou, A. 2005. A study on the utility of bismuth-film electrodes for the determination of In(III) in the presence of Pb(II) and Cd(II) by square wave anodic stripping voltammetry. *Analytica Chimica Acta* **547** (1): 53-58.
- Chen, R., Xu, D., Guo, G. and Gui, L. 2003. Preparation of Ag₂Se and Ag₂SeI - xTex nanowires by electrodeposition from DMSO baths. *Electrochemistry Communications* **5** (7): 579-583.
- Chen, W., Duan, L. and Zhu, D. 2007. Adsorption of Polar and Nonpolar Organic Chemicals to Carbon Nanotubes. *Environ. Sci. Technol.* **41** (24): 8295-8300.
- Chen, Z. L. and Hibbert, D. B. 1997. Simultaneous amperometric and potentiometric detection of sugars, polyols and carboxylic acids in flow systems using copper wire electrodes. *Journal of Chromatography A* **766** (1-2): 27-33.
- Cheng, B. and Samulski, E. T. 2001. Fabrication and characterization of nanotubular semiconductor oxides In₂O₃ and Ga₂O₃. *J. Mater. Chem.* **11**: 2901-2902.
- Cheng, F., Wang, H., Sun, Z., Ning, M., Cai, Z. and Zhang, M. 2008. Electrodeposited fabrication of highly ordered Pd nanowire arrays for alcohol electrooxidation. *Electrochemistry Communications* **10**: 798-801.
- Christian, G. D. and O'Reilly, J. E. 1986. Instrumental Analysis. 2 Boston, Allyn and Bacon, Inc.
- Ciucanu, I., Caprita, A., Chiriac, A. and Barna, R. 2003. Helical Sorbent Microtrap for Continuous Sampling by a Membrane and Trap Interface for On-Line Gas Chromatographic Monitoring of Volatile Organic Compounds. *Anal. Chem.* **75** (4): 736-741.

- Compton, R. G., Wildgoose, G. G., Rees, N. V., Streeter, I. and Baron, R. 2008. Design, fabrication, characterisation and application of nanoelectrode arrays. *Chemical Physics Letters* **459** (1-6): 1-17.
- Cookeas, E. G. and Efstathiou, C. E. 2000. Flow injection-pulse amperometric detection of ephedrine at a cobalt phthalocyanine modified carbon paste electrode. *The analyst* **125**: 1147-1150.
- Creaser, C. S., Lamarca, D. G., Santos, L. M. F. d., New, A. P. and James, P. A. 2003. A universal temperature controlled membrane interface for the analysis of volatile and semi-volatile organic compounds. *The Analyst* **128** (9): 1150-1156.
- Creaser, C. S., Stygall, J. W. and Weston, D. J. 1998. Developments in membrane inlet mass spectrometry. *Analytical Communications* **35** 9H-11H.
- Cui, H.-F., Ye, J.-S., Liu, X., Zhang, W.-D. and Sheu, F.-S. 2006. Pt-Pb alloy nanoparticle/carbon nanotube nanocomposite: a strong electrocatalyst for glucose oxidation. *Nanotechnology* **17**: 2334-2339.
- Cusmà, A., Curulli, A., Zane, D., Kaciulis, S. and Padeletti, G. 2007. Feasibility of enzyme biosensors based on gold nanowires. *Mat. Sci. Eng. C* **27**: 1158-1161.
- Dadarwal, R., Namvar, A., Thomas, D. F., Hall, J. C. and Warriner, K. 2008. Organic conducting polymer electrode based sensors for detection of Salmonella infecting bacteriophages. *Materials Science and Engineering: C* **In Press**, **Corrected Proof**.
- Darling, R. B. 2005. Microfabrication: Photolithography. **EE527**.
- Dauginet-De Pra, L., Ferain, E., Legras, R. and Demoustier-Champagne, S. 2002. Fabrication of a new generation of track-etched templates and their use for the

synthesis of metallic and organic nanostructures. *Nuclear Instruments and Methods in Physics Research Section B: Beam Interactions with Materials and Atoms* **196** (1-2): 81-88.

David, F. and Sandra, P. 2007. Stir bar sorptive extraction for trace analysis. *Journal of Chromatography A* **1152** (1-2): 54-69.

Demetriades, D., Economou, A. and Voulgaropoulos, A. 2004. A study of pencil-lead bismuth-film electrodes for the determination of trace metals by anodic stripping voltammetry. *Analytica Chimica Acta* **519** (2): 167-172.

Dettmer, K. and Engewald, W. 2002. Adsorbent materials commonly used in air analysis for adsorptive enrichment and thermal desorption of volatile organic compounds. *Anal Bioanal Chem* **373**: 490-500.

Dewulf, J. and Van Langenhove, H. 1999. Anthropogenic volatile organic compounds in ambient air and natural waters: a review on recent developments of analytical methodology, performance and interpretation of field measurements. *Journal of Chromatography A* **843** (1-2): 163-177.

Dinçkaya, E., Sezgintürk, M. K., Akyilmaz, E. and Ertaş, F. N. 2007. Sulfite determination using sulfite oxidase biosensor based glassy carbon electrode coated with thin mercury film. *Food Chemistry* **101** (4): 1540-1544.

Economou, A. 2005. Bismuth-film electrodes: recent developments and potentialities for electroanalysis. *TrAC Trends in Analytical Chemistry* **24** (4): 334-340.

Economou, A. and Fielden, P. R. 1997. Applications, potentialities and limitations of adsorptive stripping analysis on mercury film electrodes *TrAC Trends in Analytical Chemistry* **16**: 286-292.

Eisert, R. and Pawliszyn, J. 1997. Design of automated solid-phase microextraction for trace analysis of organic compounds in aqueous samples. *Journal of Chromatography A* **776** (2): 293-303.

- Elke, K., Jermann, E., Begerow, J. and Dunemann, L. 1998. Determination of benzene, toluene, ethylbenzene and xylenes in indoor air at environmental levels using diffusive samplers in combination with headspace solid-phase microextraction and highresolution gas chromatography-flame ionization detection. *Journal of Chromatography A* **826**: 191-200.
- EPA, 1995. Product Safety Commission "The Inside Story: A Guide to Indoor Air Quality. www.USEPA.com, U.S. Environmental Protection Agency and the United States Consumer
- EPA, 1996. METHOD 515.3 Determination of chlorinated acids in drinking water by liquid-liquid extraction, derivatization and gas chromatography with electron capture detection EPA Method 515.3.
- Erdogdu, G. and Karag zler, A. E. 1997. Investigation and comparison of the electrochemical behavior of some organic and biological molecules at various conducting polymer electrodes. *Talanta* **44** (11): 2011-2018.
- Erlebacher, J., Aziz, M. J., Karma, A., Dimitrov, N. and Sieradzki, K. 2001. Evolution of Nanoporosity In Dealloying. *Nature* **410**: 450-453.
- Fang, G.-Z., He, J.-X. and Wang, S. 2006. Multiwalled carbon nanotubes as sorbent for on-line coupling of solid-phase extraction to high-performance liquid chromatography for simultaneous determination of 10 sulfonamides in eggs and pork. *Journal of Chromatography A* **1127**: 12-17.
- Farahani, H., Yamini, Y., Shariati, S., Khalili-Zanjani, M. R. and Mansour-Baghahi, S. 2008. Development of liquid phase microextraction method based on solidification of floated organic drop for extraction and preconcentration of organochlorine pesticides in water samples. *Analytica Chimica Acta* **In Press**, **Corrected Proof**.

- Fei, X. L., Tang, S. L., Wang, R. L., Su, H. L. and Du, Y. W. 2007. Fabrication and magnetic properties of Fe-Pd nanowire arrays *Solid State Communications* **141**: 25-28.
- Feng, C. and Mitra, S. 2000. Breakthrough and desorption characteristics of a microtrap. *Journal of Microcolumn Separations* **12**: 267-275.
- Finkel, N. H., Lou, X., Wang, C. and He, L. 2004a. Barcoding Microworld. *Anal. Chem.* **76**: 352A-359A.
- Finkel, N. H., Lou, X., Wang, C. and He, L. 2004b. Barcoding Microworld. *Anal. Chem.*: 353A.
- Forst, L. and Conroy, M. L. 1998. Odor and VOC Control Handbook, McGraw-Hill
- Forty, A. J. 1979. Corrosion Micromorphology of Noble Metal Alloys and Depletion Gilding. *Nature* **282**: 597-598.
- Forty, A. J. and Durkin, P. A. 1980. Micromorphological Study of the Dissolution of Silver-Gold Alloys in Nitric Acid. *Philos. Mag. A* **42**: 295-318.
- Giacomino, A., Abollino, O., Malandrino, M. and Mentasti, E. 2008. Parameters affecting the determination of mercury by anodic stripping voltammetry using a gold electrode. *Talanta* **75** (1): 266-273.
- Gogol, E. V., Evtugyn, G. A., Marty, J. L., Budnikov, H. C. and Winter, V. G. 2000. Amperometric biosensors based on nafion coated screen-printed electrodes for the determination of cholinesterase inhibitors. *Talanta* **53** (2): 379-389.
- Gooding, J. J. 2005. Nanostructuring electrodes with carbon nanotubes: A review on electrochemistry and applications for sensing. *Electrochimica Acta* **50** (15): 3049-3060.

- Grasset, F., Saitoa, N., Lia, D., Parka, D., Sakaguchia, I., Ohashia, N., Hanedaa, H., Roisnelc, T., Mornetd, S. and Dugueta, E. 2003. Surface modification of zinc oxide nanoparticles by aminopropyltriethoxysilane *Journal of alloys compounds* **360**: 298-311
- Grdeń, M., Lukaszewski, M., Jerkiewicz, G. and Czerwinski, A. 2008. Electrochemical behaviour of palladium electrode: Oxidation, electrodisolution and ionic adsorption. *Electrochimica Acta* **53** (26): 7583-7598.
- Green, M. J. 1996. A practical guide to analytical method validation. *Analytical Chemistry*.
- Grob, L. R. 1985. Modern practise of gas chromatography. 2 Canada, John Wiley & Sons, Inc.
- Günesa, S., Fritz, K. P., Neugebauer, H., Sariciftci, N. S., Kumar, S. and Scholesb, G. D. 2007. Hybrid solar cells using PbS nanoparticles. *Solar Energy Materials & Solar Cells* **91**: 420-423.
- Günzler, H. and Williams, A. 2002. Handbook of Analytical Techniques, Wiley-VCH.
- Guo, X. and Mitra, S. 1998a. Development of pulse introduction membrane extraction for analysis of volatile organic compounds in individual aqueous samples, and for continuous on-line monitoring. *Journal of Chromatography A* **826** (1): 39-47.
- Guo, X. and Mitra, S. 1998b. Development of pulse introduction membrane extraction for analysis of volatile organic compounds in individual aqueous, samples, and for continuous on-line monitoring. *Journal of Chromatography A* **826**: 39-47.

- Gupta, M., Jain, A. and Verma, K. K. 2007. Optimization of experimental parameters in single-drop microextraction-gas chromatography-mass spectrometry for the determination of periodate by the Malaprade reaction, and its application to ethylene glycol. *Talanta* 71 (3): 1039-1046.
- Habib, A. 2006. Optimization of Conditions for the Synthesis of Silver Nanowire. *WSSP*: 1-20.
- Han, G., Yuan, J., Shi, G. and Wei, F. 2005. Electrodeposition of polypyrrole/multiwalled carbon nanotube composite films. *Thin Solid Films* 474: 64- 69.
- Han, M., Gao, X., Su, J. Z. and Nie, S. 2001. Quantum-Dot-Tagged Microbeads for Multiplexed Optical Coding of Biomolecules. *Nature biotechnology* 19: 631-635.
- Hanaoka, T.-A., Heilmann, A., Kröll, M., Kormann, H.-P., Sawitowski, T., Schmid, G. n., Jutzi, P., Klipp, A., Kreibitz, U. and Neuendorf, R. 1998. Alumina membranes - templates for novel nanocomposites. *Applied Organometallic Chemistry* 12 (5): 367-373.
- Harper, M. 2000a. Sorbent trapping of volatile organic compounds from air. *Journal of Chromatography A* 885: 129-151.
- Harper, M. 2000b. Sorbent trapping of volatile organic compounds from air. *Journal of Chromatography A* 885: 129-151.
- Hasanoglu, A., Salt, Y., Keleser, S., Zkan, S. and Diñer, S. 2005. Pervaporation separation of ethyl acetate-ethanol binary mixtures using polydimethylsiloxane membranes. *Chemical Engineering and Processing* 44 (3): 375-381.

- Hayashi, K., Iwasaki, Y., Horiuchi, T., Sunagawa, K. and Tate, A. 2005. Selective Detection of a Catecholamine against Electroactive Interferents Using an Interdigitated Heteroarray Electrode Consisting of a Metal Oxide Electrode and a Metal Band Electrode. *Anal. Chem.* **77** (16): 5236-5242.
- He, H. and Tao, N. J. 2003. Electrochemical Fabrication of Metal Nanowires. *Encyclopedia of Nanoscience and Nanotechnology*: 1-18.
- Heald, C. G. R., Wildgoose, G. G., Jiang, L., Jones, T. G. J. and Compton, R. G. 2004. Chemical Derivatisation of Multiwalled Carbon Nanotubes Using Diazonium Salts. *ChemPhysChem*, **5**: 1794 -1799.
- Hernandez, S. C., Chaudhuri, D., Chen, W., Myung, N. V. and Mulchandani, A. 2007. Single Polypyrrole Nanowire Ammonia Gas Sensor. *Electroanalysis* **19**: 2125 - 213.
- Hippelein, M. 2006. Analysing selected VVOCs in indoor air with solid phase microextraction (SPME): A case study. *Chemosphere* **65**: 271-277.
- Hočevár, S. B., Wang, J., Deo, R. P. and Ogorevc, B. 2002. Potentiometric stripping analysis at bismuth-film electrode. *Electroanalysis* **14** (2): 112-115.
- Hong, S., Duttweiler, C. M. and Lemley, A. T. 1999. Analysis of methyl tert.-butyl ether and its degradation products by direct aqueous injection onto gas chromatography with mass spectrometry or flame ionization detection systems. *Journal of Chromatography A* **857**: 205-216.
- Hou, S., Zheng, N., Feng, H., Li, X. and Yuan, Z. 2008. Determination of dopamine in the presence of ascorbic acid using poly(3,5-dihydroxy benzoic acid) film modified electrode. *Analytical Biochemistry* **179**: 179-184.

<http://www.whatman.com/PRODAnoporeInorganicMembranes.aspx>, 2007. Anopore® Inorganic Membranes (Anodisc®)

Hulteen, J. C. and Martin, C. R. 1997. A general template-based method for the preparation of nanomaterials. *J. Mater. Chem.* **7**: 1075-1087.

Hurst, S. J., Payne, E. K., Qin, L. and Mirkin, C. A. 2006. Multisegmented One-Dimensional Nanorods Prepared by Hard-Template Synthetic Methods. *Angew. Chem., Int. Ed.* **45**: 2672-2692.

Hutton, E. A., Hočevár, S. B. and Ogorevc, B. 2005. Ex situ preparation of bismuth film microelectrode for use in electrochemical stripping microanalysis. *Analytica Chimica Acta* **537** (1-2): 285-292.

Hutton, E. A., Hočevár, S. B., Ogorevc, B. and Smyth, M. R. 2003. Bismuth film electrode for simultaneous adsorptive stripping analysis of trace cobalt and nickel using constant current chronopotentiometric and voltammetric protocol. *Electrochemistry Communications* **5** (9): 765-769.

Hutton, E. A., Ogorevc, B., Hočevár, S. B. and Smyth, M. R. 2006. Bismuth film microelectrode for direct voltammetric measurement of trace cobalt and nickel in some simulated and real body fluid samples. *Analytica Chimica Acta* **557** (1-2): 57-63.

Hutton, E. A., Ogorevc, B. ž., Hočevár, S. B., Weldon, F., Smyth, M. R. and Wang, J. 2001. An introduction to bismuth film electrode for use in cathodic electrochemical detection. *Electrochemistry Communications* **3** (12): 707-711.

Hutton, E. A., van Elteren, J. T., Ogorevc, B. and Smyth, M. R. 2004. Validation of bismuth film electrode for determination of cobalt and cadmium in soil extracts using ICP-MS. *Talanta* **63** (4): 849-855.

- Hylton, K. and Mitra, S. 2007. Automated, on-line membrane extraction. *Journal of Chromatography A* **1152** (1-2): 199-214.
- Hyötyläinen, T. 2008. On-line coupling of extraction with gas chromatography. *Journal of Chromatography A* **1186** (1-2): 39-50.
- Hyötyläinen, T. and Riekkola, M.-L. 2008. Sorbent- and liquid-phase microextraction techniques and membrane-assisted extraction in combination with gas chromatographic analysis: A review. *Analytica Chimica Acta* **614** (1): 27-37.
- Ida, H., Segawa, T., Tohyama, S. and Kawai, J. 2005. Analysis of Painted Steel by a Hand-held X-ray Fluorescence Spectrometer. *Spectrochimica Acta Part B* **60**: 249- 252.
- Jakubowska, N., Polkowska, a., Namieall nik, J. and Przyjazny, A. 2005. Analytical Applications of Membrane Extraction for Biomedical and Environmental Liquid Sample Preparation. *Critical Reviews in Analytical Chemistry* **35** (3): 217 - 235.
- James, N. M. and Jane, C. M. 2000. Statistic and Chemimetrics for Analytical Chemistry. 4 England, Prentice Hall, Pearson Education Limited,.
- Jönsson, J. and Mathiasson, L. 2001. Membrane extraction in analytical chemistry. *Journal of Separation Science* **24** (7): 495-507.
- Jérôme, C., Labaye, D. E. and Jérôme, R. 2004. Electrochemical formation of polypyrrole nanowires. *Synthetic Metals* **142** (1-3): 207-216.
- Ji, C., Oskam, Y., Ding, Y., Erlebacher, J. D., Wagner, A. J. and Searson, P. C. 2003. Deposition of $\text{AuxAg}_{1-x}/\text{AuyAg}_{1-y}$ Multilayers and Multisegment Nanowires. *J. Electrochem. Soc.* **150**: C523-C528.

- Ji, C. and Searson, P. C. 2003. Synthesis of Nanoporous Gold Nanowires. *J. Phys. Chem. B* **107**: 4494-4499.
- Ji, W., Sikdar, S. K. and Hwang, S.-T. 1994. Modeling of multicomponent pervaporation for removal of volatile organic compounds from water. *Journal of Membrane Science* **93** (1): 1-19.
- Jochmann, M. A., Yuan, X., Schilling, B. and Schmidt, T. C. 2008. In-tube extraction for enrichment of volatile organic hydrocarbons from aqueous samples. *Journal of Chromatography A* **1179** (2): 96-105.
- Jönsson, J. Å. and Mathiasson, L. 1999a. Liquid membrane extraction in analytical sample preparation: I. Principles. *TrAC Trends in Analytical Chemistry* **18** (5): 318-325.
- Jönsson, J. Å. and Mathiasson, L. 1999b. Liquid membrane extraction in analytical sample preparation: II. Applications. *TrAC Trends in Analytical Chemistry* **18** (5): 325-334.
- Jönsson, J. Å. and Mathiasson, L. 2000. Membrane-based techniques for sample enrichment. *Journal of Chromatography A* **902** (1): 205-225.
- Jönsson, J. Å. and Mathiasson, L. 2003. Membrane Extraction for Sample Preparation. *LC•GC Europe*
- Jurado, L., Alicia, de Castro, L. and Maria, D. 2006. X-Ray Fluorescence Analysis of Valuable Metals. *Current Analytical Chemistry* **2** (3): 271-277.
- Kapturski, P. and Bobrowski, A. 2008. The silver amalgam film electrode in catalytic adsorptive stripping voltammetric determination of cobalt and nickel. *Journal of Electroanalytical Chemistry* **617** (1): 1-6.

- Keating, C. D. N., M. J. 2003. Striped Metal Nanowires as Building Blocks and Optical Tags. *Advanced Materials* **15** (5): 451-454.
- Kefala, G., Economou, A. and Sofoniou, M. 2006. Determination of trace aluminium by adsorptive stripping voltammetry on a preplated bismuth-film electrode in the presence of cupferron. *Talanta* **68** (3): 1013-1019.
- Kefala, G., Economou, A., Voulgaropoulos, A. and Sofoniou, M. 2003. A study of bismuth-film electrodes for the detection of trace metals by anodic stripping voltammetry and their application to the determination of Pb and Zn in tapwater and human hair. *Talanta* **61** (5): 603-610.
- Keller, A. A. and Bierwagen, B. G. 2001. Hydrophobic Hollow Fiber Membranes for Treating MTBE-Contaminated Water. *Environ. Sci. Technol.* **35** (9): 1875-1879.
- Kerr, T. M. and Mike, J. H. 1998. Post-column oxidation of purpald-aldehyde adducts at nickel electrodes. *Journal of Chromatography A* **813** (2): 213-222.
- Ketola, R. A., Virkki, V. T., Ojala, M., Komppa, V. and Kotiaho, T. 1997. Comparison of different methods for the determination of volatile organic compounds in water samples. *Talanta* **44** (3): 373-382.
- Kim, J.-H., Ayalasomayajula, T., Gona, V. and Choi, D. 2008. Fabrication and electrochemical characterization of a vertical array of MnO₂ nanowires grown on silicon substrates as a cathode material for lithium rechargeable batteries. *Journal of Power Sources* **183** (1): 366-369.
- Kim, K., Kim, M. and Cho, S. M. 2006. Pulsed electrodeposition of palladium nanowire arrays using AAO template. *Materials Chemistry and Physics* **96**: 278-282.

- Klabunde, K. J. 2001. Nanoscale materials in chemistry, John Wiley and Sons, Inc.
- Knupp, V. F., Leite, E. M. A. and de Lourdes Cardeal, Z. 2005. Development of a solid phase microextraction-gas chromatography method to determine N-hydroxymethyl-N-methylformamide and N-methylformamide in urine. *Journal of Chromatography B* **828** (1-2): 103-107.
- Kolahgar, B., Hoffmann, A. and Heiden, A. C. 2002. Application of stir bar sorptive extraction to the determination of polycyclic aromatic hydrocarbons in aqueous samples. *Journal of Chromatography A* **963** (1-2): 225-230.
- Kolb, B. and Ettre, L. S. 1997. Static Headspace-Gas Chromatography: Theory and Practice New York, A Wiley & Sons Inc., Publication.
- Kot-Wasik, A., Debska, J. and Namiesnik, J. 2004. Monitoring of organic pollutants in coastal waters of the Gulf of Gdansk, Southern Baltic. *Marine Pollution Bulletin* **49** (3): 264-276.
- Kou, D., Juan, A. S. and Mitra, S. 2001. Gas Injection Membrane Extraction for Fast On-Line Analysis Using GC Detection. *Anal. Chem.* **73**: 5462-5467.
- Koziel, J. A. and Novak, I. 2002. Sampling and sample-preparation strategies based on solid-phase microextraction for analysis of indoor air. *TrAC Trends in Analytical Chemistry* **21** (12): 840-850.
- Królicka, A., Pauliukaite, R., Švancara, I., Metelka, R., Bobrowski, A., Norkus, E., Kalcher, K. and Vytřas, K. 2002. Bismuth-film-plated carbon paste electrodes. *Electrochemistry Communications* **4** (2): 193-196.
- Kumar, A., Gaurav, Malik, A. K., Tewary, D. K. and Singh, B. 2008. A review on development of solid phase microextraction fibers by sol-gel methods and their applications. *Analytica Chimica Acta* **610** (1): 1-14.

- Kun Yang a, b., Baoshan Xing 2007. Desorption of polycyclic aromatic hydrocarbons from carbon nanomaterials in water. *Environmental Pollution* **145**: 529-537.
- Kuntasal,^a O., Karman, D., Wang, D., Tuncel, S. G. and Tuncel, G. r. 2005. Determination of volatile organic compounds in different microenvironments by multibed adsorption and short-path thermal desorption followed by gas chromatographic-mass spectrometric analysis. *Journal of Chromatography A* **1099** (1-2): 43-54.
- Kyriakou, G., Davis, D. J. and Lambert, R. M. 2006. Sensitivity and selectivity of Pt electrodes for hydrocarbon sensing in an ultra high vacuum environment. *Sensors and Actuators B: Chemical* **114** (2): 1013-1018.
- Lallemant, F., Plumier, F., Delhalle, J. and Mekhalif, Z. 2008. Electrochemical elaboration of adherent poly(3,4-ethylenedioxythiophene) films and hybride nanowires on nickel. *Applied Surface Science* **254** (11): 3318-3323.
- Lambropoulou, D. A., Konstantinou, I. K. and Albanis, T. A. 2007. Recent developments in headspace microextraction techniques for the analysis of environmental contaminants in different matrices. *Journal of Chromatography A* **1152** (1-2): 70-96.
- Laocharoensuk, R., Burdick, J. and Wang, J. 2008. Carbon-Nanotube-Induced Acceleration of Catalytic Nanomotors. *ACS Nano* **2** (5): 1069-1075.
- Lara-Gonzalo, A., Sanchez-Ufa, J. E., Segovia-García, E. and Sanz-Medel, A. 2008. Critical comparison of automated purge and trap and solid-phase microextraction for routine determination of volatile organic compounds in drinking waters by GC-MS. *Talanta* **74** (5): 1455-1462.

- Leach, A. M., McDowell, M. and Gall, K. 2007. Deformation of Top-Down and Bottom-Up Silver Nanowires. *Advanced Functional Materials* 17 (1): 43-53.
- Lee, J.-W. and Yeo, I.-H. 2001. Integrated pulsed amperometry for the analysis of organic compounds. *Microchemical Journal* 70 (3): 173-177.
- Lee, J. H., Wu, J. H., Liu, H. L., Cho, J. U., Cho, M. K., An, B. H., Min, J. H., Noh, S. J. and Kim, Y. K. 2007. Iron-Gold Barcode Nanowires. *Angew. Chem. Int. Ed.* 46: 3663 -3667.
- Lee, J. Y., Connor, S. T., Cui, Y. and Peumans, P. 2008. Solution-Processed Metal Nanowire Mesh Transparent Electrodes. *Nano Lett.* 8 (2): 689-692.
- Legeai, S. and Vittori, O. 2006. A Cu/Nafion/Bi electrode for on-site monitoring of trace heavy metals in natural waters using anodic stripping voltammetry: An alternative to mercury-based electrodes. *Analytica Chimica Acta* 560 (1-2): 184-190.
- Leprince-Wang, Y., Yacoubi-Ouslim, A. and Wang, G. Y. 2005. Structure study of electrodeposited ZnO nanowires. *Microelectronics Journal* 36 (7): 625-628.
- Leva, E., Buchholt, K., Colaianne, L., Cioffi, N., van der Werf, I. D., Spetz, A. L., Kall, P. O. and Torsi, L. 2007. Gold nanoparticle sensors for environmental pollutant monitoring. *Advances in Sensors and Interface. 2nd International workshop*: 1-4.
- Li, J. and Lin, X. 2007. Electrocatalytic oxidation of hydrazine and hydroxylamine at gold nanoparticle--polypyrrole nanowire modified glassy carbon electrode. *Sensors and Actuators B: Chemical* 126 (2): 527-535.
- Li, J. J. and Tan, W. 2002. A Single DNA Molecule Nanomotor. *Nano Lett.* 2 (4): 315-318.

- Li, L., Xiao, Z., Tan, S., Pu, L. and Zhang, Z. 2004a. Composite PDMS membrane with high flux for the separation of organics from water by pervaporation. *Journal of Membrane Science* **243** (1-2): 177-187.
- Li, Q.-L., Yuan, D.-X. and Lin, Q.-M. 2004b. Evaluation of multi-walled carbon nanotubes as an adsorbent for trapping volatile organic compounds from environmental samples. *Journal of Chromatography A* **1026**: 283-288.
- Li, X. and Li, Y. 2003. Electrochemical preparation of polythiophene in acetonitrile solution with boron fluoride-ethyl ether as the electrolyte. *Journal of Applied Polymer Science* **90** (4): 940-946.
- Li, Y., Meng, G. W., Zhang, L. D. and Phillipp, F. 2000. Ordered semiconductor ZnO nanowire arrays and their photoluminescence properties. *Applied Physics Letters* **76** (15): 2011-2013.
- Liang, L., Cai, Y., Mou, S. and Cheng, J. 2005. Comparisons of disposable and conventional silver working electrode for the determination of iodide using high-performance anion-exchange chromatography with pulsed amperometric detection. *Journal of Chromatography A* **1085** (1): 37-41.
- Lin, H. Y., Chen, H. A. and Lin, H. N. 2008a. Fabrication of a Single Metal Nanowire Connected with Dissimilar Metal Electrodes and Its Application to Chemical Sensing. *Anal. Chem.* **80** (6): 1937-1941.
- Lin, T., Bajpai, V., Ji, T. and Dai, L. 2003. Chemistry of Carbon Nanotubes. *Australian Journal of Chemistry* **56** (7): 635-651.
- Lin, Z., Takahashi, Y., Kitagawa, Y., Umemura, T., Shiku, H. and Matsue, T. 2008b. An Addressable Microelectrode Array for Electrochemical Detection. *Anal. Chem.* **80** (17): 6830-6833.

- Liu, S.-f., Li, X.-h., Li, Y.-c., Li, Y.-f., Li, J.-r. and Jiang, L. 2005. The influence of gold nanoparticle modified electrode on the structure of mercaptopropionic acid self-assembly monolayer. *Electrochimica Acta* **51** (3): 427-431.
- Liu, Y. and Shi, B. Hollow fiber supported liquid membrane for extraction of ethylbenzene, nitrobenzene from aqueous solution: A Hansen Solubility Parameter Approach. *Separation and Purification Technology* **In Press**, **Accepted Manuscript**.
- Liu, Z. and Searson, P. C. 2006. Single Nanoporous Gold Nanowire Sensors. *J. Phys. Chem. B* **110**: 4318-4322.
- Liu, Z. and Serson, P. C. 2006. Single Nanoporous Gold Nanowire Sensors. *J. Phys. Chem. B* **110**: 4318-4322.
- Loaiza, Óscar A., Laocharoensuk, R., Burdick, J., Rodríguez, Marcella C., Pingarron, Jose M., Pedrero, M. and Wang, J. 2007. Adaptive Orientation of Multifunctional Nanowires for Magnetic Control of Bioelectrocatalytic Processes13. *Angewandte Chemie International Edition* **46** (9): 1508-1511.
- Long, G. L. and Wineforner, J. D. 1983. The Limit of Detection. *Analytical Chemistry* **55**: 712A-724A.
- Long, G. L. and Winetordner, J. D. 1983. Limit of detection: A closer look at the IUPAC definition. *Analytical chemistry* **55**: 712A-724A.
- Long, L. and Wineforder, J. D. 1983. The Limit of Detection. *Analytical Chemistry* **55**: 712A.
- Lou, D.-W., Lee, X. and Pawliszyn, J. 2008. Extraction of formic and acetic acids from aqueous solution by dynamic headspace-needle trap extraction:

Temperature and pH optimization. *Journal of Chromatography A* **1201** (2): 228-234.

Lu, C., Chung, Y.-L. and Chang, K.-F. 2005. Adsorption of Trihalomethanes from Water with Carbon Nanotubes. *Water Research* **39**: 1183-1189.

Lu, Y., Yang, M. and Qu, F. 2007. Enzyme-functionalized gold nanowires for the fabrication of biosensors. *Bioelectrochem.* **71**: 211-216.

Lukomska, A. and Sobkowski, J. 2004. Potential of zero charge of monocrystalline copper electrodes in perchlorate solutions. *Journal of Electroanalytical Chemistry* **567** (1): 95-102.

Lund, H. and Hammerich, O. 2001. Organic electrochemistry. 4 New York, Marcell Dekker, Inc.

Luo, P., Zhang, F. and Baldwin, R. P. 1991. Comparison of metallic electrodes for constant-potential amperometric detection of carbohydrates, amino acids and related compounds in flow systems. *Analytica Chimica Acta* **244**: 169-178.

Luo, Y. Z., Adams, M. and Pawliszyn, J. 1997. Aqueous Sample Direct Extraction and Analysis by Membrane Extraction With a Sorbent Interface. *Analyst* **122**: 1461-1469.

Mackie, D. S., van den Berg, C. M. G. and Readman, J. W. 2004. Determination of pyriithione in natural waters by cathodic stripping voltammetry. *Analytica Chimica Acta* **511** (1): 47-53.

Mangani, E., Lattanzi, L. and Maione, M. 1998. Fast Determination of VOCs in Workplace Air by Solid-Phase Extraction and Gas Chromatography- Mass Spectrometry. *Chromatographia* **47**: 57-62.

- Matthias, S., Schilling, J., Neilsch, K., Müller, F., Wehrspohn, R. B. and Gösele, U. 2002. Monodisperse Diameter Modulated Gold Microwires. *Adv. Mater.* **14**: 1618-1621.
- Matz, G., Kibelka, G., Dahl, J. and Lennemann, F. 1999. Experimental study on solvent-less sample preparation methods: Membrane extraction with a sorbent interface, thermal membrane desorption application and purge-and-trap. *Journal of Chromatography A* **830** (2): 365-376.
- Meenach, Samantha A., Burdick, J., Kunwar, A. and Wang, J. 2007a. Metal/Conducting-Polymer Composite Nanowires. *Small* **3** (2): 239-243.
- Meenach, S. A., Burdick, J. and Wang, J. 2007b. Metal/Conducting Polymer Composite Nanowires. *Small* **3**: 239-243.
- Melcher, R. G. and Morabito, P. L. 1990. Membrane/gas chromatographic system for automated extraction and determination of trace organics in aqueous samples. *Anal. Chem.* **62** (20): 2183-2188.
- Meloan, C. E. 1999. Chemical Separations: Principles, Technique, and Experimentants New York, A John Wiley & Sons, Inc., Publication.
- Melquiades, F. and Appoloni, C. 2004. Application of XRF and Field Portable XRF for Environmental Analysis. *Journal of Radioanalytical and Nuclear Chemistry* **262** (2): 533-541.
- Melwanki, M. B. and Fuh, M.-R. 2008. Dispersive liquid-liquid microextraction combined with semi-automated in-syringe back extraction as a new approach for the sample preparation of ionizable organic compounds prior to liquid chromatography. *Journal of Chromatography A* **1198-1199**: 1-6.

- Meyer, M. J., Gress, M. F. and Borgerding, A. J. 2001. Rapid aqueous sample extraction of volatile organic compounds: effect of sample matrix and analyte properties. *Talanta* **55** (4): 755-764.
- Michulec, M., Wardencki, W., Partyka, M. and Namiecalnik, J. 2005. Analytical Techniques Used in Monitoring of Atmospheric Air Pollutants. *Critical Reviews in Analytical Chemistry* **35** (2): 117-133.
- Miriam, B., ccaron and kovu, P. G. n. G.-U. F. 2005. Adsorptive Stripping Voltammetric Detection of Daunomycin at a Bismuth Bulk Electrode. *Electroanalysis* **17** (5-6): 440-444.
- Mitra, S. 2003. Sample Preparation Techniques in Analytical ChemistryNew Jersey, A John Wiley & Sons, Inc., Publication.
- Morfobos, M., Economou, A. and Voulgaropoulos, A. 2004. Simultaneous determination of nickel(II) and cobalt(II) by square wave adsorptive stripping voltammetry on a rotating-disc bismuth-film electrode. *Analytica Chimica Acta* **519** (1): 57-64.
- Morrin, A., Ngamna, O., O'Malley, E., Kent, N., Moulton, S. E., Wallace, G. G., Smyth, M. R. and Killard, A. J. 2008. The fabrication and characterization of inkjet-printed polyaniline nanoparticle films. *Electrochimica Acta* **53** (16): 5092-5099.
- Mousty, C. 2004. Sensors and biosensors based on clay-modified electrodes--new trends. *Applied Clay Science* **27** (3-4): 159-177.
- Moxom, J., Reilly, P. T. A., Whitten, W. B. and Ramsey, J. M. 2003. Analysis of Volatile Organic Compounds in Air with a Micro Ion Trap Mass Analyzer. *Anal. Chem.* **75** (15): 3739-3743.

- Ndungu, K. and Mathiasson, L. 2000. Microporous membrane liquid-liquid extraction technique combined with gas chromatography mass spectrometry for the determination of organotin compounds. *Analytica Chimica Acta* **404** (2): 319-328.
- Nicewarner-Peña, S. R., Freeman, R. G., Reiss, B. D., He, L., Peña, D. J., Walton, I. D., Cromer, R., Keating, C. D. and Natan, M. J. 2001. Submicrometer Metallic Barcodes. *SCIENCE* **294**: 137-141.
- NIOSH. 1994. "National Institute for Occupational Safety and Health, NIOSH."
- Núñez-Vergara, L. J., Bontá, M., Sturm, J. C., Navarrete, P. A., Bollo, S. and Squella, J. A. 2001. Electrochemical reduction of nitroso compounds: voltammetric, UV-vis and EPR characterization of ortho- and meta-nitrosotoluene derivatives. *Journal of Electroanalytical Chemistry* **506** (1): 48-60.
- Ochiai, N., Sasamoto, K., Kanda, H. and Pfannkoch, E. 2008. Sequential stir bar sorptive extraction for uniform enrichment of trace amounts of organic pollutants in water samples. *Journal of Chromatography A* **1200** (1): 72-79.
- Ohgai, T., Gravier, L., Hoffer, X. and Ansermet, J.-P. 2005. CdTe semiconductor nanowires and NiFe ferro-magnetic metal nanowires electrodeposited into cylindrical nano-pores on the surface of anodized aluminum. *Journal of Applied Electrochemistry* **35** (5): 479-485.
- Page, J. A., Maxwell, J. A. and Graham, R. P. 1962. Analytical applications of the mercury electrode. A review. *Analyst* **87**: 245 - 272.
- Palaharn, S., Charoenraks, T., Wangfuengkanagul, N., Grudpan, K. and Chailapakul, O. 2003. Flow injection analysis of tetracycline in pharmaceutical formulation with pulsed amperometric detection. *Analytica Chimica Acta* **499** (1-2): 191-197.

- Parida, S., Kramer, D., Volkert, C. A., Rösner, H., Erlebacher, J. and Weissmüller, J. 2006. Volume of Change during the Formation of Nanoporous Gold by Dealloying. *Phys. Rev. Lett.* **97**: 035504.
- Pavón, J. L. P., Martín, S. H., Carmelo García Pinto and Moreno Cordero, B. 2008. Determination of trihalomethanes in water samples: A review. *Analytica Chimica Acta* **In Press, Corrected Proof**.
- Pearce, M. E., Melanko, J. B. and Salem, A. K. 2007. Multifunctional Nanorods for Biomedical Applications *Pharmaceutical Research* **24**: 2335-2352.
- Pedersen-Bjergaard, S. and Rasmussen, K. E. 2008. Liquid-phase microextraction with porous hollow fibers, a miniaturized and highly flexible format for liquid-liquid extraction. *Journal of Chromatography A* **1184** (1-2): 132-142.
- Peng, M., Vane, L. M. and Liu, S. X. 2003a. Recent advances in VOCs removal from water by pervaporation. *Journal of Hazardous Materials* **B98**: 69-90.
- Peng, M., Vane, L. M. and Liu, S. X. 2003b. Recent advances in VOCs removal from water by pervaporation. *Journal of Hazardous Materials* **98** (1-3): 69-90.
- Peng, Y., Zhang, H.-L., Pan, S.-L. and Li, H.-L. 2000. Magnetic properties and magnetization reversal of a-Fe nanowires deposited in alumina film. *J. Appl. Phys.* **87**: 1405-1408.
- Periago, J. F. and Prado, C. 2005. Evolution of Occupational Exposure to Environmental Levels of Aromatic Hydrocarbons in Service Stations. *Ann Occup Hyg* **49** (3): 233-240.
- Perrin, D. D. and Dempsey, B. 1974. Buffers for pH and metal ion control London, Chapman and hall.

- Pijper, D., vanDelden, R. A., Meetsma, A. and Feringa, B. L. 2005. Acceleration of a Nanomotor: Electronic Control of the Rotary Speed of a Light-Driven Molecular Rotor. *J. Am. Chem. Soc.* **127** (50): 17612-17613.
- Pingarrón, J. M., Hernández, I. O., González-Cortés, A. and Yáñez-Sedeño, P. 2001. Carbon fibre microelectrodes modified with rhodium for the electrocatalytic determination of hydrazine. *Analytica Chimica Acta* **439** (2): 281-290.
- Pinto, C. G., Laespada, M. E. F., Pavón, J. L. P. and Cordero, B. M. 1999. Analytical applications of separation techniques through membranes. *Laboratory Automation & Information Management* **34** (2): 115-130.
- Polkowska, Z. 2004. Determination of volatile organohalogen compounds in urban precipitation in Tricity area (Gdansk, Gdynia, Sopot). *Chemosphere* **57** (10): 1265-1274.
- Price, P. B. and Walker, R. M. 1962. Chemical Etching of Charged-Particle Tracks in Solids. *Journal of Applied Physics* **33** (12): 3407-3412.
- Psillakis, E. and Kalogerakis, N. 2001. Solid-phase microextraction versus single-drop microextraction for the analysis of nitroaromatic explosives in water samples. *Journal of Chromatography A* **938** (1-2): 113-120.
- Qin, D., Zhou, J., Luo, C., Liu, Y., Han, L. and Cao, Y. 2006. Surfactant-assisted synthesis of size-controlled trigonal Se/Te alloy nanowires. *Nanotechnology* **17**: 674-679.
- Qu, F., Yang, M., Shen, G. and Yu, R. 2007. Electrochemical biosensing utilizing synergic action of carbon nanotubes and platinum nanowires prepared by template synthesis. *Biosen. Bioelectron.* **22**: 1749-1755.
- Rafson, H. J. 1998. Odor and VOC Control handbook, McGraw-Hill.

- Ramanathan, K., Bangar, M. A., Yun, M., Chen, W., Mulchandani, A. and Myunga, N. V. 2007. In Situ Fabrication of Single Poly(methyl pyrrole) Nanowire. *Electroanalysis* **19**: 793 - 797.
- Reiff, Reiff, F., Bartels, Bartels, M., Gastel, Gastel, M., Ortner and Ortner, H. 2001. Investigation of Contemporary Gilded Forgeries of Ancient Coins. *Fresenius' Journal of Analytical Chemistry* **371** (8): 1146-1153.
- Reiss, B. D., Freeman, R. G., Walton, I. D., Norton, S. M., Smith, P. C., Stonas, W. G., Keating, C. D. and Natan, M. J. 2002. Electrochemical synthesis and optical readout of striped metal rods with submicron features. *Journal of Electroanalytical Chemistry* **522**: 95-103.
- Restek 2003. Optimizing the Analysis of Volatile Organic Compounds.
- Ridgway, K., Lalljie, S. P. D. and Smith, R. M. 2006. Comparison of in-tube sorptive extraction techniques for non-polar volatile organic compounds by gas chromatography with mass spectrometric detection. *Journal of Chromatography A* **1124** (1-2): 181-186.
- Roco, M. C., Williams, R. S. and Alivisatos, P. 1996. Vision for Nanotechnology R and D in the decade, Interagency working group in nanoscience engineering and technology (IWGN) Workshop report: Nanotechnology research direction, Kluwer Academic Publisher.
- Romann, T., Kallip, S., Sammelselg, V. and Lust, E. 2008. Bismuth microelectrode system with in situ renewable surface for electroanalysis and adsorption studies. *Electrochemistry Communications* **10** (7): 1008-1011.
- Romero, J., López, P., Rubio, C., Batlle, R. n. and Nefn, C. 2007. Strategies for single-drop microextraction optimisation and validation: Application to the

detection of potential antimicrobial agents. *Journal of Chromatography A* **1166** (1-2): 24-29.

Saedi, A. and Ghorbani, M. 2005. Electrodeposition of Ni-Fe-Co Alloy Nanowire in Modified AAO Template. *Materials Chemistry and Physics* **91** (2-3): 417-423.

Sandahl, M., Mathiasson, L. and Jönsson, J. a. 2002. On-line automated sample preparation for liquid chromatography using parallel supported liquid membrane extraction and microporous membrane liquid-liquid extraction. *Journal of Chromatography A* **975** (1): 211-217.

Santos, F. J. and Galceran, M. T. 2002. The application of gas chromatography to environmental analysis. *TrAC Trends in Analytical Chemistry* **21** (9-10): 672-685.

Saraji, M. 2005. Dynamic headspace liquid-phase microextraction of alcohols. *Journal of Chromatography A* **1062** 15-21.

Saridara, C., Brukh, R., Iqbal, Z. and Mitra, S. 2005. Preconcentration of Volatile Organics on Self-Assembled, Carbon Nanotubes in a Microtrap. *Anal. Chem.* **77**: 1183-1187.

Sarkar, J., Khan, G. G. and Basumallik, A. 2007. Nanowires: properties, applications and synthesis via porous anodic aluminium oxide template. *Bull. Mater. Sci., Vol. 30*: 271-290.

Savitsky, A. C. and Siggia, S. 1972. Improved Diffusion Dilution cell for introducing Known Small Quantities of Liquids into Gases. *Analytical Chemistry* **44** (9): 1712-1713.

- Schmidt, T. C. 2003. Analysis of methyl tert-butyl ether (MTBE) and tert-butyl alcohol (TBA) in ground and surface water. *TrAC Trends in Analytical Chemistry* **22** (10): 776-784.
- Schonenberger, C., van der Zande, B. M. I., Fokkink, L. G. J., Henny, M., Schmid, C., Kruger, M., Bachtold, A., Huber, R., Birk, H. and Staufer, U. 1997. Template Synthesis of Nanowires in Porous Polycarbonate Membranes: Electrochemistry and Morphology. *J. Phys. Chem. B* **101** (28): 5497-5505.
- Segal, A., Górecki, T., Mussche, P., Lips, J. and Pawliszyn, J. 2000. Development of membrane extraction with a sorbent interface-micro gas chromatography system for field analysis. *Journal of Chromatography A* **873** (1): 13-27.
- Shankar, K. S. and Raychaudhuri, A. K. 2005. Fabrication of nanowires of multicomponent oxides: Review of recent advances. *Materials Science and Engineering C* **25** 738 – 751.
- Shawn A. Sapp, B. B. L. C. R. M. 1999. Template Synthesis of Bismuth Telluride Nanowires. *Advanced Materials* **11** (5): 402-404.
- Silva, R. G. d. C. and Augusto, F. 2005. Highly porous solid-phase microextraction fiber coating based on poly(ethylene glycol)-modified ormosils synthesized by sol-gel technology. *J. Chromatogr. A* **1072**: 7-12.
- Smart, J., Schucker, R. C. and R. Lloyd, D. 1998. Pervaporative extraction of volatile organic compounds from aqueous systems with use of a tubular transverse flow module.: Part I. Composite membrane study. *Journal of Membrane Science* **143** (1-2): 137-157.
- Smitha, B., Suhanya, D., Sridhar, S. and Ramakrishna, M. 2004. Separation of organic-organic mixtures by pervaporation--a review. *Journal of Membrane Science* **241** (1): 1-21.

Snow, N. H. and Slack, G. C. 2002. Head-space analysis in modern gas chromatography. *TrAC Trends in Analytical Chemistry* **21** (9-10): 608-617.

Sofia GmbH, 2007. Research and development for chemical analysis: Solid Phase Dynamic Extraction.

Srinivasana, C., Andersonb, M. E., Jayaramana, R., Weissb, P. S. and H, M. W. 2006. Electrically isolated nanostructures fabricated using self-assembled multilayers and a novel negative-tone bi-layer resist stack *Microelectronic engineering* **83**: 1517-1520

Stoermer, R. L., Cederquist, K. B., McFarland, S. K., Sha, M. Y., Penn, S. G. and Keating, C. D. 2006. Coupling Molecular Beacons to Barcoded Metal Nanowires for Multiplexed, Sealed Chamber DNA Bioassays. *J. AM. CHEM. SOC.* **128**: 16892-16903.

Strem Chemicals, I. 2005. Strem Nanomaterials for Defense & Security.

Suede, R., Seechamnaturakit, V., Canyuk, B., Ovatlarnporn, C. and Martin, G. P. 2006. Temperature sensitive dopamine-imprinted (N,N-methylene-bis-acrylamide cross-linked) polymer and its potential application to the selective extraction of adrenergic drugs from urine. *Journal of Chromatography A* **1114** (2): 239-249.

Suede, R., Srichana, T., Chuchome, T. and Kongmark, U. 2004. Use of molecularly imprinted polymers from a mixture of tetracycline and its degradation products to produce affinity membranes for the removal of tetracycline from water. *Journal of Chromatography B* **811** (2): 191-200.

Sun, Y., Graff, R. A., Strano, M. S. and Rogers, J. A. 2005. Top-Down Fabrication of Semiconductor Nanowires with Alternating Structures along their Longitudinal and Transverse Axes. *small* **1**: 1052 - 1057.

- Sunesson, A.-L., Nilsson, C.-A. and Andersson, B. 1995. Evaluation of adsorbents for sampling and quantitative analysis of microbial volatiles using thermal desorption-gas chromatography. *J. Chromatogr. A* **699** (1-2): 203-214.
- Supelco, 1998. Guide to solid phase extraction: Bulletin 910.
- Švancara, I., Baldrianová, L., Tesařová, E., Hočevár, S. B., Elsuccary, S. A. A., Economou, A., Sotiropoulos, S., Ogorevc, B. and řas, K. V. 2006. Recent Advances in Anodic Stripping Voltammetry with Bismuth-Modified Carbon Paste Electrodes. *Electroanalysis* **18** (2): 177-185.
- Tamayo, F. G., Turiel, E. and Martn-Esteban, A. 2007. Molecularly imprinted polymers for solid-phase extraction and solid-phase microextraction: Recent developments and future trends. *Journal of Chromatography A* **1152** (1-2): 32-40.
- Tan, S., Li, L., Xiao, Z., Wu, Y. and Zhang, Z. 2005. Pervaporation of alcoholic beverages--the coupling effects between ethanol and aroma compounds. *Journal of Membrane Science* **264** (1-2): 129-136.
- Tarkiainen, V., Kotiaho, T., Mattila, I., Virkajärvi, I., Aristidou, A. and Ketola, R. A. 2005. On-line monitoring of continuous beer fermentation process using automatic membrane inlet mass spectrometric system. *Talanta* **65** (5): 1254-1263.
- Tena, M. T. and Carrillo, J. D. 2007. Multiple solid-phase microextraction: Theory and applications. *TrAC Trends in Analytical Chemistry* **26** (3): 206-214.
- Thammakhet, C. 2007. Development of Analytical techniques for Trace and Ultra Trace Analysis, Prince of Songkla University. **Degree of Doctor of Philosophy in Chemistry**

- Thammakhet, C., Muneesawang, V., Thavarungkul, P. and Kanatharana, P. 2006. Cost effective passive sampling device for volatile organic compounds monitoring *Atmos. Environ.* **40**: 4589-4596.
- Thammakhet, C., Thavarungkul, P., Brukh, R., Mitra, S. and Kanatharana, P. 2005. Microtrap modulated flame ionization detector for on-line monitoring of methane. *Journal of Chromatography A* **1072** (2): 243-248.
- Thomsen, V., Schatzlein, D. and Mercuro, D. 2003. Limits of Detection in Spectroscopy. *Spectroscopy* **18** (12): 112-114.
- Tian, M., Wang, J., Kumar, N., Han, T., Kobayashi, Y., Liu, Y., Mallouk, T. E. and Chan, M. H. W. 2006. Observation of Superconductivity in Granular Bi Nanowires Fabricated by Electrodeposition. *NANO LETTERS* **6**: 2773-2780.
- Tok, J. B.-H., Chuang, F. Y. S., Kao, M. C., Rose, K. A., Pannu, S. S., Sha, M. Y., Chakarova, G., Penn, S. G. and Dougherty, G. M. 2006. Metallic Striped Nanowires as Multiplexed Immunoassay Platforms for Pathogen Detection. *Angew. Chem. Int. Ed.* **45**: 6900 -6904.
- Tóth, K., Štulík, K., Kutner, W., Fehér, Z. and Lindner, E. 2004. Electrochemical detection in liquid flow analytical techniques: Charecterization and classification. *Pure Appl. Chem.*, **76**: 1119-1138.
- Uchiyama, S., Asai, M. and Hasegawa, S. 1999. A sensitive diffusion sampler for the determination of volatile organic compounds in ambient air. *Atmos. Environ.* **33** (12): 1913-1920.
- US EPA 1994. Indoor Air Pollutant: An introduction for health professionals.

- Van Baelen, D., Van der Bruggen, B., Van den Dungen, K., Degreve, J. and Vandecasteele, C. 2005. Pervaporation of water-alcohol mixtures and acetic acid-water mixtures. *Chemical Engineering Science* **60** (6): 1583-1590.
- Vittal, R., Gomathi, H. and Kim, K.-J. 2006. Beneficial role of surfactants in electrochemistry and in the modification of electrodes. *Advances in Colloid and Interface Science* **119** (1): 55-68.
- Vlachopoulou, M. E., Tserepi, A., Vourdas, N., Gogolides, E. and Misiakos, K. 2005. Patterning of thick polymeric substrates for the fabrication of microfluidic devices. *Journal of Physics: Conference Series* **10**, Second Conference on Microelectronics, Microsystems and Nanotechnology: 293-296.
- Volden, J., Thomassen, Y., Greibrokk, T., Thorud, S. and Molander, P. 2005. Stability of workroom air volatile organic compounds on solid adsorbents for thermal desorption gas chromatography. *Anal. Chim. Acta* **530**: 263-271.
- Vrana, B., Allan, I. J., Greenwood, R., Mills, G. A., Dominiak, E., Svensson, K., Knutsson, J. and Morrison, G. 2005. Passive sampling techniques for monitoring pollutants in water. *TrAC Trends in Analytical Chemistry* **24** (10): 845-868.
- Walton, I. D., Norton, S. M., Balasingham, A., He, L., Oviso, D. F., Jr., D. G., Raju, P. A., Natan, M. J. and Freeman, R. G. 2002. Particles for Multiplexed Analysis in Solution: Detection and Identification of Striped Metallic Particles Using Optical Microscopy. *Anal. Chem.* **74**: 2240-2247.
- Wanekaya, A. K., Chen, W., Myung, N. V. and Mulchandani, A. 2006. Nanowire-Based Electrochemical Biosensors. *Electroanalysis* **18**: 533-550.

- Wang, A., Fang, F. and Pawliszyn, J. 2005. Sampling and determination of volatile organic compounds with needle trap devices. *J. Chromatogr. A* **1072**: 127-135.
- Wang, J. 2003. Nanoparticle-based electrochemical DNA detection. *Analytica Chimica Acta* **500**: 247-257
- Wang, J. 2006. Analytical Chemistry, WILEY-VCH.
- Wang, J., Bunimovich, Y. L., Sui, G., Savvas, S., Wang, J., Guo, Y., Heath, J. R. and Tseng, H.-R. 2006a. Electrochemical fabrication of conducting polymer nanowires in an integrated microfluidic system. *Chemical Communications* (29): 3075-3077.
- Wang, J., Kirgöz, Ü. A. and Lu, J. 2001a. Stripping voltammetry with the electrode material acting as a 'built-in' internal standard. *Electrochemistry Communications* **3** (12): 703-706.
- Wang, J. and Liu, G. 2006. Templated One-Step Synthesis of Compositionally Encoded Nanowire Tags. *Anal. Chem.* **78** (7): 2461-2464.
- Wang, J., Liu, G. and Rivas, G. 2003. Encoded Beads for Electrochemical Identification. *Anal. Chem.* **75**: 4667-4671.
- Wang, J., Lu, D., Thongngamdee, S., Lin, Y. and Sadik, O. A. 2006b. Catalytic adsorptive stripping voltammetric measurements of trace vanadium at bismuth film electrodes. *Talanta* **69** (4): 914-917.
- Wang, J., Lu, J., Hočevár, S. B., Farias, P. A. M. and Ogorevc, B. 2000a. Bismuth-Coated Carbon Electrodes for Anodic Stripping Voltammetry. *Anal. Chem.* **72** (14): 3218-3222.

- Wang, J., Lu, J., Kirgöz, Ü. A., Hočevár, S. B. and Ogorevc, B. 2001b. Insights into the anodic stripping voltammetric behavior of bismuth film electrodes. *Analytica Chimica Acta* **434** (1): 29-34.
- Wang, J. and Musameh, M. 2004. Carbon nanotube screen-printed electrochemical sensors. *Analyst* **129**: 1-2.
- Wang, J., Thongngamdee, S. and Lu, D. 2006c. Adsorptive Stripping Voltammetric Measurements of Trace Molybdenum at the Bismuth Film Electrode. *Electroanalysis* **18** (1): 59-63.
- Wang, L., Qiu, H. Z. and Zhoua, Z. 2006d. Determination of four benzodiazepine residues in pork using multiwalled carbon nanotube solid-phase extraction and gas chromatography-mass spectrometry. *J. Chromatogr. A* **1136**: 99-105.
- Wang, N., Cai, Y. and Zhang, R. Q. 2008. Growth of nanowires. *Materials Science and Engineering R* **60**: 1-51.
- Wang, Z., Xiao, C., Wu, C. and Han, H. 2000b. High-performance polyethylene glycol-coated solid-phase microextraction fibers using sol-gel technology. *J. Chromatogr. A* **893** 157-168.
- Wangfuengkanagul, N., Siangproh, W. and Chailapakul, O. 2004. A flow injection method for the analysis of tetracycline antibiotics in pharmaceutical formulations using electrochemical detection at anodized boron-doped diamond thin film electrode. *Talanta* **64** (5): 1183-1188.
- Wardencki, W., Curylo, J. and Namiesnik, J. 2007. Trends in solventless sample preparation techniques for environmental analysis. *Journal of Biochemical and Biophysical Methods* **70** (2): 275-288.

- Whitney, T. M., Searson, P. C., Jiang, J. S. and Chien, C. L. 1993. Fabrication and Magnetic Properties of Arrays of Metallic Nanowires. *Science* **261** (5126): 1316-1319.
- Wildgoose, G. G., Banks, C. E., Leventis, H. C. and Compton, R. G. 2006. Chemically Modified Carbon Nanotubes for Use in Electroanalysis. *Microchim Acta* **152**: 187-214.
- Wildt, B., Mali, P. and Searson, P. C. 2006. Electrochemical template synthesis of multisegment nanowires: Fabrication and protein functionalization. *Langmuir* **22**: 10528-10534.
- Winston, W. S. H. and Sirkar, K. K. 2001. Membrane handbook, Kluwer Academic Pub., Group.
- Wu, C.-H., Feng, C.-T., Lo, Y.-S., Lin, T.-Y. and Lo, J.-G. 2004. Determination of volatile organic compounds in workplace air by multisorbent adsorption/thermal desorption-GC/MS. *Chemosphere* **56**: 71-80.
- Wu, C.-H., Lin, M.-N., Feng, C.-T., Yang, K.-L., Lo, Y.-S. and Lo, J.-G. 2003. Measurement of toxic volatile organic compounds in indoor air of semiconductor foundries using multisorbent adsorption/ thermal desorption coupled with gas chromatography-mass spectrometry *Journal of Chromatography A* **996**: 225-231.
- Xu, C., Li, H., Xue, T. and Li, H. 2006. Fabrication of CoPd alloy nanowire arrays on an anodic aluminum oxide/Ti/Si substrate and their enhanced magnetic properties *Scripta Materialia* **54** (9): 1605 - 1609.
- Xu, X., Chen, L., Wang, C., Yao, Q. and Feng, C. 2005. Template synthesis of heterostructured polyaniline/Bi₂Te₃ nanowires. *Journal of Solid State Chemistry* **178**: 2163-2166.

- Yamamoto, N., Okayasu, H., Hiraiwa, T., Murayama, S., Maeda, T., Morita, M. and Suzuki, K. 1998. Continuous determination of volatile organic compounds in the atmosphere by an automated gas chromatographic system. *J. Chromatogr. A* **819**: 177-186.
- Yamini, Y., Hojjati, M., Haji-Hosseini, M. and Shamsipur, M. 2004. Headspace solvent microextraction: A new method applied to the preconcentration of 2-butoxyethanol from aqueous solutions into a single microdrop. *Talanta* **62** (2): 265-270.
- Yang, M., Zhang, Z., Hu, Z. and Li, J. 2006a. Differential pulse anodic stripping voltammetry detection of metallothionein at bismuth film electrodes. *Talanta* **69** (5): 1162-1165.
- Yang, M. J., Harms, S., Luo, Y. Z. and Pawliszyn, J. 1994. Membrane Extraction with a Sorbent Interface for Capillary Gas Chromatography. *Anal. Chem.* **66** (8): 1339-1346.
- Yang, W., Wu, Z., Lu, Z., Yang, X. and Song, L. 2006b. Template-electrodeposition preparation and structural properties of CdS nanowire arrays. *Microelectronic Engineering* **83** (10): 1971-1974.
- Yogeswaran, U. and Chen, S.-M. 2008. A Review on the Electrochemical Sensors and Biosensors Composed of Nanowires as Sensing Material. *Sensors* **8**: 290-313.
- Yosypchuk, B. and Novotný, L. 2002. Cathodic stripping voltammetry of cysteine using silver and copper solid amalgam electrodes. *Talanta* **56** (5): 971-976.
- Yosypchuk, B., Sestuková, I. and Novotný, L. 2003. Voltammetric determination of phytochelatin using copper solid amalgam electrode. *Talanta* **59** (6): 1253-1258.

- Zeng, Y., Chen, H., Pang, D.-W., Wang, Z.-L. and Cheng, J.-K. 2002. Microchip Capillary Electrophoresis with Electrochemical Detection. *Anal. Chem.* **74**: 2441-2445.
- Zhang, Q., Li, Y., Xu, D. and Gu, Z. 2001a. Preparation of silver nanowire arrays in anodic aluminum oxide templates. *Journal of Materials Science Letters* **20**: 925- 927.
- Zhang, S., Zhao, H. and John, R. 2001b. A dual-phase biosensing system for the determination of phenols in both aqueous and organic media. *Analytica Chimica Acta* **441** (1): 95-105.
- Zheng, M., Li, G., Zhang, X., Huang, S., Lei, Y. and Zhang, L. 2001a. Fabrication and Structural Characterization of Large-Scale Uniform SnO₂ Nanowire Array Embedded in Anodic Alumina Membrane. *Chem. Mater.* **13** (11): 3859-3861.
- Zheng, M. J., Zhang, L. D., Li, G. H., Zhang, X. Y. and Wang, X. F. 2001b. Ordered indium-oxide nanowire arrays and their photoluminescence properties. *Applied Physics Letters* **79** (6): 839-841.
- Zhou, J., Gerhardt, G. C., Baranski, A. and Cassidy, R. 1999. Capillary electrophoresis of some tetracycline antibiotics coupled with reductive fast cyclic voltammetric detection. *Journal of Chromatography A* **839** (1-2): 193-201.
- Zhou, Q., Xiao, J. and Wang, W. 2006. Using multi-walled carbon nanotubes as solid phase extraction adsorbents to determine dichlorodiphenyltrichloroethane and its metabolites at trace level in water samples by high performance liquid chromatography with UV detection. *J. Chromatogr. A* **1125**: 152-158.

- Zhou, Q. X., Xie, G. H. and Pang, L. 2008. Rapid determination of atrazine in environmental water samples by a novel liquid phase microextraction. *Chinese Chemical Letters* **19** (1): 89-91.
- Zoccolillo, L., Amendola, L., Cafaro, C. and Insogna, S. 2005. Improved analysis of volatile halogenated hydrocarbons in water by purge-and-trap with gas chromatography and mass spectrometric detection. *Journal of Chromatography A* **1077** (2): 181-187.
- Zogorski, J. S. 2006. Volatile Organic Compounds in the Nation's Ground Water and Drinking-Water Supply Wells—A Summary. *USGS Promotes Public Access to Water-Quality Information*.
- Zorita, S., Barri, T. and Mathiasson, L. 2007. A novel hollow-fibre microporous membrane liquid-liquid extraction for determination of free 4-isobutylacetophenone concentration at ultra trace level in environmental aqueous samples. *Journal of Chromatography A* **1157** (1-2): 30-37.

Appendices

Appendix A

Short Communication

Bismuth Film Electrode for Analysis of Tetracycline in Flow Injection System

Sirilak Sattuyasamitsathit,^a Panote Thavarungkul,^{a,b} Proespichaya Kanatharana^{a,b*}^a Analytical and Environmental Chemistry/Trace Analysis Research Unit (AECTA-RU), Department of Chemistry, Faculty of Science, Prince of Songkla University, Hat Yai, Songkhla 90112, Thailand^b Biophysics Research Unit: Biosensors and Biochemicals, Department of Physics, Faculty of Science, Prince of Songkla University, Hat Yai, Songkhla 90112, Thailand

*e-mail address: proespichaya.K@psu.ac.th

Received: September 20, 2006

Accepted: November 27, 2006

Abstract

A bismuth film was prepared on glassy carbon electrode (GCE) and used in a flow injection amperometric system to analyze tetracycline. Bismuth film electrode (BiFE) preparation and flow injection amperometric parameters were optimized. System performances of BiFE were compared to GCE. BiFE was validated with three different lots of real sample, 250 mg tetracycline capsules, the results showed good agreement, i.e., between 240 and 260 mg per capsule. Good relative recoveries were also obtained in the range of 86–106%.

Keywords: Bismuth film electrode (BiFE), Tetracycline, Cyclic voltammetry, Amperometry, Flow injection analysis (FIA)

DOI: 10.1002/elan.200603726

Bismuth film electrode (BiFE) has recently been proposed as an alternative to mercury film electrode (MFE) due to its environmental friendly nature [1]. BiFE can be prepared by depositing thin bismuth film on a suitable substrate material such as glassy carbon [1–14], carbon paste [12, 15–16], pencil-lead [17], copper [18], carbon fiber [1, 19–20] and have been widely applied for trace metal analysis by anodic stripping voltammetry, adsorptive stripping voltammetry, voltammetry and potentiometric stripping analysis. These include nickel (II) and cobalt(II) [20], cadmium(II) [3, 5, 8, 15–16, 18, 20–21], zinc(II) [5, 15, 17, 18, 21] and lead(II) [3–5, 8, 15–17, 20–21]. However, only a few reports used BiFE and bismuth bulk electrode (BiBE) to determine organic compounds. These include amperometric detection of 2-nitrophenol and bromofenoxim [2], adsorptive stripping voltammetry of daunomycin [22], and for trace analysis of several metals by forming a complex with dimethylglyoxime (DMG) such as cadmium (II) [6], lead (II) [13], cobalt (II) [6–7, 19], nickel (II) [7, 19], molybdenum [9] and vanadium [10]. It was also used to detect aluminum by forming intermetallic compound with cupferron [12]. Recently, BiFE has been applied to detect metallothionein (protein with low molecular weight) [14]. Most of the studies using BiFE were performed in a batch system and to the best of our knowledge no one has applied BiFE in a flow system. Therefore, it would be interesting to applied BiFE for the analysis of some other organic compounds in a flow system. In this report BiFE was prepared and used to determine tetracycline, which was selected as a test compound, in a flow injection system with amperometric detection.

BiFE was prepared by depositing Bi(III) onto the GCE surface and the influences of the concentration of the bismuth solution, deposition potential and time were studied by using anodic stripping voltammetry technique. Five replications were performed for each parameter with % RSD less than 4.0. The concentration of bismuth was varied in the range 0.2 to 1.7 mM. After each deposition, the potential was increased to 0.25 V to strip the bismuth film from GCE surface and the current peaks were recorded. The anodic stripping peak current increased with the concentration of Bi(III) solution and reached a steady value at 1.5 mM. Using the optimum concentration at 1.5 mM, the deposition potential and time were investigated in the range of –0.2 to –1.0 V and 1 to 7 min. Using the same criteria, –0.3 V and 6 min were the optimum deposition potential and time, respectively.

Using optimum preparation conditions, 10 different preparations of BiFE were investigated. Anodic stripping peak currents, of Bi(III) from GCE surface, of these preparations provided a relative standard deviation of 4.7 %, showing good reproducibility. The potential window of BiFE and GCE (working electrode) were tested in 25.0 mM borate buffer pH 8.7 in a batch system, using a Ag/AgCl (3 M KCl) reference electrode and a platinum wire counter electrode. The potential windows were found between –0.9 to –1.5 V for BiFE and –1.0 to –1.3 V for GCE (Fig. 1). Although, the potential windows of GCE and BiFE narrower than that of mercury film micro electrode (–0.6 to –2.0 V) [23], they were wide enough for tetracycline detection (see later).

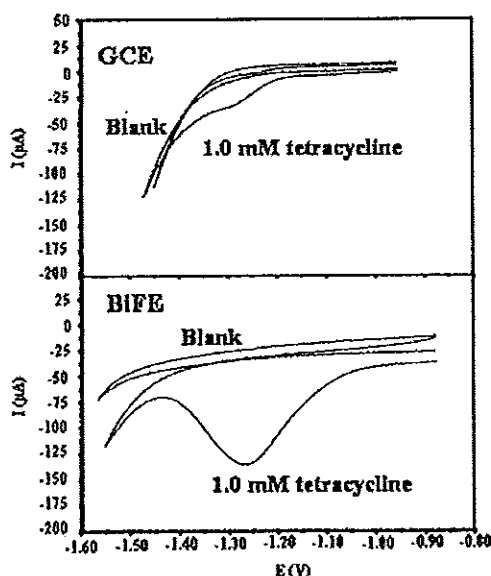


Fig. 1. Cyclic voltammograms on GCE and BiFE of blank, 25.0 mM borate buffer pH 8.7, and 1.0 mM of tetracycline in 25.0 mM borate buffer pH 8.7 containing 0.1 M KCl. Scan rate 50 mV s⁻¹.

The reduction potential of tetracycline was studied by adding 1.0 mM tetracycline into the system. The cyclic voltammogram was scanned between -0.9 to -1.5 V for BiFE and -1.0 to -1.3 V for GCE. Ten scans were performed in each running. The first voltammogram of tetracycline scan of each injection was used since subsequent scans provided lower peak current due to rapid desorption of tetracycline from the electrode surface. Reduction reaction of 1.0 mM tetracycline occurred at -1.25 V. This was slightly less than mercury film micro electrode where the reduction peak of tetracycline was found between -1.4 to -1.5 V [23]. The shift of reduction potential is possible either from slightly higher electron transfer kinetics of tetracycline on BiFE than mercury film micro electrode or a difference in electrical double layer region of BiFE and mercury film micro electrode [2, 25]. In the case of a bare GCE, although it has a potential window between -1.0 to -1.3 V, no current peak of tetracycline was obtained under the same condition probably because GCE is less sensitive to tetracycline than BiFE. To improve the sensitivity, supporting electrolyte, KCl, was added to increase the conductivity of the running buffer solution [24]. Using cyclic voltammetry the responses could be obtained from GCE but were still much less than BiFE (Fig. 1). The cyclic voltammogram of tetracycline using BiFE shows good adsorption and rapid desorption of tetracycline. At 0.1 M KCl the response of 1.0 mM tetracycline obtained from BiFE increased by 50%. This supporting electrolyte was studied further in the flow injection system.

GCE and BiFE were tested in the flow injection system. A constant potential of -1.0 V was applied until a stable baseline was obtained. The detection potential was then optimized to recheck the reduction potential of tetracycline in the flow injection system since the distance between working, reference and auxiliary electrodes were different from the batch system. In addition, auxiliary electrode in the flow and the batch systems were different (stainless steel and platinum wire). The detection potential was tested at -1.00, -1.20, -1.25, 1.30, -1.35 -1.40 V for BiFE and -1.00, -1.20, -1.25, -1.30 V for GCE. Tetracycline, 200 μ L of 1.0 mM, was injected into the amperometric flow injection system. Current peak of tetracycline increased with potential and provided the highest response at -1.30 V for both BiFE and GCE and this was used as the detection potential. Effect of carrier flow rate was investigated between 0.1 and 0.4 mL min⁻¹. Between 0.2–0.4 mL min⁻¹ the same value of current was obtained, however, at 0.1 mL min⁻¹ the peak of 1.0 mM tetracycline was quite broad and the peak height was lower than the others. This was probably caused by the dispersion of the sample in the flow system at a slow flow rate. Therefore, 0.2 mL min⁻¹ was selected. In the study of injection volume, 150–225 μ L, peak height increased with volume from 150 to 175 μ L and reached a constant value. Therefore, 175 μ L was selected. Concentration of KCl was then tested between 0.05–1.0 M using amperometric detection. The current response of 1.0 mM tetracycline increased with KCl concentration from 0.05–0.1 M due to the reduction of the resistance of the solution. However, at higher concentration of KCl, 0.2, 0.3, 0.4, 0.5 and 1.0 M, the current of 1.0 mM tetracycline decreased because larger amount of KCl can shift the reduction potential of analyte to a more negative value resulting in decrease response in amperometric detection. Moreover, the baseline noise at high KCl concentration is also quite high. Therefore, 0.1 M was selected as the optimum value.

In this work, borate buffer was used as a running buffer because basic solution was needed to provide the reduction reaction of tetracycline at negative potential and provide a wide potential window suitable for reduction potential of tetracycline where the highest response was obtained at pH 8.7. This buffer was used to prepare standard tetracycline in order to reduce the effect of background current and it can only dissolve tetracycline up to 6.0 mM. Therefore, tetracycline could only be tested up to 6.0 mM. At optimum conditions, system performance was investigated. Tetracycline standard solution (0–6.0 mM) was injected to the flow injection system. Figure 2 shows the actual amperometric responses of GCE and BiFE to 1.0, 2.0, 3.0 and 4.0 mM tetracycline in 25.0 mM borate buffer solution (pH 8.7) containing 0.1 M KCl where the peak height increase is proportional to the concentration of tetracycline. The calibration curve shows the linearity of BiFE between 0.5 and 6.0 mM with a sensitivity (slope) of 7.7 μ A mM⁻¹, intercept 1.8 μ A and $r=0.9968$. GCE gave the same linear range ($r=0.9973$) but was 4.5 times less sensitive (slope 1.7 μ A mM⁻¹, intercept 0.3 μ A) than BiFE. The limit of detection was obtained at 1.2 μ M for BiFE and 7.0 μ M for

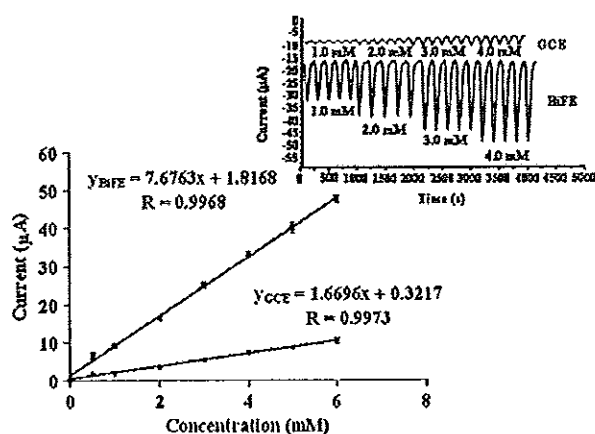


Fig. 2. Relationship between concentration and current response of GCE and BiFE to tetracycline at different concentration in the flow injection amperometric detection system with 25.0 mM borate buffer pH 8.70 containing 0.1 M KCl, applied potential -1.3 V. Inset shows the current responses of tetracycline obtained from GCE and BiFE at 1.0, 2.0, 3.0, 4.0 mM.

GCE by using IUPAC method [26]. The linearity and detection limit of BiFE and GCE were in a higher concentration range than mercury film micro electrode used in capillary electrophoresis-end column detection with small dead volume (linearity and detection limit were 1.0–500.0 μ M and 0.7 μ M for mercury film micro electrode [23]). However, this range of concentration would be sufficient for determination of tetracycline capsule.

The stability of BiFE was evaluated by injecting 2.0 mM of tetracycline for 50 times into the amperometric flow injection system at optimum conditions. The results indicated that the cathodic peaks were relatively constant up to 40 injections (16.3 ± 0.9 μ A) and the peak currents decreased to about half thereafter. This is probably caused by the deterioration of bismuth film, similar to mercury film [27]. However, when this occurred, a new BiFE can be easily prepared by applying a potential of 0.25 V to strip off the bismuth film. The surface of GCE was then rinsed with deionized water before a new layer of bismuth was deposited. The advantage of this technique is no mechanical polishing was needed to reactivate electrode surface prior to a new preparation because of the impurities on the electrode surface. To test the reproducibility of electrode responses three preparations of BiFE were used to analyze tetracycline at 1.0, 4.0 and 6.0 mM. The peak currents of the three concentrations were 9.4 ± 0.3 , 34.2 ± 1.0 and 47.2 ± 0.6 μ A, respectively. The results showed that each preparation of BiFE provided good reproducibility. Therefore, when the BiFE has reached its operation life a new film can be prepared and new calibration would not be required.

Tetracycline contents of capsules obtained from local drug-store were determined by BiFE with amperometric flow injection system. Three different lot numbers were analyzed. For each lot, the content of twenty capsules of 250 mg tetracycline were weighed and mixed. Then 73.1 mg

of the powder was dissolved in 25.0 mL of the running buffer solution (this would be equivalent to 4.0 mM) and injected to the amperometric flow injection system. Five replications were performed with % RSD ≤ 4.0 in all running. The responses were used to calculate the amount of tetracycline from the regression equation of the calibration graph. The results obtained for the three lots were 245 ± 5 mg, 260 ± 10 mg and 245 ± 10 mg of tetracycline per capsule. Relative recoveries were also studied by spiking 1.0 mM and 2.0 mM of tetracycline standard solution into each of the three lots of real samples. The percentage relative recoveries were 102 ± 5 , 86 ± 1 and 87 ± 1 for 1.0 mM and 106 ± 1 , 96 ± 2 and 93 ± 2 for 2.0 mM. The results showed that the percentage relative recoveries were within the acceptance criteria (80–125%) providing sufficiently precise technique for medicine analysis [28].

In conclusion, BiFE was applied to determine tetracycline in an amperometric flow injection system. The major advantages of BiFE are low toxicity of Bi(III), higher sensitivity when compared to bare GCE and simple to prepare. One preparation of bismuth film electrode can be used up to 40 times. When the responses have declined the bismuth layer can be easily stripped off and redeposited with good reproducibility. Therefore, analysis can be carried on without recalibration. When the system was applied for real sample analysis of tetracycline capsule, good agreement was obtained between the value obtained from the flow injection analysis system and the labeled value. The system provided good recoveries and the analysis required only 3 minutes for each injection.

Experimental

$\text{Bi}(\text{NO}_3)_3 \cdot 5\text{H}_2\text{O}$ (Fluka, Switzerland) was dissolved in 0.5 M HNO_3 (Carlo Erba Reagent, France) to obtain 2.0 mM of

bismuth solution. Sodium acetate buffer, 100.0 mM pH 4.50 [3–4, 9–10, 13, 15, 17–20], was used for the deposition of bismuth film on GCE. Sodium tetraborate buffer (25.0 mM pH 8.70) was prepared from sodium tetraborate (Sigma-Aldrich, USA) and HCl [24] and used to prepare standard and running buffer solutions in all experiments. Stock standard solution of tetracycline (Sigma-Aldrich, Germany) was prepared in running buffer solution and stored at -20°C . Working standard solution was diluted from stock standard solution, stored at -4°C and used within three days [23]. GCE was polished with 5.0 μm , 1.0 μm and 0.3 μm alumina powder (Metkon Instruments Ltd., Turkey), respectively, to mirror-like and then sonicated for 15 minutes in deionized water before use. An electrochemical cell composed of a 3 mm diameter GCE working electrode (or BiFE), a Ag/AgCl (3 M KCl) reference electrode and a platinum wire (Metrohm, Netherlands) counter electrode. Anodic stripping voltammetry technique was performed using a μ -Autolab type III (Metrohm, Netherlands) connected to a personal computer and driven by GPES 4.9 software (Eco Chemie, Switzerland) to optimize the deposition of bismuth film onto GCE.

Flow injection system was set for tetracycline analysis. A peristaltic pump (Minipuls 2, Gilson, France) was used to deliver buffer solution while a six-port valve (Valco, Houston, TX, USA) was used as a sample injector to control an exact sample volume. A bare GCE (3 mm) or BiFE served as a working electrode with a Ag/AgCl (3 M KCl) and a stainless steel tube acting as the reference and counter electrode, respectively. All electrodes were held in a laboratory-built flow cell. All system performances were investigated. Tetracycline capsules, containing 250 mg tetracycline, were purchased at a local drugstore in Hat Yai, Songkhla, Thailand and applied for real sample analysis.

Acknowledgements

This project was supported by the Thailand Research Fund under the Royal Golden Jubilee Ph.D. Program, the Postgraduate Education and Research Program in Chemistry (PERCH), Department of Chemistry, Faculty of Science and Graduate School, Prince of Songkla University, Hat Yai, Thailand.

References

- [1] J. Wang, J. Lu, S. B. Hocevar, P. A. M. Farias, *Anal. Chem.* 2000, 72, 3218.
- [2] E. A. Hutton, B. Ogorevc, S. B. Hocevar, F. Weldon, M. R. Smyth, J. Wang, *Electrochem. Commun.* 2001, 3, 707.
- [3] J. Wang, J. Lu, Ü. A. Kirgöz, S. B. Hocevar, B. Ogorevc, *Anal. Chim. Acta* 2001, 434, 29.
- [4] J. Wang, Ü. A. Kirgöz, J. Lu, *Electrochem. Commun.* 2001, 3, 703.
- [5] G. Kefala, A. Economou, A. Voulgaropoulos, M. Sofoniou, *Talanta* 2003, 61, 603.
- [6] E. A. Hutton, T. Y. Elterren, B. Ogorevc, R. M. Smyth, *Talanta* 2004, 63, 849.
- [7] M. Morfobos, A. Economou, A. Voulgaropoulos, *Anal. Chim. Acta* 2004, 519, 57.
- [8] A. Charalambos, A. Economou, *Anal. Chim. Acta* 2005, 547, 53.
- [9] J. Wang, S. Thongngamdee, D. Lu, *Electroanalysis* 2006, 18, 59.
- [10] J. Wang, D. Lu, S. Thongngamdee, Y. Lin, O. A. Sadik, *Talanta* 2006, 69, 914.
- [11] A. Economou, *Trends in Anal. Chem.* 2005, 24, 334.
- [12] G. Kefala, A. Economou, M. Sofoniou, *Talanta* 2006, 68, 1013.
- [13] E. A. Hutton, S. B. Hocevar, B. Ogorevc, M. R. Smyth, *Electrochem. Commun.* 2003, 5, 765.
- [14] M. Yang, Z. Zhang, Z. Hu, J. Li, *Talanta* 2006, 69, 1162.
- [15] A. Króllicka, R. Pauliukaitė, I. Švancara, R. Metela, A. Bobrowski, E. Norkus, K. Kalcher, K. Vytas, *Electrochem. Commun.* 2002, 4, 193.
- [16] I. Švancara, L. Baldrianová, E. Tesařová, S. B. Hocevar, S. A. A. Elsuccary, A. Economou, *Electroanalysis* 2006, 18, 177.
- [17] D. Demetriades, A. Economou, A. Voulgaropoulos, *Anal. Chim. Acta* 2004, 519, 167.
- [18] S. Legeal, O. Vittori, *Anal. Chim. Acta* 2006, 560, 184.
- [19] E. A. Hutton, B. Ogorevc, S. B. Hocevar, M. R. Smyth, *Anal. Chim. Acta* 2006, 557, 57.
- [20] E. A. Hutton, S. B. Hocevar, B. Ogorevc, *Anal. Chim. Acta* 2005, 537, 285.
- [21] S. B. Hocevar, J. Wang, R. P. Deo, B. Ogorevc, *Electroanalysis* 2002, 14, 112.
- [22] M. Buková, P. Gründler, G.-U. Flechsig, *Electroanalysis* 2005, 17, 440.
- [23] Z. Jinkui, C. G. Geoff, B. Andrej, C. Richard, *J. Chromatogr. A* 1999, 839, 193.
- [24] D. D. Perrin, B. Dempsey, *Buffers for pH and Metal Ion Control*, Chapman and Hall, New York 1974, p. 148.
- [25] A. J. Bard, L. R. Faulkner, *Electrochemical methods*, Wiley, New York 2000, pp. 580–582.
- [26] G. L. Long, J. D. Winefordner, *Anal. Chem.* 1983, 55, 712A.
- [27] D. Erhan, S. K. Mustafa, M. S. Kemal, A. Erol, E. F. Nil, *Food Chem.* 2007, 101, 1540.
- [28] B. Lokesh, D. Roger, H. Waller, S. Eric, Y. Lynn, W. Roger, *AAPS J.* 2005, 7, B786.

Appendix B

Alloy Nanowires Bar Codes Based on Nondestructive X-ray Fluorescence Readout

Sirilak Sattayasamitsathit,^{†,‡} Jared Burdick,[†] Ralph Bash,[†] Proespichaya Kanatharana,[‡] Panote Thavarungkul,[‡] and Joseph Wang^{*,†}

Departments of Chemical Engineering and Chemistry and Biochemistry and Biodesign Institute, Arizona State University, Tempe, Arizona, 85287, and Faculty of Science, Prince of Songkla University, Hat Yai, Songkhla, 90112 Thailand

We demonstrate here the ability to generate ternary Co–Ni–Cu alloy nanowires with distinct X-ray fluorescence (XRF) barcode patterns using a one-step template-guided electrodeposition. Such coupling of one-step templated synthesis with a nondestructive XRF readout of the composition patterns greatly simplifies practical applications of barcoded nanomaterials. The new protocol leads to alloy nanowires with broad composition range and hence to an extremely large number of distinguishable XRF signatures. The resulting fluorescence barcodes correlate well with the composition of the metal mixture plating solution, indicating a reproducible plating processes. Factors affecting the coding capacity and identification accuracy are examined, and potential tracking and authenticity applications involving embedding the nanowires within plastics or inks are demonstrated and discussed.

There has been a considerable recent interest in nanomaterial-based barcode systems for a wide range of important applications, ranging from product tracking to multiplexed biodetection.^{1–3} Widespread use of barcoded nanomaterials requires high coding capacity, a low-cost large-scale particle production, and a portable and accurate detection system.¹ Multistriped metal nanowires, prepared by sequential templated electrodeposition of metal segments of different lengths, have been particularly useful for barcoding applications.^{3–5} However, the preparation of such encoded multisegment nanowires relies on a time-consuming synthesis involving multiple plating steps from different metal solutions.⁵

Recently we demonstrated that compositionally encoded alloy nanowire tags, with a large number of recognizable electrochemical signatures, can be prepared by a single-step electrodeposition from a metal-mixture plating solution.⁶ Such a template-directed

alloy preparation route obviates the need for sequential plating steps (from different metal solutions) common for the synthesis of multisegment barcoded nanowires. This single-step preparation of one-segment alloy nanowires thus offers a substantial simplification and speed advantages over the multistep preparation of multisegment nanowires. However, the simplicity of this attractive synthetic route has been greatly compromised by a destructive and time-consuming measurement, involving acid dissolution of the alloy nanowires, followed by electrochemical readout of the voltammetric signatures.⁶

Here we present a greatly simplified nondestructive x-ray fluorescence (XRF) readout of the composition profiles of alloy nanowires. XRF has been widely used in various fields for rapid and accurate nondestructive metal measurements without sample preparation.^{7,8} The technique provides both qualitative and quantitative analyses and offers the simultaneous multielement nondestructive readout of samples over a wide concentration range.⁹ XRF has thus been used for detecting the chemical composition of different alloys, ranging from steel¹⁰ to coins¹¹ and jewelry.¹² Portable (hand-held) XRF analyzers have been particularly useful for on-site nondestructive forensic or archeological analyses¹⁰ in which destructive sampling is not permitted. However, there are no early reports on XRF analyses of barcoded nanowires, in general, and of alloy nanowires, in particular.

In the present study we demonstrate that alloy nanowires with a broad variety of compositions, and hence with a large number of unique XRF signatures, can be easily produced by a one-step template-guided electrodeposition from a mixture of Ni, Co, and Cu ions in an aqueous sulfate plating bath (Figure 1). These metals lead to well-resolved and close K- $L_{2,3}$ XRF peaks and hence to a large coding capacity. The resulting XRF barcode patterns reflect the alloy composition and correlate well with the concentration of the different metal ions in the plating solution. Such coupling of a one-step templated synthesis of alloy nanowires with a nondestructive XRF readout (without dissolution of the encoded

* Corresponding author. E-mail: Joseph.Wang@asu.edu

[†] Arizona State University.

[‡] Prince of Songkla University.

- (1) Finkel, N. H.; Lou, X.; Wang, C.; He, L. *Anal. Chem.* 2004, 76, 353A.
- (2) Han, M.; Gao, X.; Su, J. Z.; Nie, S. *Nat. Biotechnol.* 2001, 19, 631.
- (3) Nkwawue-Peña, S.; Freeman, R. G.; Reiss, B. D.; He, L.; Peña, D. J.; Walton, I. D.; Cromer, R.; Keating, C. D.; Natan, M. J. *Science* 2001, 294, 137.
- (4) Keating, C. D.; Natan, M. J. *Adv. Mater.* 2003, 15, 451.
- (5) Reiss, B. D.; Freeman, R. G.; Walton, I. D.; Norton, S. M.; Smith, P. C.; Stosias, W. G.; Keating, C. D.; Natan, M. J. *J. Electroanal. Chem.* 2002, 522, 55.
- (6) Wang, J.; Liu, G. *Anal. Chem.* 2006, 78, 2461.
- (7) Melquiesdes, F. I.; Appoloni, C. R. *J. Radioanal. Nucl. Chem.* 2004, 262, 533.
- (8) Jurado-Lopez, A.; de Castro, M. D. L. *Curr. Anal. Chem.* 2006, 2, 271.
- (9) Berendes, A.; Neimke, D.; Schumacher, R.; Barth, M. *J. Ferrous Sci.* 2006, 51, 1085.
- (10) Ida, H.; Segawa, T.; Tohyama, S.; Kuraai, J. *Spectrochim. Acta, Part B* 2005, 60, 249.
- (11) Reil, F.; Bartels, M.; Gastel, M.; Ortner, H. M. *Fresenius J. Anal. Chem.* 2001, 371, 1146.
- (12) Bonizzoni, L.; Maloni, A.; Mizzaro, M. *X-Ray Spectrosc.* 2006, 35, 300.

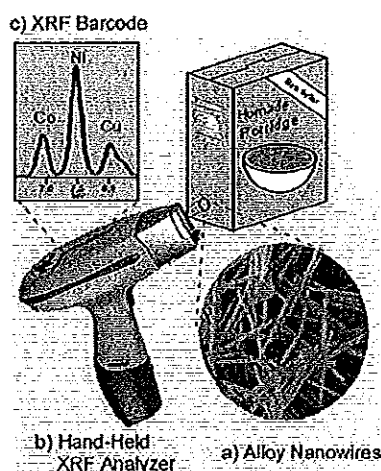


Figure 1. Nondestructive XRF readout of barcoded alloy nanowires: toward product tracking and authenticity testing. Barcoded nanowires (shown in the SEM photomicrograph of inset (a)) are dispensed or embedded in packaging materials of a commercial product are detected with a hand-held XRF analyzer (b). The resulting XRF signature (c) is used for the product identification.

tags) greatly simplifies practical applications of barcoded nanomaterials, making the new strategy extremely attractive for different on-site tagging applications.

EXPERIMENTAL SECTION

Apparatus. Sputtering of the alumina membrane was accomplished with a Denton Vacuum Desk III TSC (Moorestown, NJ). Electroplating was accomplished using a CHI 440 electrochemical analyzer controlled by CHI 2.06 software (CH Instruments, Austin, TX). The sputtered gold was removed from the membrane using a standard 8 in. SEM sample polishing machine (model 900 grinder/polisher, South Bay Technology Inc., VA) along with 3.0 μm alumina powder (Fisher, Pittsburgh, PA). Kevex spectrometer model 0810A, (Kevex, Foster City, CA) was used for detecting the composition of the encoded alloy nanowires. Hand-held XRF measurements were performed with a NITON XL1 791 thin sample analyzer (Thermo Fisher Scientific, NITON Analyzers, Billerica, MA). Scanning electron microscopy (SEM) images were obtained with an XL30 SEM instrument (FEI Co., Hillsboro, OR) using an acceleration potential of 19 kV.

Reagents. The gold target used for sputtering the membrane (99.9+ % pure) was purchased from Denton Vacuum (Moorestown, NJ). The commercial gold and silver plating solutions (Orotech 24 RTU RACK and 1025 RTU@4.5 Troy/Gallon, respectively) were obtained from Technic Inc. (Anaheim, CA). All standard solutions were prepared with ultrapure (18.2 M Ω) water (BEGA-Ultra-Pure water polishing system model PURELAB Ultra Scientific). Sodium hydroxide, cupric sulfate pentahydrate ($\text{CuSO}_4 \cdot 5\text{H}_2\text{O}$), and nickel sulfate hexahydrate ($\text{NiSO}_4 \cdot 6\text{H}_2\text{O}$) were obtained from Sigma (St. Louis, MO). Cobalt sulfate heptahydrate ($\text{CoSO}_4 \cdot 7\text{H}_2\text{O}$) was purchased from Alfa Aesar (Ward Hill, MA). Anodisc 25 alumina membranes (25 mm diameter, 200 nm pore size, and 60 μm

thickness) were received from Whatman (Maldstone, UK). Cyclic olefin copolymer (COC) sheets, 1.1 mm thickness, were obtained from Knightsbridge Plastic Inc. (Fremont, CA), while the standard black inkjet ink was received from Hewlett Packard (Palo Alto, CA).

Preparation of Co-Ni-Cu Nanowires. Alumina membranes were used as templates for the nanowire growth. Before use, a gold layer was sputtered on one side of the membrane (where the pores are branched) to serve as the working electrode during the electrodeposition (in connection to an aluminum foil contact). Ag/AgCl (3 M KCl) and platinum wires were used as the reference and counter electrodes, respectively. The sputtered membrane was placed in the bottom of a plating cell with the sputtered side contacting the aluminum foil. Silver was deposited using the amperometric mode at -0.9 V and a charge of 2 C. Following this, gold was deposited at -0.9 V using a charge of 1 C. The metal-mixture plating solution was subsequently introduced to the cell. Plating solutions composed of 40 g L^{-1} of H_3BO_3 and differing concentrations of the metal salts [cobalt ($\text{CoSO}_4 \cdot 7\text{H}_2\text{O}$), nickel ($\text{NiSO}_4 \cdot 6\text{H}_2\text{O}$), and copper ($\text{CuSO}_4 \cdot 5\text{H}_2\text{O}$)] were employed (final pH ~ 3.8). The deposition from these plating solutions was carried out at a fixed potential of -1.4 V using a total charge of 15 C.

After completion of the deposition, the membrane was removed from the cell and was polished to remove the sputtered gold as previously stated. The alumina membrane was then rinsed with ultrapure water and was divided into two equal pieces. One piece was placed in a 3 M NaOH solution for about 30 min to allow complete dissolution of the membrane. The nanowires were separated magnetically from the NaOH solution and were rinsed with ultrapure water until a neutral pH was obtained. The final 2.0 mL suspension contained ~ 3 mg of wire (one-half of the membrane). The second piece of the nanowire-containing membrane was kept intact for direct XRF analysis of the embedded nanowires. Inks containing the encoded nanowires were prepared by mixing 3.0 mg of the wires within 1.5 mL of a commercial black inkjet ink. A 30.0 μL droplet of the resulting ink was then dispensed dropwise with a pipet onto standard white printing paper (Xerox, Business 4200, 20 lb, Rochester, NY) and was allowed to dry prior to the XRF readout. Bar-coded nanowires were also embedded in COC plastics by sandwiching varying amounts of the encoded nanomaterials between fused COC sheets.

Analytical Procedure. XRF readouts of the nanowire composition profiles were performed on nanowires embedded in the membrane and nanowires suspended in water after dissolution of the membrane. Some spectra measurements were performed using a NITON handheld XRF analyzer, while most XRF spectra were obtained using the Kevex XRF system, with the high voltage power supply operated at 20 kV and 1.5 mA. X-rays that bombarded the nanowire samples in the Kevex system fluoresced from a germanium secondary target with $\text{K}_{\text{L}\alpha}$ and $\text{K}_{\text{M}\alpha}$ lines at 9.90 and 11.03 keV, respectively. The XRF spectrum for each sample was acquired over 200 s with the Kevex XRF system and for 60 s with the NITON handheld unit. Acquired data, in counts per second for the NITON system and in total number of counts for the Kevex system, were recorded with reference to discrete energy levels (25 and 20 eV for NITON and Kevex, respectively) over the energy range of interest (0 eV to ~ 20 keV). The XRF

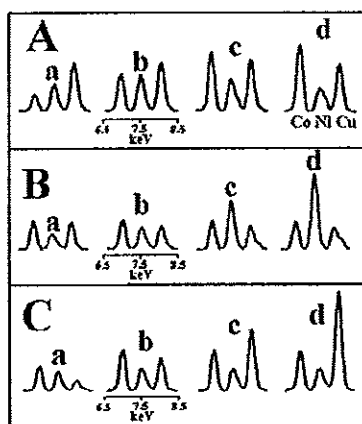


Figure 2. X-ray fluorescence of multimetall alloy nanowires prepared by changing the concentration of one of the metals (Co (A), Ni (B), and Cu (C)) while keeping the level of others constant. (A) Changing the Co concentration (a–d, 10 g L⁻¹, 20 g L⁻¹, 30 g L⁻¹, and 40 g L⁻¹) with Ni and Cu at 50 g L⁻¹ and 10 g L⁻¹, respectively. (B) Changing the Ni concentration (a–d, 40 g L⁻¹, 60 g L⁻¹, 80 g L⁻¹, and 120 g L⁻¹) with Co and Cu at 30 g L⁻¹ and 10 g L⁻¹, respectively. (C) Changing the Cu concentration (a–d, 5 g L⁻¹, 10 g L⁻¹, 15 g L⁻¹ and 20 g L⁻¹) with Co and Ni at 30 g L⁻¹ and 50 g L⁻¹, respectively. All given concentrations are of metal salts present in aqueous solution. All alloy nanowires were electrodeposited at a potential of -1.4 V using a total charge of 15 C. XRF spectra were obtained with the nanowires embedded in the membrane template and using a laboratory Kevex XRF system.

data were normalized using Microsoft Excel, and this was done with respect to counts corresponding to a given K_{L2} value of one of the unchanged metals. The intensity extraction for characterizing and normalizing the remaining peaks was performed by measuring the peak height at the corresponding approximate K_{L2} energies for Co, Ni, or Cu as defined in the Results and Discussion.

RESULTS AND DISCUSSION

The one-step templated synthesis of Ni–Co–Cu alloy nanowires of different metal contents leads to a large number of characteristic XRF barcoding patterns, reflecting the composition of the corresponding nanowires. Such ability to tune the XRF peak intensities by controlling the composition of the alloy nanowires, through the composition of the plating solution, is illustrated in Figure 2. This figure displays XRF readouts of ternary wires with different composition patterns, obtained by changing the content of one metal [Co (A), Ni (B), and Cu (C); red peak], while keeping the level of the other metals constant. The alloy nanowires yield a distinct multiplex spectra, reflecting mostly the emission of K_{L2} photons and the relatively minor contributions of K_{M3} photons from Co and Ni. The approximate peak energies for the K_{L2} lines are 6.9 keV for Co, 7.5 keV for Ni, and 8.0 keV for Cu, and the K_{M3} lines are 7.7 keV for Co, 8.3 keV for Ni, and 8.9 keV for Cu. The influence of the Co and Ni K_{M3} lines can be seen as tiny growing shoulders on the Ni and Cu peaks with increasing Co and Ni concentrations, respectively (e.g., the influence of the

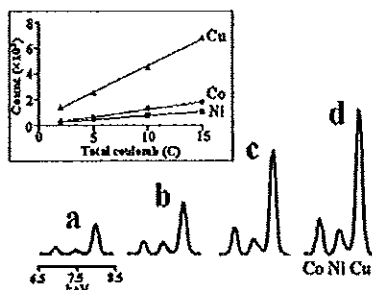


Figure 3. XRF readout of Co–Ni–Cu alloy nanowires of different lengths, prepared by using different plating charges: 2 C (a), 5 C (b), 10 C (c), and 15 C (d) and a plating solution containing 5 g L⁻¹ of the corresponding metal salts. Other conditions are as in Figure 2.

Ni K_{M3} line on the Cu peak is visible in B). Such a K_{M3} line adds to the information content and distinct signature of the corresponding nanowires by adding more data for the identification of all three constituent metals.

The resulting fluorescence signatures correlate well with the composition of the plating solution, with the corresponding peak intensities following the levels of the corresponding metal in the plating solution. A slight deviation from linearity of the corresponding intensity–concentration plots was observed at the lower concentration values (not shown). Linear intensity–concentration correlations were reported earlier for voltammetric signatures of alloy nanowires following their acid dissolution.⁶ The slight nonlinearity, observed at the lowest metal concentrations, is attributed to a potential composition gradient along the nanowires, associated with differences in the ion diffusion rates.²³ Since the number of identifiable nanowires depends upon the number of distinguishable metals and the number of peak intensities, it is possible to obtain thousands of readable XRF signatures with three or four metals present at four to six loadings. In our study using three metals, we found that when evaluating a sample of wires grown from a solution containing 5 g L⁻¹ Co, 5 g L⁻¹ Ni, and 5 g L⁻¹ Cu, the detection limit (calculated following the IUPAC method¹⁹) of the wires, dried on paper, was 30 µg/cm². The uniformity of the plating process was indicated from the low relative standard deviations of 3.4, 4.8, and 6.5% obtained for the intensity of the copper, nickel and cobalt peaks, respectively, in six different sections of one membrane template. Also, the reproducibility of the wires was measured by comparing several samples of wires grown from the same solution. The XRF peak heights of these data (normalized as described earlier) yielded relative standard deviations ranging between 4.3 and 8.5% for the three metals. In addition, uniform length-independent alloy compositions should greatly facilitate practical applications of the new bar-coded nanowires.

Figure 3 examines the influence of the nanowire length (reflected by the deposition charge) upon the corresponding XRF peak intensities for ternary Ni–Co–Cu nanowires prepared using charges ranging from 2 to 15 C (Figure 3a–d). As expected, the

(19) Sedi, A.; Ghorbani, M. *Mater. Chem. Phys.* 2003, 91, 417.

(14) Long, G. L.; Winckler, J. D. *Anal. Chem.* 1983, 55, 712A.

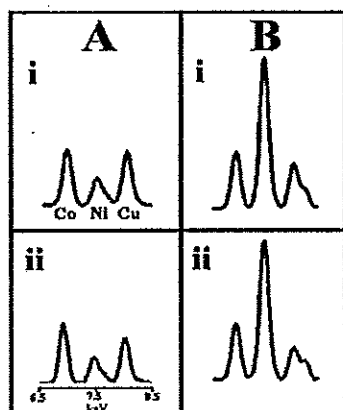


Figure 4. Comparison of the alloy nanowire XRF signatures obtained in various experiments. (A) XRF spectra obtained using (i) the laboratory-based (Kevex XRF) instrument and (ii) a compact handheld XRF analyzer (NITON). The nanowires were prepared using a plating solution containing 30 g L⁻¹, 45 g L⁻¹, and 10 g L⁻¹ of the Co, Ni, and Cu salts. (B) XRF spectra of (i) nanowires embedded in the alumina membrane and of (ii) the nanowires in solution (after the membrane dissolution). The nanowires were prepared using a plating solution containing 30 g L⁻¹, 120 g L⁻¹, and 10 g L⁻¹ of the Co, Ni and Cu salts.

signals of the three metals increase linearly with the deposition charge over the entire 2–15 C charge range (see inset for the corresponding plots), indicating a uniform alloy composition along the length of the nanowires. The peak ratios in the corresponding fluorescence signatures, and hence the overall nanowire signatures, are thus independent of the charge used during the plating process (i.e., length of the resulting nanowires).

Portable XRF analyzers have found extensive field applications¹⁶ and could greatly facilitate numerous practical on-site applications of the encoded alloy nanowires. Accordingly, we compared the XRF signatures obtained with an easy-to-use and compact handheld XRF unit (shown in Figure 1) with those recorded with a centralized large laboratory analyzer. Such comparison, shown in Figure 4A, indicates that both the stationary and portable systems yield similar XRF profiles and that the identification accuracy is not compromised by the use of the handheld analyzer.

The XRF readout of the alloy nanowires can be accomplished while the wires are embedded in the membrane or after dissolving the membrane. Figure 4B compares XRF signatures of ternary alloy nanowires (prepared from a 30 g L⁻¹, 120 g L⁻¹, and 10 g L⁻¹ Co/Ni/Cu solution), as obtained before (i) and after (ii) dissolving the membrane template. Both cases yielded similar XRF signatures, with similar peak energies, intensities, and peak ratios, indicating that the corresponding bar codes are not affected by the membrane dissolution. Notice again the distinct Ni K α shoulder peak, on the copper signal (B), and also the less distinct Co K α shoulder peak on the Ni response (A,ii) that provide additional identification capability. The nanowires analyzed in the membrane represent a highly concentrated two-dimensional array of nanowires ($\sim 1 \times 10^6$ nanowires/cm²) and in suspension a dilute

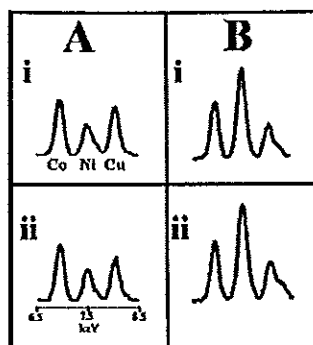


Figure 5. XRF signatures of alloy nanowires incorporated within inks or plastics. (A) Nanowire XRF signatures recorded with the nanowires (i) embedded in the membrane template or (ii) dispersed within an ink dispensed on a white printing paper. The nanowires were prepared using a plating solution containing 30 g L⁻¹, 50 g L⁻¹, and 10 g L⁻¹ of the Co, Ni, and Cu salts. (B) Nanowire XRF signatures for (i) nanowires embedded in the membrane template or (ii) nanowires embedded between fused plastic (COC) sheets. The nanowires were prepared using a plating solution containing 30 g L⁻¹, 90 g L⁻¹, and 10 g L⁻¹ of the Co, Ni, and Cu salts.

three-dimensional scattering of nanowires. This figure shows that a relatively small sample of nanowires can produce the same normalized XRF response as a highly concentrated sample.

Finally, to demonstrate potential tracking and authenticity (counterfeit) applications, the barcoded nanowires were embedded within host materials relevant to product packaging. Figure 5 illustrates the ability to read XRF signatures of alloy nanowires incorporated in a printable ink (A) or within fused plastic (COC) plates (B). Well-defined XRF signals are observed for both the ink- and plastic-embedded nanowires (ii) even with the nanowires embedded between 1.1 mm thick plastic sheets (much thicker than standard packaging plastics). In our study, the resulting fingerprints are similar enough to those of the corresponding freshly prepared nanowires to make a positive identification (within the membrane template; i versus ii). However, the exact definition of a positive identification will be left up to those using this technology, as it would depend on their specific needs. Overall, the data of Figure 5 clearly indicate that compositionally encoded alloy nanowires maintain their distinct XRF signatures upon incorporation in relevant host materials (with no apparent matrix effect) and that XRF leads to a convenient nondestructive readout of such fingerprints.

CONCLUSIONS

In this note, we demonstrated that XRF provides an effective nondestructive readout of compositionally encoded alloy nanowires. The template-directed alloy co-deposition preparation route obviates the need for sequential deposition steps (from different metal solutions) common for the synthesis of multisegment nanowire barcodes. Such coupling of one-step synthesis with a nondestructive readout (without prior dissolution) greatly simplifies practical applications of nanomaterial tags. The ability to prepare alloy nanowires with a large variety of compositions and visualize these compositions by XRF makes these alloy nanowires

promising candidates for a wide variety of tagging applications ranging from product tracking and protection, counterfeit testing to bioaffinity assays.

ACKNOWLEDGMENT

This work was supported by the National Science Foundation (Grant Number CHE 0506529). S.S. acknowledges a fellowship

from the Thailand Research Fund (Royal Golden Jubilee Ph.D. Program). Special thanks to Barry Wilkens (Center for Solid-State Science, ASU) for his help in using the Kevex XRF system.

Received for review June 7, 2007. Accepted July 23, 2007.
AC071206M

Appendix C

Shape-Tailored Porous Gold Nanowires: From Nano Barbells to Nano Step-Cones

Rawiwan Laocharoensuk,¹ Sirilak Sattayasamitsathit,^{1,2} Jared Burdick,¹ Proespichaya Kanatharana,³ Panote Thavarungkul,⁴ and Joseph Wang^{1,*}

¹Biodesign Institute, Departments of Chemical Engineering and Chemistry, Arizona State University, Tempe, Arizona 85287, and ²Faculty of Science, Prince of Songkla University, Hat Yai, Songkhro, 90112 Thailand

Nanowires are critically important building blocks of nanotechnology.^{1,2} An attractive and versatile route for preparing nanowires involves the electrodeposition into the cylindrical nanopores of a host porous membrane template, followed by dissolution of the template.³ Such a template-assisted electrochemical synthesis route permits a convenient and reproducible preparation of nanowires of a variety of sizes or compositions. Any material that can be electroplated can be used as a portion of the resulting nanowire. Multisegment nanowires, based on different materials, can be readily prepared by sequential electrochemical deposition of several segments (of metals, polymers, and composites), with different predetermined lengths, into the pores of the membrane template.⁴ In addition to solid metal nanowires, it is possible to prepare porous nanowires by a membrane-templated electrodeposition of a bimetallic alloy followed by the selective dissolution (de-alloying) of the less noble component.⁵ The electropolymerization of polypyrrole within the resulting nanopores led to metal/polymer composite nanowires of controllable composition.⁶ All of the above nanostructures have been characterized by a cylindrical shape of uniform diameter.

Here we report on the fabrication of shape-tailored porous gold nanowires via silver dissolution from multisegment gold-silver alloy nanowires with segments of different compositions. The new membrane-template protocol leads to novel step-like nanowire configurations (e.g., barbell or step-cone) containing segments with different diameters. As illustrated in Figure 1, such a protocol relies on sequentially depositing alloy segments of

ABSTRACT: Step-like porous gold nanowires of different shapes and diameters have been prepared by sequentially depositing alloy segments composed of different gold-silver ratios and de-alloying the silver component. For example, step-cone and nano-barbell porous gold nanowires were generated by a membrane-templated sequential deposition of gold-silver alloy segments from plating solutions of respectively decreasing or alternating gold-silver composition ratios. Alloy segments of different gold-silver ratios, prepared by using different plating potentials, also lead to multistep nanowires. In addition to step-like nanowires, we describe the preparation of cone- and bone-shaped porous nanowires from alloy nanowires of longitudinally changing compositions, generated via deposition from a flowing plating solution of a continuously changing composition. Such customization of the porous gold nanostructure is attributed to the chemical removal of silver and the different extents of gold reordering from alloy segments of different compositions. The latter leads to porous gold segments of smaller diameters from silver-rich alloy segments. The new "nanosculpting" concept is versatile and could be extended to nanowires of diverse shapes with a variety of properties, generating an attractive assortment of nano hardware.

KEYWORDS: nanowires • shape • alloys • porosity • gold • configurations

different gold/silver ratios (from plating solutions of decreasing or alternating gold/silver composition ratios) and etching the silver component. Taking advantage of earlier findings reported by Liu and Searson⁷ that the diameter of single-composition nanowires decreases upon dissolution of the less noble component, we now demonstrate that changing the alloy composition (by controlling the plating conditions) allows remarkable control of the shape and dimensions of the resulting wires. The different diameters of the resulting multistep nanowires reflect the larger void spaces formed between the nanowire and the template for alloy segments with higher silver content when free gold atoms (released during the silver dissolution) diffuse toward the gold-rich center. In addition to multistep nanowires, we describe for the first time the preparation of cone- and bone-shaped porous nanowires based on

*Address correspondence to Joseph.wang@asu.edu.

Received for review September 25, 2007 and accepted November 27, 2007.

Published online December 14, 2007.
10.1021/nm700255a.CC0: \$37.00

© 2007 American Chemical Society

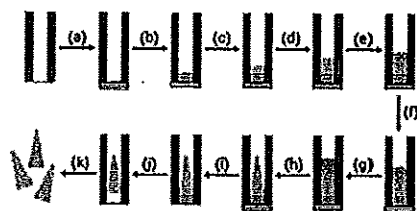


Figure 1. Scheme illustrating the template-assisted electrochemical preparation of the asymmetric porous gold nanowires: (a) sputtering gold on an alumina membrane; (b) copper deposition for a total charge of 10 C; (c) Au deposition; (d–g) deposition from Au/Ag solutions of (d) 9/1, (e) 8/2, (f) 7/3, and (g) 6/4 ratios; (h) etching the silver component using a 35% HNO_3 solution; (i) removal of the sputtered gold layer by polishing with a polishing machine and 1 μm alumina powder; (j) removal of the copper layer using 0.1 M CuCl_2 with 20% HCl ; and (k) dissolution of the membrane template using 3 M NaOH . All alloy deposition steps (d–g) were performed at -0.9 V using a charge of 0.2 C each.

gradually changing the composition of a flowing plating solution and hence the longitudinal composition of the corresponding nanowires. As will be illustrated below, such versatile tailor-made "nanomachining" results in nanoscopic objects with a wide range of shapes and dimensions.

RESULTS AND DISCUSSION

The ability to tailor the shape of porous gold nanowires and create unique and diverse stepwise nanostructures through the controlled plating of multisegment gold–silver alloy nanowires and selective silver etching is illustrated by the scanning electron microscopy (SEM) and transmission electron microscopy (TEM) images in Figure 2. Such images show well-defined step-cone (A,B) and nano-barbell (C,D) porous gold nanowires. The step-cone nanostructures were prepared by sequentially depositing binary alloy segments from plating solutions of decreasing gold/silver ratios (10/0, 9/1, 8.5/1.5, 8/2, 7.5/2.5, and 7/3) to yield alloy segments containing different compositions. In contrast, the nano-barbell configurations were synthesized by alternating between plating solutions with gold/silver ratios of 9/1 and 7/3. Etching the silver component from the corresponding alloy segment results in a significant change in the diameter of the porous gold nanowire section, hence leading to distinct step-cone and barbell nanostructures. The normalized diameter of each segment of the porous gold nanostructure was calculated with respect to the diameter of the solid gold segment (bright segment in SEM and dark segment in TEM). The diameter of the step-cone porous nanowires decreased in a stepwise manner from 91% to 41% (of the pure gold segment) upon decreasing the gold/silver ratio in the plating solution from 9/1 to 7/3, respectively. In contrast, the diameter of the nano-barbell alternates reproducibly between 100% and 64% upon switching between the 9/1 and 7/3 gold/silver solutions, respectively. The diameters of each segment of the nano-barbell structure are the same when the same composition of the Au/Ag plating solution was employed. Consequently, alternating between plating solutions of high-to-low Au/Ag ratios, or in an inverse fashion, does affect the diameter of the corresponding segments and the shape of the resulting nanostructures. In general, these images confirm the ability to create step-like porous nanostructures of different shapes based on the new synthesis protocol.

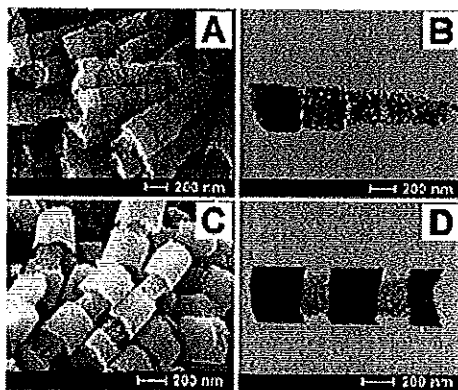


Figure 2. SEM and TEM images of multisegment asymmetric porous gold nanowires prepared at a deposition potential -0.9 V and using plating solutions of different gold/silver composition ratios. (A) SEM and (B) TEM images of the porous step-cone nanostructure prepared by plating sequentially alloy segments from plating solutions with gold/silver ratios of 10/0, 9/1, 8.5/1.5, 8/2, 7.5/2.5, and 7/3. (C) SEM and (D) TEM images of porous nano-barbell nanostructures prepared by alternating between gold/silver plating solutions of 9/1 and 7/3 composition ratios.

copy (SEM) and transmission electron microscopy (TEM) images in Figure 2. Such images show well-defined step-cone (A,B) and nano-barbell (C,D) porous gold nanowires. The step-cone nanostructures were prepared by sequentially depositing binary alloy segments from plating solutions of decreasing gold/silver ratios (10/0, 9/1, 8.5/1.5, 8/2, 7.5/2.5, and 7/3) to yield alloy segments containing different compositions. In contrast, the nano-barbell configurations were synthesized by alternating between plating solutions with gold/silver ratios of 9/1 and 7/3. Etching the silver component from the corresponding alloy segment results in a significant change in the diameter of the porous gold nanowire section, hence leading to distinct step-cone and barbell nanostructures. The normalized diameter of each segment of the porous gold nanostructure was calculated with respect to the diameter of the solid gold segment (bright segment in SEM and dark segment in TEM). The diameter of the step-cone porous nanowires decreased in a stepwise manner from 91% to 41% (of the pure gold segment) upon decreasing the gold/silver ratio in the plating solution from 9/1 to 7/3, respectively. In contrast, the diameter of the nano-barbell alternates reproducibly between 100% and 64% upon switching between the 9/1 and 7/3 gold/silver solutions, respectively. The diameters of each segment of the nano-barbell structure are the same when the same composition of the Au/Ag plating solution was employed. Consequently, alternating between plating solutions of high-to-low Au/Ag ratios, or in an inverse fashion, does affect the diameter of the corresponding segments and the shape of the resulting nanostructures. In general, these images confirm the ability to create step-like porous nanostructures of different shapes based on the new synthesis protocol.

Such fine and reproducible control of the diameter of the resulting porous gold segments (and hence the shape of the resulting nanostructures) reflects the different extents of gold reordering during etching of silver from alloy segments of different compositions. The de-alloying process starts when the alloy surface comes in contact with nitric acid solution. Silver atoms, connected to gold atoms in a face-centered-cubic (fcc) unit structure, are preferentially dissolved. Gold atoms with no coordination (adatoms) reorganize themselves by diffusing to a gold-rich zone and combining into a larger gold island. The atomic relocation of gold adatoms results in exposure of a new ("virgin") alloy surface that allows the acid to penetrate toward the center and dissolve silver atoms.^{8–10} Such continuous etching of the alloy nanowires eventually creates a 3D nanoporous structure with an axially symmetric cylindrical shape (templated by the alumina membrane). Porous nanowires have been shown to decrease in diameter and increase in porosity during the initial 10 min of the etching process.⁷ Negligible changes in the porosity and diameter were observed over longer dissolution

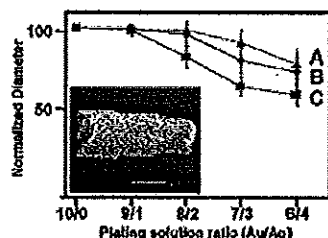


Figure 3. Normalized diameters of asymmetric porous gold nanowires obtained using different compositions of the Au/Ag plating solution (Au/Ag ratios of 10/0, 9/1, 8/2, 7/3, and 6/4) and various deposition potentials of -1.1 (A), -1.0 (B), and -0.9 V (C). The Au atom percent in the Au/Ag alloys ranged from 15% for the smallest diameter section to 85% for the largest diameter section. The normalized diameter was calculated with respect to the solid gold segment. The inset shows a SEM image of a step-cone nanowire prepared by using a 7.5/2.5 Au/Ag plating solution, with the individual alloy segments deposited at different potentials (-1.1 , -1.0 , and -0.9 V).

periods. The initial decrease of the diameter reflects the fact that free gold atoms (released from alloy during the silver dissolution) tend to diffuse toward the gold-rich center of the wire (since there is no gold on the extremities), leaving a "void space" between the nanowires and the template. Larger void spaces (i.e., small outside dimensions (diameters)) are thus expected for silver-rich alloy segments. The decreased diameter of the porous gold nanowires is also in agreement with a microscopic shrinkage of bulk Au/Ag alloy structures during electrochemical (rather than acidic) dealloying.¹¹ The initial change in morphology (from a solid alloy to nanoporous structure) results in an increase in porosity. Yet, with sufficiently long etching times (e.g., the 30 min used here), the various porous gold segments—corresponding to different alloy compositions—appear to reach a similar final density (i.e., porosity), as indicated from Figure 2A,B and from additional images below. Note also (from Figure 2 and subsequent data) that alloy segments with different compositions lead to gold islands of a similar ligament size (~ 15 – 20 nm). These observations that all segments reach the same final gold density and porosity imply that "silver-rich" segments of the alloy exhibit a faster rate of gold reordering than segments with lower silver content and that the time scale for dissolution is large enough that all segments reach the same asymptotic coarsening. Consequently, alloy segments with lower gold content result in porous nanowires of smaller outside dimension.

The alloy plating potential has a profound effect upon the diameter of the resulting porous gold segments. Figure 3 displays the dependence of the normalized diameter of segments of the step-cone nanostructure upon the plating potential and the composition of the plating solution. Using a plating potential of -1.1 V, the segment diameter decreased from 100% to 78%

upon reducing the Au/Ag ratio from 9/1 to 6/4 (Figure 3A). Larger changes (reductions) in the diameter of the porous segment, down to 74% and 60% (for the 6/4 gold/silver solution), are observed using plating potentials of -1.0 V (Figure 3B) and -0.9 V (Figure 3C), respectively. This behavior reflects the different standard reduction potentials of the silver cyanide ($\text{Ag}(\text{CN})_2^-$) and gold cyanide ($\text{Au}(\text{CN})_2^-$) major components of the silver and gold plating solutions (-0.53 and -0.82 V, respectively). These result in different reduction rates of silver and gold at the different plating potentials. Searson's group¹² illustrated that the deposition current of gold starts to increase at a potential of -0.9 V and reaches its potential-independent region above -1.2 V, while that of silver is already near its plateau at -0.7 V and changes only slightly over the entire -0.7 to -1.2 V potential range. The different reduction rates lead to changes in the amount of gold plated (i.e., to different alloy compositions) and, in turn, to different diameters of the corresponding nanoporous segments (after the silver dissolution). Energy-dispersive X-ray (EDX) analysis performed on the 7/3, 7.5/2.5, 8/2, and 8.5/1.5 Au/Ag segments of the alloy nanowires (grown at -0.9 V) yielded gold atom percent values of 18%, 19%, 24%, and 38%, respectively.

The profiles in Figure 3 indicate that it is possible to tailor the dimensions of the multistep nanowires by using the same plating solution while changing the deposition potential. For example, the inset in Figure 3 displays a SEM image of a step-cone porous gold nanowire prepared by using a 7.5/2.5 Au/Ag plating solution, with the individual alloy segments deposited at three different potentials (-1.1 , -1.0 , and -0.9 V). This image indicates that such stepwise electrodeposition yields a well-defined three-segment step-cone nanostructure with normalized segment diameters of 100%, 87%, and 74%. Such a multipotential single-solution protocol simplifies the preparation procedure, as it obviates the need for replacing the plating solution in connection to the different segments. Notice again the similar porosities and gold densities of the different segments of the step-cone structure (corresponding to the different alloy compositions).

It is possible also to combine the new nanomachining protocols with an electropolymerization step for preparing metal/polymer composites based on different shapes of the metal component. This can be accomplished after leaching the silver, by "backfilling" the resulting pores and surrounding gap with an electropolymerized polypyrrole while the wires are still inside the membrane template. Earlier we described a procedure for producing cylindrical (single-segment) metal/polymer composite nanowires.⁶ Figure 4 presents SEM and TEM images of a composite gold/polypyrrole nanostructure prepared by using a stepwise alloy deposition at -0.9 V from Au–Ag solutions with descending composition ratios (8.8/1.2, 8.2/1.8, and 7.8/

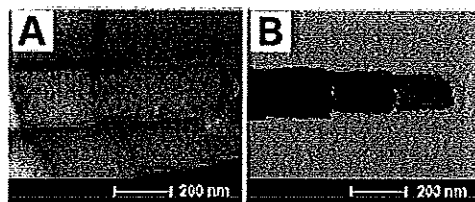


Figure 4. (A) SEM and (B) TEM images of a polymer (PPy)-covered step-cone nanowire. The porous gold step-cone was prepared by decreasing sequentially the composition of the gold in the Au/Ag mixture plating solution (Au/Ag ratios of 8.8/1.2, 8.2/1.8, and 7.8/2.2) while depositing at -0.9 V, with a 0.3 C charge for each segment. Following the silver etching, PPy was electropolymerized at $+1.2$ V for 12 s.

2.2). These images indicate that cylindrical composite nanostructures are formed with a defined internal porous gold step-cone (as in Figure 2A), but filled and surrounded with polypyrrole. This concept of metal/polymer composites can be extended to different shapes of porous gold and different polymers. Further dissolution of porous gold structure within the polypyrrole coverage could lead to porous polymer nanowires with pores reflecting the shape of the internal metal component.

In addition to step-like nanowire structures, we developed an alloy-based protocol for creating cone- and bone-shaped nanostructures based on continuously changing the composition of the Au/Ag plating solution (i.e., creating alloy nanowires with a longitudinal composition gradient). Figure 5C–H demonstrates the ability to design such conical nanostructures and to tailor their diameter, length, and hence sharpness. It shows SEM and TEM images of nanocones grown by adding silver to the gold-containing growth cell at increasing flow rates of 0.37 (C,D), 1.0 (E,F) and 2.0 $\text{mL} \cdot \text{min}^{-1}$ (G,H) until a final $1:1$ Au/Ag ratio was obtained. The rate of silver addition, and thus the time needed to reach the final Au/Ag ratio (5/5), determines

the overall plating time and hence the final length of the nanowires. The different longitudinal composition gradients along the alloy nanowires, associated with the different silver flow rates, lead to different diameters of the nanocone porous wires (i.e., to nanocones of different sharpness). For example, increasing the silver flow rates from 0.37 $\text{mL} \cdot \text{min}^{-1}$ (Figure 5C,D) to 2.0 $\text{mL} \cdot \text{min}^{-1}$ (Figure 5G,H) leads to reductions in the diameter per unit length ($\Delta d/L$) from 3% to 37% , respectively. Careful examination of these images indicates that the porosity and gold density are relatively uniform along the nanocones, analogous to earlier observations of step-cone nanowires (Figure 2).

In addition to one-directional conical nanowires, it is possible to prepare nanobone-like objects with two-directional changes. Figure 5I,J illustrates TEM and SEM images, respectively, of such nanobone porous nanowires grown by selectively adding and removing silver plating solution into a continuously flowing gold plating solution, delivered to a constant volume (~ 1.6 mL) growth flow cell. Figure 5A,B displays the experimental setup of the growth cell. (See Methods section for more details.) The addition of silver plating solution into the gold one results in a descending Au/Ag gradient in the plating solution, leading to the first conical segment (with decreasing diameter). At the reverse point, the flow of the silver plating solution was stopped, resulting in an ascending Au/Ag concentration profile in the plating solution and in the second conical segment (with an inverse direction of diameter change). Overall, this leads to a nanobone structure with lower diameter (in the central point of reversal), corresponding to 63% of the diameter of the solid-metal sections (on both ends). The exact time-dependent composition of the Au/Ag plating solution can be determined by solving an elementary first-order differential equation for solution mixing. Such versatile use of the flow of constituents to control the time-dependent composition of the

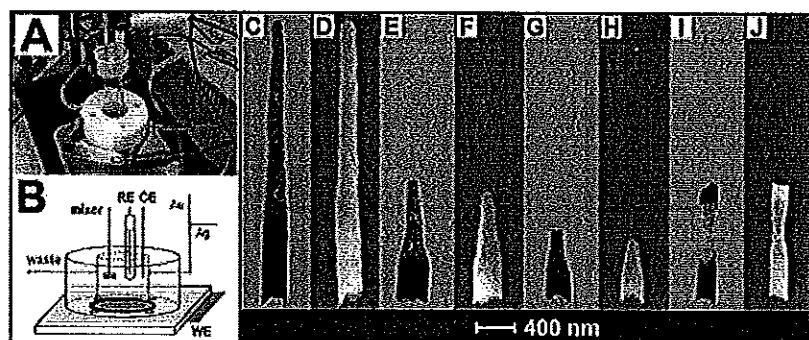


Figure 5. Nanocone (C–H) and nanobone (I, J) wires prepared by gradually changing the compositions of the plating solution. Nanocone nanowires were grown by adding 5.0 mL of silver plating solution to 5.0 mL of already present gold plating solution at varying flow rates. (C,E,G) TEM and (D,F,H) SEM images obtained using silver flow rates of 0.37 , 1.0 , and 2.0 $\text{mL} \cdot \text{min}^{-1}$, respectively. Insets (A) and (B) show the constant volume flow cell setup used to create the porous nanobone.

plating solution represents an elegant route for constructing shaped wires of different configurations.

In conclusion, we have described an attractive template-assisted electrochemical protocol for preparing shape-tailored multisegment nanowires of different shapes and diameters. This versatile shape-tailored concept can be extended to nanowires of diverse configurations with a variety of properties, based on different metals and polymers, leading to an attractive arsenal of assorted nano-hardware. The production of such shape-tailored wires could lead to wide range of potential applications, including barcoding/tagging, imaging, or del-

ivery, and could have an impact in microelectronics and sensing devices. For example, the new nanomachining protocol can be used for generating barcode nanowires based on segments of different diameters and lengths, i.e., of distinct shape-dependent "signatures", analogous to the much larger lithographically prepared diameter-modulated microwires of Matthias *et al.*,¹² leading to a wide range of tagging or multiplexed sensing applications. The tailoring of both diameter and porosity could possibly be used to tune the near-infrared absorbance of *in vivo* nanowires, aiding in pathological imaging and drug release.

METHODS

Materials. Anodic alumina membranes with a specified pore size of 200 nm and thickness of 60 μm were purchased from Whatman (Catalog No. 6809-6022; Midstone, UK). The pyrrole monomer was purchased from Sigma-Aldrich. The pyrrole was distilled regularly and stored at 4 °C. Gold targets fused to sputter the membranes were purchased from Denton Vacuum (Moorestown, NJ). The gold and silver plating solutions (Oxotemp 24 RTU PACK; and 1025 RTU @ 4.5 Troy/oz) were obtained from Technic Inc. (Anaheim, CA). A 161 mM pyrrole in 200 mM HCl solution was used for electropolymerizing the polypyrrole (PPy). All other chemicals were of analytical grade purity and were used as received. All solutions were prepared using nanopure water (18 M Ω , ELGA purelab-ultra model, Ultra Scientific, Marlow, Buckinghamshire, UK).

Instrumentation. All controlled-potential experiments were performed with a CHI 621A potentiostat (CHI Instruments, Austin, TX). Platinum wire and Ag/AgCl (3 M KCl, CHI Instruments) served as the counter and reference electrodes, respectively. All working electrode potentials are given with respect to Ag/AgCl reference electrodes. Scanning electron microscopy (SEM) images and metal compositions were obtained with a FEI XL 30 SEM instrument (FEI Co., Hillsboro, OR), equipped with an energy-dispersive X-ray analyzer (Amatek Inc., Mahwah, NJ) under an accelerating voltage of 30 kV.

Template Preparation of Multistep and Conical Nanowires. For all asymmetric nanowires, a thin film of gold was first sputtered on the branched side of the alumina membrane to provide an electrical contact for the subsequent electrochemical plating. For the asymmetric nanowires (not containing PPy), a copper base was plated first into the branched section of the membrane using a 1 M cupric sulfate pentahydrate ($\text{CuSO}_4 \cdot 5\text{H}_2\text{O}$) solution and a charge of 10 C; this was followed by 0.2 C of gold from an Oxotemp 24 plating solution. Both plating steps were carried out at a potential of -0.9 V. Asymmetric gold nanowires containing PPy were grown using an initial gold base (1 C at -0.9 V), as opposed to copper and gold.

The asymmetric step-cone nanowires were prepared on top of the previously mentioned bases by sequentially depositing (at -0.9 V) alloy segments (of 0.2 C) from gold/silver plating solutions of different ratios: 9/1, 8.5/1.5, 8/2, 7.5/2.5, and 7/3 (with intermediate rinsing with nanopure water). The nano-barbells were constructed by depositing alternately (at -0.90 V) alloy segments from gold/silver mixture plating solutions with ratios of 9/1 and 7/3 for five segments of 0.2 C each (starting with the 9/1 solution). The alloy sections of the nanowires were then de-alloyed with the removal of the less noble silver component by placing approximately 1 mL of a 35% (v/v) nitric acid solution in the growth cell (containing the nanowires-embedded membrane) for 15 min and then rinsing with nanopure water and repeating the process once. The membranes were then "released" from the growth cells and rinsed with nanopure water to remove all residues. After rinsing, the membranes containing copper were swabbed (on the gold-sputtered side) with a cotton-tip applicator soaked in 0.1 M CuCl_2 in 20% HCl for ca. 2 min. This

removed both the copper and the sputtered gold. The wires were then released from the alumina membrane as described below.

The asymmetric cone-shaped porous nanowires were constructed on the previously mentioned copper and gold bases by growing nanowires from a continuously changing Au/Ag plating solution. The solution consisted initially of 5 mL of the gold plating solution, and its composition was varied gradually by adding the silver plating solution at a fixed flow rate while plating (at -0.9 V) until obtaining a final volume of 10 mL. Different flow rates of the silver solution led to conical nanowires of different sharpnesses. Nanobone nanowires were prepared using a constant-volume growth cell setup with solution mixer. The growth cell was connected to both a 7 cm prebubbling tube (that delivered the plating solution) and a waste tube (that removed extraneous plating solution from the cell to maintain the total volume of ca. 1.6 mL). The nanobone wires were plated (at -0.9 V) from the changing solution in the growth cell. The first conical segment of the nanobone structure was deposited while flowing the silver plating solution at 0.3 mL \cdot min $^{-1}$ into a continuously flowing (at 0.7 mL \cdot min $^{-1}$) gold plating solution for 300 s. To obtain the second inverse-cone segment, the flow of silver plating solution was stopped, and only the gold plating solution was allowed to flow (at 0.7 mL \cdot min $^{-1}$) for an additional 100 s. The cone- and nanobone-containing membranes were de-alloyed as described earlier for the step-cone and barbell nanowires and were released from the membrane template as described below.

The asymmetric PPy-covered step-cone nanowires were prepared atop the solid gold base by sequentially depositing at -0.9 V alloy segments of decreasing gold contents from Au/Ag solutions with descending composition ratios (87.5/12.5, 82.4/17.6, and 77.8/22.2). The silver was then removed from the alloy as aforementioned, and PPy was electropolymerized from a 160 mM pyrrole solution in 0.2 M HCl for 12 s at a potential of $+1.2$ V. After removing the membrane from the growth cell and rinsing with nanopure water, the gold side of the membrane was polished with a standard 6-in. SEM sample polisher (South Bay Technology, Inc., San Clemente, CA) using 3- μm alumina powder and a final B polishing cloth (Electron Microscopy Sciences, Washington, PA). The membrane was polished until the gold color (from the solid gold segment) on the back of the membrane was no longer visible. The wires were then released from the alumina membrane as described below.

The release of the nanowires was carried out by first thoroughly rinsing the membrane with nanopure deionized water to remove any plating solution residue. This was followed by immersing the membrane in 3 M NaOH for 10 min with only slight agitation (owing to the delicate nature of the wires). The resulting nanowire-containing NaOH solution was removed to 1.5 mL Eppendorf tubes for precipitation. Nanowires were precipitated from the solution via centrifugation (for 3 min at 3000 rpm) and were washed several times with nanopure water until a neutral pH was achieved. All nanowire solutions were stored at room temperature.

The diameters of the individual segments of the new nanostructures were measured from calibrated SEM images. The diameter ratio reflects the ratio of the porous gold to the solid gold segments (the latter used as 100%). For each potential (-0.9 , -1.0 , and -1.1 V), the data were collected from 20 step-cone wires of five segments each, where five measurements were performed on each segment for a total of 1500 measurements.

Acknowledgment. This work was supported by the National Science Foundation (Grant No. CHE 0506529). R.L. and S.S. acknowledge fellowships from the DPST Program and the Thailand Research Fund (Royal Golden Jubilee Ph.D. Program), Thailand, respectively.

REFERENCES AND NOTES

- Hurst, S. J.; Payne, E. K.; Qin, L.; Mitlin, C. A. Multisegmented One-Dimensional Nanorods Prepared by Hard-Template Synthetic Methods. *Angew. Chem., Int. Ed.* 2006, 45, 2672–2692.
- Wanekaya, A. K.; Chen, W.; Myung, N. V.; Mukhandani, A. Nanowire-Based Electrochemical Biosensors. *Electroanalysis* 2006, 18, 533–550.
- Bentley, A. K.; Farhoud, M.; Ellis, A. B.; Lisensky, G. C.; Nickel, A. M.; Crone, W. C. Template Synthesis and Magnetic Manipulation of Nickel Nanowires. *J. Chem. Educ.* 2005, 82, 765–769.
- Keating, C. D.; Natan, M. J. Striped Metal Nanowires as Building Blocks and Optical Tags. *Adv. Mater.* 2003, 15, 451–454.
- Ji, C.; Searson, P. C. Synthesis of Nanoporous Gold Nanowires. *J. Phys. Chem. B* 2003, 107, 4494–4499.
- Meenach, S. A.; Burdick, J.; Wang, J. Metal/Conducting-Polymer Composite Nanowires. *Solid* 2007, 3, 239–243.
- Liu, Z.; Searson, P. C. Single Nanoporous Gold Nanowire Sensors. *J. Phys. Chem. B* 2006, 110, 4318–4322.
- Erlacher, J.; Aziz, M. J.; Karma, A.; Dimitrov, N.; Sieradzki, K. Evolution of Nanoporosity in Dealloying. *Nature* 2001, 410, 450–453.
- Forty, A. J. Corrosion Micromorphology of Noble Metal Alloys and Depletion Gilding. *Nature* 1979, 282, 597–598.
- Forty, A. J.; Durkin, P. A. Micromorphological Study of the Dissolution of Silver–Gold Alloys in Nitric Acid. *Philos. Mag. A* 1980, 42, 295–318.
- Pardo, S.; Kramer, D.; Volkert, C. A.; Rösner, H.; Erlacher, J.; Weissmüller, J. Volume Change during the Formation of Nanoporous Gold by Dealloying. *Phys. Rev. Lett.* 2006, 97, 035504.
- Ji, C.; Oskam, Y.; Ding, Y.; Erlacher, J. D.; Wagner, A. J.; Searson, P. C. Deposition of $\text{Au}_{1-x}\text{Ag}_x$ / $\text{Au}_{1-x}\text{Ag}_x$ Multilayers and Multisegment Nanowires. *J. Electrochem. Soc.* 2003, 150, C523–C528.
- Matthias, S.; Schilling, J.; Neitsch, K.; Möller, F.; Wehrspohn, R. B.; Gösele, U. Monodisperse Diameter-Modulated Gold Nanowires. *Adv. Mater.* 2002, 14, 1618–1621.

Appendix D

Nanowires

DOI: 10.1002/sml.200701047

Striped Alloy Nanowire Optical Reflectance Barcodes Prepared from a Single Plating Solution**

Andrea Bulbarello, Sirilak Sattayasamitsathit, Agustin G. Crevillen, Jared Burdick, Saverio Mannino, Proespichaya Kanatharana, Panote Thavarungkul, Alberto Escarpa, and Joseph Wang*

Nanowires have received considerable recent attention as tagging systems for a variety of product-tracking, identification, and protection applications.^[1,2] Such barcoded nanowire tags are commonly prepared by sequential electro-deposition of different metals within a porous template and display stripes of different metals (commonly silver and gold) that can be distinguished by optical reflectivity microscopy.^[3–6] While leading to high coding capacities such nanowires require a time-consuming synthesis involving multiple plating steps from different metal solutions.^[1] Recent efforts have demonstrated that encoded single-segment alloy nanowires can be synthesized by a single deposition step and encoded electrochemically^[9] or by X-ray fluorescence (XRF).^[9] However, such a greatly simplified preparation route is compromised by the corresponding destructive^[8] or expensive^[9] readout tools.

We demonstrate here that multisegment alloy nanowire barcodes with distinct optical-reflectance striping patterns and large coding capacity can be prepared by a template-assisted

electro-deposition from a single gold-silver plating solution mixture in connection to different potentials. The different reduction rates of silver and gold at different plating potentials over the -0.50 to -1.20 V range (versus Ag/AgCl)^[10] lead to alloy segments of different Au-Ag compositions and to 3–4 optically distinct, readily decoded alloy segments. Extremely large varieties of optical-reflectance striping patterns can thus be produced by plating these alloy segments in different orders and charges.

The new multisegment alloy nanowire preparation route greatly simplifies the code production when compared with the solution-changing sequential deposition of common bimetal nanowire barcodes.^[5,7] Scheme 1 illustrates the template-assisted electro-deposition of the multisegment alloy nanowires. The different deposition potentials are applied sequentially in a predetermined order and for different durations (A,B,C) to produce alloy segments of controlled length. This is followed by the template dissolution (D) and optical readout of the reflectance patterns (E). Compared to recently developed single-segment alloy nanowire electrochemical^[8] and XRF^[9] barcodes, the new striped alloy nanowires can be readily decoded on the basis of differences in optical reflectivity (which is a faster and cheaper diagnostic tool).

The ability to tune the optical properties by adjusting the deposition potential and to generate multisegment alloy nanowires with distinct optical reflectance barcode patterns from a single plating solution is illustrated in Figure 1. For example, Figure 1A displays an optical microscopy image, and the corresponding intensity profile, for a 5-segment nanowire involving four different alloy compositions. This nanowire was prepared from an 85/15 (v/v) Au/Ag plating solution by applying four different potentials in the following sequence: a) -1.20 , b) -0.73 , c) -0.96 , d) -0.50 , and e) -1.20 V versus Ag/AgCl. Such sequential deposition from the same solution results in four alloy segments that can be distinguished on the basis of the intensity of their reflectivity. As will be illustrated below, the four intensity levels reflect the stepwise increase of the gold content in the alloy upon increasing the deposition potential from -0.50 to -1.20 V.^[10] The corresponding intensity (line) profile (bottom of Figure 1A) clearly illustrates the ability to distinguish between the four segments of different alloy compositions. Each segment yields a characteristic intensity level, allowing convenient distinction of adjacent alloy stripes and of the four compositions. A large number of unique codes can thus be prepared by simply varying the deposition conditions while using the same plating solution. For example, Figure 1B–D shows reflectance images (top) and intensity lines (bottom) for three nanowires prepared by applying different potentials (-0.50 , -0.85 , and -1.20 V versus Ag/AgCl) using different preset orders and charges. Such change in the deposition conditions results in distinct striping patterns involving three visibly distinguishable reflectance intensity levels (bright, dark, and intermediate), corresponding to the individual alloy segments. Also shown in Figure 1C is an SEM image of the corresponding nanowire. The individual segments are clearly visible, and as expected,^[8] their intensities are the opposite of the corresponding optical-reflectance intensities.

* Prof. J. Wang, A. Bulbarello, S. Sattayasamitsathit, A. G. Crevillen, J. Burdick
Department of Chemical Engineering
Blodesign Institute at ASU
1001 S. McAllister Ave., P.O. Box 875801
Tempe, AZ 85287-5801 (USA)
E-mail: joseph.wang@asu.edu

Prof. J. Wang, A. Bulbarello, S. Sattayasamitsathit, A. G. Crevillen, J. Burdick
Department of Chemistry and Biochemistry
Blodesign Institute at ASU
1001 S. McAllister Ave., P.O. Box 875801
Tempe, AZ 85287-5801 (USA)

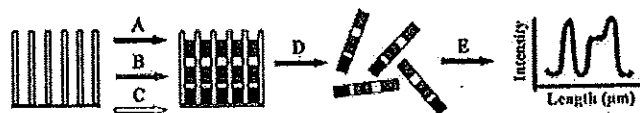
A. Bulbarello, Prof. S. Mannino
Department of Food Science and Technology
Università degli Studi di Milano
20133, Milano (Italy)

S. Sattayasamitsathit, Prof. P. Kanatharana, Prof. P. Thavarungkul
Faculty of Science, Prince of Songkla University
Hat Yai, Songkhla, 90112 (Thailand)

A. G. Crevillen, Prof. A. Escarpa
Department of Analytical Chemistry, Universidad de Alcalá
Alcalá de Henares, 28871 (Spain)

** This work was supported by the National Science Foundation (Grant number CHE 0506529). A.B., S.S., and A.G.C. acknowledge fellowships from Milan University, from the Thailand Research Fund and from the Spanish Ministry of Education and Science, respectively.

communications



Scheme 1. Synthesis of multisegment alloy nanowire barcodes using one gold–silver mixture plating solution with electro-deposition of segments occurring at different potentials (A–C) in various preset orders and durations. (D) and (E) represent the template dissolution and optical reflectance (intensity profile) readout, respectively.

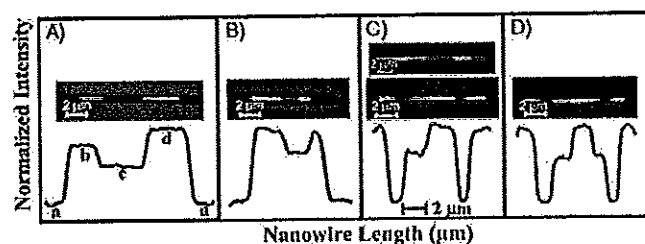


Figure 1. Reflectance images (top) and intensity lines (bottom) for different multisegment alloy nanowire barcodes prepared from an 85/15 (v/v) Au/Ag plating solution. The sequences of the deposition potentials for each nanowire image are (from left to right): A) -1.20 , -0.73 , -0.96 , -0.50 , and -1.20 V; B) -1.20 , -0.50 , -0.85 , -0.50 , and -1.20 V; C) -0.50 , -1.20 , -0.85 , -0.50 , and -0.50 V; D) -0.50 , -1.20 , -0.85 , -0.50 , -0.85 , -1.20 , and -0.50 V. The upper image (in C) shows the corresponding SEM image.

This concept can lead to a huge number of uniquely identifiable nanowires. Theoretically, varying the number of intensities, segment length and order can generate an unlimited number of codes. The coding capacity is effectively n^m where n is the number of intensity levels (i.e., alloy compositions) and m is the number of segments in the nanowire (assuming that the direction of the nanowire can be determined).^[7] In practice, however, given the current resolution, up to 5 intensity levels can be distinguished and up to 10 segments can be resolved within a typical $10\ \mu\text{m}$ long nanowire. This combination corresponds to 9,765,625 distinguishable nanowires. Such ability to generate 4–5 distinct alloy segments (and hence a huge coding capacity) using a single plating solution represents a major improvement over commonly used bimetal nanowire code ($n=2$) prepared by a solution-changing sequential deposition.^[5,7] The plating process can be computer-controlled for the simultaneous synthesis of multiple striping patterns in different membranes.

The multipotential templated deposition from a single plating solution results in distinct stepwise variation of the alloy composition along the length of the nanowires. Such tunable composition and optical properties are illustrated in Figure 2, which shows the dependence of the segment composition (A) and reflectance intensity (B) upon the deposition potential for a wire containing four different alloy segments, along with pure gold and silver segments (on both ends). These darkest (Au) and brightest (Ag) pure metal segments were added to normalize the intensity of the alloy segments and were assigned intensity values of 0.0 (Au) and 1.0 (Ag), respectively. An optical reflectance image of this nanowire, with the four alloy segments and the pure metal segments, is also shown in Figure

2. The silver content decreases in a nearly sigmoidal fashion from 92 to 53% upon raising the deposition potential from -0.50 to -1.20 V (A). This profile reflects the larger extent of gold co-deposition at more negative potentials associated with the different standard reduction potentials of the silver cyanide (-0.53 V) and gold cyanide (-0.82 V), major components of the silver and gold plating solutions. Searson's group^[10] illustrated that the deposition current of gold starts to increase around -0.9 V and reaches its potential-independent region

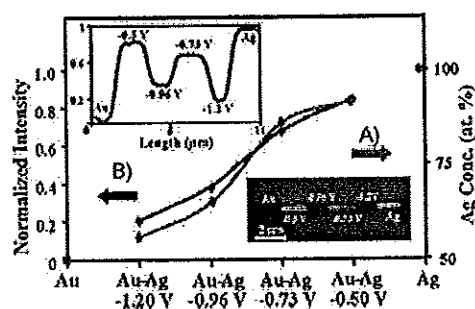


Figure 2. Dependence of the alloy composition (A) and the normalized reflectance intensity (B) upon the deposition potential. Insets show a reflectance microscopy image (bottom) and the intensity profile (top) of a multisegment nanowire containing four alloy compositions (deposited over the -0.50 to -1.20 V range) and pure gold and silver segments (at the ends, deposited at -0.90 V). The alloy composition was obtained by EDX analysis.

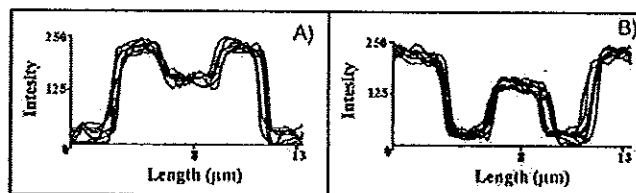


Figure 3. Reproducibility of the intensity profiles for multisegment alloy nanowire barcodes ($n = 10$ from two batches A and B). The alloy nanowire barcodes are composed of 5 segments (2 C charge each), deposited using the following sequence of plating potentials: A) -1.20 V, -0.50 V, -0.85 V, -0.50 V, -1.20 V. B) -0.50 V, -1.20 V, -0.85 V, -1.20 V, -0.50 V. Intensity is measured using an 8-bit grayscale.

above -1.20 V, while that of silver is already near its plateau and changes only slightly over the -0.7 to -1.20 V range. As indicated by Figure 2B, the optical intensity increases in a nearly linear fashion upon lowering the deposition potential from -1.20 to -0.50 V. The small difference in profiles A and B (with the larger curvature of the composition dependence) is attributed to the nonlinear correlation between the alloy silver content and the intensity of the reflected image.^[10]

The template preparation of multisegment alloy nanowires results in highly reproducible striping patterns. Figure 3 illustrates the reproducibility of two populations ($n = 10$) of nanowires based on different coding patterns (A, B). The relative standard deviation (RSD) for the respective intensity of each segment ranges from 3.8 to 13.7% for A and from 3.7 to 10.0% for B. The average lengths of the nanowires are $13.59 \mu\text{m}$ (A) and $13.32 \mu\text{m}$ (B) (RSD of 1.9 and 4.1%, respectively). The length of the respective individual segments had RSDs ranging from 4.9 to 7.4% (A) and from 4.1 to 7.6% (B).

In conclusion, we have demonstrated the template-assisted preparation of alloy nanowires with distinct optical reflectance coding patterns based on different alloy segments deposited from the same solution. The different reflectivity of adjacent alloy stripes enables convenient identification of the striping patterns by conventional light microscopy. The new multisegment alloy protocol combines a remarkably high coding capacity with a greatly simplified code production method as compared to that of commonly used bimetal nanowires, and hence holds great promise for different tagging applications.

Experimental Section

Sputtering of the alumina membrane was accomplished with a Denton Vacuum Desk III TSC (Moorestown, NJ). Electroplating was performed using a CHI 440 electrochemical analyzer (CH Instruments, Austin, TX). The sputtered gold was removed from the membrane using a standard 8-inch SEM sample polishing machine (Model 900 Grinder/Polisher, South Bay Technology Inc., San Clemente, CA) along with $1 \mu\text{m}$ alumina powder (Struers, Cleveland, OH). Optical images were acquired on a Nikon Eclipse 80i microscope (Nikon Corp., Tokyo, Japan) equipped with an X-Cite 120 fluorescence illumination system (EXFO, Mississauga, Ontario, Canada) as a light source and using a band-pass filter centered at 390 nm (with a bandwidth of 120 nm). Digital images

from the microscope were acquired with a Photometrics CoolSnap CF camera (Roper Scientific, Duluth, GA) and MetaMorph 7 software (Molecular Devices Corp., Sunnyvale, CA). Scanning electron microscopy (SEM) images were obtained with an XL30 SEM instrument (FEI Co., Hillsboro, OR) using an acceleration potential of 30 kV . Energy dispersive X-ray analysis (EDX) of the segmented nanowires was performed with an EDAX acquisition system (Ametek Inc., Mahwah, NJ) installed on the XL30 SEM instrument.

The gold target used for the membrane sputtering (99.9+ % pure) was purchased from Denton Vacuum (Moorestown, NJ). The commercial gold and silver plating solutions (Orotec 24 RTU RACK and 1025 RTU@4.5 Troy/Gallon) were obtained from Technic Inc. (Anahelm, CA). Sodium hydroxide was obtained from Sigma (St. Louis, MO). Anodisc 25 alumina membranes (25-mm diameter, 200-nm pore size and $60\text{-}\mu\text{m}$ thickness) were purchased from Whatman (Maldstone, U.K.) and used for all experiments. All solutions (except the commercial plating solutions) were prepared using nanopure deionized ($18 \text{ M}\Omega$) water (ELGA purelab-ultra model Ultra Scientific, High Wycombe, UK).

Alumina membranes were used as templates for the nanowire growth. Before use, a gold layer was sputtered on one side of the membrane (where the pores are branched) to serve as the working electrode during electrodeposition (in connection to an aluminum foil contact). Ag/AgCl and platinum wires were used as reference and counter electrodes, respectively. The sputtered membrane was placed in the bottom of a plating cell with the sputtered side contacting aluminum foil. The Au-Ag plating solution was introduced into the cell and the wires were deposited potentiostatically (as shown in Scheme 1). Three or four different potentials (-0.50 , -0.85 and -1.20 V or -0.50 , -0.73 , -0.96 and -1.20 V) were applied sequentially in a preselected order and charge to deposit the individual alloy segments. The length of each segment was controlled by the total deposition charge.

After completing the deposition, the membrane was removed from the growth cell and a polishing step was performed to remove the sputtered gold layer and the branched membrane section. The alumina membrane was then rinsed with distilled water and subsequently placed in a 3 M NaOH solution for 30 min until the membrane was dissolved. The resulting nanowire dispersion was washed using separation and dilution by centrifuging for 5 min at 6000 rpm , followed by removal of the supernatant and addition of distilled water. This process was repeated until a neutral pH was obtained. The wires used for obtaining the profiles of Figure 3 included also solid gold and silver segments

communications

on the opposite ends of the nanowires. This was accomplished by changing solutions from the silver plating medium to the Au–Ag mixture alloy plating solution and finally to the gold solution. The solid gold and silver segments were both plated at a constant potential of -0.9 V (versus Ag/AgCl).

The optical images were acquired using the 100x objective (LU Plan BD ELWD, Nikon Corp., Tokyo, Japan) on the Nikon 801 optical microscope, outfitted with the monochrome 12-bit dynamic range CoolSnap CF camera (previously mentioned). After the acquisition of the images, the optical pictures were processed using an internally developed protocol. First, using Photoshop CS2 (Adobe Systems Incorporated, San Jose, CA) the central part (along the axis of the nanowire) of the alloy nanowire barcode was selected (width of 4 pixels vs. different lengths), pasted into a new 8-bit grayscale image and subsequently the autocontrast filter built into Photoshop was applied on the nanowire strip image. The processed image was then fed to a Matlab (The Mathworks Inc., Natick, MA) program which averaged the pixel intensity across the 4-pixel columns and graphed this profile versus length of the wires. Using different plotting modes it is possible to obtain quickly the raw data or the normalized plots. The reflectance intensity was normalized using the highest intensity value corresponding to a prevalently silver segment deposited at -0.50 V . Normalization was performed with respect to the highest intensity value along the nanowire barcode. In order to obtain the dependence between the deposition potential and the reflectance intensity (Figure 3B) the above procedure was slightly modified. The same amount of pixels from each segment was selected and averaged to estimate intensity value of the segment. This segment intensity value was then plotted versus the corresponding plating

potential. For normalizing the reflectance intensity, the brightest segment (pure silver) was assigned a value of 1.0, while the darkest segment (pure gold) was set to be 0.0. Every segment was measured 5 times.

Keywords:

alloys · barcodes · nanowires · reflectance

- [1] H. H. Finkel, X. Lou, C. Wang, L. He, *Anal. Chem.* 2004, 76, 352A.
- [2] C. D. Keating, M. J. Natan, *Adv. Mater.* 2003, 15, 451.
- [3] S. R. Niekewamer-Pena, R. G. Freeman, B. D. Reiss, L. He, D. J. Pena, I. D. Walton, R. Cromer, C. D. Keating, M. J. Natan, *Science* 2001, 294, 137.
- [4] B. D. Reiss, R. G. Freeman, I. D. Walton, S. M. Norton, P. C. Smith, W. G. Stonas, C. D. Keating, M. J. Natan, *J. Electroanal. Chem.* 2002, 522, 95.
- [5] S. R. Niekewamer-Pena, A. J. Carado, K. E. Shale, C. D. Keating, *J. Phys. Chem. B* 2003, 107, 7360.
- [6] R. L. Stoermer, K. B. Cederquist, S. K. McFarland, M. Y. Sha, S. G. Penn, C. D. Keating, *J. Am. Chem. Soc.* 2006, 128, 16892.
- [7] I. D. Walton, S. M. Norton, A. Balasingham, L. He, D. F. Ovislo, D. Gupta, P. A. Raju, M. J. Natan, R. G. Freeman, *Anal. Chem.* 2002, 74, 2240.
- [8] J. Wang, G. Liu, *Anal. Chem.* 2006, 78, 2461.
- [9] S. Sattayasamitsathit, J. Burdick, R. Bash, P. Kanatharana, P. Thavavongkul, J. Wang, *Anal. Chem.* 2007, 79, 7571.
- [10] C. Ji, G. Oskam, Y. Oskam, Y. Ding, J. D. Erlebacher, A. J. Wagner, P. C. Searson, *J. Electrochem. Soc.* 2003, 150, C523.

Received: October 29, 2007
Revised: December 17, 2007
Published online: April 9, 2008

VITAE

Name Miss Sirilak Sattayasamitsathit

Student ID 4623008

Education Attainment

Degree	Name of Institute	Year of Graduation
Bachelor of Science (Chemistry), Second Class Honor	Prince of Songkla University	2002

Scholarship Awards during Enrolment

1. The Development and Promotion of Science and Technology Talent Project (DPST)
2. The Royal Golden Jubilee Ph.D. Program (RGJ) of the Thailand Research Fund (TRF)
3. The Center of Excellence for Innovation in Chemistry (PERCH-CIC), Commission on Higher Education, Ministry of Education and Graduate School

List of Publications and Proceedings

Publications

1. Sirilak Sattayasamitsathit, Panote Thavarungkul and Proespichaya Kanatharana "Bismuth Film Electrode for Analysis of Tetracycline in Flow Injection System" *Electroanalysis*, 19, 2007, No. 4, 502-505.
2. Sirilak Sattayasamitsathit, Jared Burdick, Ralph Bash, Proespichaya Kanatharana, Panote Thavarungkul and Joseph Wang "Alloy Nanowires Bar Codes Based on Nondestructive X-ray Fluorescence Readout" *Anal. Chem.* 79, 2007, 7571-7575.
3. Rawiwan Laocharoensuk, Sirilak Sattayasamitsathit, Jared Burdick, Proespichaya Kanatharana, Panote Thavarungkul and Joseph Wang "Shape-Tailored Porous Gold Nanowires: From Nano Barbells to Nano Step Cones" *ACSNANO*, 1, 2007, No.5, 403-408.
4. Andrea Bulbarello, Sirilak Sattayasamitsathit, Agustin G. Crevillen, Jared Burdick, Saverio Mannino, Proespichaya Kanatharana, Panote Thavarungkul,

Alberto Escarpa, and Joseph Wang "Striped Alloy Nanowire Optical Reflectance Barcodes Prepared from a Single Plating Solution" *Small*, 4, 2008, No. 5, 597-600.

Presentation

Oral presentations

1. Sirilak Sattayasamitsathit, Panote Thavarungkul and Proespichaya Kanatharana "Determination of Trihalomethanes in Drinking Water by Headspace Technique": A Clean Environment towards Sustainable Development, Malaysia, August, 2003
2. Sirilak Sattayasamitsathit, Rawiwan Laocharoensuk, Jared Burdick, Panote Thavarungkul, Proespichaya Kanatharana, and Joseph Wang "Single-Step Preparation of Alloy Nanowires Barcodes" RGJ-Ph.D. Congress IX, Pattaya, Thailand, April 4-6, 2008

Poster presentations

1. Sirilak Sattayasamitsathit, Panote Thavarungkul, Somenath Mitra and Proespichaya Kanatharana "*On-line system for alcohols*" RGJ- Ph.D. Congress IIV, Pattaya, Thailand, April, 2005
2. Sirilak Sattayasamitsathit, Panote Thavarungkul, Somenath Mitra and Proespichaya Kanatharana "*Membrane-based System to Separate Alcohol in Aqueous Sample*" PERCH Congress VI, Pattaya, Thailand, May, 2005
3. Sirilak Sattayasamitsathit, Panote Thavarungkul and Proespichaya Kanatharana "Fast Detection of Chloramphenicol Using Bismuth and Carbon Nanotubes Modified Electrode in Flow System" The 6th Princess Chulabhorn International Science Congress, Bangkok, Thailand, November 25-29, 2007
4. Sirilak Sattayasamitsathit, Panote Thavarungkul, Jared Burdick, Joseph Wang and Proespichaya Kanatharana "Electrochemical Synthesis of Multifunction Nanowires" 1st Regional Electrochemistry Meeting of South-East Asia 2008 REMSEA 2008 at Singapore, August 5-7, 2008
5. Sirilak Sattayasamitsathit, Panote Thavarungkul, Joseph Wangd, Jared Burdickd, Rawiwan Laocharoensukd, Andrea Bulbarelloe and Proespichaya Kanatharana

“Electrochemical Synthesis and Characterizations of Versatile Nanowires” 9th
Trends in Nanotechnology International Conference (TNT2008), Oviedo,
Asturias, Spain, September 1-5, 2008